Short Title of Thesis:

METHYL TUNNELING AND VISCOELASTIC RELAXATION IN PMMA

METHYL GROUP TUNNELING AND VISCOELASTIC RELAXATION IN POLY(METHYL METHACRYLATE)

by

John Richard Williams

A thesis submitted to the Faculty of Graduate Studies and Research in partial fulfillment of the requirements for the degree of Doctor of Philosophy.

Department of Chemistry
McGill University
Montreal, Quebec, Canada

January, 1978

To Elizabeth

METHYL GROUP TUNNELING AND VISCOELASTIC RELAXATION IN POLY(METHYL METHACRYLATE)

ABSTRACT

This thesis describes a dynamic mechanical investigation of the backbone methyl relaxation in poly(methyl methacrylate), (PMMA); the normal and fully deuterated polymers were studied by high precision torsional pendulum, vibrating reed and ultrasonic techniques, in the region of ~-200 to +50°C. Two very small relaxations observed for free-radically prepared PMMA were interpreted as due to motions of backbone methyls corresponding to syndiotactic and heterotactic main chain configurations. Evidence of quantum mechanical tunneling was present for the syndiotactic methyl relaxation, which showed not only pronounced curvature in the log ν versus 1/T plot but also a large isotope effect. Both results have been predicted from theoretical considerations and have now been verified experimentally. This represents the first demonstration of an isotope effect in the field of polymer mechanical properties.

Extrapolation of viscoelastic data for PMMA to high temperatures suggests that the various relaxations may all converge in a frequency/temperature region near 10^9 Hz and 200°C.

L'EFFET DE TUNNEL DU GROUPE METHYLE ET LA RELAXATION VISCOELASTIQUE DANS LE POLYMETHACRYLATE DE METHYLE

RESUME

Cette thèse décrit une étude dynamique et mécanique de la relaxation du groupe méthyle de l'épine dorsale dans la structure moléculaire du polyméthacrylate de méthyle, (PMMA); le deutéro-PMMA et les polymères normales ont été étudiées par des techniques de haute précision: le pendule de torsion, le 'roseau vibrant' et l'ultrasonique, pour des températures de -200 à 50°C. Deux relaxations très petites ont été observées dans le PMMA préparé par la méthode à radical libre et sont interprétées comme causées par les déplacements des méthyles de l'épine dorsale correspondant aux configurations syndiotactique et hétérotactique de la principale chaîne moléculaire. La relaxation syndiotactique du méthyle montrait un effet de tunnel quantique mécanique évident par la courbe marquée dans le graphique de $\log \nu$ versus $1/T$ ainsi que par un grand effet isotopique. Les deux résultats ont été prédits par des considérations théoriques et ont maintenant été vérifiés par expérience. Ceci représente la première démonstration d'un effet isotopique dans le sujet des propriétés mécaniques des polymères.

L'extrapolation des résultats viscoélastiques du PMMA à de hautes températures suggère que les relaxations divers peuvent tous converger dans la région fréquence/température près de 10^9 Hz et 200°C.

ACKNOWLEDGEMENTS

It is a pleasure to thank my research director, Dr. Adi Eisenberg, for his sustained interest, great enthusiasm, and constant encouragement throughout the project. Special thanks are also due to Dr. Esther Shohamy, who synthesized the deuterated polymer used in this study, to Messrs. Kluck, Gaulin and Kopp of the Chemistry Department workshops for expert apparatus design and fabrication, and to Nancy Dawes and Shelly Katz who helped with syntheses and dynamic mechanical experiments. I am also indebted to Dr. John Krause of the Bell Laboratories for help with the ultrasonic design and to Dr. Betty Ginsburg of Rohm and Haas for supplying several samples.

I would especially like to thank Susanne Chatterjee who very kindly typed the manuscript, my colleagues Kerry Burns, Richard Yeo and Melvin Croucher, and Lisa Arenson for their considerable assistance. Finally, I would like to acknowledge the financial assistance of the J.W. McConnell Memorial Fellowship and McGill University.

FOREWORD

'Methyl Group Tunneling and Viscoelastic Relaxation in Poly(methyl methacrylate)' is presented in six chapters as follows: Chapter I contains an introduction to the subject and a literature review of the molecular motions (especially the backbone methyl relaxation) of PMMA; Chapter II outlines the experimental techniques employed in the study and Chapter III contains the dynamic mechanical results obtained for normal and fully deuterated PMMA specimens; Chapter IV consists of a discussion of these results with Chapter V emphasizing the contributions to original knowledge and suggestions for future work; Chapter VI contains supporting references.

For the convenience of the reader, the tunneling frequency calculation for a deutero-methyl group in a barrier of 5.89 Kcal/mole has been reproduced from the private communication of Dr. S. Reich as Appendix I. Descriptions of the high precision Vibrating Reed and Ultrasonic instruments employed in the study are given as Appendices II and III respectively. Numerical and graphical data in support of Vibrating Reed and Ultrasonic results quoted in the text are included as Appendices IV and V respectively, with Appendix VI containing the supporting numerical data for text Figures.

A preliminary report of this work, presented in Phys. Rev. Lett. 35, 951 (1975), is included as Appendix VII.

TABLE OF CONTENTS

LIST OF SYMBOLS

a_T	WLF equation shift factor
b	overall specimen shape factor (torsional pendulum)
db	decibel level
f	frequency (ultrasonic)
f_o	resonance frequency
$(\Delta f)_{HW}$	width of resonance curve at half peak height
h	Planck's constant
$\hbar$	$h/2\pi$
k	Boltzmann constant
k'	spring constant
k_i	constants in vibrating reed calculations (i = 1,2,3)
ℓ	specimen length
log	logarithm to base 10
m	mass
n	quantum number (also number of points in ultrasonic calculation)
S_A, S_y	standard deviation of slope and Δy values
t	specimen thickness
t'	time (in the ultrasonic derivation)
v	ultrasonic velocity
w	specimen width
x	distance (also variable in ultrasonic data treatment)
y	variable in ultrasonic data treatment
A, B	constants
A_2	slope of time versus distance in ultrasonic data treatment
CAD	continuously adjustible decade (vibrating reed)

LIST OF SYMBOLS (contd)

E	Young's modulus
E', E'', E*	storage, loss and complex Young's moduli respectively
E	apparent activation energy
E_n	energy level
ENDOR	electron nuclear double resonance
G	modulus of rigidity or shear modulus
G', G'', G*	storage, loss and complex shear moduli respectively
I	moment of inertia of rotor (also ultrasonic intensity)
ISO	isotactic
K	bulk modulus
L_m	curvature of the hindering potential (of a methyl group) at its top
M	moment of inertia of oscillating system
M_L	mass of metal tab (vibrating reed)
MDBP	4-methyl-2,6-ditertiarybutyl phenol
MMA-H_8	methyl methacrylate, normal
MMA-D_8	methyl methacrylate, deuterated
N	Avogadro constant
NMR	nuclear magnetic resonance
P	pressure
PEMA	poly(ethyl methacrylate)
PMMA	poly(methyl methacrylate)
PMMA-H_8	poly(methyl methacrylate), normal
PMMA-D_8	poly(methyl methacrylate), deuterated
QM	quantum mechanical
R	ideal gas constant
RF	radiofrequency
S	scale factor (vibrating reed)
SYNDIO	syndiotactic
T	absolute temperature
T_c	Christov characteristc temperature
T_g	glass transition temperature
T_m	melting temperature

LIST OF SYMBOLS (contd)

T_o	period of oscillating system (no sample present)
T_A	period of oscillating system (sample in place)
T_1	spin-lattice relaxation time
V	volume
V (x,y,z) or V (ϕ)	potential function
V_o	barrier height
V_3	barrier height for a symmetric three-wall potential
ΔV	noise level (vibrating reed)
W_{st}	energy stored
ΔW	energy dissipated in one cycle
WLF	Williams, Landel and Ferry
Z	impedance
α, β, γ, δ	sub-Tg relaxations
α	attenuation coefficient
α-methyl	backbone methyl group
γ	shear strain
δ	phase angle (or chemical shift)
tan δ	loss tangent or internal friction
tan δ_E, tan δ_G	loss tangent in elongation or shear respectively
tan δ_a, tan δ_c	apparent and corrected loss tangent respectively
ε	elongation
η	viscosity
λ	ultrasonic wavelength
μ	Poisson's ratio (also shape factor in torsional pendulum)
ν	relaxation frequency
ν_o	frequency corresponding to infinite temperature
ν_c	correlation frequency (transition probability)
ν_t	tunneling frequency
ρ	sample density

LIST OF SYMBOLS (contd)

σ	tensile stress
τ.	shear stress
ϕ, ϕ_m	methyl rotation angle; angle at potential maximum
ψ	wave function
ω	angular velocity
Δ	logarithmic decrement

LIST OF TABLES

LIST OF FIGURES

I. INTRODUCTION

A. MECHANICAL PROPERTIES OF POLYMERIC SOLIDS:

1. Elasticity:

A deformation applied to an elastic solid gives rise to a restoring force within the material. If the deformation is sufficiently small, the stress (force/unit area) is proportional to the extent of deformation or the strain where the material is said to be in its "linear region". The constant of proportionality is called the modulus of elasticity or, more commonly, the stiffness of the material.

There are three distinct types of modulus: the shear modulus or modulus of rigidity G; the tensile or Young's modulus, E; and the bulk modulus K. These are given by:[1]

$$G = \frac{\tau}{\gamma}$$

$$E = \frac{\sigma}{\varepsilon}$$

$$\text{and} \quad K = \frac{P}{-\Delta V/V}$$

where τ and σ represent shear and tensile stresses respectively, P is pressure exerted on all sides of a body, and γ, ε $(= \Delta\ell/\ell)$, and $(\Delta V/V)$ are the shearing angle, the elongation or relative increase in length ℓ, and the relative increase in volume V, respectively.

The total volume of an isotropic material is not preserved under axial deformation, with experiments showing that lateral dimensions decrease (or increase) in proportion to the

axial elongation (or shortening). This 'factor of lateral contraction' is known as the Poisson's ratio μ, which, for a cylindrical specimen of unstressed diameter d and length ℓ, is defined by the equations:[2]

$$\ell_1 = (1 + \varepsilon)\ \ell;\ d_1 = (1 - \mu\varepsilon)\ d \qquad \ldots \text{for tension}$$

and $$\ell_1 = (1 - \varepsilon)\ \ell;\ d_1 = (1 + \mu\varepsilon)\ d \qquad \ldots \text{for compression}$$

where ℓ_1 and d_1 are the dimensions after stressing. The Poisson's ratio for isotropic plastics ranges from $\sim$0.3 (glass) to $\sim$0.49 (rubber).[3]

The various moduli of isotropic materials are interconnected through the Poisson's ratio as follows:

$$E = 2\ G\ (1 + \mu)$$

and $$E = 3\ K\ (1-2\mu).$$

2. Viscoelasticity:

A polymeric material exhibits simultaneously the properties of an elastic solid (stress proportional to strain) and a viscous liquid (stress proportional to rate of strain). The behavior of such 'viscoelastic' materials may be studied by various techniques, including dynamic mechanical testing, in which a very low amplitude cyclic strain (i.e. a vibration) is applied to the specimen. It is found that the resulting stress is not completely in phase with the strain, as illustrated schematically in Figure 1; the in-phase stress (stress which is proportional to strain) reflects elastic behavior, while the out-of-phase stress(stress proportional to the rate of strain) is a viscous response. The modulus therefore

FIGURE 1.

SCHEMATIC DIAGRAM ILLUSTRATING STRESS WHICH IS OUT OF PHASE WITH STRAIN, WHICH WOULD BE OBSERVED FOR A VISCOELASTIC MATERIAL.

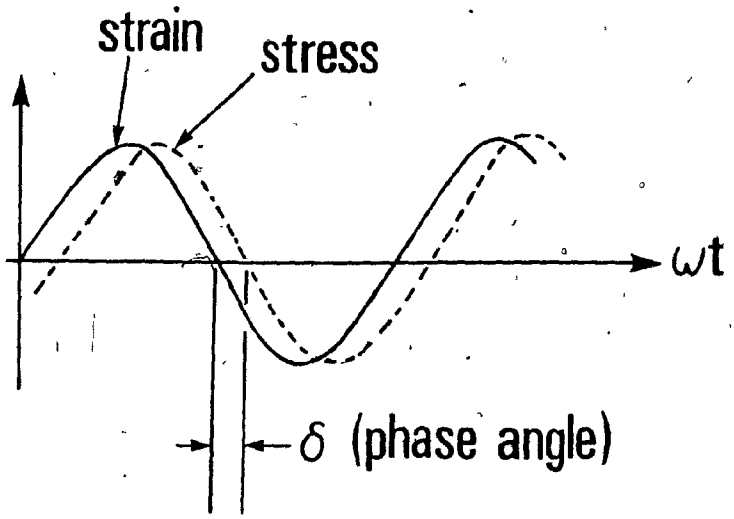
strain
stress
ωt
δ (phase angle)

consists of two orthogonal components, and can be written as a complex quantity; thus the complex modulus of rigidity G* is defined as:

$$G^* = G' + iG''$$

where G' is the in-phase (stress/strain) ratio or storage modulus, and G'' is the out-of-phase (stress/strain) ratio or loss modulus. G' and G'' relate to energy stored and dissipated (as heat) in the same sense as G and η (the viscosity) determined in static tests.[4]

The internal friction, $\tan \delta_G$, which is also known as the specific loss or damping factor, is defined as follows:

$$\tan \delta_G = \frac{G''}{G'}$$

Similarly, the complex Young's modulus, E*, may be written:

$$E^* = E' + iE''$$

with $\tan \delta_E = \frac{E''}{E'}$.

It may be shown that, for hard isotropic solids,[5] $\tan \delta_E \approx \tan \delta_G$, which allows the general use of tan δ (without a subscript) for damping.

3. Temperature Dependence of Polymer Mechanical Properties:

If the dynamic mechanical properties of an amorphous linear polymer are measured as a function of temperature at constant frequency, a progression of peaks in tan δ and corresponding steps in the modulus is generally observed. This is depicted schematically

in Figure 2A which might represent a torsional pendulum experiment at (say) 1 Hz. The peak regions, which are referred to as dispersions or relaxations in recognition of the time-dependent nature of the phenomena, appear when the frequency of a molecular motion matches the test frequency and are labeled α, β, γ, δ ....[6] with decreasing temperature; the α peak corresponds to the softening point or glass transition and involves mutual slippage of large numbers of main chain segments, while the lower temperature peaks are indicative of side group motions (such as hindered rotations) or movements of smaller parts of the main chain. Relaxations may be characterized by means of their tan δ peak heights and corresponding relaxation strengths, which is defined as the difference in modulus across a relaxation region divided by the average modulus in that region.[5,7]

At the glass transition temperature (T_g) region, a dramatic change in the mechanical properties occurs, with the material typically passing from a deformable rubber far above T_g to a brittle glass below that temperature; a thousand-fold increase in stiffness or rigidity may take place over a relatively small temperature range. Modulus changes across sub-T_g relaxations are less spectacular; nevertheless, the so-called 'tough' polymers may experience brittle to ductile transitions across lower temperature dispersions, especially if they involve motion of a backbone group - say the hindered rotation of a benzene ring contained in the polymer backbone.[8]

FIGURE 2A

SCHEMATIC DIAGRAM ILLUSTRATING TYPICAL G' (OR E') AND TAN δ BEHAVIOUR AS A FUNCTION OF TEMPERATURE FOR AN AMORPHOUS LINEAR POLYMER, AT A FREQUENCY OF (SAY) 1 Hz.

FIGURE 2B

SCHEMATIC DIAGRAM OF A TRANSITION MAP OF AN AMORPHOUS LINEAR POLYMER, CONTAINING, AS EXPERIMENTAL POINTS, THE HYPOTHETICAL EXPERIMENT AT 1 Hz SHOWN IN FIGURE 2A. THE FREQUENCY RANGES OF MECHANICAL TESTING TECHNIQUES ARE ALSO SHOWN.

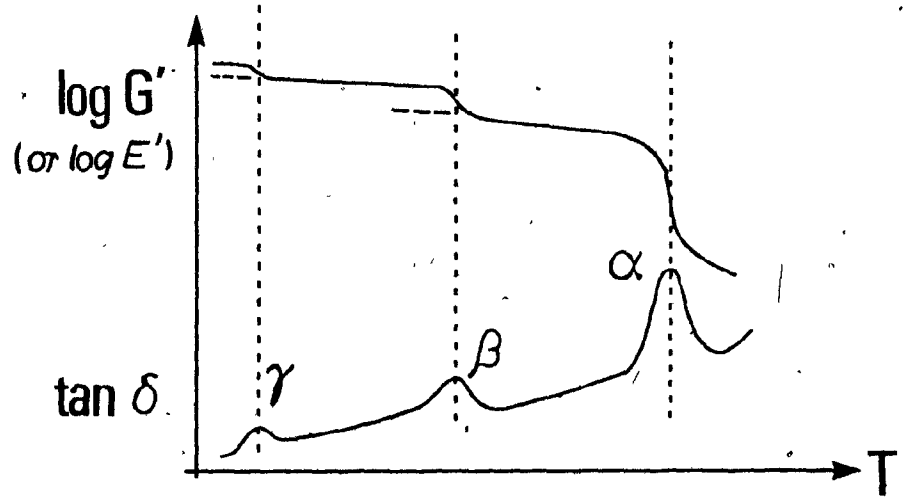
log G'
(or log E')
tan δ
γ
β
α
T

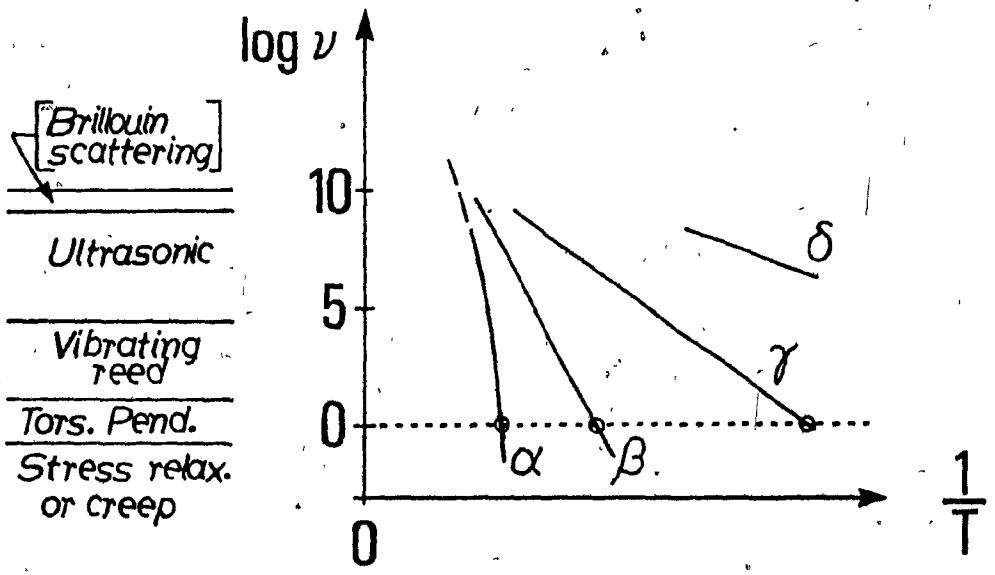
Brillouin scattering
Ultrasonic
Vibrating reed
Tors. Pend.
Stress relax. or creep
log ν
10
5
0
0
δ
γ
α
β
1/T

It is important to realize that under optimum conditions, dynamic mechanical testing permits the location in temperature and frequency of the various molecular motions taking place within the material although frequently the identification of the detailed molecular mechanisms may be difficult. If tests of the type depicted in Figure 2A are conducted at several frequencies (ν), a 'transition map' or plot of log ν versus $1/T$ for the relaxations may be constructed, where T is the absolute temperature. Figure 2B represents schematically a transition map containing, as experimental points, the hypothetical experiment at 1 Hz shown in Figure 2A.

As Figure 2B indicates, the sub-Tg relaxations (β, γ, δ) generally follow Arrhenius or straight-line log ν versus $1/T$ relations whose slopes define apparent activation energies (E_a's) for the several molecular motions occurring. For a movement which is a hindered rotation of a group, the activation energy E_a would be related to the barrier to rotation. A wide range of activation energies, from 1 to $\sim$ 25 kcal/mole, has been noted for the secondary relaxations of a variety of polymers.[6] The Arrhenius relation may be expressed mathematically as:[9]

$$\nu = \nu_o e^{-E_a/RT}$$

where ν_o is the frequency corresponding to infinite temperature, for which a value of $\log \nu_o = 13.5 \pm 1$ has been suggested.[5]

The α or glass transition relaxation follows a curvilinear log ν versus $1/T$ relation which is well described by the WLF

(Williams, Landel and Ferry) equation:[10]

$$\log a_T = \frac{-17.44\ (T-T_g)}{51.6 + (T-T_g)}$$

where a_T is a shift factor (analogous to a change in timescale or frequency) which is related to the change in T_g, given by $(T-T_g)$. Thus, if T_g is the glass transition temperature at $\log \nu = 0$, then the equation affords an estimate of T_g at a frequency given by $\nu = a_T$.

Dynamic dielectric and proton nuclear magnetic resonance (NMR) experimental data have been successfully combined with dynamic mechanical results in order to generate transition maps for polymers.[6,11] The dielectric and NMR techniques have limitations, however; the former is only able to follow molecular group motions which give rise to dipole moment changes, while the latter (NMR), although especially sensitive to the movement of proton-containing groups, cannot respond to motions of atoms not possessing nuclear spin, and has until recently been limited to frequencies greater than $\sim 10^4$ Hz.

Dynamic mechanical experiments appear capable of detecting all types of molecular motion. However, different types of instruments are required to span a wide frequency range. As indicated in Figure 2B, the torsional pendulum is generally employed in the 0.1 to 10 Hz region, the vibrating reed for $\sim$ 10 to 10^4 Hz, and ultrasonic methods for still higher frequencies ($> \sim 2 \times 10^4$ Hz). Stress relaxation and creep have also been used to study α and β relaxations at low frequencies. The use of such tests to elucidate molecular mechanisms

occurring in solid polymers has become known as 'Mechanical Spectroscopy', which has recently been reviewed.[12]

4. Molecular Identification of Mechanical Loss Peaks in Polymers:

Due to the enormous industrial importance of the mechanical properties of polymers, these types of measurements have been carried out extensively, with some identifications of molecular mechanisms progressing very far. Perhaps the best example of this is the case of polymers containing the cyclohexyl moiety, for which Heijboer[5] has shown that the chair-chair conformational change of the cyclohexyl group attached to a polymer chain (or present in a plasticizing molecule) gives rise to a γ relaxation at $\sim -80^{\circ}C$ at 1 Hz, with an activation energy of 11.5 Kcal/mole. In this case, the activation energy is equal to the barrier height, the barrier being strictly intramolecular, arising from within the ring itself. Indeed frequency/temperature data for the loss peak in liquid cyclohexanol are in agreement with results for the cyclohexyl-substituted polymers, suggesting a remarkable insensitivity of the molecular mechanism to the molecular environment. Heijboer showed not only that the γ peak was absent in PMMA plasticized with 1,1-dichlorocyclohexane, in which both chair conformers are identical, but also that the peak disappeared when the chair-chair conformational change was blocked through steric hindrance. In addition, he found that dielectric measurements on chlorinated derivatives were qualitatively what would be expected from geometrical considerations of the chair-chair transition for a cyclohexyl ring linked to a chain. It is worth

pointing out that Heijboer's assignment of the γ relaxation in cyclohexyl-containing materials to the chair-chair flip has been amply confirmed by subsequent NMR and theoretical work.

B. QUANTUM MECHANICAL TUNNELING AND VISCOELASTICITY:

1. Reality of Quantum Effects:

In the early part of the present century it was evident that Newtonian and Maxwellian concepts were unable to explain many phenomena occurring at the submicroscopic level of the atomic and subatomic particle. In particular, the frequency dependence of the blackbody radiation rate and the temperature dependence of the specific heat of a solid could not be understood in terms of classical mechanics.[13] An entirely new physical approach was needed. Max Planck laid the groundwork for this by boldly associating discrete energy levels with standing waves in a box. Einstein and later Debye extended Planck's concept to solids, identifying the thermal atomic motions with internal standing sound waves of different frequencies ν up to a maximum frequency corresponding to a wavelength approximately twice the lattice spacing. These oscillators were assumed to possess discrete energies of $nh\nu$, where n is a positive integer and h is Planck's constant, and an adequate description of the specific heat behavior was achieved. These developments launched the field of quantum mechanics.

Other experiments[13] indicated that electromagnetic radiation

(light) very often exhibited particle-like behavior as in the photoelectric effect, whereas entities which were considered to be particles (such as electrons) could display wave-like behavior. The wave-particle duality concept arose, necessitating a wave mechanical theory of particle behavior. In this formalism, the motion of a particle of mass m is described by a wave function ψ which obeys the Schrödinger equation:

$$\left[-\frac{\hbar^2}{2m} \nabla^2 + V(x,y,z) \right] \psi = i\hbar \frac{\partial \psi}{\partial t}$$

where $V(x,y,z)$ is the potential energy of the particle and $\hbar = h/2\pi$. Here $|\psi|^2$ is interpretable as a probability density.

As a one-dimensional illustration of the use of the Schrödinger wave equation, the case of a particle or system of particles behaving as a simple harmonic oscillator (i.e., as a spring) may be presented.[13,14] Here, the potential may be represented by $V(x) = \frac{1}{2}kx^2$, which has the form of a parabolic well. The wave equation reduces to:

$$-\frac{\hbar^2}{2m} \frac{d^2\psi}{dx^2} + \frac{kx^2}{2} \psi = E\psi$$

A set of solutions exists for this equation such that

$$E_n = \hbar \omega_o (n+\tfrac{1}{2})$$

where $n = 0, 1, 2, \ldots$ and $\omega_o^2 = k/m$. The wave functions ψ_n corresponding to these discrete energy values are characterized by maxima and minima and also nodes, where $\psi = 0$. A total of (n+1) maxima and minima, and n nodes exists. A schematic diagram of the potential function and the ground state ($n = 0$) wave function ψ_o is given in Figure 3A. It is clear from the Figure that the wave function extends beyond the confines of the hindering potential. Since $|\psi|^2$

FIGURE 3A

SCHEMATIC DIAGRAM OF THE SIMPLE HARMONIC OSCILLATOR POTENTIAL FUNCTION AND GROUND STATE WAVE FUNCTION, ILLUSTRATING THAT PENETRATION OF THE WALL TAKES PLACE (SHADED REGION).

FIGURE 3B

SCHEMATIC DIAGRAM OF TWO SIMPLE HARMONIC OSCILLATORS IN CLOSE PROXIMITY, ILLUSTRATING THE CONCEPT OF TUNNELING THROUGH A BARRIER.

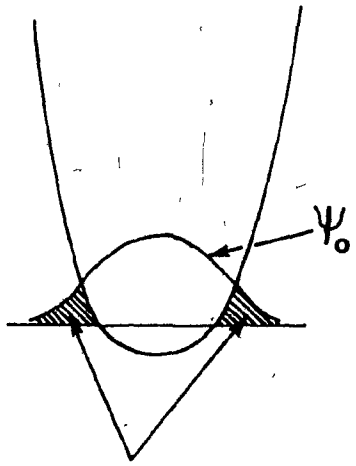

regions where particle penetrates the potential well

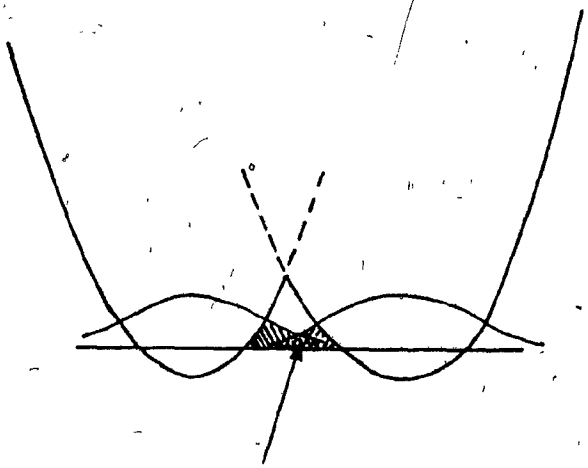

region where particle is within both wells

is interpreted as a particle probability density, there is therefore a finite probability of finding that particle outside the barrier, especially in the shaded regions. Thus the particle (or system of particles) penetrates the barrier to a very real extent.

If two such simple harmonic oscillators are in close proximity, as illustrated schematically in Figure 3B, then an interesting situation exists: overlap of the individual ground state wave functions is occurring, so that a particle moving under the influence of one potential function may find itself within the other well (as understood from quantum mechanical concepts), despite the fact that the particle energy is less than that required to hop over the barrier! Such a particle is said to have 'tunneled' through the barrier, a situation absolutely without classical counterpart.

Examples of quantum mechanical tunneling abound: α-particles decaying from radioactive nuclei are observed to penetrate the strong repulsive coulombic barrier provided by the charge on the radioactive nucleus, despite a total energy which is less than this barrier;[13] conversely, shooting particles at a nucleus usually involves tunneling. Tunneling of electrons through a potential hill occurs as in the case of the tunnel diode.[14] In addition, very high frequency (electromagnetic) effects which reflect tunneling are known, for instance the "umbrella" inversion of ammonia,[15] which is observed at normal temperatures, and is, in fact, well represented by the picture presented in Figure 3B. Quantum effects are however, very often encountered at low temperatures, an example being the superfluidity of liquid helium,[16] which is a mechanical manifestation of quantum mechanical

behavior. In addition, considerable evidence of tunneling phenomena in solids is also accumulating.[17,18] These illustrations of quantum effects show clearly the reality of the phenomenon, however foreign to our classical way of thinking it may be.

2. Development of the Quantum Mechanical Tunneling Hypothesis for Methyl Group Motions in Solids:

Methyl group motions in methyl-containing solids have long been investigated by various experimental techniques, especially proton NMR methods such as spin-lattice relaxation, line width and second moment studies.[19] As the temperature is lowered, minima in the spin-lattice relaxation time T_1, and increases in line width and second moment occur, corresponding to freezing-in of the methyl motion. In each type of experiment, a frequency ν may be associated with the motion[20] and correlated with the temperature. In this way, frequency-temperature relationships can be established for particular methyl group motions.

The temperature dependence of group motions such as barrier hopping of various side chains, including methyl groups has, in the past, frequently been expressed by the Arrhenius equation which has been described earlier (Introduction, Part A). This equation predicts a straight line relationship between log ν and $1/T$ with the slope proportional to the barrier height E_a.

Low temperature NMR tests on methyl-containing solids have not always, however, shown an Arrhenius type of behavior. This can be seen, for example, from Figure 4, which contains the frequency-temperature relation calculated by Das[21] from line width measurements for

FIGURE 4

FREQUENCY-TEMPERATURE RELATIONSHIP FOR 1,1,1-TRICHLOROETHANE (CALCULATED BY DAS[21] FROM NMR LINE WIDTH MEASUREMENTS CONDUCTED BY POWLES AND GUTOWSKY[22]).

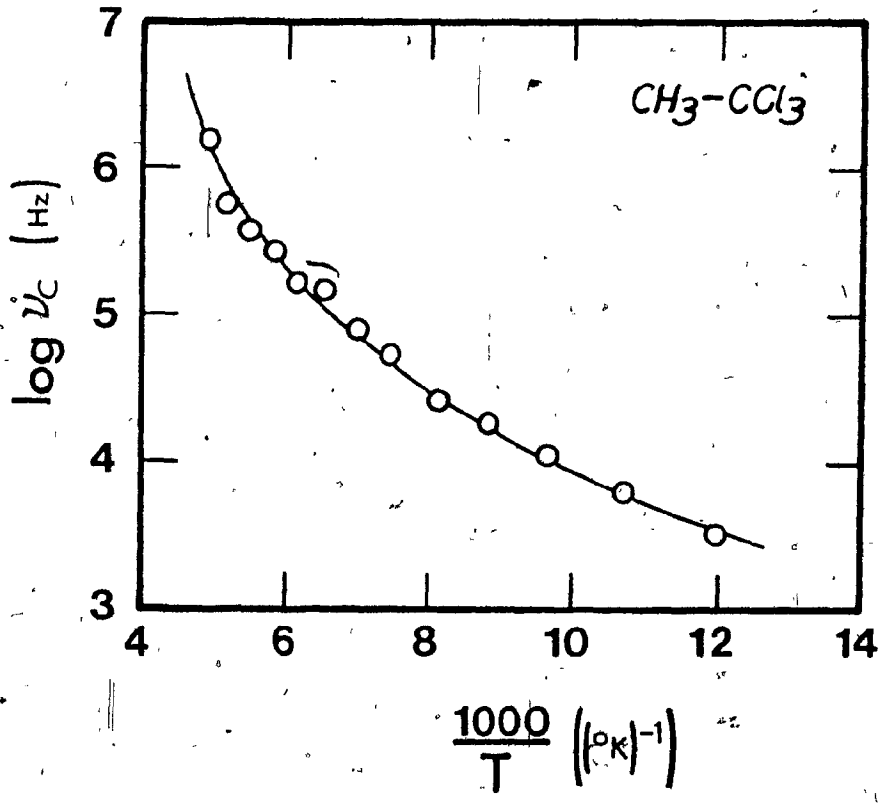
7
6
5
4
3
4
6
8
10
12
14
CH_3-CCl_3
$\log \nu_c$ (Hz)
$\frac{1000}{T}$ $(^\circ K)^{-1}$

1,1,1-trichloroethane (CH_3-$CC\ell_3$) conducted by Powles and Gutowsky[22] as early as 1953. It is clear that the log ν versus 1/T graph is curvilinear over the region studied. Such deviations from Arrhenius behavior have been correlated with rotational quantum mechanical (QM) tunneling of methyl groups in these materials at low temperatures.

The mathematical treatment of rotational tunneling only differs from the one-dimensional illustration given previously (the case of the simple harmonic oscillator) in that particle mass and linear distance must be replaced by the moment of inertia I and the angle of rotation ϕ of the rotating species. Figure 5 depicts the hindered rotation of a methyl group within a three-fold sinusoidal potential barrier for the case of ethane, assuming a barrier height of 2.75 Kcal/mole. The energy minima and maxima correspond to the staggered and eclipsed configurations of the methyl protons as shown in the Figure. Here, the ethane molecule is being viewed along the C-C axis. The first three vibrational energy levels calculated from the wave equation are given. It is clear that rotation of a methyl group in the ethane molecule implies that potential hills must be overcome, in the same sense as for a single particle approaching a coulombic barrier.

Quantum mechanical treatments (to be described later) indicate that, at a given temperature, there is not only a probability that the rotating system will hop over the barrier (the classical case) but also a probability that tunneling through the barrier will occur, with the tunneling frequency dependent on the barrier height and the moment of inertia. This picture would be similar for methyls in other molecular environments, except that the hindering potential barriers would differ.

FIGURE 5

SINUSOIDAL POTENTIAL FUNCTION FOR METHYL GROUP ROTATION IN ETHANE.

ETHANE

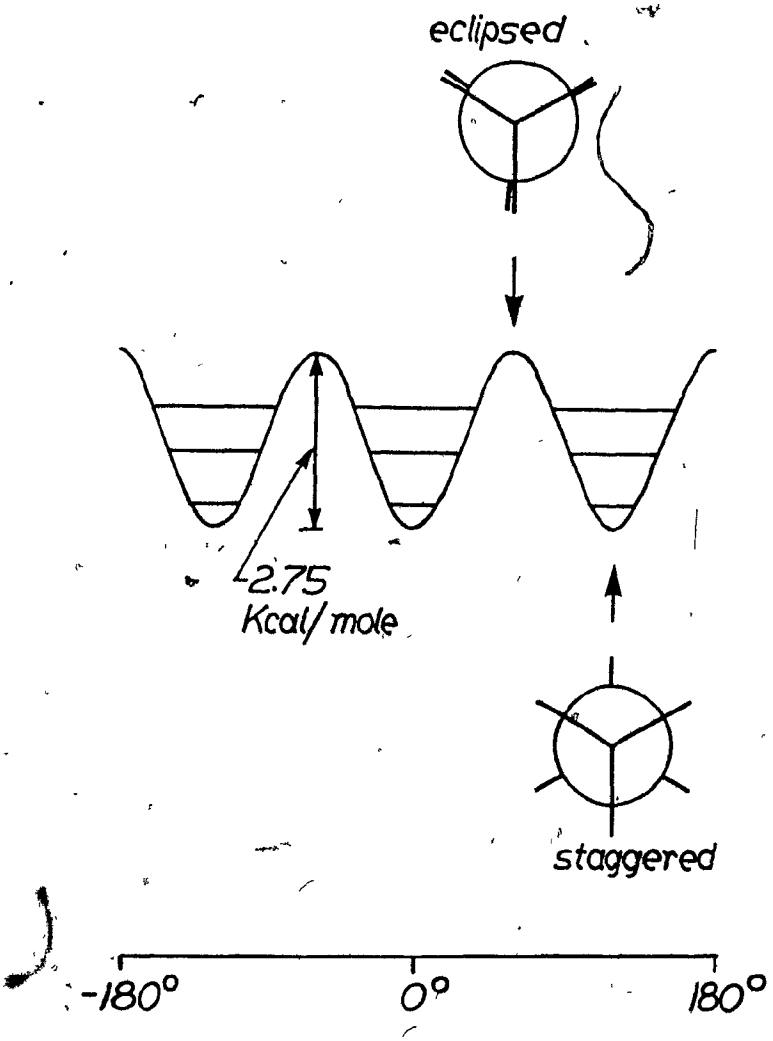

Rotational QM tunneling of methyl groups has been treated from a theoretical point of view by Das[21] in 1957, Stejskal and Gutowsky[23] in 1958, and more recently by Apaydin and Clough,[24] Allen and Clough,[25]* Davidson and Miyagawa,[26] Bloom,[27] Allen,[28] Hüller and Kroll[29] and Johnson and Mottley.[30] These theoretical approaches have followed quite different lines: Das, Stejskal and Gutowsky, Apaydin and Clough, Allen and Clough, Bloom, and Johnson and Mottley dealt with NMR phenomena; Davidson and Miyagawa, and Allen attempted to explain electron spin resonance (ESR) effects; and Hüller and Kroll considered neutron scattering evidence of methyl group rotational tunneling.

Das[21] applied a theory of tunneling through n-fold periodic barriers which previously had been used to explain fine structure in rotational microwave spectra, to the problem of calculating barrier heights from NMR data in solids. The theory, applicable to one dimensional potential barriers only, was applied to line width versus temperature data and T_1 versus temperature data for various low molecular weight compounds, most containing CH_3, CF_3 or NH_3^+ groups capable of hindered rotational motion. In particular, he deduced a barrier height of ∿6 Kcal/mole for the rotation of the methyl group in 1,1,1-trichloroethane (for which data was given in Figure 4).

Stejskal and Gutowsky calculated the average tunneling frequency ν_t as a function of temperature for barrier heights V_o in the range of 2.36 to 7.92 Kcal/mole, for a methyl group attached to a rigid framework, assuming a potential of the form

$$V = \tfrac{1}{2}V_o (1 + \cos 3\phi)$$

* It should be noted that Clough (References 24 and 25) has recently retracted parts of his theory.

where ϕ is the angle of rotation of the methyl group. Substitution of this potential function into the Schrödinger wave equation yields an expression of the Mathieu equation type, for which numerical solutions were obtained. These solutions were considered more rigorous than the approximate expressions derived by Das.

Stejskal and Gutowsky's theoretical results, which are shown in Figure 6, predict that, at high temperatures, or in the absence of tunneling, the frequency obeys an Arrhenius temperature dependence, while, at low temperatures, in the presence of tunneling, it levels off, ultimately becoming independent of temperature. A wide range of experimental NMR results is in general agreement with this hypothesis;[21,31-36] Odajima, Woodward and Sauer[31] found that the correlation frequency ν_c calculated from line width data above 77°K for poly(methyl methacrylate), (PMMA), poly(methacrylic acid), poly(sodium methacrylate), poly(α-methyl styrene) and the α-methyl styrene monomer began to level off with decreasing temperature, indicative of the onset of tunneling there. Kosfeld and von Mylius[34] have observed similar effects in wide line NMR measurements on PMMA and poly(methyl acrylate) in studies over the temperature range of 5 to 293°K. Knutson and Spitzer[32] studied the NMR line shape of poly(methyl-α-chloroacrylate) at temperatures as low as 1.5°K, concluding that the CH_3 group reorients rapidly at that temperature, i.e. at an average rate greater than 10^5/second. This would be consistent with quantum tunneling of the methyl group through a barrier of less than ∿3Kcal/mole.

FIGURE 6

THE AVERAGE TUNNELING FREQUENCY AS A FUNCTION OF TEMPERATURE FOR A METHYL GROUP, FOR BARRIER HEIGHTS IN THE RANGE OF 2.36 TO 7.92 KCAL/MOLE (CALCULATED BY STEJSKAL AND GUTOWSKY[23]).

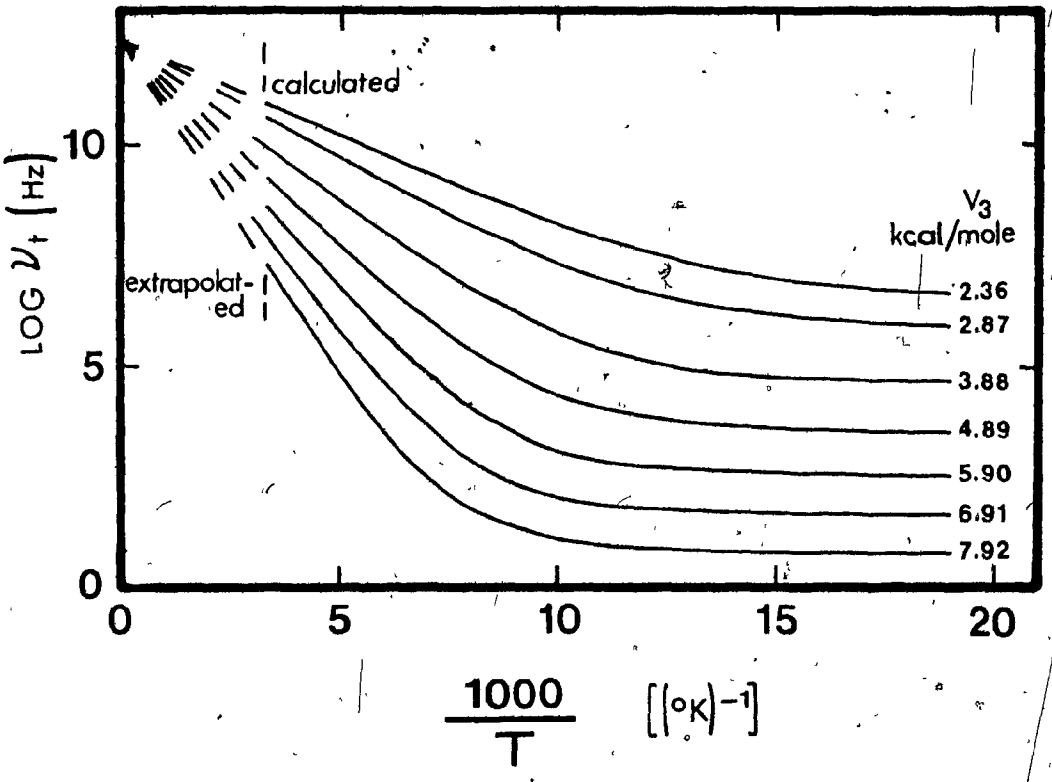
calculated
extrapolat-
ed
LOG ν_t (Hz)
10
5
0
V_3
kcal/mole
2.36
2.87
3.88
4.89
5.90
6.91
7.92
0
5
10
15
20
$\frac{1000}{T}$ [(°K)$^{-1}$]

Haupt and Müller-Warmuth[33] performed nuclear spin-lattice relaxation rate measurements at 14.5 and 40.7 MHz on toluene and several fluorotoluenes down to liquid helium temperatures and found low temperature methyl relaxations stronger than those predicted by classical theory. They suggest that "at low temperatures, the motion causing spin-lattice relaxation is reduced to certain torsional transitions between the lowest states, which are connected with tunneling". This interpretation appears consistent with the theory of Allen and Clough[25] which attributes a low temperature T_1^{-1} peak observed at $\sim 45^{\circ}K$ and 25 MHz in pentamethyl benzene[35] to a secondary tunneling-assisted relaxation. Recent T_1 measurements at 60 MHz on poly(isobutylene) and poly(carbonate) performed by Lammel and Kosfeld[36] have indeed found indications of two T_1 minima in each polymer, the lower relaxation (occurring at $\sim 7^{\circ}K$ (60 MHz) in both cases) considered due to tunneling methyl groups. Allen's[28] theory of QM tunneling suggests that the average tunneling frequency will increase with decreasing temperature at very low temperatures; this implies that the frequency of methyl reorientation will first decrease with decreasing temperature (Arrhenius behavior) and then level off as tunneling ensues, finally increasing again at very low temperatures. Thus a minimum frequency may exist, so that a constant frequency experiment would show two relaxations of a methyl group or none, depending on the magnitude of the frequency. Lammel and Kosfeld's data[36] and that of Allen and Cowking[35] appear consistent with this.

Evidence that methyl groups are indeed capable of rotational tunneling at low temperatures has also emerged from several other types

of experiments on methyl-containing materials. Among the most recent are studies of electron spin resonance[26,37-41,43] and electron nuclear double resonance (ENDOR);[42,43] Davidson and Miyagawa[26] studied the ESR absorption of the intermediate radical $CH_3\dot{C}HR$ from L-alanine at 4.2°K and developed a simple methyl rotational tunneling model to explain their observations; Clough and co-workers[37,38,39] investigated the ESR spectrum of γ-irradiated 4-methyl-2,6-ditertiarybutyl phenol (MDBP). It was demonstrated[37] that a change in the ESR hyperfine structure and maxima in the NMR spin-lattice relaxation rate both occurred near 14°K in MDBP and it was suggested that both effects were due to rotational tunneling of the hindered methyl. It was claimed that the two types of experiments represented similar dynamics of the methyl group. Later,[38] peaks in the magnetic field dependence of the proton spin-lattice relaxation rate were observed at liquid helium temperatures and attributed to resonances between the methyl tunneling frequency and the Larmor frequency associated with the unpaired electron. It was later[39] shown that, for an MDBP specimen thermally quenched to 4°K, a cross relaxation between the electron spin transition in a magnetic field and the transition between tunneling rotational states could be detected thermally; it was claimed that this "cross relaxation releases the stored mechanical energy of tunneling rotation to heat the sample". Temperature rises of the order of 1 mK degree were observed in this study. Clough's group also investigated methyl group tunneling rotation in γ-irradiated methyl malonic acid crystals by ESR[40,41] and by ENDOR;[42] a sample containing deutero-methyl groups was also studied.[43] It was shown that the frequency of methyl (CH_3)

tunneling appears to decrease with increasing temperature above ~25°K,[41] in reasonable agreement with the theory of Allen.[28] The work on deutero-methyls (CD_3)[43] indicated that CD_3 groups also undergo rapid tunneling rotation at 4°K with a possibly lower barrier to rotation than that for the non-deuterated analogue.

3. Proposal for Viscoelastic Relaxation:

In 1969, it was proposed by Eisenberg and Reich[44] that rotational tunneling of methyl groups could be involved in viscoelastic relaxation, the basis for this suggestion being the existence of low temperature mechanical loss peaks in methyl-containing polymers at temperatures too low to be explained by the classical approach. Too few methyls possess sufficient energy at (say) 40°K (a reasonable temperature for the low temperature relaxations) to overcome barriers of greater than ~2 Kcal/mole (also reasonable for methyl motions[21]) to account for the observed energy dissipation. The proposal made use of the Stejskal and Gutowsky theoretical treatment of methyl group tunneling around the C_3 axis.[23] It was pointed out by Eisenberg and Reich that the prediction that the average tunneling frequency levels off with decreasing temperature could explain not only the low temperatures of the observed loss peaks, but also the relatively large width of the peaks (half-width ~20 to 70°K for the methyl-substituted polystyrene peaks which occur at ~40°K.[45]) A success of the approach was that the application of the QM hypothesis to the observed dispersions led to quite reasonable estimates of the barrier heights for the different methyl groups based on structural considerations. It was observed that the barriers clustered around two values, ~4 Kcal/mole and ~7 Kcal/mole,

the former being considered appropriate for methyls attached to ester side chains and those attached to carbon-oxygen backbones (as in poly(propylene oxide)) and the latter felt reasonable for methyls bonded directly to a carbon backbone (as in the methacrylate polymers and polypropylene).

A more detailed mechanistic picture supporting the tunneling involvement was later given by Reich and Eisenberg.[46] Their proposed explanation considered that a dynamic viscoelastic test imposed a cyclic strain on the polymer specimen, modulating the interatomic distances at the experimental frequency (say 0.1 to 10^8 Hz), and resulting in a corresponding modulation of the barrier height restricting methyl rotation. This change in V_3 causes a change in the torsional energy states of the methyl rotors. It is suggested that, at low temperatures, methyl tunneling rotation may occur between the same torsional states (but differing slightly in energy due to a barrier modulation also occurring), with the difference in energy carried away by a phonon. The emitted phonon would ultimately be thermalized, leading to energy dissipation as heat. Several well-known processes were cited as support for the proposal; these were the cases of inelastic electron tunneling from one conduction band to a lower one through a barrier, the energy difference being carried off by a phonon, and an optical analogue, in which a monochromatic beam incident on a transparent medium where the refractive index is modulated in time, yields transmitted waves with the original frequency (say ν_1) and also two components at frequencies above and below ν_1 by the modulation frequency.

Reich and Eisenberg claim that the most pronounced viscoelastic relaxation should occur when $\langle \nu_t \rangle$ is approximately equal to the experimental

frequency, since, if tunneling occurs at a slower rate, then it is mainly barrier modulation (which is elastic) that is occurring, and, if tunneling is taking place at a faster rate, then most tunneling events are elastic. The authors carried out a simple calculation illustrating that the expected energy change in the proposed inelastic tunneling was of the same order as the most probable phonon at low temperatures (say $\sim 10^{\circ}K$); therefore phonons produced by the suggested mechanism could interact with thermal phonons, resulting in energy dissipation. It was also shown that only a small fraction of the methyls would have to participate in such a mechanism to explain the size of the low temperature loss peaks in the methyl-containing polymers.

The proposed connection between methyl group tunneling and viscoelasticity was not, however, universally accepted. Tanabe et al.[47] detected small mechanical relaxations in ultrasonic tests at 10 MHz in several methyl-containing polymers - polypropylene, poly(methyl methacrylate), poly(ethyl methacrylate), and poly(isobutyl methacrylate); the relaxations were observed at $\sim 220^{\circ}K$ for the methacrylate polymers and at $\sim 160^{\circ}K$ for polypropylene and were ascribed to the motion of methyls attached directly to the polymer backbones. These authors concluded that methyl group motion led to mechanical relaxation, but suggested that QM tunneling was ineffective as a mechanism. They arrived at this conclusion via a summary of dynamic mechanical and NMR log ν versus 1/T data for methyl groups in four types of molecular environment - those attached to tertiary carbon atoms, secondary carbon atoms, CH_2 units and oxygen atoms, it being assumed that the barriers to rotation would be comparable for each type. (It is interesting to note that Eisenberg and Reich[44] also compared similar polymer types in their proposal

and came to the opposite conclusion as Tanabe et al., i.e. that quantum tunneling could explain the low temperature viscoelastic data.)

Support for an interrelation of methyl rotational tunneling and viscoelastic relaxation has also emerged; Sauer[48] has reviewed the low temperature relaxation phenomena observed in several methyl-containing polymers and has noted that the general pattern followed by methyl motions is intermediate to that predicted by classical and tunneling theories, suggesting that quantum effects will be manifest at very low temperatures. Golub' and Perepechko[49] measured the velocity of longitudinal and transverse ultrasonic waves in PMMA at 1 and 5 MHz and temperatures from 2.1 to 240°K; they found that the velocity continued to increase with decreasing temperature all the way down to 2.1°K, and attributed this result to the occurrence of rotational QM tunneling of methyl groups, along the lines of the Reich and Eisenberg model.[46] In addition, they claim that a dispersion in the velocity exists at ∿140°K at 1 MHz and ∿160°K at 5 MHz, and that this relaxation might be due to the side chain methyl motion. It would seem more reasonable to ascribe this to the hindered rotation of backbone methyls, however, in rough agreement with the observations of Tanabe et al.[47] It should be noted also, that the relative error in their velocity measurements is stated by Golub' and Perepechko as being ∿1%; this would be expected to make the observation of the small methyl dispersion very difficult, as will become apparent from the data reported in this thesis. Indeed, what they observe is a change in slope of the velocity/temperature curves, and not inflections which are characteristic of mechanical relaxations. Thus the temperatures they suggest for the relaxation may be

only approximate. Nevertheless, the observed velocity increases at very low temperatures may indeed suggest a QM tunneling phenomenon, perhaps related to motion of the ester methyl in PMMA.

Additional support for the QM hypothesis has arisen from the neutron incoherent inelastic scattering studies of Allen and co-workers,[50,51] who calculated the three-fold barriers to rotation (V_3) of the α-(or backbone) methyl group in syndiotactic and isotactic PMMA from measured torsional frequencies of the group. (It was necessary to prepare isotactic PMMA-$COOCD_3$ in order to obtain a reliable value for the isotactic polymer.) The improved results[51] led to potential barriers which agreed better with V_3's calculated from existing NMR experimental data for PMMA by assuming that methyl tunneling was operative than with activation energies calculated by assuming Arrhenius relationships.

For several non-methyl containing systems, tunneling has been connected with viscoelastic and dielectric relaxation: Jackle[52] considered a model for a glassy solid in which atoms (or groups of atoms) possess two equilibrium positions within an asymmetric double well potential. At low temperatures, transitions between the two ground states are possible by tunneling, with a phonon absorbed or emitted, providing a mechanism of structural relaxation. This picture seems similar to that proposed by Reich and Eisenberg[46] to explain energy dissipation by a tunneling methyl group where asymmetry in the barrier results from modulation by an external excitation. Jackle derived the sound absorption from this relaxation process and compared the result with recent experimental data for the ultrasonic attenuation in fused silica at 2 GHz and 1 to 2°K, obtaining qualitative agreement between

theory and experiment. Very recently, Yano et al.[53] studied the dielectric loss in high density polyethylene from 1.5 to 4.2°K at 10 Hz to 10 KHz, concluding that low temperature peaks were due to phonon-assisted tunneling of hydroxyl protons accidentally attached to tertiary carbon atoms. A potential calculation for the OH rotation within the distorted polyethylene lattice suggested that protons could be present in a double well potential, which (as has just been discussed) can lead to tunneling-related structural relaxation. It may also be mentioned here that the anomalous thermal properties of glasses at low temperatures[54] can be explained qualitatively by theory involving "tunneling-level-pairs".[55]

Literature data on mechanical relaxations of methyl groups in polymers[6,11] has, however, proved insufficient to distinguish between tunneling and thermal activation. This is because very little viscoelastic data, especially high precision results, exist for methyl relaxations in general, and those which do exist cover only limited temperature and frequency regions. Even the occurrence of methyl peaks is surprising, since methyl rotation under a symmetrical three-fold potential is not expected to result in mechanical loss.[11] Nevertheless several mechanical peaks have been ascribed to methyl groups.[48,56,57]

The principal objective of this thesis is to resolve experimentally the question of the involvement of methyl tunneling in viscoelastic relaxation. For this purpose an experimental examination of the γ relaxation in poly(methyl methacrylate) was launched. This relaxation was chosen, since it had been identified as due to rotational motion of the backbone methyl

group,[6,47,58,59] and is experimentally accessible in convenient frequency and temperature regions. Of great importance to this investigation is the effect of isotopic substitution on tunneling, which is well known. In particular, the influence of deuteration on the rotational tunneling frequencies of methyl groups was examined by S. Reich,[60] whose calculation (based on the theory of Stejskal and Gutowsky[23]) is given in detail in Appendix I, for the convenience of the reader. Reich's treatment showed that deuteration should lead to only very minor changes in the classical region, while producing a profound shift to lower frequency in the tunneling region. This is illustrated in Figure 7 for methyl and deuteromethyl groups in a potential well of 5.9 Kcal/mole.

Two features apparent in Figure 7 provide the basis for this experimental study. First, if the temperature dependence of the viscoelastic energy dissipation peak is of the Arrhenius type over the entire range, then tunneling is unlikely, while a levelling-off would support tunneling. Our accessible frequency-temperature region (shown as the area enclosed by the dotted lines in Figure 7) indicates that this levelling-off, if present, should be seen for the non-deuterated polymer.

The second feature which can be investigated is the isotope effect. If it were shown that the behavior of the material containing deuteromethyls is very close to that of the non-deuterated analogue, then tunneling would be excluded, while the presence of an isotope effect of the type shown in Figure 7 would prove that tunneling is indeed involved in viscoelastic relaxation. It should be emphasized that these criteria are based on the assumption that the theory of Stejskal and Gutowsky is valid in its essential features in its description of the tunneling process.

FIGURE 7

THEORETICAL FREQUENCY-TEMPERATURE RELATIONS FOR METHYL AND DEUTEROMETHYL REORIENTATIONS BY CLASSICAL ROTATION AND QUANTUM MECHANICAL TUNNELING FOR A BARRIER HEIGHT OF 5.9 KCAL/MOLE. THE DASHED LINES REPRESENT THE CLASSICAL CASE AND THE AREA ENCLOSED BY THE DOTTED LINES IS THE REGION ACCESSIBLE BY THE EXPERIMENTAL TECHNIQUES USED HERE.

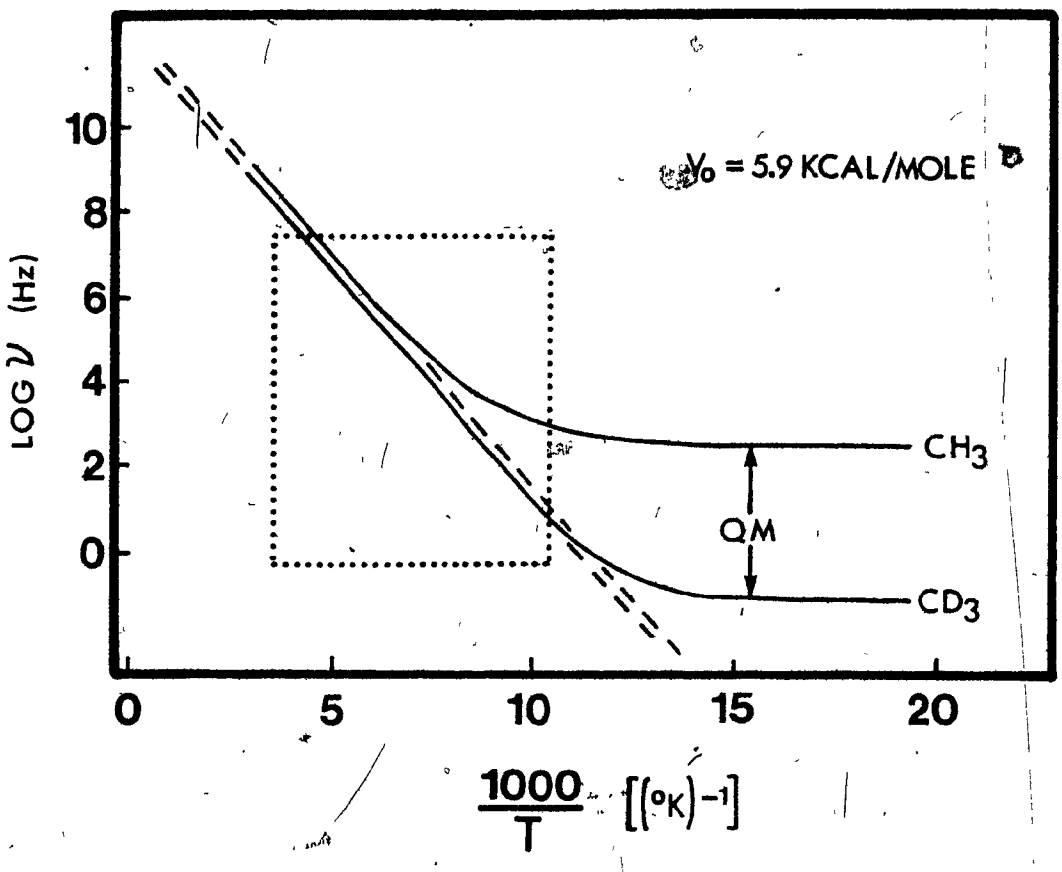
LOG ν (Hz)
10
8
6
4
2
0
V_0 = 5.9 KCAL/MOLE
CH_3
QM
CD_3
0
5
10
15
20
$\frac{1000}{T}$ [(°K)⁻¹]

C. LITERATURE REVIEW OF MOLECULAR MOTIONS IN PMMA

1. The Overall Transition Map:

As a material of great commercial importance, conventional PMMA, the structure of which is given in Figure 8, has been much studied by dynamic mechanical, dielectric and NMR techniques. The literature data up to 1967 have been quite thoroughly reviewed by McCrum, Read and Williams[11] and by McCall[6] who presented the results in the form of log ν versus 1/T plots. The combined data from these two studies have been augmented by additional literature results for methyl group motions in PMMA[31,34,47,49,56,61] to yield the transition map given in Figure 9. This shows, with decreasing temperature, the glass transition relaxation (α), the ester side group motion (β) and a dispersion due to water impurity (labeled 'H_2O'). All of the points at still lower temperatures are ascribed to motion of backbone methyl groups (γ), with the exception of the points in the vicinity of $1000/T = 13$, which are attributed to the side chain or ester methyl group (δ).

The methyl motions are interpreted as rotations of the group, and are not expected to be dielectrically active since no change in dipole moment would be occurring. This appears to be confirmed by the absence of dielectric data for the methyl regions of Figure 9. It can be seen that previous literature data for the backbone methyl or γ relaxation are very scattered; there have been few mechanical values and the NMR information has been limited to fairly high frequencies, greater than about 10^3 Hz. From previous results, it has been difficult to draw any conclusions insofar as the mechanism of relaxation is concerned.

FIGURE 8

THE STRUCTURAL FORMULA FOR THE REPEATING UNIT IN PMMA.

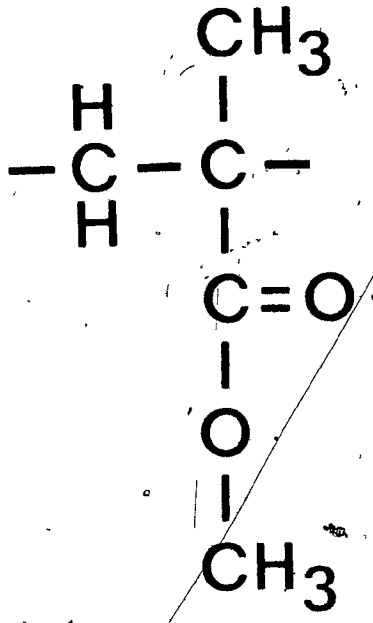

PMMA

FIGURE 9

TRANSITION MAP OF LITERATURE DATA FOR CONVENTIONAL POLY(METHYL METHACRYLATE).

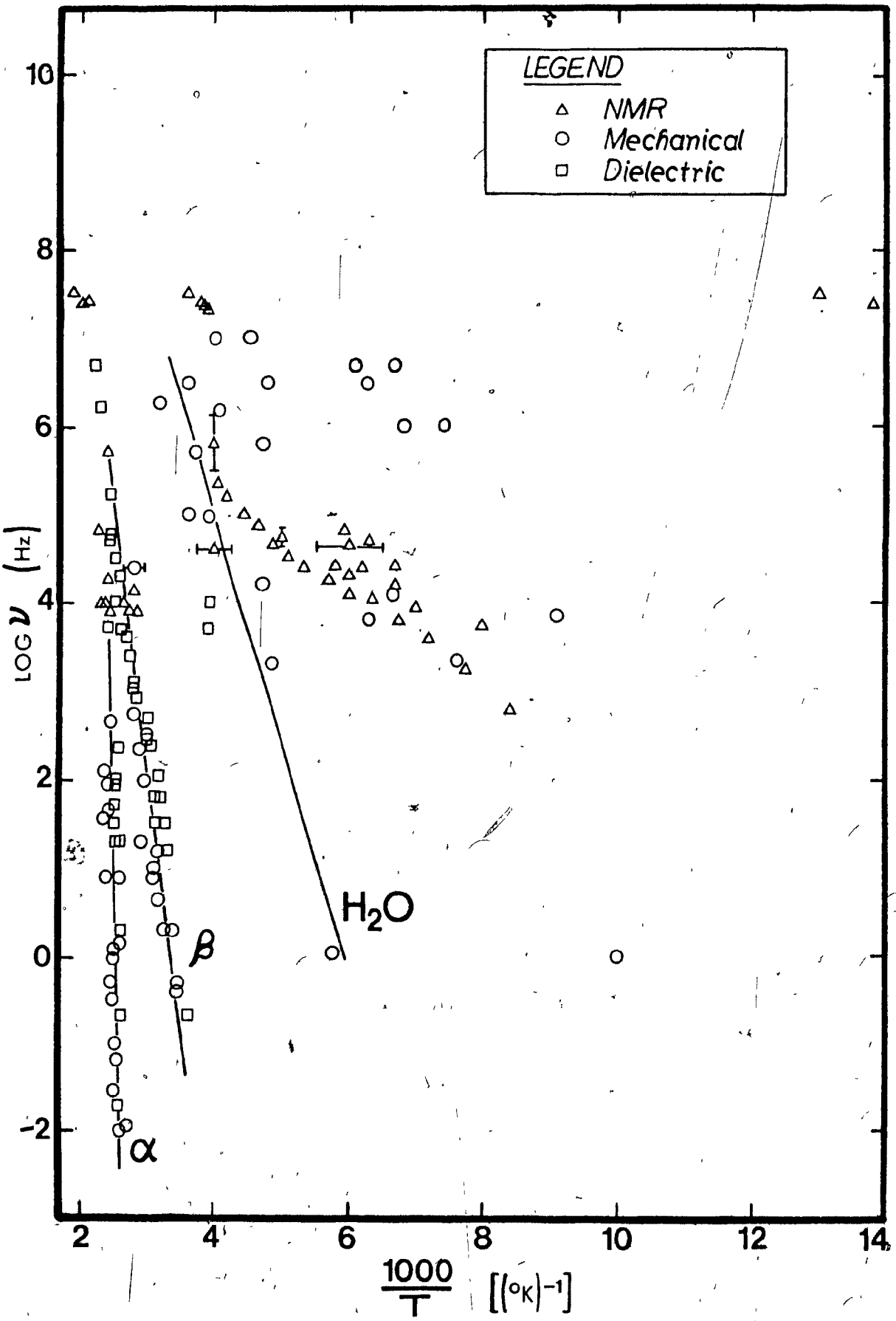
LEGEND
NMR
Mechanical
Dielectric
10
8
6
4
2
0
-2
LOG ν (Hz)
α
β
H2O
2
4
6
8
10
12
14
1000/T [(°K)-1]

2. Literature Results for the Backbone Methyl Relaxation:

a) NMR Data:

It is worthwhile, at this point, to consider the literature results for the backbone methyl motion in some detail, since it is to this relaxation that the tunneling hypothesis is to be applied in this thesis. The NMR evidence is more extensive than the mechanical data, and will be discussed first.

Powles[58] appears to have been one of the first researchers to observe the backbone methyl relaxation in PMMA; in 1956, he carried out line width and second moment studies on that material over the temperature range -196 to + 200°C, and discovered a transition at ~-110°C corresponding to a frequency of molecular motion of $\sim 10^4$ Hz. Powles suggested that both main and side chain methyl groups might be responsible for the motional narrowing, but it now seems evident that only α-methyls are involved. Three years later Hendus and others,[62] observed the same effect in PMMA containing 0.2% water, finding a change in line width centered around 167°K at $\sim 4.4 \times 10^4$ Hz. Sinnott[59] also measured the NMR line width and second moment in PMMA as a function of temperature from 77°K to ~400°K. He found evidence of a molecular relaxation occurring over a very wide temperature region (~130-230°K) at $\sim 10^4$ Hz which he attributed to motion of the α-methyl groups for the following reasons: theoretical calculations of the magnitude of the second moment and of the NMR line shape for (i) a completely rigid

structure, (ii) hindered rotation of one methyl group and (iii) hindered rotation of both methyl groups, when compared with experimental values of second moment and the observed line shapes at 77°K and 300°K, suggested that at 77°K (i.e. at a temperature below the wide relaxation region) rotation of one methyl group was occurring, while at 300°K (above the transition) both methyls were reorienting. Moreover, poly(methyl acrylate) which was also studied showed no similar relaxation in the 77-250°K range, yet had its methyl undergoing rotation at 77°K, as theoretical calculations indicated. Thus it was very reasonable to conclude that the methyl group which was moving at 77°K (at $>\sim 10^4$ Hz) in both polymers was the ester methyl and that it was the α-methyl of PMMA which began to move at ∿130°K, producing the second moment decrease centered around 180°K in that polymer. Odajima, Woodward and Sauer[31] effectively confirmed Sinnott's identification in their study (from 77°K) of the NMR line width and second moments of four polymers, including PMMA, which contained backbone methyl groups: all four polymers displayed marked second moment changes in the 100-250°K region undoubtedly due to the occurrence of the α-methyl motion. Odajima et al. calculated correlation frequencies at various temperatures within the relaxation regions and observed deviations from linearity in log ν versus 1/T (as has been noted previously). Their points for PMMA have been included in the literature transition map presented as Figure 9. Kosfeld and von Mylius,[34] in a more recent wide line NMR study which covered

temperatures down to 5°K, have presented results for the α-methyl transition in the same way; these results have similarly been placed in Figure 9. It is interesting to note that this low temperature study detected what is presumably the ester methyl relaxation below ∿75°K ($\nu \sim 10^5$ Hz) for which a levelling off of the frequency with decreasing temperature (indicative of a QM tunneling mechanism) is apparent.

In addition to NMR line shape studies, several investigations of the spin lattice relaxation time T_1 as a function of temperature have provided evidence of the α-methyl relaxation in PMMA. Kawai,[63] in 1961, located a T_1 minimum at ν_c ∿40 MHz and 263°K in PMMA, which he attributed to the main chain methyl groups on the basis of the occurrence at about that temperature of a T_1 minimum in two other methacrylate polymers studied. Kawai, however, also suggested that ester methyls were involved in this relaxation (which is what Powles[58] originally thought) but the reasoning behind this suggestion is not clear. Moreover, a decrease in T_1 below ∿-150°C is occurring, probably due to the freezing-in of the ester methyl motion. Powles and Mansfield[64] observed a T_1 minimum at ∿250°K in an experiment at ν_c ∿35 MHz on commercial PMMA containing ∿0.1% monomer, in close agreement with Kawai's result, and tentatively assigned the relaxation to the main chain methyl motion. Powles, Strange and Sandiford[65] later presented results for PMMA which was more than 90% syndiotactic and for an isotactic specimen which

was stated as containing less than 24% atactic material. The T_1 minimum (at ν_c ~35 MHz) moved from ~260°K in the syndiotactic material to ~220°K in the isotactic polymer - a shift of ~40°K, which, interestingly, was almost the same as the observed shift in the higher temperature softening transition. Connor and Hartland[66] later extended these experiments to lower frequency, via $T_{1\rho}$ measurements (ν_c ~$10^{4.7}$ Hz) on commercial and isotactic PMMA (the latter again containing <24% atactic material) finding $T_{1\rho}$ minima at 1000/T values of ~6.3 and 8.0 respectively.

b) Dynamic Mechanical Literature Data:

The evidence for a dynamic mechanical relaxation corresponding to the backbone methyl motion in PMMA is somewhat limited. Hendus et al.[62] have reported mechanical loss peaks at four frequencies in the temperature and frequency regions of 250 to 120°K and $10^{6.5}$ to 10^3 Hz respectively in PMMA containing 0.2% water; these data are consistent with their observation of an NMR line width narrowing located at ~167°K (ν_c ~4.4×10^4 Hz), which has been ascribed to α-methyl motion. The authors did not report the actual tan δ versus temperature curves, however. Sinnott[67] measured the shear modulus and internal friction of PMMA between 4.2 and 100°K with a low temperature torsional pendulum operating at ~8 Hz. Within the precision of the test, no relaxation was detected over the temperature region studied. An increase in tan δ was, however, observed for decreasing temperature below ~20°K; it was postulated that this might be due to the onset of the ester methyl group reorientation. In a later publication, which dealt mainly with NMR

evidence of methyl motion, Sinnott[59] stated that a small loss peak had been observed in PMMA at 100°K and approximately 1 Hz, and assigned it to the main chain methyl motion. Except for this single point (for which, incidentally, the tan δ curve did not appear) there is no other dynamic mechanical evidence for an α-methyl relaxation at frequencies below $\sim 10^3$ Hz!

Bordoni, Nuovo and Verdini[56] have, however, carried out some high precision dynamic mechanical tests of the flexural vibration type on both plasticized and unplasticized PMMA specimens, locating small relaxations for those materials which are in the frequency/temperature region expected for the α-methyl motion (as indicated by the NMR results). In the unplasticized specimen, the transition was observed at ~110°K at a frequency of ~7 KHz as both a peak in tan δ (peak height ~0.0002) and an inflection in the resonant frequency (relaxation strength of the order of one part per thousand). A second very small inflection in the frequency is possibly present at ~160°K. Powles et al.[65] have suggested that Bordoni's peak may be due to plasticizer. There is some support for this in the work of Crissman, Sauer and Woodward,[68] who carried out dynamic mechanical tests in the 6-300°K range at $\sim 10^4$ Hz on a longitudinal vibration apparatus; they found that unpurified commercial PMMA gave two loss maxima at ~14 KHz - one at 42°K and the other at 140-170°K, which were not evident in a test at ~9 KHz on more purified material. There is, however, a hint of an inflection in the modulus in the latter test at ~130°K, although the test precision is insufficient

to confirm this. Such a temperature and frequency location would be consistent with the α-methyl coordinates from NMR work; it may be suggested here that detection of the α-methyl relaxation in dynamic mechanical studies may require a high degree of precision in the test, and that it is for this reason that the mechanical evidence for this dispersion is so meagre. It should be added here that Shen, Strong and Schlein[69] have observed a very small loss peak (tan δ peak height of the order of 0.0001) in an acoustic spectrometer test on both water-swollen and unswollen PMMA at ∿40°K (and probably ∿800 Hz, although the exact test frequency is not given), which may have its origin with the α-methyl motion.

Ultrasonic tests have perhaps given the clearest indications of the α-methyl motion in PMMA. It has already been mentioned that Tanabe et al.[47] detected a peak at ∿220°K and 10 MHz in PMMA which they assigned to the backbone methyl hindered rotation. This was a fairly large peak, with a tan δ peak height of ∿0.03. Another much smaller shoulder (say one-tenth the peak height) may be present at ∿250°K. Hayakawa et al.[61] measured the velocity and attenuation of ultrasonic waves at 3 MHz in PMMA and found a similar pattern - a loss peak at ∿160°K with a tan δ peak height of ∿0.003 which the authors assigned to α-methyl rotation, and a smaller shoulder (height ∿0.001) at ∿210°K. Lastly, the ultrasonic velocity data of Golub' and Perepechko,[49] which was previously described in some detail, should be summarized: dispersions were observed at 147°K (1 MHz) and 165°K (5 MHz) for longitudinal waves, and at 135°K

(1 MHz) and 150°K (5 MHz) for shear waves; it should be re-emphasized, though, that changes in slope of the velocity/temperature curves were found, and not inflections characteristic of mechanical relaxations.

II. EXPERIMENTAL TECHNIQUES

A. SAMPLE PREPARATION AND CHARACTERIZATION BY HIGH RESOLUTION NMR:

Non-deuterated PMMA-H_8 and its fully deuterated analogue, PMMA-D_8, were prepared, the latter synthesis having been accomplished in collaboration with Dr. E. Shohamy. Commercial methyl methacrylate (MMA-H_8) was first purified by extraction with an aqueous solution of NaOH and NaCl to remove the hydroquinone inhibitor present, and dried over sodium carbonate; it was then bulk polymerized under nitrogen at 80-100°C by the free radical method using azo-bis-isobutyronitrile (0.05 weight %) as initiator, after several freeze/thaw cycles under vacuum to remove dissolved oxygen. The polymer formed was purified by dissolving in methylene chloride and reprecipitating with methanol.

The deuterated monomer was synthesized by the standard modified acetone - cyanohydrin process[70] using deuterated reagents (>99% D) throughout. This reaction proceeds in two steps as follows:

Step 1: Preparation of Acetone Cyanohydrin:

$$CD_3\text{-}\overset{O}{\overset{\|}{D}}\text{-}CD_3 \xrightarrow[NaCN]{D_2SO_4} CD_3\text{-}\overset{CD_3}{\overset{|}{\underset{C\equiv N}{\underset{|}{C}}}}\text{-}OD$$

acetone-D_6 — acetone cyanohydrin-D_7

Step 2: Preparation of Methyl Methacrylate:

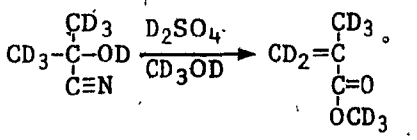

acetone cyanohydrin-D_7 — methyl methacrylate-D_8

The synthesis of deuterated acetone cyanohydrin (Step 1) involved the dropwise addition of 40% sulphuric acid to a chilled aqueous solution of sodium cyanide and acetone, with vigorous stirring. The final reaction mixture was allowed to stand overnight in a cooled state, during which time a separation into two liquid phases had occurred. The organic phase was collected and the aqueous phase was extracted with diethyl ether, with the ether extracts added to the previously separated organic phase, which was then dried over anhydrous magnesium sulphate and suction filtered. The ether was removed by rotary evaporation and the remaining material was vacuum distilled, with the deuterated acetone cyanohydrin collected at 56-57°C at 0.6-0.8 mm Hg. For a charge of 50 g acetone-D_6, 31 g of acetone-cyanohydrin-D_7 product was recovered by this procedure. To ensure complete deuteration, the synthesis was carried out in D_2O media, since acetone can exchange its protons with the solvent via keto-enol tautomerism.

The synthesis of deuterated methyl methacrylate from acetone cyanohydrin-D_7 (Step 2) consisted of adding the latter dropwise into a flask containing hot concentrated D_2SO_4 to which a small quantity of

tannic acid had been added. Upon completion of the addition, the temperature was raised from 80-90°C to 135°C for one-half hour, and then allowed to fall to 60°C at which time D_2O followed by the methanol-D_4 were added to the reaction mixture. A simple distillation was then carried out on the final flask contents with the distillate boiling at 68-75°C collected. This distillate (an azeotrope of methyl methacrylate and water) was dried over magnesium sulphate and filtered. An NMR spectrum taken of the MMA-D_8 produced showed no hydrogen peaks. For 25 g acetone-cyanohydrin-D_7, ~8.5 g of MMA-D_8 were produced and used for polymerization by the free-radical procedure also used for MMA-H_8. Again purification of the polymer by dissolving in methylene chloride and reprecipitating with methanol was carried out.

Samples of isotactic and syndiotactic PMMA-H_8 (kindly supplied by Dr. B. Ginsburg, Rohm and Haas) were also used in the present study. The tacticity of PMMA-H_8 samples can be determined by high resolution proton NMR studies of the backbone methyl absorption.[71,72] Typically, three closely spaced peaks are found at a chemical shift of about 1 ppm; these correspond to syndiotactic, heterotactic and isotactic triads in order of increasing chemical shift. Figure 10 contains 100 MHz spectra for the backbone methyl regions of the PMMA-H_8 samples used in this study, as obtained on a Varian HA-100 spectrometer. The polymers were tested in methylene chloride solution (8.0% weight/volume) at 30°C, CH_2Cl_2 having been selected as solvent since it gives better separation of the three backbone methyl peaks than do other solvents.[73] The syndiotactic methyl peak can be seen at ~0.9 ppm, the heterotactic at ~1.1 ppm and

FIGURE 10

100 MHz SPECTRA OF FREE-RADICAL, 'SYNDIOTACTIC' AND ISOTACTIC PMMA-H_8 IN CH_2Cl_2 AT 30°C, SHOWING BACKBONE METHYL PEAKS.

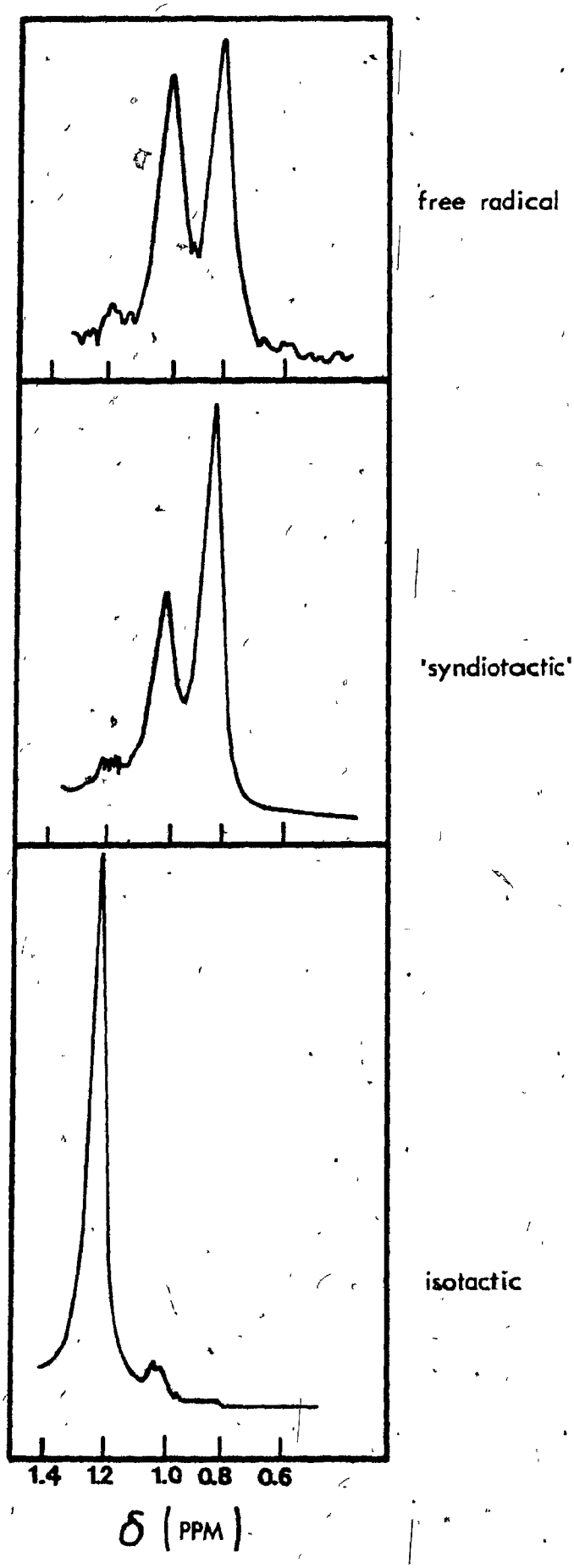
free radical
'syndiotactic'
isotactic
1.4
1.2
1.0
0.8
0.6
δ (PPM)

the isotactic at ∿1.25 ppm. The relative percentages of the three tactic species as calculated from peak areas are given in Table 1 below, along with the densities (at room temperature) of the molded samples.

TABLE 1

AREAS OF BACKBONE METHYL NMR PEAKS AND DENSITIES FOR PMMA SAMPLES

Polymer Type	Density of Molded Samples (g/cm^3)	Content of Triads		
		% Iso	% Hetero	% Syndio
Free Radical PMMA-H_8	1.18	8	37	55
'Syndiotactic' PMMA-H_8	1.16	6	32	62
Isotactic PMMA-H_8	1.22	93	7	-
Free Radical PMMA-D_8	1.28			

From Table 1 it is evident that the free-radically polymerized PMMA-H_8 used in this study contains mainly syndiotactic and heterotactic triads in an approximate ratio of 3 to 2, which is generally found for free radical PMMA. (This ratio may be assumed to hold for the PMMA-D_8, which was polymerized in the same way as the free radical PMMA-H_8.) The 'syndiotactic' PMMA-H_8 is similar to the free radical PMMA, except that it has a higher syndiotactic to heterotactic ratio of about 2 to 1. The isotactic sample consists almost entirely of isotactic triads.

B. DYNAMIC MECHANICAL TEST INSTRUMENTS:

In order to elucidate the backbone methyl relaxation in PMMA, it was necessary to carry out dynamic mechanical tests over a wide frequency and temperature region. Accordingly, specimens of free-radically prepared PMMA-H_8 and its fully deuterated analogue (PMMA-D_8) were compression molded at $\sim 20^{\circ}C$ above their T_g of approximately $105^{\circ}C$[74] and investigated using a free vibration torsional pendulum with a frequency range of 0.2 to 10 Hz, a high precision vibrating reed device operating in the frequency region 2×10^2 to 2×10^4 Hz, and an ultrasonic apparatus employing the single crystal pulse echo technique over the 10^6 to 10^8 Hz region. The loss tangent and modulus were measured as a function of temperature at approximately constant frequency, over the ranges of the three instruments, using liquid nitrogen as coolant. Isotactic and syndiotactic PMMA specimens compression molded at $\sim 20^{\circ}C$ above their T_g's of $\sim 45^{\circ}C$ and $120^{\circ}C$ respectively[74] were also studied ultrasonically.

It has been indicated in the Introduction that dynamic mechanical peaks and relaxation strengths due to methyl motions in general - and the backbone methyl motion in PMMA in particular - are exceedingly small, so that a very high precision is required in the measurements in order to detect them. Previously, moduli have seldom been measured to better than (say) 1% precision, with methyl motions quite likely going unnoticed. In the present study, considerable effort has been made to improve the precision of the usual dynamic mechanical instruments: an existing torsional pendulum[75] could be used directly but with a modified measurement and calculation technique; the existing vibrating reed instrument

which employed an optical detection system[76] did not afford the required precision, necessitating development of an entirely new instrument (new to this lab) operating with a piezoelectric detection system similar to that described by Fielding-Russell and Wetton[77], but with a data acquisition system capable of providing extremely high precision modulus measurements. In addition to the development of this sensitive vibrating reed instrument, an ultrasonic apparatus also capable of very precise measurements, was assembled. This design utilized MATEC Corporation electronics and an oscilloscope measuring technique which has been described fairly recently by Chung.[78] The principles involved in the use of these instruments will be outlined in the next section, with detailed descriptions of the vibrating reed and ultrasonic techniques given in Appendices II and III; these will enable the reader to evaluate the test precision or to repeat the experiments if he so desires.

1. The Torsional Pendulum:

This instrument is of the inverted type and has been described previously in detail.[75] A schematic diagram of the experimental set-up is given in Figure 11A; a specimen of rectangular cross-section is held in a fixed clamp from below and an inertial clamp from above. The inertial clamp is attached to a crossbar (the so-called inertial arms) which may or may not carry weights; and the whole assembly is supported by a wire. In a test a twist is applied to the inertial arms, setting up a torsional oscillation in the specimen; this motion is detected either optically or otherwise and recorded, providing a signal with the appearance of the one shown schematically in Figure 11B. The form of the signal is that of an exponentially decaying sinusoidal wave.

FIGURE 11A

SCHEMATIC DIAGRAM OF A TORSIONAL PENDULUM OF THE INVERTED TYPE.

FIGURE 11B

SCHEMATIC DIAGRAM OF THE EXPONENTIALLY DECAYING SINUSOIDAL AMPLITUDE OBTAINED IN A TORSIONAL PENDULUM TEST.

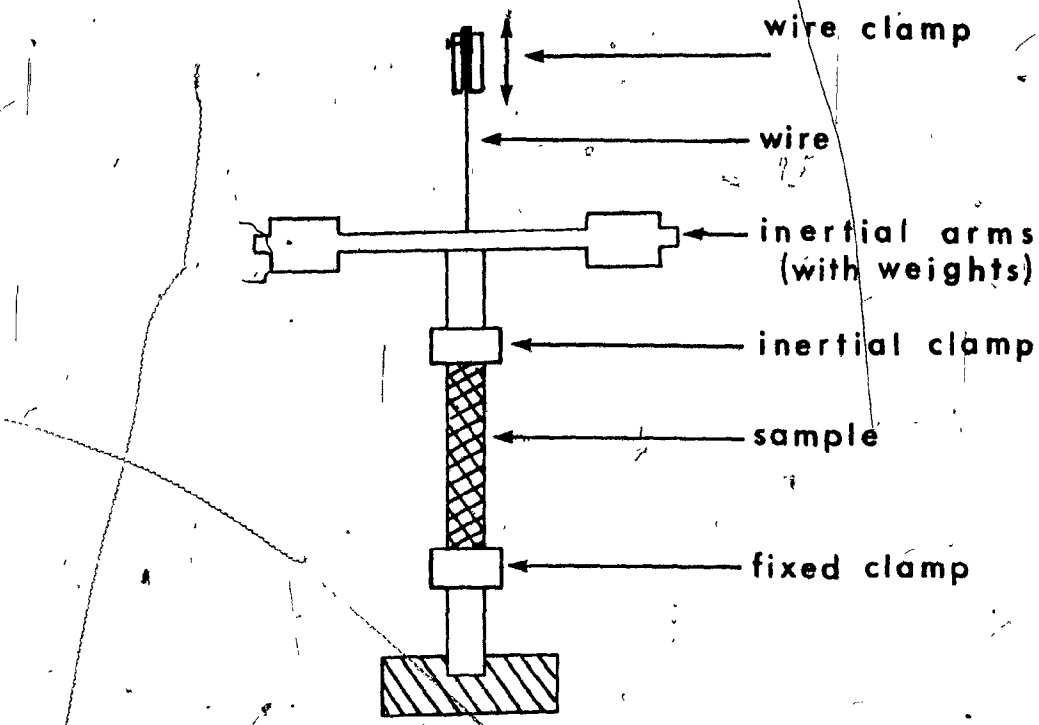
wire clamp
wire
inertial arms
(with weights)
inertial clamp
sample
fixed clamp

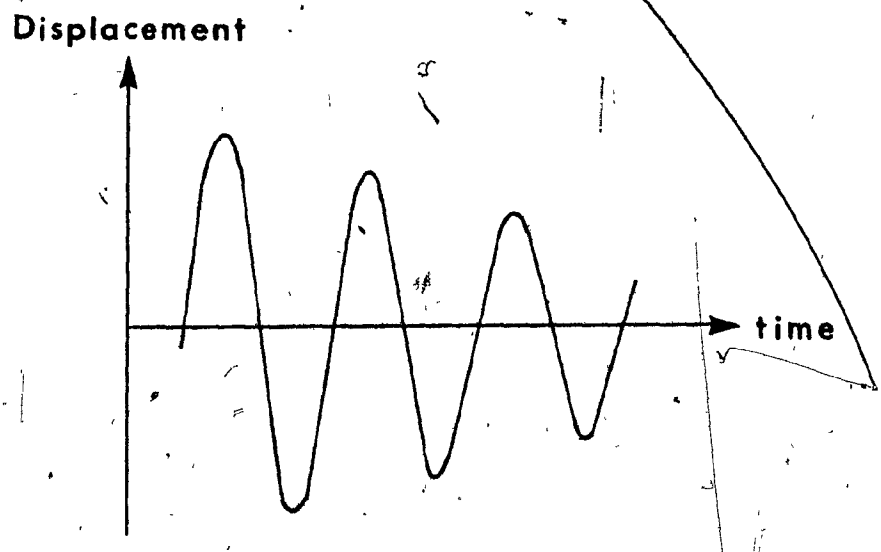
Displacement
time

The real and imaginary shear moduli (G' and G'' respectively) and corrected loss tangent ($\tan \delta_c$) were calculated from the following equations:[79]

$$G' = \frac{4\Pi^2 M}{b}\left[\frac{1}{T_A^2} - \frac{1}{T_o^2} + \frac{(\tan \delta_a)^2}{4T_A^2}\right]$$

$$G'' = \frac{4\Pi^2 M}{b} \cdot \frac{\tan \delta_a}{T_A^2}$$

and $$\tan \delta_c = \frac{G''}{G'}$$

where $b = wt^3\mu/16\ell$ is a factor depending on sample shape, and $\tan \delta_a = \Delta/\Pi$ is the apparent loss tangent. Here, M and T_o, the moment of inertia and period of the oscillating system respectively, are instrumental constants, measured without the specimen in place; w, t, ℓ and μ are specimen width, thickness, length and shape factor[80] respectively. The logarithmic decrement Δ, which is the slope of the plot of the natural logarithm of amplitude versus number of oscillations, and T_A, the oscillation period with the specimen in place, are measured as a function of temperature. The design was such that specimens could be cooled from room to liquid nitrogen temperature, while under an atmosphere of dry nitrogen.

In order to attain the high precision in G' necessary to detect very low strength relaxations, accurate measurements of oscillation period were performed; at each temperature, the decay was allowed to proceed until oscillations were no longer well defined (which depends on the magnitude of tan δ and on the noise level), and the time corresponding to a large number of cycles was measured directly from

the chart. For PMMA-D_8, at temperatures less than $\sim -150^{\circ}C$, 400 cycles could be counted in this way, leading to a precision in G' approaching 1 part in 1000. Accuracy in tan δ was obtained by measuring every twentieth oscillation amplitude and least squares fitting this data (corrected for noise) to yield the logarithmic decrement. Only data corresponding to low torsional amplitudes (i.e. less than $\sim 1^{\circ}$) were treated, since higher amplitude oscillations did not always follow a logarithmic decay.

2. The Vibrating Reed Instrument:

The Vibrating Reed technique is a dynamic mechanical technique by which the loss tangent (tan δ) and the Young's modulus E' of a solid (modulus range ca. 10^8 to 10^{12} dynes/cm^2) can be determined over the frequency range of $\sim$100 Hz to 5000 Hz. The method involves the forced vibration in the region of the resonance frequency of a rod of material clamped at one end as a cantilever, with vibration usually excited by means of magnetic coils.

The vibrating reed instrument adopted for this study was a high precision device in which vibration amplitude was measured by means of a piezoelectric detection technique; it was based on the design of Fielding-Russell and Wetton,[77] (denoted FRW), as has been previously mentioned. A lower frequency vibrating reed with a novel optical detection technique[76] and an acoustic spectrometer based on the design of Schlein and Shen[81] also saw some limited use. The FRW method employs thicker specimens than the optical technique and is generally used in the frequency range of $\sim$500 to 5000 Hz; use of weights may extend the

technique to lower frequencies, however, while use of overtone frequencies may extend it to higher frequencies. The temperature of the specimens could be varied from room temperature to -210°C, which was achieved by pumping on liquid nitrogen. Pressure within the low temperature cell was generally maintained at 2 cm Hg, controlled to ±0.05 cm, to optimize heat transfer within the cell on the one hand and minimize energy loss due to gas pressure on the other.

A schematic diagram of the apparatus, with component descriptions, is given in Figure 12. Operation of the components is as follows: triangular wave generator G acts on Frequency Synthesizer A to produce a steadily changing frequency which is applied to magnet M. The magnet attracts and repels a metal tab glued to sample S, setting up a vibration. Transducer T detects the vibration sending a low-level signal via shielded connections to amplifier D. The amplified signal is applied to the Y-axis of X-Y recorder E and the triangular wave is simultaneously applied to the X-axis, resulting in the plotting-out of a resonance curve. Thus a curve of amplitude versus frequency is plotted for the resonance region, and analyzed to yield the desired mechanical properties, tan δ, E' and E'', through the use of the following equations:[82]

$$\text{Loss tangent:} \quad \tan\delta = \frac{(\Delta f)_{H.W.}}{\sqrt{3}\, f_o}$$

$$\text{Moduli:} \quad E' = 38.33 \left(\frac{\ell^4 \rho}{t^2}\right) f_o^{\,2} \quad \text{(fundamental)}$$

$$\text{and} \quad E'' = E'(\tan\delta)$$

where $(\Delta f)_{H.W.}$ is the width at half peak height of the resonance curve

FIGURE 12

SCHEMATIC DIAGRAM OF VIBRATING REED APPARATUS

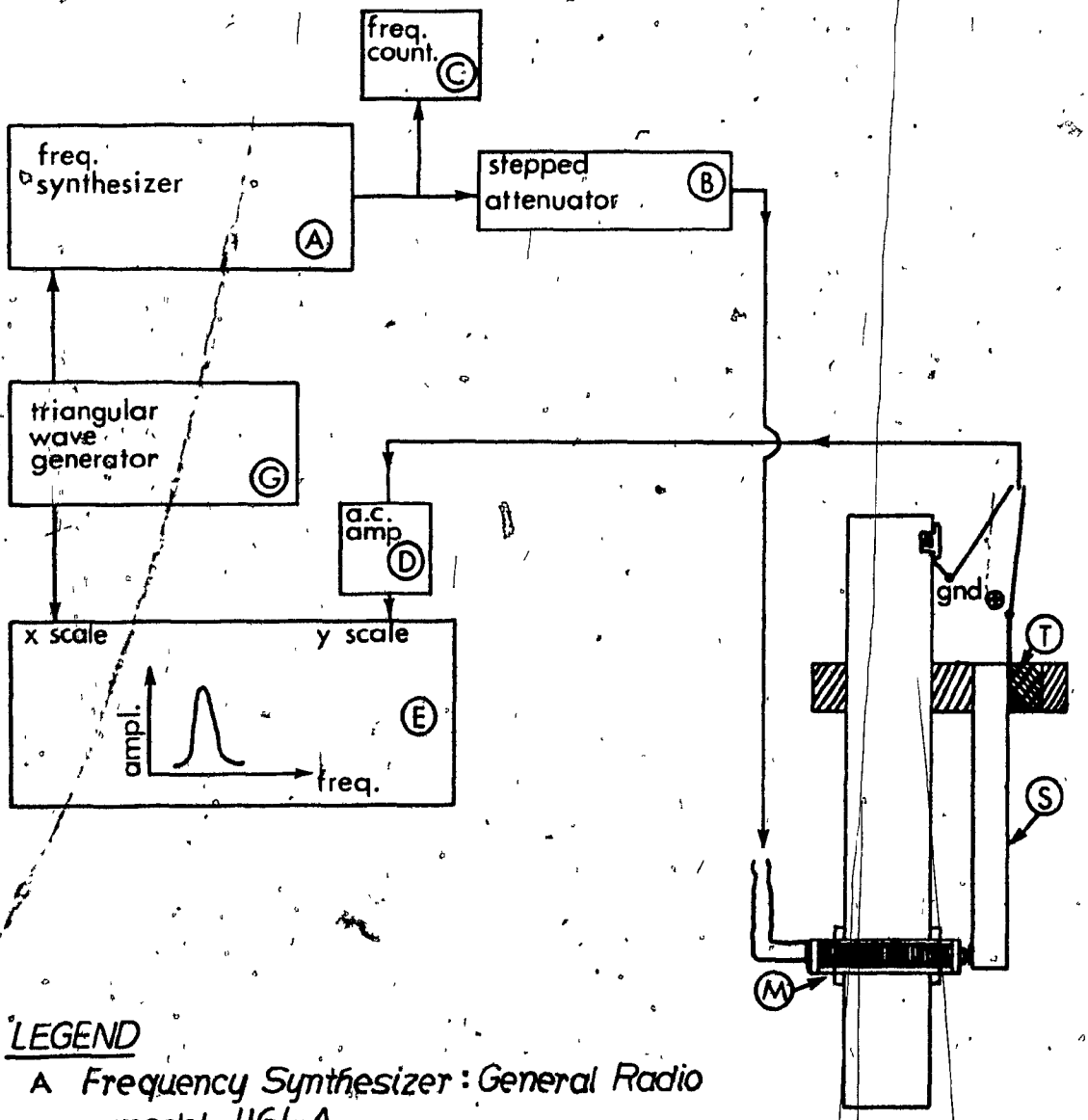

LEGEND

- A Frequency Synthesizer : General Radio model 1161-A
- B Stepped Attenuator, 0-80 db : Texscan LA series
- C Frequency Counter, 5Hz-80MHz : Fluke model 1900A
- D A.C. Amplifier : Hewlett Packard model 465-A
- E X.Y. Recorder : H.P. model 7000 A
- G Triangular Wave Generator : H.P. model 3310A
- M Magnet : Electro Products model 3055-A
- S Sample, rod with metal tab attached to lower end
- T Transducer PZT-4 disc .25" x .100" thick : Vernitron part # 4100-4

(in frequency units); f_o is the resonance frequency or frequency of maximum amplitude; ℓ, t and ρ are specimen length, thickness and density respectively. If the specimen is being vibrated at the first or the second overtone, it is necessary to replace the constant 38.33 in the equation for the storage modulus E' by 0.9758 or 0.1244 respectively.

An electronic frequency counter (C in Figure 12) was incorporated into the FRW design, allowing measurement of the resonance frequency f_o to approximately 1 part in 50,000 for polymer specimens at low temperatures (where tan $\delta \sim 0.001$). This permitted the calculation of the Young's modulus E' with a precision of better than 1 part in 10^4, enabling the detection of the small methyl dispersion. It should be emphasized, however, that the absolute accuracy of the measurements is obviously much less than that number. In fact the FRW paper gives a standard error of ±8% in E' and ±0.001 in tan δ for regions of low loss, which the authors attributed to variations in sample preparation conditions and accuracy of measurement of specimen dimensions. (For a more detailed discussion of the errors involved in the vibrating reed test, which considers also the effects of noise, of measurements made from the charts, of the metal tab, and of pressure and temperature, please refer to Appendix II.)

3. The Ultrasonic Apparatus:

The dynamic mechanical properties of materials at higher-than-audible frequencies (greater than ~20,000 Hz) can be determined from tests utilizing ultrasonic waves. These waves are generated by

piezoelectric transducers (e.g. quartz crystal sections) which change dimensions in an electric field. In the commonly-used pulse echo experimental technique a single crystal is used both to generate an initial ultrasonic pulse which is coupled into a sample and to detect echoes from the opposite face of the sample. The method has been successfully applied to polymeric solids from room to cryogenic temperatures.

The apparatus used in this study allowed measurement of attenuation coefficient and speed of sound for longitudinal waves in low loss solid samples (tan δ less than $\sim$0.02) over a frequency range of 1 to 20 MHz. A schematic diagram of the ultrasonic pulse echo apparatus is given in Figure 13. The Pulse Generator main frame - R.F. plug-in combination (A+B) generates pulses of radio frequency at the desired frequency; these pulses are applied via impedance matching network D to piezoelectric transducer T, which vibrates at the frequency of the electrical signal. The transducer is attached by means of a thin layer of suitable bonding agent X to solid sample S which has closely parallel faces (as compared to the wavelength of the ultrasound). The ultrasonic pulse is coupled into the sample where it travels at a characteristic speed and undergoes a series of internal reflections from the sample faces until all the sound energy has been dissipated. The transducer also acts as a detector for the returning pulse echoes, producing electrical pulses which pass back through the matching network D and the stepped attenuator C to R.F. plug-in B where they are amplified and then rectified (leaving only the R.F. pulse envelopes). This video output is then displayed on Oscilloscope E where an exponentially decaying series of evenly spaced pulses is observed.

FIGURE 13

SCHEMATIC DIAGRAM OF ULTRASONIC PULSE ECHO APPARATUS

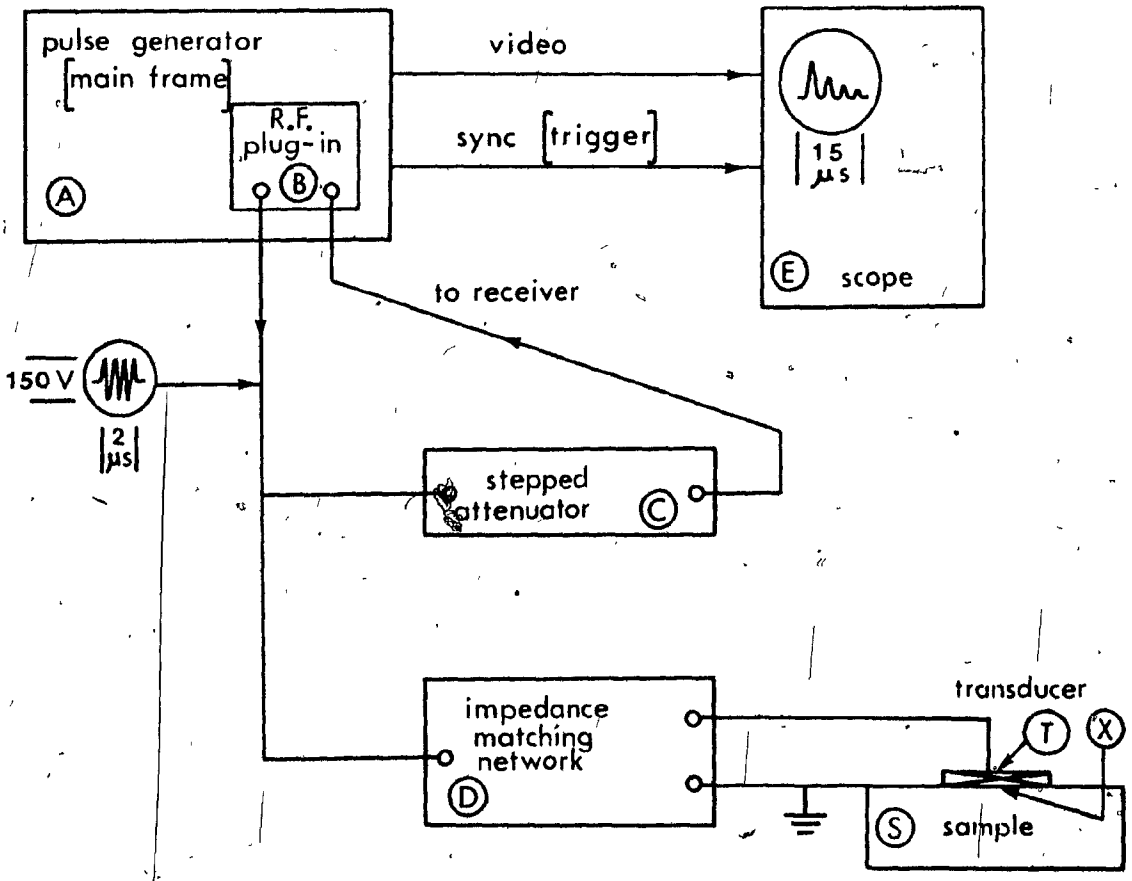

LEGEND

A Pulse Generator, main frame: Matec model 6600
B Radiofrequency plug-in: Matec model 950, 1-20 MHz range
C Stepped Attenuator, 0-80 db in 0.1 db steps: Texscan LA's
D Impedance Matching Network, 0-28 μh: Matec model 65, rated 5-30 MHz
E Oscilloscope: Tektronix model 535A with type L amplifier
T Transducer: quartz, Valpey-Fisher Corp.; ceramic, Automation Industries
S Sample: cylindrical, with closely parallel faces (top face requires an electrode for use with quartz transducer)
X Bonding liquid layer between transducer and sample

(numbers given in the figure are typical for 15 MHz operation)

An essential feature of the test was the selection of a Tektronix 535A oscilloscope operated in the 'A DELAYED BY B' mode.[78] This permitted very accurate measurement of the time between successive ultrasonic echoes, which, in conjunction with measurements of relative attenuation levels (obtained by means of a stepped attenuator (C in Figure 13) which was accurate to 0.1 db in 70 db), led to sufficient precision in tan δ to enable observation of methyl relaxations. From the experimental time and db readings thus obtained, the loss tangent (tan δ), real Young's modulus (E') and imaginary Young's modulus (E'') can be calculated from the following equations (discussed in detail in Appendix III:)[11,83]

$$\tan \delta = \frac{\alpha\lambda}{\pi} \qquad (\alpha\lambda << 1)$$

$$E' = \rho v^2$$

$$\text{and } E'' = (\tan \delta)\, E',$$

where α is the attenuation coefficient defined by the equation

$$I = I_o e^{-2\alpha x}$$

Here I is ultrasonic intensity which decays exponentially with distance x in the solid due to dissipative mechanisms (such as molecular motion), I_o being the intensity at x=0. The attenuation coefficient α has units of nepers/unit distance in the direction of propagation and is proportional to the change in db level per unit distance, where the db level is the usual logarithmic scale of sound intensity: $db = 10 \log(I/I_o)$. λ and v are the ultrasonic wavelength and velocity respectively, which are connected through the frequency f by the relation $v = \lambda f$, and ρ is the specimen density.

The ultrasonic test is carried out as a function of temperature, by placing the specimen/transducer assembly in a suitable low temperature cell (described in Appendix III). The temperature range achieved was from liquid nitrogen temperature (-196°C) to +50°C, the latter being achieved with the use of a low wattage heater. The pressure was normally 1 atmosphere throughout a test, but vacuum operation was also possible, with suitable experimental technique.

III. DYNAMIC MECHANICAL RESULTS:

A. VIBRATING REED RESULTS:

In view of the fact that the proof of a QM tunneling involvement in methyl relaxation hinges primarily on the vibrating reed results, these are presented first. A large body of data was obtained on the vibrating reed apparatus for PMMA-H_8 and PMMA-D_8 prepared by free-radical polymerization, over the frequency region of ∿230 Hz to ∿9250 Hz, achieved through the use of fundamental and overtone vibration frequencies. The real Young's modulus E' and (in some cases) tan δ have been measured as a function of temperature, covering the region from ∿-200°C to room temperature. Experimentally, samples were warmed from pumped liquid nitrogen temperature under partial vacuum (pressure ∿2 cm of Hg) at warming rates varying from ∿10°C/hour (the usual case) to ∿50°C/hour. Under these conditions, using the high precision instrument described in Appendix II, very low strength mechanical relaxations were detected. Two such relaxations, denoted γ_1 and γ_2 in order of decreasing temperature location, are evident from the data, generally as inflections in modulus, and sometimes as peaks in tan δ. Figure 14 shows data from one such experiment

FIGURE 14.

EXPERIMENTAL VIBRATING REED CURVES OF E' and TAN δ VERSUS TEMPERATURE FOR FREE-RADICAL PMMA-H_8 AT ~565 Hz.

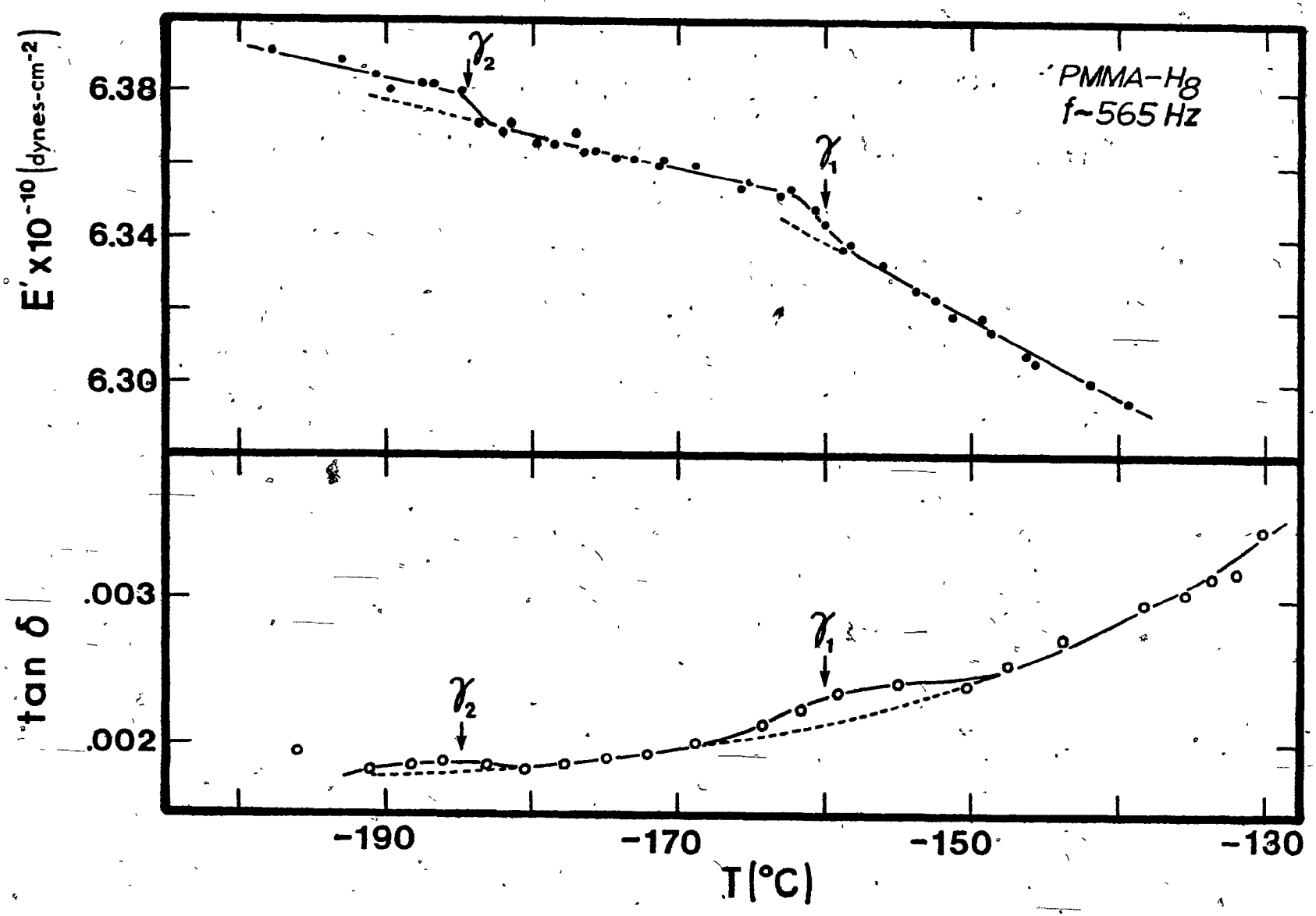
E' x10^{-10} (dynes-cm^{-2})
6.38
6.34
6.30
PMMA-H8
f~565 Hz
γ2
γ1
tan δ
.003
.002
γ1
γ2
-190
-170
-150
-130
T(°C)

obtained on the vibrating reed apparatus for PMMA-H_8 at a frequency of ∿565 Hz, while Figure 15 shows corresponding data for PMMA-D_8 at ∿540 Hz. Both of these Figures show the γ relaxations as inflections in modulus and also as tan δ peaks. This was not always the case, however; often tan δ curves showed too much scatter to permit detection of small peaks. Nevertheless, inflections were almost always observed in the modulus.

The frequency and temperature positions of the low temperature γ relaxations found in vibrating reed tests on PMMA-H_8 are summarized in Table 2 along with relevant experimental quantities (the warming rate, pressure and vibration mode). Table 3 shows the corresponding vibrating reed data for PMMA-D_8. The complete set of graphs of modulus (E') and tan δ versus temperature which support these observations is given in Appendix IV along with the corresponding numerical values. It is evident from the data of Tables 2 and 3 that the peak positions are quite reproducible.

For PMMA-H_8, the average relaxation strength ($\Delta E'/E'$) of the γ_1 relaxation is 1.1×10^{-3} while that of the γ_2 dispersion is 0.75×10^{-3}. Where observed, tan δ peak heights are of the order of 1×10^{-4} above background levels. The average γ_1 and γ_2 relaxation strengths for PMMA-D_8 are similar - 1.2×10^{-3} and 0.78×10^{-3} respectively. Here, however, tan δ peak heights are of the order of 2×10^{-4} above background. The reason for the difference in the tan δ peak heights is, conceivably, the lower precision of these measurements. The γ relaxation strengths are summarized along with their standard deviations in Table 4 below. It is interesting to note that the γ_1 and γ_2 relaxation strengths are roughly in the ratio of three to two for both PMMA-H_8 and PMMA-D_8.

FIGURE 15.

EXPERIMENTAL VIBRATING REED CURVES OF E' AND TAN δ VERSUS TEMPERATURE FOR FREE-RADICAL PMMA-D_8 AT $\sim$540 Hz.

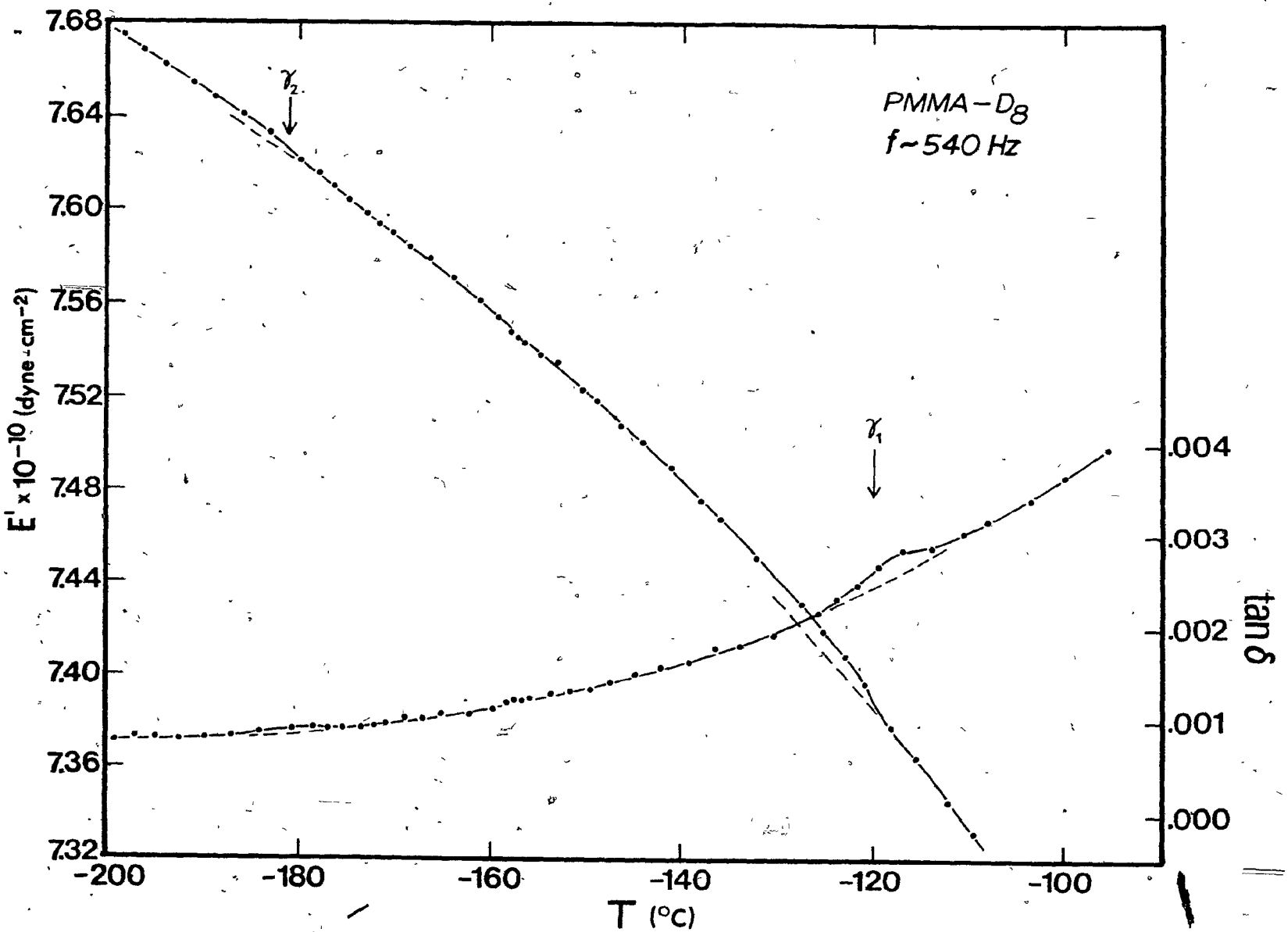
PMMA – D_8
f ~ 540 Hz
γ_2
γ_1
E' x 10^{-10} (dyne-cm^{-2})
7.68
7.64
7.60
7.56
7.52
7.48
7.44
7.40
7.36
7.32
tan δ
.004
.003
.002
.001
.000
-200
-180
-160
-140
-120
-100
T (°C)

TABLE 2.

SUMMARY OF VIBRATING REED EXPERIMENTAL DATA FOR THE γ RELAXATION REGION OF FREE RADICAL PMMA-H_8.

Relaxation Position			Relax. Strength	Tan δ Peak Height	Experimental Conditions			
ν (Hz)† (γ_1 or γ_2)	T (°C) γ_1	T (°C) γ_2	$\Delta E'/E'$ ($\times 10^{-3}$)	($\times 10^{-4}$)	Warm Rate (°C/hour)	Pressure (cm Hg)	Vibration Mode*	Figure #
225.3		-200.5	1.0		8.	1.4	f	IV-1
274.	-162.		0.9		7.	1.3	f	IV-2
277.		-198.		~1.	7.	1.3	f	IV-3
295.3		-196.5	0.5		10.	3.0	f	IV-4
496.	-167.5		0.6		21.	2.0	f	IV-5
497.)	-170.		0.6	~0.8	~41.	2.0	f	IV-6
499.)		-190.		~0.7	~50.	2.0	f	"
565.)	-160.		1.5	~2.	~30.	2.75	f	14
566.)		-184.	0.9	~1.	~30.	2.75	f	"
568.	-156.		1.8		16.	1.35	f	IV-7
569.5)	-162.5		0.9		7.	1.3	f	IV-8
571.)		-188.	0.6		7.	1.3	f	"
710.	-145.		1.4		11.	1.3	f	IV-9
712.5	-151.		0.8	~0.5	6.	1.2	f	IV-10
1322.		-179.5	0.6		7.	1.3	1	IV-11
1633.		-179.		~1.5	8.	1.3	1	"
1761.	-147.		1.1		9.	2.0	1	IV-12
1770		-175.	0.6		10.	3.0	1	IV-13
3025.	-118.		0.9		14.	2.0	1	IV-14
3025.	-117.		0.9		10.	2.0	1	IV-15
3036.	-121.		0.8		26.	2.0	1	IV-16
4319.)	-125.		1.7		12.	1.3	1	IV-17
4379.)		-172.5	0.9		10.	1.3	1	"
9105.	-116.		2.0		12.	1.3	2	IV-18
9243.		-164.	0.9		7.	1.3	2	IV-19

† ≡ brackets indicate results from the same run
*f ≡ fundamental
1 ≡ first overtone
2 ≡ second overtone

TABLE 3.

SUMMARY OF VIBRATING REED EXPERIMENTAL DATA FOR THE γ RELAXATION REGION OF FREE-RADICAL PMMA-D_8.

Relaxation Position			Relax. Strength	Tan δ Peak Height	Experimental Conditions			
ν (Hz)† (γ_1 or γ_2)	T (°C) γ_1	T (°C) γ_2	$\Delta E'/E'$ ($\times 10^{-3}$)	($\times 10^{-4}$)	Warm Rate (°C/hour)	Pressure (cm Hg)	Vibration Mode*	Figure #
368.	-119.		1.7	7.5	~10.	2.5	f	IV-20
540.5	-120.		1.1	2.	8.	1.4	f	IV-21
538.5	-120.		1.2	2.	15.	2.0	f	15
547.		-181.	0.6	0.7	15.	2.3	f	"
1007.	-118.		1.1	1.6	12.	2.0	f	IV-22
1017.		-175.	0.7		~20.	2.0	f	"
1392.	-119.		1.2		~11.	1.4	1	IV-23
1416.		-176.	0.8		9.	1.4	1	"
1731.	-118.5		1.0	2.	10.	1.4	f	IV-24
3934.	-106.		~1.3	~10.	12.	1.4	2	IV-25
4015.		-175.	1.0	1.5	9.	1.4	2	"

† ≡ brackets indicate results from the same run

*f ≡ fundamental

1 ≡ first overtone

2 ≡ second overtone

TABLE 4.

AVERAGE RELAXATION STRENGTHS FOR γ RELAXATIONS IN FREE-RADICAL PMMA-H_8 AND PMMA-D_8.

Polymer	γ_1 Relaxation Strength $(\frac{\Delta E'}{E'} \times 10^3)$			γ_2 Relaxation Strength $(\frac{\Delta E'}{E'} \times 10^3)$		
	average	std. devn.	# of obs.	average	std. devn.	# of obs.
PMMA-H_8	1.14	0.46	14	0.75	0.19	8
PMMA-D_8	1.23	0.23	7	0.78	0.17	4

Several preliminary vibration tests revealed a mechanical dispersion at temperatures greater than -100°C for PMMA-H_8 samples which had been exposed to moisture. These results are shown in Figure 16 and summarized in Table 5. It should be noted that the three sets of data were obtained on three different vibration instruments, to which previous reference has been made in the section on Experimental Techniques. This "water" relaxation has a strength of ~0.025 with a tan δ peak height of ~0.0015.

TABLE 5. SUMMARY OF ACOUSTIC EXPERIMENTAL DATA (GIVEN IN FIGURE 16) FOR THE 'WATER' RELAXATION REGION OF FREE RADICAL PMMA-H_8.

Relaxation Position		Relaxation Strength $\Delta E'/E'$	Tan δ Peak Height	Experimental Conditions		Pressure (cm Hg)
ν (Hz)	T (°C)			Type of Apparatus	Warm or Cool Rate (°C/hr)	
269.	-80.		0.0015	Vibrating Reed-Optical	Not Recorded (warming)	~1.
1075.	-50.	0.020		Vibrating Reed-Piezoelectric	~50. (cooling)	76.
1365.	-42.	0.032		Acoustic Spectometer	~80. (cooling)	76.

FIGURE 16.

E' AND TAN δ VERSUS TEMPERATURE FOR THE "WATER" PEAK REGION OF FREE-RADICAL PMMA-H_8 BY SEVERAL ACOUSTIC TECHNIQUES.

TYPE OF APPARATUS

■ ACOUSTIC SPECTROMETER

● VIBRATING REED - PIEZOELECTRIC DETECTION

▲ VIBRATING REED - OPTICAL DETECTION

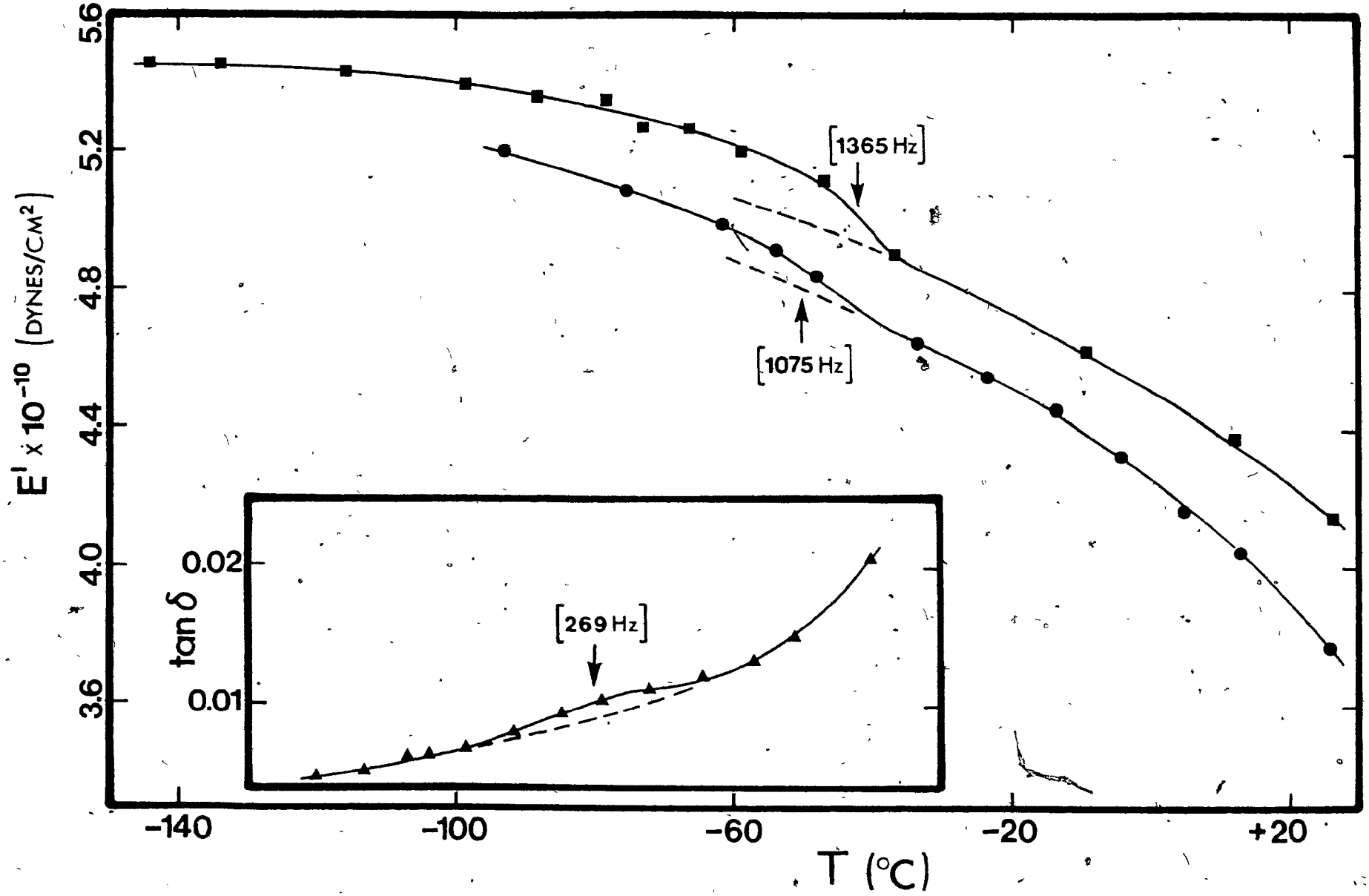
5.6
5.2
4.8
4.4
4.0
3.6
E' x 10⁻¹⁰ (DYNES/CM²)
[1365 Hz]
[1075 Hz]
0.02
0.01
tan δ
[269 Hz]
-140
-100
-60
-20
+20
T (°C)

Although considerable care was taken to keep subsequent PMMA samples free of moisture, it was difficult to exclude water completely, as indicated by more recent ultrasonic tests on free-radical PMMA-H_8, which still contain a hint of the 'water' dispersion.

B. ULTRASONIC RESULTS:

Ultrasonic tests were performed on the PMMA samples using the single crystal pulse echo technique described in the experimental section, and detailed in Appendix III. The free-radical PMMA-H_8 was investigated at several frequencies from 1.3 to 20.0 MHz, while free-radical PMMA-D_8 and both isotactic and 'syndiotactic' PMMA-H_8 were tested at ∿13.5 MHz only, for comparison purposes. Mechanical relaxations were detected either as shoulders in the tan δ versus temperature curve, as inflections in the velocity/temperature curve, or as local minima in the db level of a single echo. In most of the experiments, warming (or cooling) rates of ∿30°C/hour were employed, with nonaq cement as the specimen-to-transducer bonding agent.

Corresponding to the vibrating reed tests, very small mechanical dispersions were detected in the temperature interval from -100°C to +50°C. In two samples, as many as four relaxations (denoted H_2O, γ_1, γ_2 and γ_3 in order of decreasing temperature) were observed in the PMMA's. Figure 17 shows ultrasonic curves of tan δ and velocity versus temperature for free-radical PMMA-H_8 at 8.4 MHz which illustrate the γ_1 relaxation; the peak is easily seen from the tan δ plot but the suggested inflection in the velocity is only barely evident. In fact, owing to the scatter in the velocity data, the transition seems smeared out, so that only a change in slope of the curve is really evident. (It is interesting to recall that Golub' and Perepechko[49] identified methyl relaxations in

FIGURE 17

TAN δ AND SPEED OF ULTRASOUND AS A FUNCTION OF TEMPERATURE FOR FREE-RADICAL PMMA-H_8 AT 8.4 MHz, ILLUSTRATING THE RELAXATION AT APPROXIMATELY -10°C.

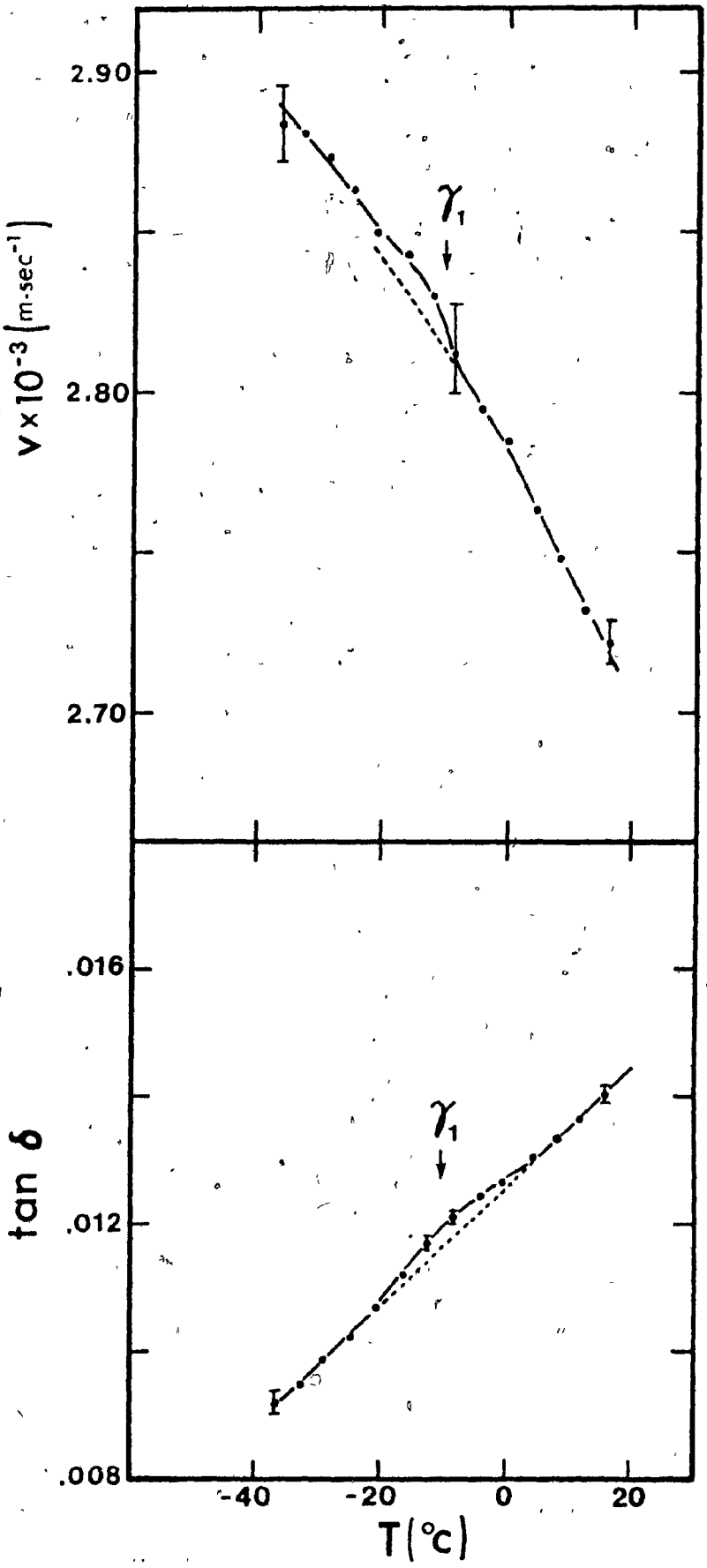
2.90
2.80
2.70
v x 10⁻³ (m·sec⁻¹)
γ1
.016
.012
.008
tan δ
γ1
-40
-20
0
20
T(°C)

their ultrasonic velocity studies with changes in slope of the velocity versus temperature curve.) Free-radically prepared PMMA-H_8 was studied ultrasonically at several frequencies: 1.3, 3.4, 8.4, 12.9, 13.6, 18.5 and 20.0 MHz; the results of these experiments are summarized in Table 6, with the graphical and numerical data supporting the observations being given in Appendix V.

Figure 18 shows tan δ versus temperature for free-radical PMMA-D_8, for a frequency of 13.4 MHz. Here, the results of two separate experiments at that frequency have been combined; the two sets of data overlap well in the vicinity of $-20^{\circ}C$ indicating the very good repeatability of the test. These data (included in Table 6) show the γ_1 and γ_2 relaxation regions near $0^{\circ}C$ and $-60^{\circ}C$ respectively.

Ultrasonic data for isotactic and syndiotactic PMMA-H_8 are given in Figures 19 and 20 respectively. The test frequency was $\sim$13.5 MHz for both cases, this value having been chosen so that all four types of PMMA could be compared at this frequency. The isotactic polymer appears to undergo only one relaxation at $\sim -100^{\circ}C$, while the syndiotactic polymer shows two distinct dispersions in the vicinity of $-20^{\circ}C$ and $-60^{\circ}C$, with a possible (although extremely small) transition near $-100^{\circ}C$. These results are also included in Table 6.

The tan δ peak heights for the several relaxations detected all fall within the range 10^{-4} to 10^{-3}; relaxation strengths ($\Delta v/v$) are approximately 2×10^{-3}, with the exception of the γ_1 and γ_2 dispersions in the syndiotactic polymer where much higher velocity changes are apparent. The reason for these larger relaxation strengths is not known.

TABLE 6.

SUMMARY OF ULTRASONIC DATA OBTAINED FOR PMMA SAMPLES OF VARIOUS COMPOSITION AND TACTICITY. THE SAMPLE-TO-TRANSDUCER BONDING AGENT WAS NONAQ CEMENT, UNLESS OTHERWISE NOTED.

Material	Relaxation Position					Relax. Strength $\Delta v/v(x10^{-3})$	Tan δ Peak Height $(x10^{-4})$	Warming or Cooling Rate (°C/hr)	Figure #
	ν (MHz)	T_{γ_1} (°C)	T_{γ_2} (°C)	T_{γ_3} (°C)	T_{H_2O} (°C)				
PMMA-H_8 (free-radical)	1.3				+ 6.	2.	3.	25. (cool)	V-1
	1.3	-38.				2.	4.	25. (cool)	"
	3.4	-22.				2.	5.	35. (warm)	V-2
	8.4	-10.				2.	4.	30. (warm)	17
	12.9*		-56.			2.	3.	25. (cool)	V-3
	13.6				+34.		(∿4.)**	25. (warm)	V-4
	13.6	- 1.					4.	12. (warm)	"
	18.5				+42.		(∿2.)**	30. (warm)	V-5
	18.5			(-92.5)			∿1.	30. (warm)	"
	20.0	- 1.					(∿5.)**	35. (warm)	V-6
PMMA-D_8 (free-radical)	13.4	- 2.					10.	25. (warm)	18
	13.4		-58.				7.	50. (warm)	"
PMMA-H_8 (isotactic)	13.7			-97.		3.	4.	30. (cool)	19
PMMA-H_8 ('syndiotactic')	13.5	-16.				8.	7.	35. (warm)	20
	13.5		-56.			11.	6.	35. (warm)	"

* Bonding agent ≡ 3-chloropropyl benzene. A peak thought due to bonding agent was observed at -85°C.

** Estimated from local minimum in db curve for a single echo.

FIGURE 18.

TAN δ AS A FUNCTION OF TEMPERATURE FOR FREE-RADICAL PMMA-D_8 AT 13.4 MHz. (RESULTS OF TWO SEPARATE EXPERIMENTS AT THAT FREQUENCY ARE SHOWN.)

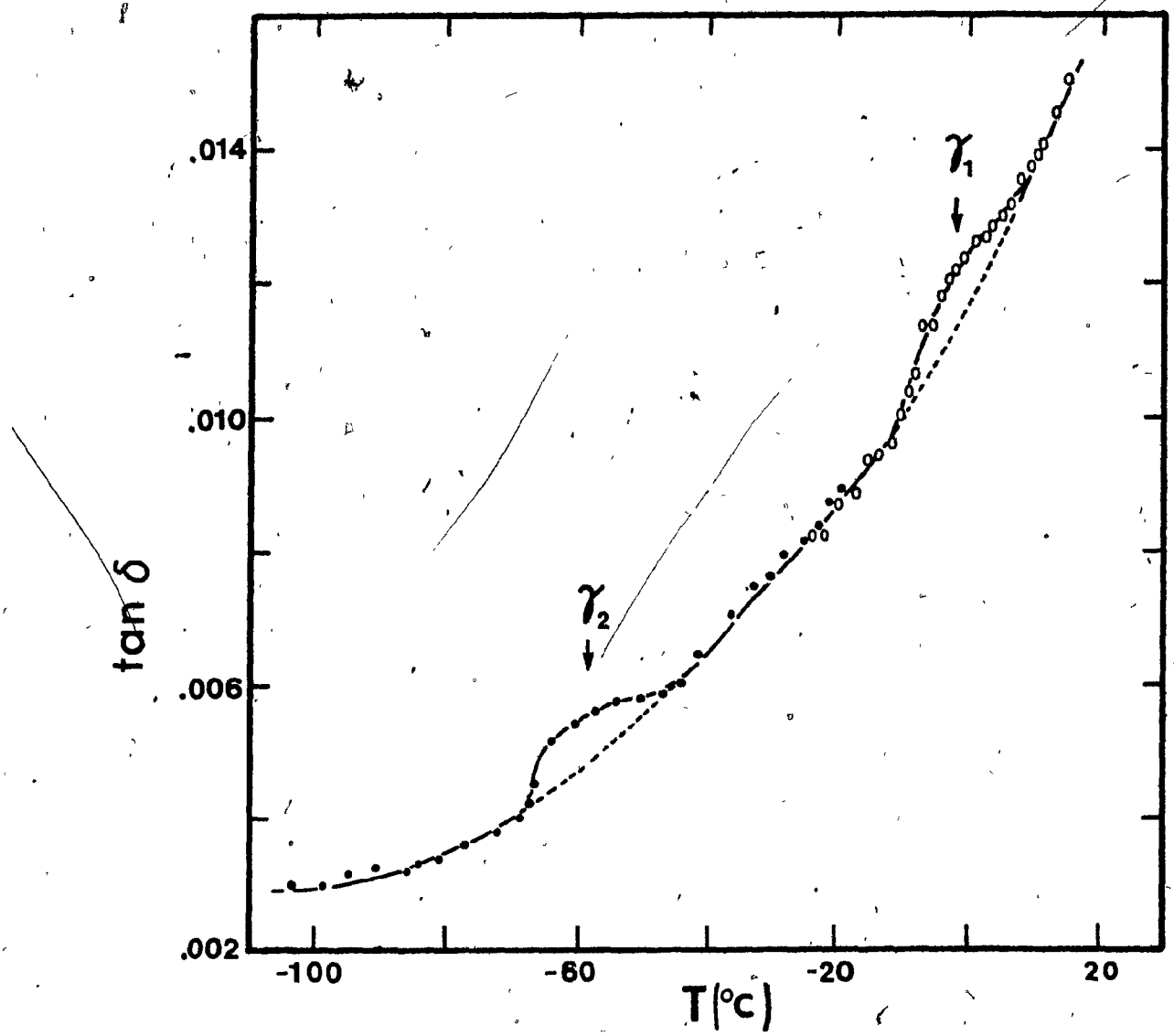
.014
.010
.006
.002
tan δ
γ1
γ2
-100
-60
-20
20
T(°C)

FIGURE 19.

TAN δ AND SPEED OF SOUND VERSUS TEMPERATURE FOR ISOTACTIC PMMA-H_8 AT 13.7 MHz.

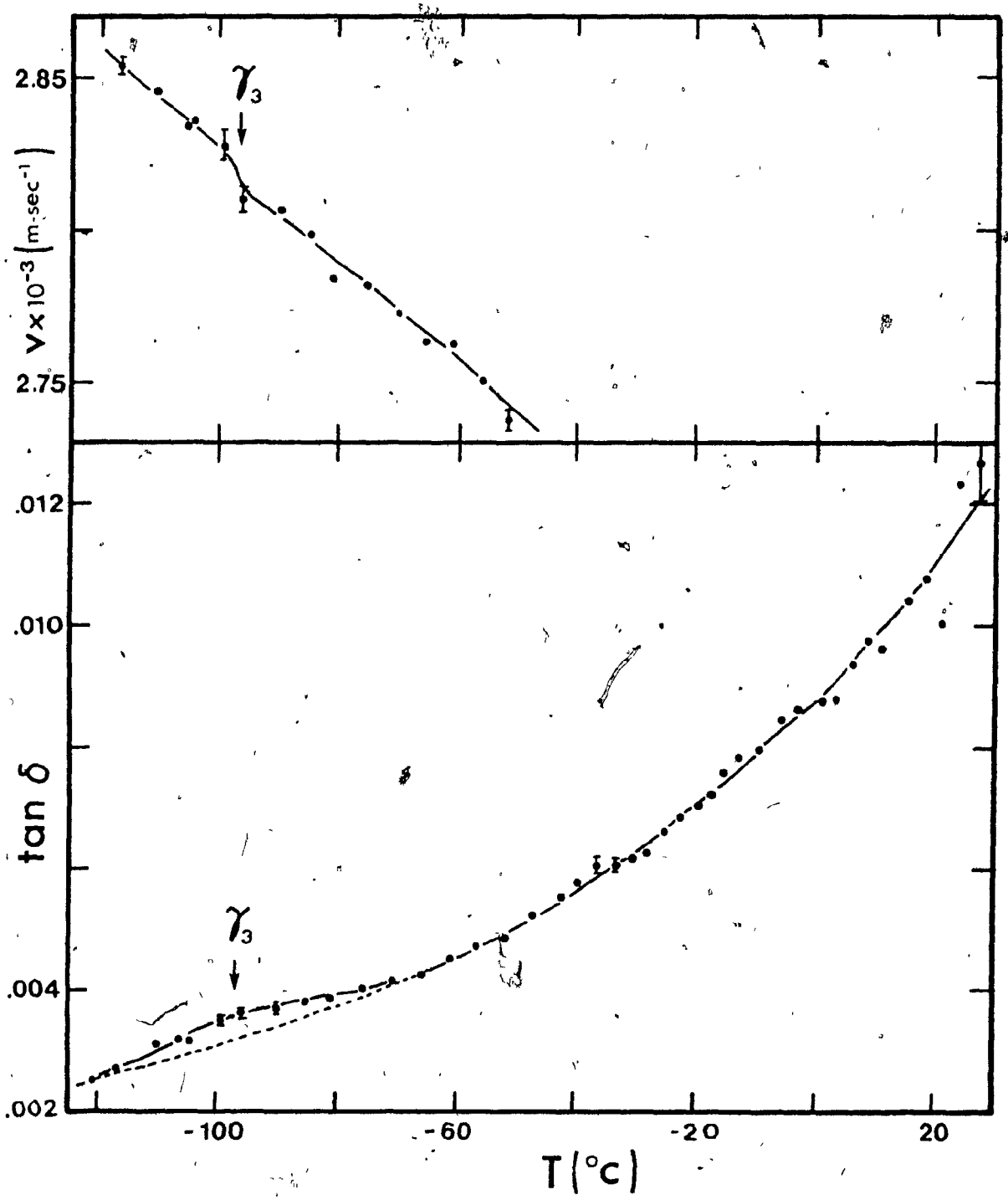
2.85
2.75
$V \times 10^{-3}$ (m-sec^{-1})
γ_3
.012
.010
.004
.002
tan δ
γ_3
-100
-60
-20
20
T (°C)

FIGURE 20.

TAN δ AND SPEED OF SOUND VERSUS TEMPERATURE FOR 'SYNDIOTACTIC' PMMA-H_8 AT 13.5 MHz.

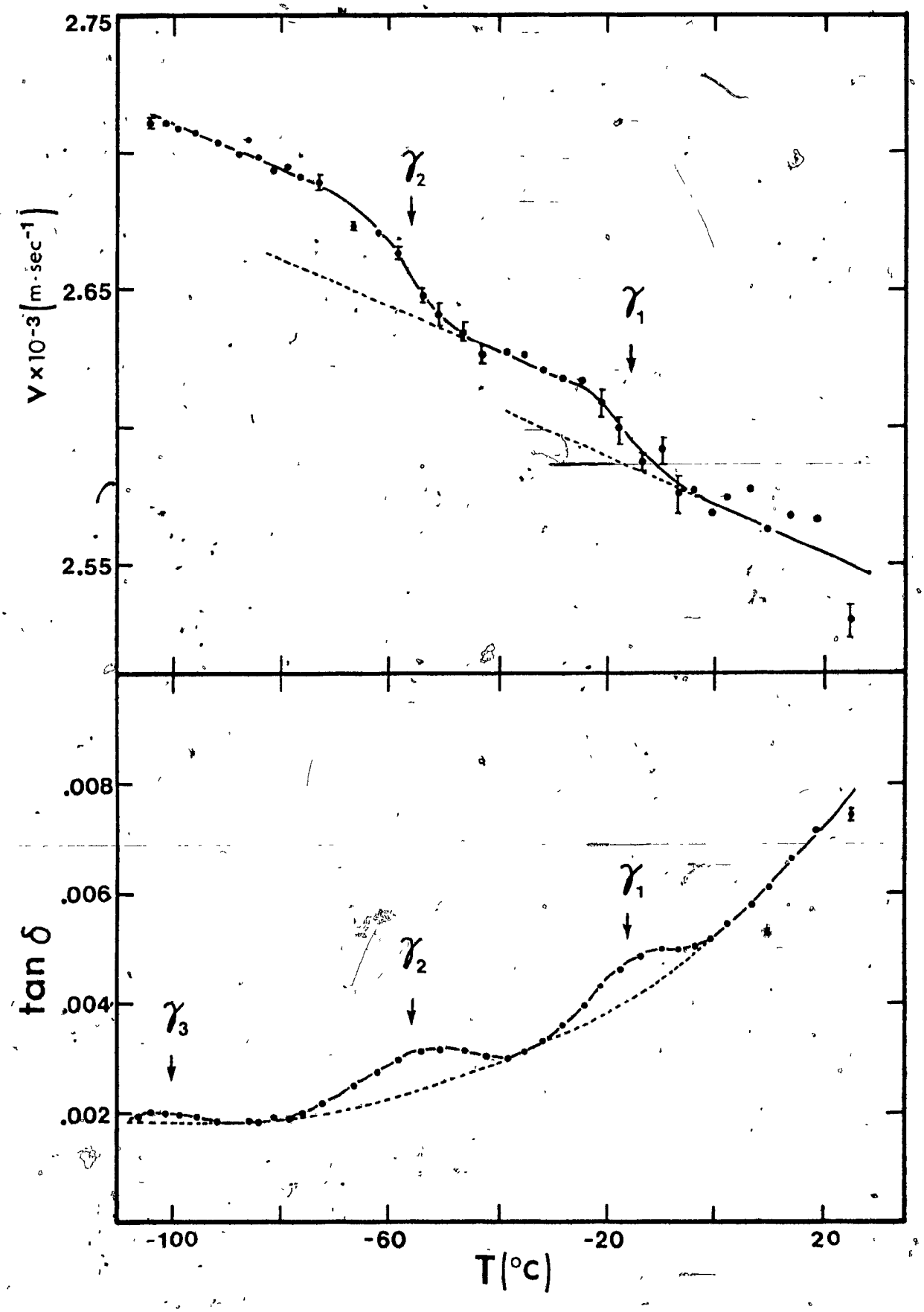
2.75
2.65
2.55
V x 10-3 (m·sec-1)
γ2
γ1
.008
.006
.004
.002
tan δ
γ1
γ2
γ3
-100
-60
-20
20
T(°C)

C. TORSIONAL PENDULUM RESULTS:

The torsional pendulum technique which has already been described in the experimental section was applied to PMMA-D_8 samples in a nitrogen atmosphere at two frequencies: 0.75 and 2.35 Hz. The results are given in Figure 21. The G' curves provide evidence of a very low strength relaxation near -157°C at 0.75 Hz and -153°C at 2.35 Hz; the tan δ curves also hint at the presence of a dispersion in this region. Despite the low warming rate of 15 to 20°C/hour employed for these tests, a sizeable temperature gradient of ∿10°C at -150°C existed inside the sample chamber. This must contribute toward limiting the size of mechanical dispersion observable in the test.

An experiment on PMMA-H_8 at 2.35 Hz over the same temperature region as above was also attempted, but results were too scattered to permit observation of a relaxation even if one were present. In this case, due to a higher tan δ, only 260 cycles could be counted, leading to reduced accuracy in the period measurement. (As many as 400 cycles were counted for PMMA-D_8.)

The relaxations observed in these torsional pendulum tests are summarized in Table 7 below:

TABLE 7.

SUMMARY OF TORSIONAL PENDULUM DATA OBTAINED FOR DEUTERATED PMMA SAMPLES.

Material	Relaxation Position		Relax. Type	Relax. Strength	Tan δ Peak Height	Figure #
	ν (Hz)	T (°C)		$\Delta G'/G'(\times 10^{-3})$	$(\times 10^{-4})$	
PMMA-D_8 (free-radical)	0.75	-157.	γ_1	1.5	∿1.	21
	2.35	-153.	γ_1	2.	∿1.	21

FIGURE 21.

EXPERIMENTAL CURVES OF G' AND TAN δ_c AS A FUNCTION OF TEMPERATURE FOR FREE-RADICAL PMMA-D_8 OBTAINED ON THE TORSIONAL PENDULUM:

	FREQUENCY (Hz)
○	0.75
●	2.35

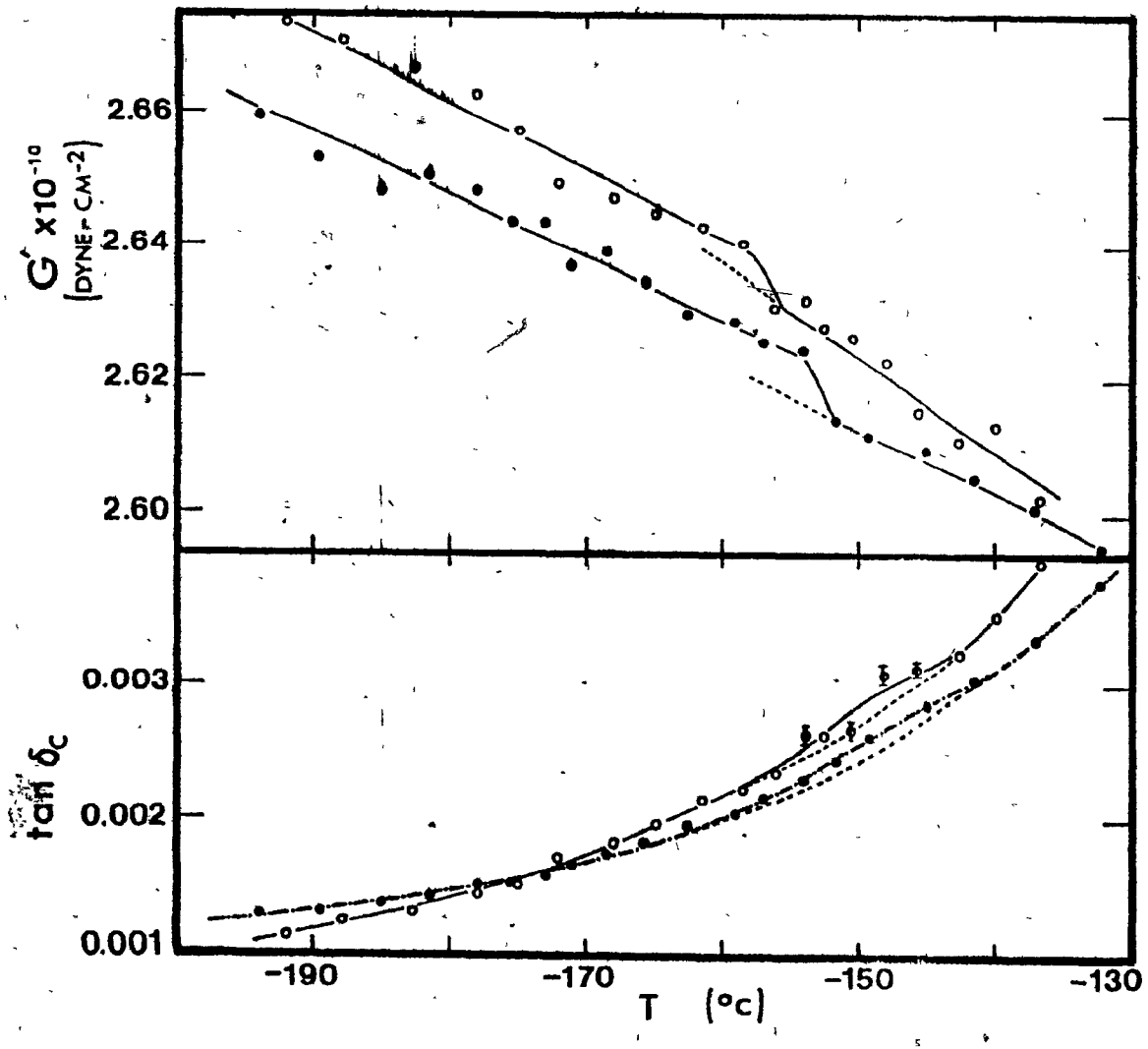
G' x10^-10 (DYNE-CM^-2)
2.66
2.64
2.62
2.60
tan δc
0.003
0.002
0.001
-190
-170
-150
-130
T (°c)

IV. DISCUSSION

A. DEMONSTRATION OF METHYL GROUP TUNNELING:

The experimental frequency-temperature positions of those dynamic mechanical methyl relaxations labeled γ_1 have been plotted in Figure 22 for both PMMA-H_8 and PMMA-D_8. The dashed lines represent calculations from the theory of Stejskal and Gutowsky[23] for methyl rotation within barrier heights of 6.4, 6.9 and 7.4 Kcal/mole. This Figure shows clearly that both criteria for tunneling are met, i.e. that log ν vs 1/T is non-Arrhenius for the non-deuterated polymer, tending to level off at low temperatures, and that a CH_3/CD_3 isotope effect also exists, the deuterated polymer following a linear Arrhenius-type relation over the whole frequency/temperature range studied. It can be seen that the behavior for PMMA-H_8 is of the type predicted by the tunneling theory but that the agreement is only qualitative. This may be due to the fact noted by Ingold[84] that a slight change in the shape of the potential barrier can result in significant changes in the log ν versus 1/T plot. Thus, from the shape of the curves and from the presence of the isotope effect, it can be concluded that tunneling of methyl groups is indeed involved in viscoelastic relaxation, if the theory of Stejskal and Gutowsky is correct in its essential features. The present study represents the first observation of an isotope effect in the field of viscoelastic properties of polymers.

FIGURE 22.

EXPERIMENTAL FREQUENCY-TEMPERATURE MAP FOR THE γ_1 RELAXATION IN PMMA-H_8 AND PMMA-D_8. (THE REGION COVERED BY THE GRAPH CORRESPONDS TO THAT OUTLINED IN DOTS ON FIGURE 7.) THE DASHED LINES REPRESENT CALCULATIONS FROM THE THEORY OF STEJSKAL AND GUTOWSKY FOR BARRIER HEIGHTS OF 6.4, 6.9 AND 7.4 KCAL/MOLE.

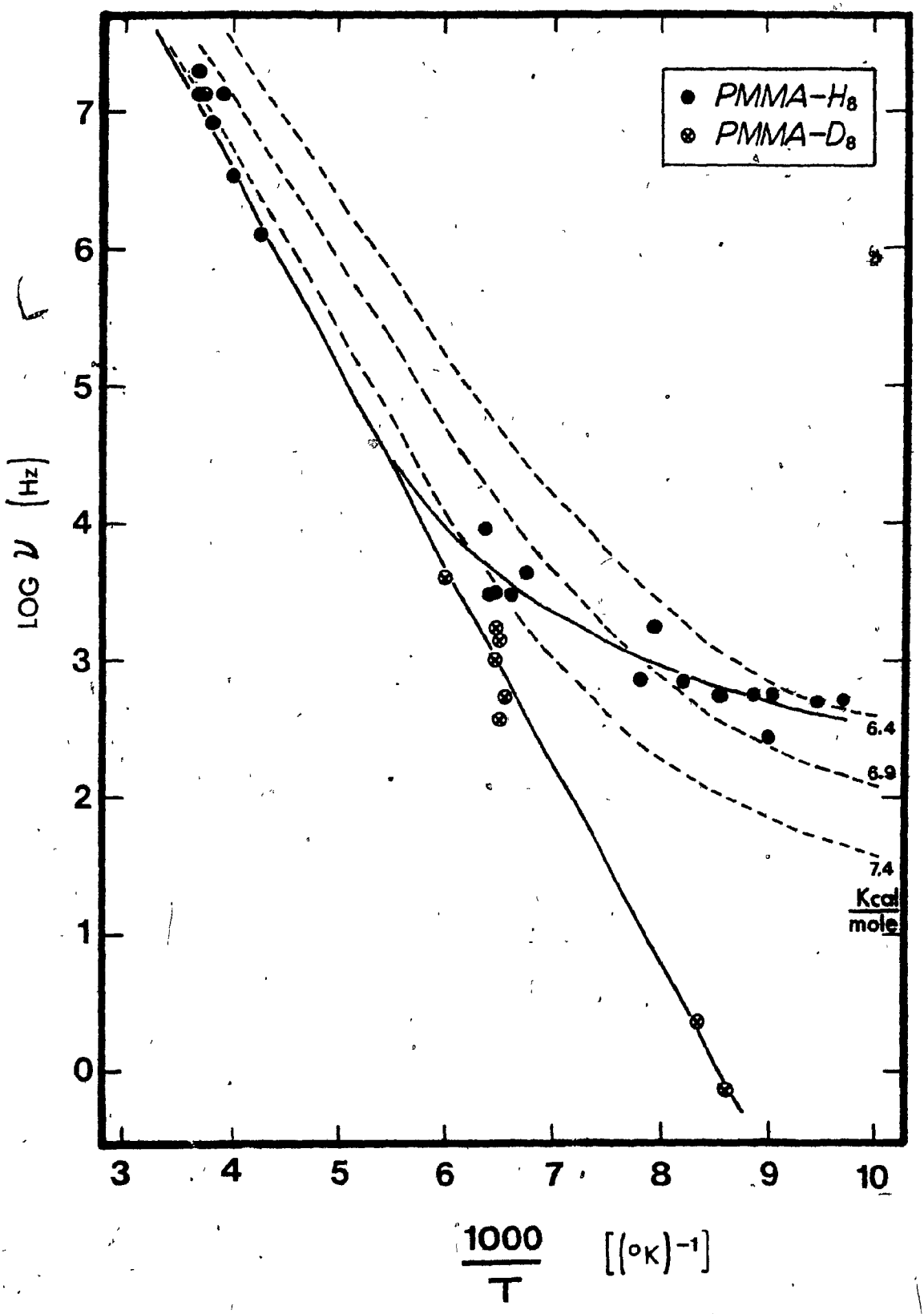
PMMA-H8
PMMA-D8
LOG ν (Hz)
7
6
5
4
3
2
1
0
3
4
5
6
7
8
9
10
1000/T [(°K)⁻¹]
6.4
6.9
7.4
Kcal/mole

B. TACTICITY EFFECT IN PMMA:

Figure 23 contains the complete transition map for PMMA, showing both the literature data given in Figure 9 (open symbols) and the relaxations observed in the present study (filled symbols, Tables 2, 3, 5, 6 and 7). Two NMR literature points for isotactic PMMA-H_8[65,66] have also been included. For simplicity, the α and β relaxations are shown only as lines.

Figure 23 shows clearly that two separate relaxations are occurring in the backbone methyl region of free radical PMMA; they are labeled γ_1 and γ_2 in order of decreasing temperature and have activation energies of 6.7 and 3.3 Kcal/mole; they may be assigned to reorientations of syndiotactic and heterotactic backbone methyl groups respectively. This interpretation is suggested by the high resolution NMR data (Table 1) which indicated a syndiotactic to heterotactic triad number ratio of about three to two, in close agreement with the average ratio of relaxation strengths found in the vibrating reed studies (1.5 for PMMA-H_8 samples and 1.6 for PMMA-D_8 samples). It is doubtful whether the lower temperature γ_2 relaxation can be ascribed to isotactic groups because very little (<10%) isotactic material is present in the free radical polymer.

The log ν versus 1/T plot of the γ_2 relaxation, here assigned to heterotactic backbone methyls, shows the beginnings of the curvature and CH_3/CD_3 isotope effect indicative of QM rotational tunneling, but measurements need to be extended to lower frequencies and temperatures for confirmation.

FIGURE 23.

THE COMPLETE TRANSITION MAP FOR PMMA, SHOWING THE EXPERIMENTAL RESULTS IN CONJUNCTION WITH PREVIOUS LITERATURE DATA. (THE α AND β RELAXATIONS ARE SHOWN ONLY AS LINES, FOR SIMPLICITY.)

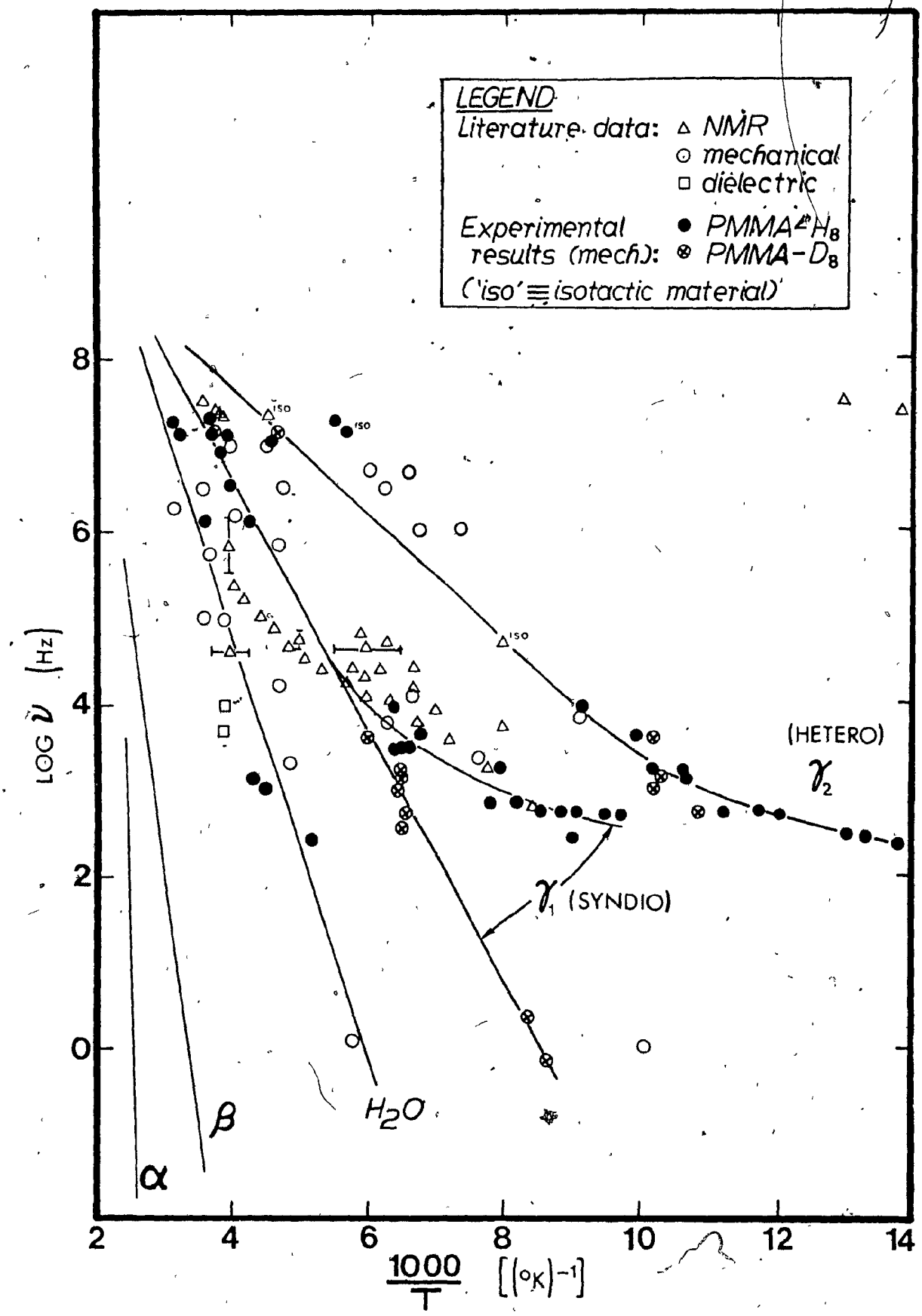
LEGEND
Literature data: △ NMR
⊙ mechanical
□ dielectric
Experimental results (mech): ● PMMA-H8
⊗ PMMA-D8
('iso' ≡ isotactic material)
LOG ν (Hz)
8
6
4
2
0
iso
iso
iso
(HETERO)
γ2
γ1 (SYNDIO)
β
α
H2O
2
4
6
8
10
12
14
1000/T [(°K)⁻¹]

It should be noted that the two NMR literature points for isotactic PMMA given in Figure 23 are close to the γ_2 relaxation of this work. It is conceivable that both the heterotactic and isotactic dispersions occur in the same temperature region. However, the high frequency ($\sim 10^7$ Hz) isotactic peaks from this study (labeled γ_3) lie at a somewhat lower temperature than that for the isotactic sample quoted in the literature (the high frequency point). Since those previous workers have not had pure isotactic material (their polymers are only stated as containing <24% atactic material), they may possibly have determined the heterotactic peak.

C. HIGH TEMPERATURE PROJECTION:

Figure 24 offers a simplified picture of the overall relaxation behavior of free radical PMMA, in that only the curves fitted to the relaxations (α, β, H_2O, γ_1, γ_2) are shown. The α or glass transition dispersion line was calculated from the WLF equation with T_g taken as 105°C. The other curves have been projected to high temperatures assuming linear Arrhenius-type relationships there. A striking feature of this plot is that all the relaxations appear to project through a region (or perhaps a single point) near log $\nu \sim 9$. and $T \sim 200$°C.

This pattern for PMMA is remarkably similar to that observed in 1968 by Starkweather[85] for several semicrystalline polymers; there, the log (ν/T) versus 1/T plots for the mechanical relaxations often converged at the crystalline melting point, T_m. Similar observations have been made informally for non-crystalline polymers by several investigators, but except for the work of G.D. Patterson, discussed

FIGURE 24.

TRANSITION MAP FOR PMMA-H_8, EXTRAPOLATED TO HIGH TEMPERATURE

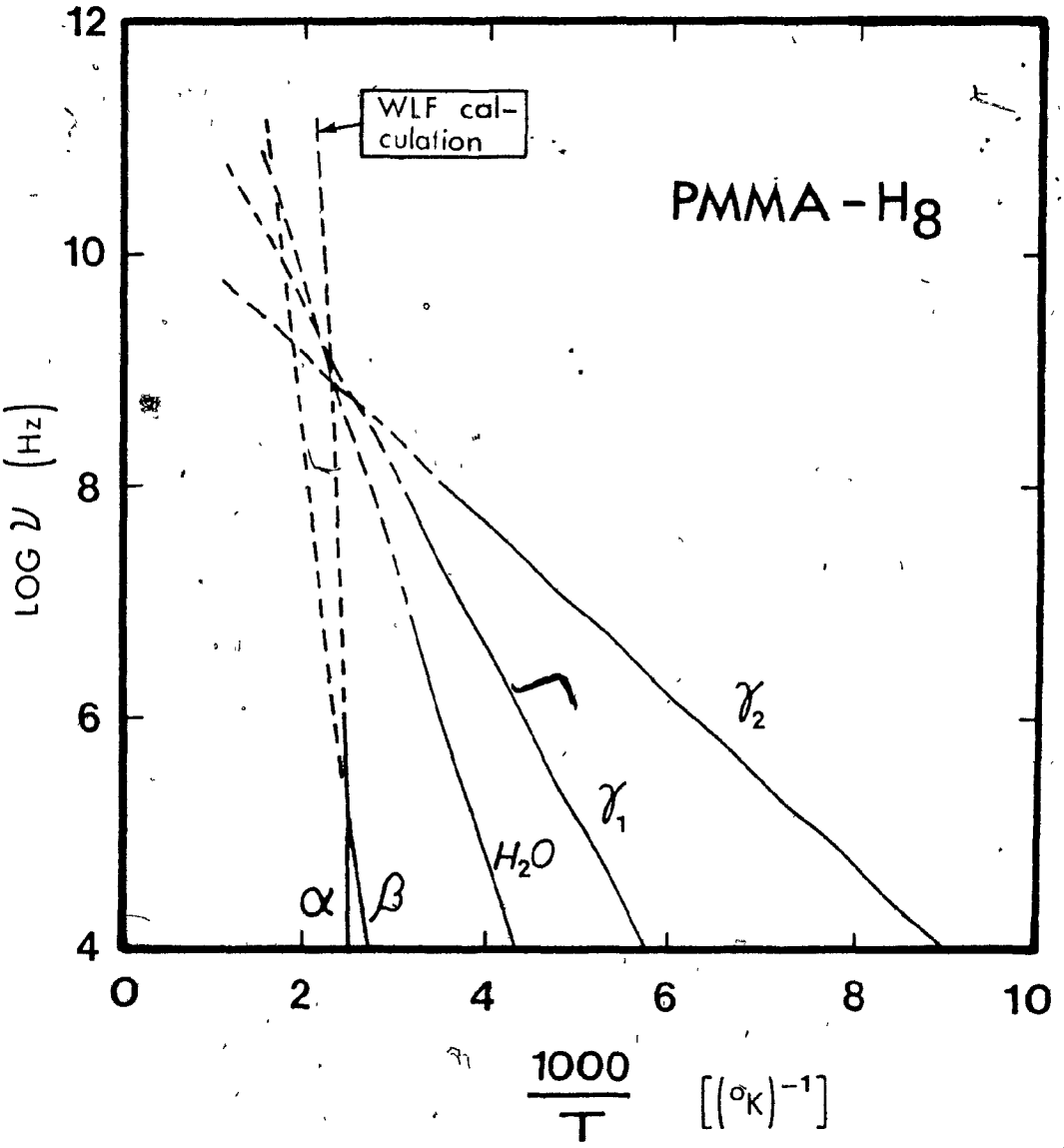
WLF calculation
PMMA - H8
LOG ν (Hz)
12
10
8
6
4
0
2
4
6
8
10
α
β
H2O
γ1
γ2
1000/T [(°K)⁻¹]

below, no literature references could be found. The intersection of the various molecular motions at a finite frequency and temperature may well be a general feature for amorphous polymers. The well-known merging at high temperatures and frequencies of the main chain (α) and secondary (β) relaxations certainly supports this concept. In recent Brillouin scattering studies, G.D. Patterson[86] observed just one loss maximum in several amorphous polymers at frequencies near $10^{9.5}$ Hz, in agreement with this merging of dispersions. He also demonstrated that the temperatures of maximum loss lay on extrapolations of the secondary β relaxations for poly(methyl acrylate), poly(isobutylene), atactic poly(propylene) and poly(vinyl acetate) and concluded that, at high temperatures, the β dispersion line extends, while the α merges with it.

V. CONTRIBUTIONS TO ORIGINAL KNOWLEDGE AND SUGGESTIONS FOR FUTURE WORK

The dynamic mechanical experiments contained in this thesis have shown that both a pronounced curvature in the log ν versus 1/T plot and a large deuteration effect are observed for the γ_1 relaxation in free-radical PMMA, in qualitative agreement with the methyl group tunneling theory of Stejskal and Gutowsky.[23] If this theory is indeed valid, then rotational QM tunneling of methyl groups is involved in viscoelastic relaxation.

It was also shown that the γ relaxation of PMMA is a function of the tacticity of the polymer, with two distinct dispersions (labeled γ_1 and γ_2) detected for the free-radically prepared polymers; these had activation energies of 6.7 and 3.3 Kcal/mole respectively. The γ_1 relaxation

was ascribed to syndiotactic backbone methyls and the γ_2 to heterotactic groups. Some evidence of a third related relaxation (labeled γ_3) was found; it is possible that this peak may correspond to isotactic material, although the evidence for this is weak. Finally, comparison of experimental and literature data for all the viscoelastic relaxations in PMMA suggests that the transitions all converge at $\sim 200^{\circ}C$ and 10^9 Hz. Although this clearly indicates an interdependency of the various molecular motions present in a polymer, an adequate explanation is lacking.

Future experimental work could be directed toward demonstrating the generality of the QM tunneling involvement in viscoelastic relaxation for a second polymer system, such as (say) poly(α-methyl styrene) which contains a hindered backbone methyl group likely to tunnel at reasonably high temperatures ($>77^{\circ}K$ at vibrating reed frequencies).

There is clearly also a need for theoretical improvements in this area: the Stejskal and Gutowsky treatment, which assumes a rigid polymer backbone, shows only qualitative agreement with experiment, and is inconsistent with the proposed existence of a common extrapolation point at a finite temperature for all the relaxations in a polymer. The detailed mechanism whereby tunneling methyl groups contribute to energy dissipation also merits further investigation.

VI. REFERENCES

1. S. Timoshenko and J.N. Goodier, Theory of Elasticity (McGraw Hill, New York, 1951).
2. O.W. Eshbach [Ed.], Handbook of Engineering Fundamentals (John Wiley, New York, 1945).
3. H. Mark, in Polymer Science and Materials, ed. by A.V. Tobolsky and H.F. Mark (John Wiley, U.S.A., 1971), p. 238.
4. R.R. Myers, J. Poly. Sci. C. 35, 3 (1971).
5. J. Heijboer, Mechanical Properties of Glassy Polymers Containing Saturated Rings, Doctoral Dissertation, University of Leiden, 1972.
6. D.W. McCall, in Molecular Dynamics and Structure of Solids, Eds. R.S. Carter and J.J. Rush, Nat. Bur. Stds. Special Publication 301, p. 475 (1969).
7. E.A.W. Hoff, D.W. Robinson and A.H. Willbourn, J. Poly. Sci. 18, 161 (1955).
8. J.M. Roe and E. Baer, Intern. J. Polymeric Mater. 1, 133 (1972).
9. K.J. Laidler, Chemical Kinetics (McGraw-Hill, U.S.A., 1965).
10. M.L. Williams, R.F. Landel and J.D. Ferry, JACS 77, 3701 (1955).
11. N.G. McCrum, B.E. Read, and G. Williams, Anelastic and Dielectric Effects in Polymeric Solids (John Wiley, New York, 1967).
12. A. Eisenberg and B.C. Eu, Ann. Rev. Matls. Sci. 6, 335 (1976).

13. R.H. Dicke and J.P. Wittke, Introduction to Quantum Mechanics (Addison-Wesley, U.S.A., 1961).

14. W.R. Beam, Electronics of Solids (McGraw Hill, U.S.A., 1965).

15. G. Herzberg, Molecular Structure and Molecular Spectra (Van Nostrand, New York, 1947), p. 221.

16. D.F. Brewer [Ed.], Quantum Fluids (North Holland Publ. Co., Amsterdam, 1966).

17. C.B. Duke, Tunneling in Solids (Academic Press, New York, 1969).

18. E. Burstein and S. Lundqvist [Eds.], Tunneling Phenomena in Solids (Plenum Press, New York, 1969).

19. See, for example, W.P. Slichter, J. Chem. Educ. 47, 193 (1970) or D.W. McCall, Accts. of Chem. Res., June 1971, p. 223.

20. V.J. McBrierty, Polymer 15, 503 (1974).

21. T.P. Das, J. Chem. Phys. 27, 763 (1957).

22. J.G. Powles and H.S. Gutowsky, J. Chem. Phys. 21, 1695 (1953).

23. E.O. Stejskal and H.S. Gutowsky, J. Chem. Phys. 28, 388 (1958).

24. F. Apaydin and S. Clough, J. Phys. C: Solid St. Phys. 1, 932 (1968).

25. P.S. Allen and S. Clough, Phys. Rev. Lett. 22, 1351 (1969).

26. R.B. Davidson and I. Miyagawa, J. Chem. Phys. 52, 1727 (1970).

27. M. Bloom, Pure and Applied Chem. 32, 99 (1972).

28. P.S. Allen, J. Phys. C: Solid State Phys. 7, L22 (1974).

29. A. Hüller and D.M. Kroll, J. Chem. Phys. 63, 4495 (1975).

30. C.S. Johnson, Jr. and C. Mottley, J. Phys. C: Solid St. Phys. 9, 2789 (1976).

31. A. Odajima, A.E. Woodward, and J.A. Sauer, J. Poly. Sci. 55, 181 (1961).

32. C.D. Knutson and D.M. Spitzer, Jr., J. Chem. Phys. 45, 407 (1966).

33. J. Haupt and W. Muller-Warmuth, Z. Naturforsch. 24a, 1066 (1969).

34. R. Kosfeld and U. von Mylius, Kolloid Z. 250, 1081 (1972).

35. P.S. Allen and A. Cowking, J. Chem. Phys. 49, 789 (1968).

36. B. Lammel and R. Kosfeld, Colloid and Polymer Science 253, 881 (1975).

37. J.L. Carolan, S. Clough, N.D. McMillan and B. Mulady, J. Phys. C: Solid St. Phys. 5, 631 (1972).

38. S. Clough and B.J. Mulady, Phys. Rev. Lett. 30, 161 (1973).

39. S. Clough, J.R. Hill and T. Hobson, Phys. Rev. Lett. 33, 1257 (1974).

40. S. Clough, J. Hill and F. Poldy, J. Phys. C: Solid St. Phys. 5, 1739 (1972).

41. S. Clough and J.R. Hill, J. Phys. C: Solid St. Phys. 7, L20 (1974).

42. S. Clough, J. Hill and F. Poldy, J. Phys. C: Solid St. Phys. 5, 518 (1972).

43. S. Clough and F. Poldy, J. Phys. C: Solid St. Phys. 6, 2357 (1973).

44. A. Eisenberg and S. Reich, J. Chem. Phys. 51, 5706 (1969).

45. J.M. Crissman, A.E. Woodward and J.A. Sauer, J. Poly. Sci. A3, 2693 (1965).

46. S. Reich and A. Eisenberg, J. Chem. Phys. 53, 2847 (1970).

47. Y. Tanabe, J. Hirose, K. Okano and Y. Wada, Polymer J. 1, 107 (1970).

48. J.A. Sauer, J. Poly. Sci. C. 32, 69 (1971).

49. P.D. Golub' and I.I. Perepechko, Sov. Phys. Acoust. 19, 391 (1974).

50. J.S. Higgins, G. Allen, and P.N. Brier, Polymer 13, 157 (1972).

51. G. Allen, C.J. Wright, and J.S. Higgins, Polymer 15, 319 (1974).

52. J. Jäckle, Z. Phys. 257, 212 (1972).

53. O. Yano, K. Saiki, S. Tarucha, and Y. Wada, J. Poly. Sci.: Phys. 15, 43 (1977).

54. See, for example, R.O. Pohl and G.L. Salinger, Annals New York Acad. of Sci. 279, 150 (1976).

55. B.I. Halperin, Annals New York Acad. of Sci. 279, 173 (1976).

56. P.G. Bordoni, M. Nuovo, and L. Verdini, Il Nuovo Cimento 20, 667 (1961).

57. T. Kajiyama and W.J. MacKnight, Macromols. 2, 254 (1969).

58. J.G. Powles, J. Poly. Sci. 22, 79 (1956).

59. K.M. Sinnott, J. Poly. Sci. 42, 3 (1960).

60. S. Reich, private communication.

61. R. Hayakawa et al., Proc. Jap. Conf. on Poly. Solid State, 1972, p. 99.

62. H. Hendus, G. Schnell, H. Thurn and K.A. Wolf, Ergeb. Exakt. Naturw. 31, 220 (1959).

63. T. Kawai, J. Phys. Soc. Jap. 16, 1220 (1961).

64. J.G. Powles and P. Mansfield, Polymer, Lond. 3, 336 (1962).

65. J.G. Powles, J.H. Strange, and D.J.H. Sandiford, Polymer, Lond. 4, 401 (1963).

66. T.M. Connor and A. Hartland, Phys. Letts. 23, 662 (1966).

67. K.M. Sinnott, J. Poly. Sci. 35, 273 (1959).

68. J.M. Crissman, J.A. Sauer, and A.E. Woodward, J. Poly. Sci. A2, 5075 (1964).

69. M. Shen, J.D. Strong, and H. Schlein, J. Macromol. Sci.-Chem. A3, 1315 (1969).

70. B. Golding, Polymers and Resins (Van Nostrand, New Jersey, 1959).

71. A. Nishioka, H. Watanabe, K. Abe and Y. Sono, J. Poly. Sci. 48, 241 (1960).

72. N.W. Johnston and P.W. Kopf, Macromols. 5, 87 (1972).

73. K.C. Ramey and J. Messick, J. Poly. Sci., Part A-2, 4, 155 (1966).

74. W.R. Krigbaum and J.V. Dawkins, in Encyclopaedia of Polymer Science and Technology 8, 764 (John Wiley, New York, 1968).

75. B. Cayrol, Segmental Mobility in Poly-p-Phenylene Ethers and Related Materials, Doctoral Thesis, McGill University, 1972.

76. S. Reich and A. Eisenberg, Rev. Sci. Instrum. 41, 1905 (1970).

77. G.S. Fielding Russell and R.E. Wetton, Plastics and Polymers, June 1970, p. 179.

78. D.Y. Chung, Rev. Sci. Instrum. 42, 878 (1971).

79. The torsional pendulum equations are presented in a number of sources and are summarized in R.S.C. Yeo, Structure-Property Studies of Ion-Containing Polymers, Doctoral Thesis, McGill University, 1976.

80. M. Navratil, Structure and Viscoelastic Properties of Styrene - based Ionomers, Doctoral Thesis, McGill University, 1973, p. A4.

81. H. Schlein and M. Shen, Rev. Sci. Instrum. 40, 587 (1969).

82. See, for example, M. Barmatz, H.J. Leamy, and H.S. Chen, Rev. Sci. Instrum. 42, 885 (1971).

83. H.F. Olson, Elements of Acoustical Engineering (Van Nostrand, New York, 1947).

84. G. Brunton, D. Griller, L.R.C. Barclay, and K.U. Ingold, JACS 98, 6803 (1976).

85. H.W. Starkweather, Jr., J. Macromol. Sci. - Phys. 2, 781 (1968).

86. G.D. Patterson, J. Poly. Sci. - Phys. 15, 455 (1977).

APPENDIX I

TUNNELING FREQUENCY CALCULATION FOR A DEUTERO-METHYL GROUP IN A BARRIER OF 5.89 KCAL/MOLE

The theoretical calculation of the isotope effect on the tunneling frequency of a methyl group has been reproduced from S. Reich's private communication strictly for the convenience of the reader.

APPENDIX I

TUNNELING FREQUENCY CALCULATION FOR A DEUTERO-METHYL GROUP IN A BARRIER OF 5.89 KCAL/MOLE

In the classical limit, the transition probability ν_c is given by:[I-1]

$$\nu_c = \frac{N}{2\pi} \left(\frac{2kT}{\pi I}\right)^{\frac{1}{2}} \exp\left(-\frac{V_o}{RT}\right) \qquad \ldots (I\text{-}1)$$

where I is the moment of inertia of the rotor, Vo the barrier height, T the absolute temperature, and N, k and R the Avogadro, Boltzmann, and ideal gas constants respectively.

Therefore, for a given temperature and barrier height,

$$\frac{\nu_c^{(CH_3)}}{\nu_c^{(CD_3)}} = \left[\frac{I_{(CD_3)}}{I_{(CH_3)}}\right]^{\frac{1}{2}} = 1.41 \qquad \ldots (I\text{-}2)$$

The Quantum Mechanical case for low enough temperatures is:

$$\nu_t \sim \exp\left[-\left(\frac{2\,V_o I}{\hbar^2}\right)^{\frac{1}{2}}\right]. \qquad \ldots (I\text{-}3)$$

Therefore,

$$\frac{\nu_t^{(CH_3)}}{\nu_t^{(CD_3)}} = \exp\left\{-\frac{(2V_o)^{\frac{1}{2}}}{\hbar}\left[I_{(CH_3)}^{\frac{1}{2}} - I_{(CD_3)}^{\frac{1}{2}}\right]\right\} \qquad \ldots (I\text{-}4)$$

which is temperature independent. ($h \equiv$ Planck's constant $= 2\pi\hbar$).

For example, with

$V_o = 2063\ cm^{-1} = 4.10 \times 10^{-13}$ erg/rotor = 5.89 Kcal/mole,

$I\ (CH_3) = 5.34 \times 10^{-40}\ g\ cm^2$,

and $I\ (CD_3) = 10.68 \times 10^{-40}\ g\ cm^2$,

$$\frac{\nu_t^{(CH_3)}}{\nu_t^{(CD_3)}} = e^{8.15} = 3.46 \times 10^3. \qquad \ldots (I\text{-}5)$$

Therefore, in the temperature range where $\nu_t \neq f\ (T)$,

$$\log \nu_t^{(CH_3)} - \log \nu_t^{(CD_3)} = 3.54. \qquad \ldots (I\text{-}6)$$

Since the curve of $\log \nu_t$ vs $1/T$ for a methyl (CH_3) rotor has been calculated [I-2], $\log \nu_t\ (CD_3)$ vs $1/T$ for small T can be calculated. The next step is to calculate the temperature T_c at which both tunneling and barrier-hopping frequencies are equal:[I-3]

$$T_c = \frac{h\, L_m^{\frac{1}{2}}}{2\pi k \sqrt{12I}}, \text{ where } L_m = -\left(\frac{\partial^2 V}{\partial \phi^2}\right)\Big|_{\phi = \phi_m} \qquad \ldots (I\text{-}7)$$

Here T_c is the Christov characteristic temperature, and L_m is the curvature of the hindering potential at its top (where coordinate $\phi = \phi_m$).

For $$V = \frac{V_o}{2}\ (1 + \cos 3\phi), \qquad \ldots (I\text{-}8)$$

$$L_m = \frac{9}{2} V_o \cos 3\phi \Big|_{\phi = 120^o} = \frac{9}{2} V_o \qquad \ldots (I\text{-}9)$$

So, for $V_o = 2063\ cm^{-1}$ and $I(CH_3) = 5.34 \times 10^{-40}\ g\ cm^2$,

$$T_c\ (CH_3) = 128^{\circ}K \text{ and } 1000/T_c\ (CH_3) = 7.8\ (^{\circ}K)^{-1},$$

which fits well with the Stejskal and Gutowsky calculation.[I-2]

In the case of the CD_3 rotor, for the same value of V_o,

$$1000/T_c\ (CD_3) = 11.04\ (^{\circ}K)^{-1}.$$

Thus, knowing the log ν_t versus 1/T curve for the CH_3 group,[I-2] the plot for the corresponding CD_3 group can now be built up: the limiting slope for high temperature is calculated from equation (I-1) and the plateau value for small T is known from equation (I-3). These two segments may be connected smoothly through $T_c\ (CD_3)$ to yield the log $\nu_t\ (CD_3)$ vs 1/T curve given in Figure 7 of the Introduction.

REFERENCES:

I-1 D.E. O'Reilly and T. Tsang, J. Chem. Phys. 46, 1291 (1967).

I-2 E.O. Stejskal and H.S. Gutowsky, J. Chem. Phys. 28, 388 (1958).

I-3 F. Gutmann, Jap. J. of Appl. Phys. 8, 1417 (1969).

APPENDIX II

VIBRATING REED INSTRUMENT, DESCRIPTION AND MODE OF OPERATION

The principal conclusion of this thesis is based on the detection of relatively low strength mechanical dispersions which have not been detectable in previous studies with conventional vibrating reed instruments. For this reason, it is considered expedient to describe the method of operation of the Vibrating Reed Instrument employed in the study in some detail. This description of the instrument will enable the reader to evaluate the test precision or to repeat the experiments if he so desires.

APPENDIX II

VIBRATING REED INSTRUMENT DESCRIPTION AND MODE OF OPERATION

"HIGH" FREQUENCY VIBRATING REED: PIEZOELECTRIC DETECTION TECHNIQUE

INDEX

'HIGH' FREQUENCY VIBRATING REED: PIEZOELECTRIC DETECTION TECHNIQUE

I PRINCIPLES OF OPERATION:

The Vibrating Reed technique is a dynamic mechanical technique by which the loss tangent (tan δ) and the Young's modulus E' of a solid (modulus range ca. 10^8 to 10^{12} dynes/cm^2) can be determined over the frequency range of ca. 100 Hz to 5000 Hz. The method involves the forced vibration near resonance of a rod of material clamped at one end as a cantilever.

Vibration is usually carried out by means of magnetic coils, with the amplitude of vibration measured either by an optical detection technique[II-1] or by a more sensitive piezoelectric detection technique[II-2] described here. This latter method employs thicker samples and is generally used in the frequency range of ca. 500 to 5000 Hz; use of weights may extend the technique to lower frequencies, however, while use of overtone frequencies may extend it to higher frequencies.

A curve of amplitude versus frequency is plotted for the resonance region, and analyzed to yield the desired properties (tan δ, E', E'').

Temperature Range: Room temperature to -210°C (achieved by pumping on liquid nitrogen).

Pressure Range: Design pressure is 2 cm Hg, controlled to ± 0.05 cm, for sufficient heat transfer within the cell and minimum energy loss due to gas pressure.

II DESCRIPTION OF INSTRUMENT:

A: APPARATUS:

A schematic diagram of the apparatus, with component descriptions has been given in Figure 12 of the Experimental section, but is reproduced here as Figure II-1 for convenience in the present discussion. Operation of the components is as follows: triangular wave generator G acts on Frequency Synthesizer A to produce a steadily changing frequency which is applied to magnet M. The magnet attracts and repels a metal tab glued to sample S, setting up a vibration. Transducer T detects the vibration sending a low-level signal via shielded connections to amplifier D. The amplified signal is applied to the Y-axis of X-Y recorder E and the triangular wave is simultaneously applied to the X-axis, resulting in the plotting-out of a resonance curve.

B: DETAILED COMPONENT DESCRIPTIONS AND SETTINGS:

Frequency Synthesizer and Triangular Wave Generator:

The Frequency Synthesizer can produce signals in the 0-100 KHz range. Frequency can be varied continuously in this range by means of the CAD (continuously adjustible decade) which can be operated manually, or externally as by a DC voltage source, in this case a triangular wave generator. Frequency is directly proportional to external voltage applied. Therefore, the triangular wave applied to the x-scale of the XY Recorder, produces an x-displacement which is proportional to frequency.

FIGURE II-1

SCHEMATIC DIAGRAM OF VIBRATING REED APPARATUS

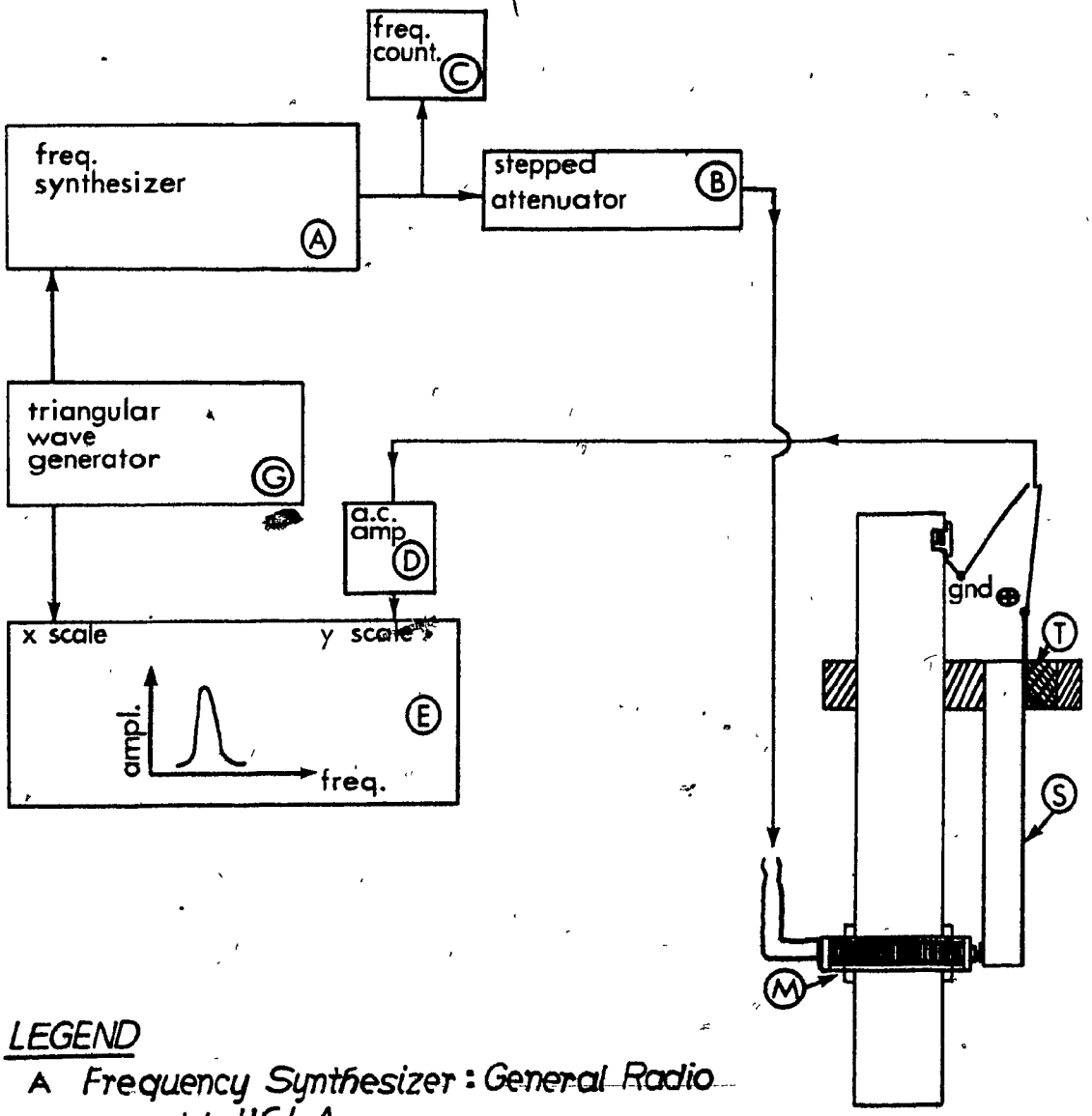

LEGEND

A Frequency Synthesizer : General Radio model 1161-A

B Stepped Attenuator, 0-80 db : Texscan LA series

C Frequency Counter, 5Hz-80MHz : Fluke model 1900A

D A.C. Amplifier : Hewlett Packard model 465-A

E X.Y. Recorder : H.P. model 7000 A

G Triangular Wave Generator : H.P. model 3310A

M Magnet : Electro Products model 3055-A

S Sample, rod with metal tab attached to lower end

T Transducer PZT-4 disc .25" x .100" thick : Vernitron part # 4100-4

The x-scale proportionality constant (frequency change/inch of displacement) can be obtained from the Frequency Synthesizer relation: 0.3 volt ≡ 1 major CAD division, and the recorder's x-scale setting in volts/inch.

An example of typical Frequency Synthesizer dial settings is given in Figure II-2A. The button beneath the x10 Hz Digit Insertion unit is depressed, indicating that the CAD dial replaces the x10 Hz and x1 Hz units. Here, the frequency setting is 624 Hz with Generator G off. With G on, frequency is varied about 624 Hz such that 0.3 volts applied externally is equivalent to 10 Hz (1 major CAD division).

The Frequency Synthesizer output voltage is constant as frequency varies. The output voltage range is 0–2 volts A.C., as monitored on the built-in voltmeter. It is set by an output level dial which is a rather coarse control. Excellent experimental results can be obtained by keeping the Frequency Synthesizer output voltage constant at 1 volt throughout the entire test, and adjusting the stepped attenuator B to keep the vibration amplitude approximately constant.

FIGURE II-2, A & B

A: TYPICAL FREQUENCY SYNTHESIZER SETTINGS, FOR A CENTRAL FREQUENCY OF 624 Hz, EXTERNALLY CONTROLLED.

B: FUNCTION GENERATOR OUTPUT SIGNAL: SCHEMATIC, SHOWING EFFECT OF SETTING CHANGES:

——— initial signal

..... signal obtained on increasing output level setting

------- signal obtained on decreasing dial (frequency) setting

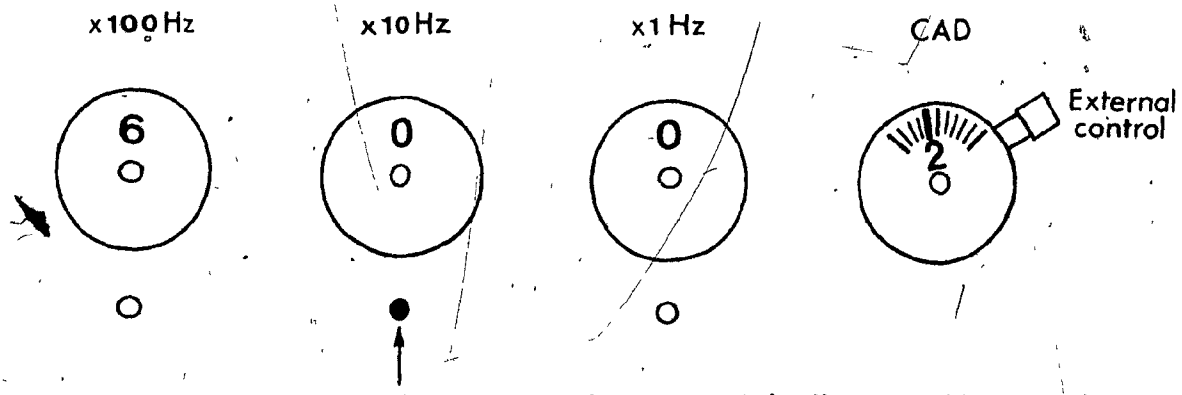
x100 Hz
x10 Hz
x1 Hz
CAD
6
0
0
2
External control
this button depressed indicates that the CAD dial replaces the x10 and x1 Digit Insertion units.

A

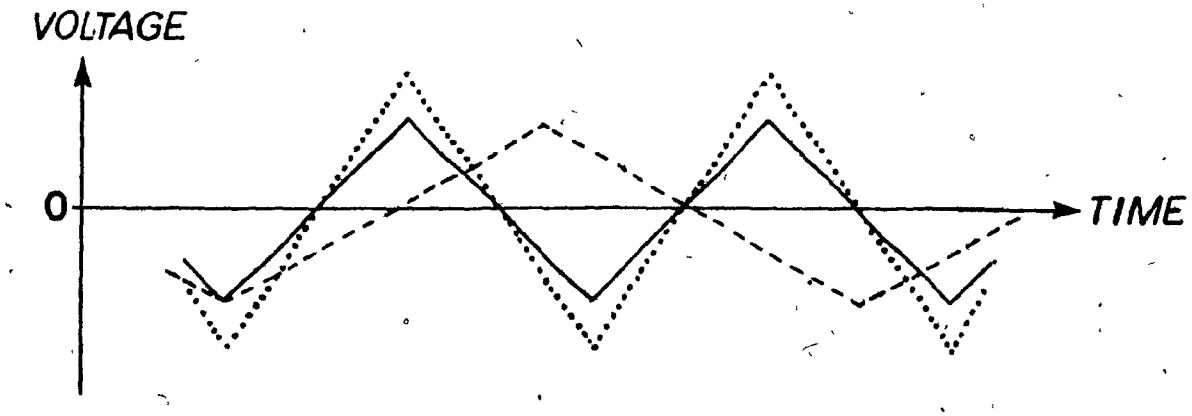
VOLTAGE
0
TIME

B

Function Generator G:

Typical Settings are as follows:

Function: TRI (angular);

Range (frequency): .001;

Dial Setting: usually 1 to 20 (variable);

DC offset level: 0;

Output level: high (variable) for 'wide' resonance peaks;

low (variable) for 'narrow' resonance peaks.

The dial is used to vary the slope of the triangular wave; a lower dial setting implies a lower slope and therefore a slower sweep across the x-axis of the recorder. Figure II-2B shows qualitatively the effects of various setting changes: the solid line is converted to the dotted one on increasing the output level setting, implying a wider range of swept voltage and a somewhat faster sweep rate (since more frequency is swept out in the same time); the solid line is changed to the dashed line on decreasing the dial (frequency) setting, implying that more time is taken for each sweep.

Frequency Counter (C):

This instrument enables quick and precise measurement of the resonance frequency or period as set manually using the Frequency Synthesizer. Five or six significant digits may be obtained, depending on the Frequency Synthesizer settings used (with greatest

precision where CAD replaces the x1 Hz Digit Insertion unit). Precision in the resonance frequency measurement is normally limited by the operator's ability to visually set the sample to resonance (maximum amplitude) on the X-Y Recorder. Precision will be best at lower temperatures where sharp loss peaks occur. The counter is best used on the period scales, since response to changes in period is very quick.

A.C. Amplifier (D):

The amplifier input signal (from the piezoelectric crystal) is shielded by means of a Pomona # 1433 connector. Amplifier gain is 40 db.

X-Y Recorder (E):

The following connections are made: the A.C. Amplifier (D) output to the Y scale (A.C. setting); the Triangular Wave voltage to the X scale (D.C. setting); and the central switch on Recycle.

FIGURE II-3

THE ASSEMBLED VIBRATING REED APPARATUS,

SHOWING VACUUM AND COOLING SYSTEMS.

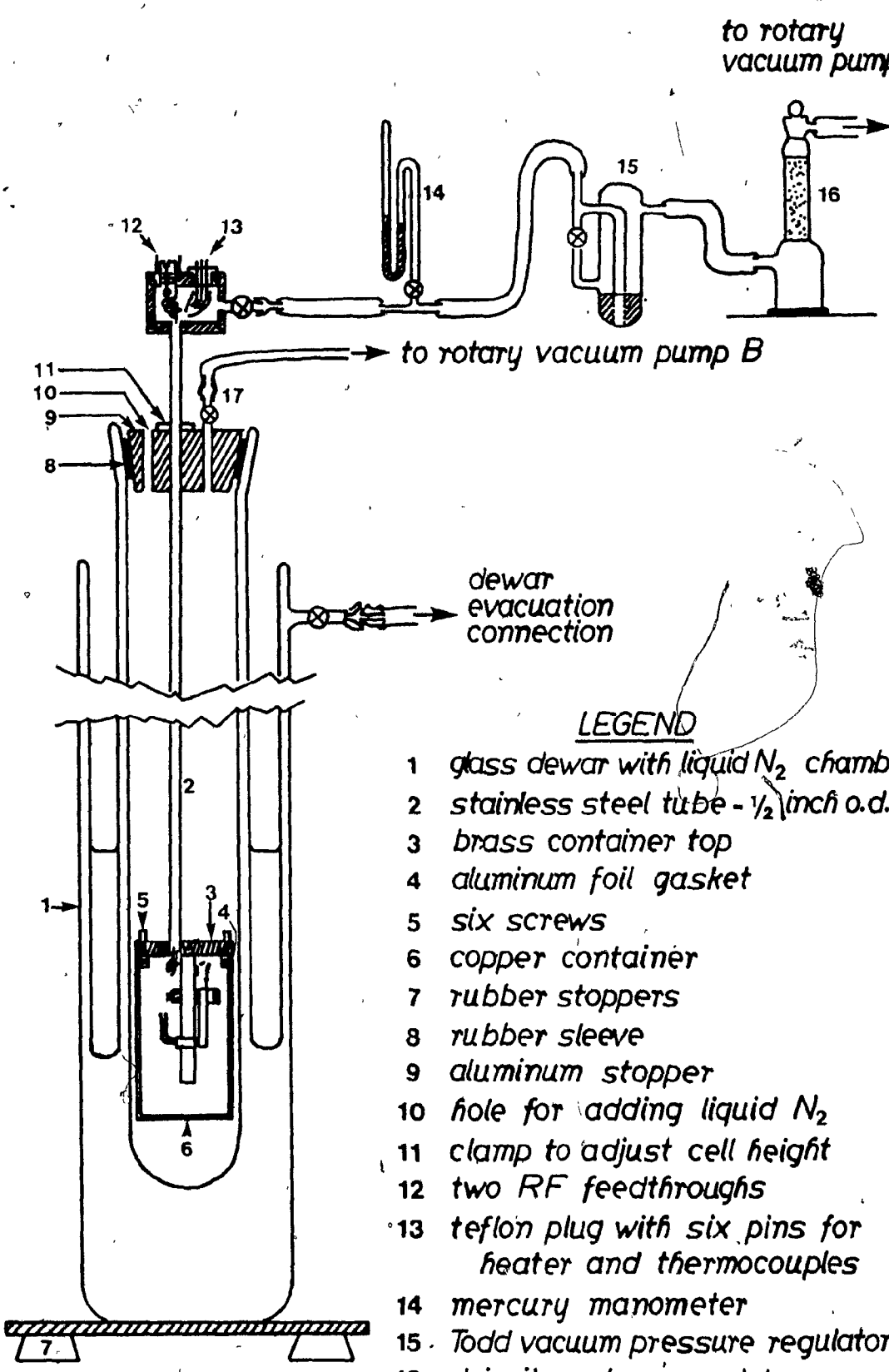

LEGEND

1 glass dewar with liquid N_2 chamber
2 stainless steel tube - ½ inch o.d.
3 brass container top
4 aluminum foil gasket
5 six screws
6 copper container
7 rubber stoppers
8 rubber sleeve
9 aluminum stopper
10 hole for adding liquid N_2
11 clamp to adjust cell height
12 two RF feedthroughs
13 teflon plug with six pins for heater and thermocouples
14 mercury manometer
15 Todd vacuum pressure regulator
16 drierite column and trap
17 connection to pump on liquid N_2

C: EXPERIMENTAL SET-UP:

The fully assembled vibrating reed apparatus, including the vacuum and cooling systems is given in Figure II-3. The low temperature dewar vessel is of glass and contains an inner and an outer annular chamber for liquid nitrogen coolant. There is provision for pumping on the liquid nitrogen in the inner container to achieve temperatures to -210°C. A second rotary pump equipped with a vacuum pressure control unit is used to maintain a low constant pressure inside the sample compartment with low temperature sealing achieved by means of an aluminum foil gasket. The dewar vessel rests on a platform supported by rubber stoppers, for vibration isolation.

III MODE OF OPERATION:

A: SAMPLE:

The sample is a molded rod with square or rectangular cross section, and typical dimensions:

ℓ - length - 2. to 5. cm;

w - width - 0.60 cm; and

t - thickness - 0.10 to 0.25 cm

An iron tab is glued to one end of the sample with epoxy glue. The tab can be a rectangular piece cut from a razor blade, with a typical weight of about 0.008 g. Figure II-4A shows the sample and tab geometry in relation to the clamp and magnet positions. It should be noted that ℓ is the 'free' length from the clamp to the end of the sample.

The tab faces the magnetic coil; when alternating current is applied to the coil, the force on the tab sets up a vibration in the sample.

The resonance frequency f_o of the rod depends on sample geometry according to the relation:

$$f_o \propto \frac{\text{thickness}}{(\text{length})^2} = \frac{t}{\ell^2}; \qquad \ldots\ldots (II\text{-}1)$$

f_o is also dependent on modulus and density as shown later.

FIGURE II-4, A & B

A: VIBRATING REED SAMPLE AND TAB GEOMETRY IN RELATION TO THE CLAMP AND MAGNET

B: THE ASSEMBLED VIBRATING REED CELL

(a) SIDE VIEW

(b) FRONT VIEW

(c) CROSS-SECTIONAL VIEW THROUGH CLAMP

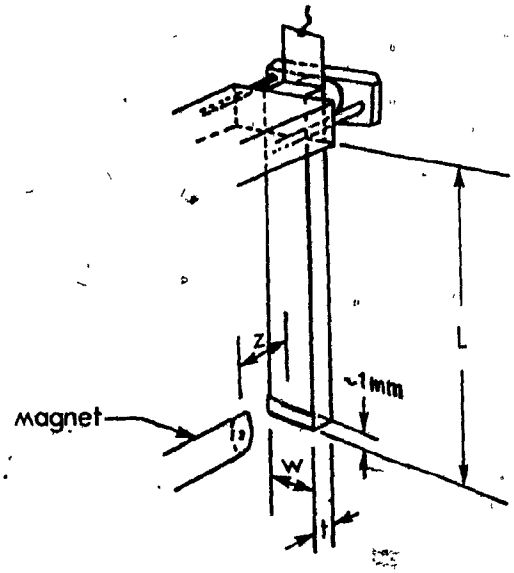
z
L
~1mm
magnet
w
t

A

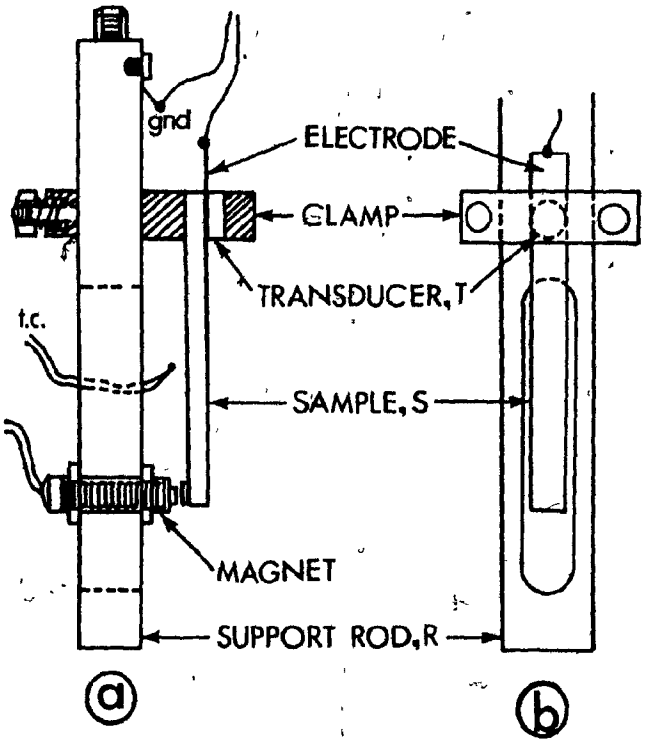
gnd
ELECTRODE
CLAMP
TRANSDUCER, T
t.c.
SAMPLE, S
MAGNET
SUPPORT ROD, R
a
b

B

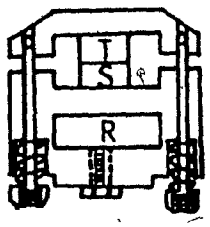
T
S
R

C

B: CELL ASSEMBLY:

The assembled cell is shown in Figure II-4B, where drawings (a), (b) and (c) represent side, front and cross-sectional views respectively. Not shown is a nichrome heating wire of resistance $\sim 10\Omega$, wound around the support rod above the clamp.

The following steps are taken on assembling the cell:

1. Position clamp on support rod using centre screw. Line up clamp, transducer, sample and electrode as perfectly as possible, as in diagram (a) of Figure II-4B. Be sure sample is centered in clamp and closely perpendicular to it (for pure transverse vibration).

2. Tighten nuts against springs (diagram (c)) of Figure II-4B for very tight clamping. Both sides should be about equally tight, to avoid cracking the transducer. (This rarely happens with PZT-4 ceramic transducers which are extremely tough, seldom cracking even under severe stress such as that due to rapid cooling.)

3. Centre metal tab exactly over the pole of the magnet and set clearance to about 5/1000 to 10/1000 inch (15/1000" for thinnest samples (about 0.1 cm thick) which might otherwise be bent causing the magnet to touch the tab), This adjustment is done using the two nuts which hold the magnet in place. Thickness

gauges may be used to measure spacing. The lower this spacing is, the greater the force will be.

4. Position thermocouples as desired either in the vapour space (such as that shown in diagram (a) of Figure II-4B) or possibly touching the fixed end of the sample.

5. Prepare the aluminum foil gasket as follows: fold several layers of foil over the mouth of the cell container and tape in place; then carefully cut away the inside area using a compass point; next press the remaining inside area onto the inner wall of the cell container; then break the foil gasket at the six screw holes (again using a compass point) and place the cell container carefully around the sample assembly; finally, insert and securely tighten the six screws.

6. If desired, place some drying agent inside the container on assembly, to ensure reasonable dryness throughout the experiment.

C: COOLDOWN AND WARMUP PROCEDURE:

1. Warming Tests:

A useful test procedure is to cool the cell down with liquid nitrogen addition to the central dewar. Once liquid N_2 temperature (ca. -195.5°C) is attained, pumping on the coolant is begun (Pump B

in Figure II-3) so as to achieve temperatures as low as -210°C. Solid nitrogen will be produced in the middle dewar. The pumping rate will be very high at first, but it will be satisfactory once the liquid nitrogen has solidified. Eventually the cell temperature will begin to rise at a rate which depends on the quality of the dewar's insulating vacuum.

Slow warming rates are advisable for several reasons: rapid rates may result in differences between sample and thermocouple temperatures, leading to errors in sample temperature measurement; also, very slow warming rates(say about 10°C/hour) appear necessary to allow detection of low strength relaxations (i.e, where $\Delta f_o/f_o \approx 1/1000$). Liquid nitrogen may be added to the outer dewar to retard the warming rate, while the heater may be used between measurements only, to speed up the warming rate. (A low heater rheostat setting of, say, 10-20 volts should be used to avoid burning out the heater.)

Controlled low pressure (say, 2.0 ± 0.05 cm Hg) in the sample container is desirable for efficient heat transfer within the cell and negligible sample energy loss due to air resistance. Pressure is controlled by means of a rotary pump (A in Figure II-3) acting through a Todd vacuum pressure regulator.

The following steps are taken in conducting a warming run:

a) pump down main dewar insulating vacuum beforehand;

b) evacuate sample chamber; (NOTE: The Todd vacuum pressure regulator must first be on bypass (stopcock open); then close for control.)

c) cool by adding liquid N_2 to inner and outer dewars;

d) when approximately at liquid N_2 temperature, pump on liquid N_2;

e) set angle of the vacuum pressure regulator to give the desired pressure (usually 2 cm). This may require occasional readjustment if leaks are present, i.e., if the aluminum foil gasket is not sealing well.

2. Cooling Tests:

With the existing cell, a cooling run may also be done, in which the sample cell (internal pressure controlled as above) is cooled with small additions of liquid N_2, measurements being made between additions. Too rapid cooling may produce spikes of transducer noise, making cooling rates lower than $1^{\circ}C$/minute advisable.

D: MEASUREMENT PROCEDURE:

Measurements are done as a function of temperature with the following steps taken:

1. Turn Frequency Synthesizer, Frequency Counter, A.C. Amplifier and X-Y Recorder on. Locate the resonance frequency by varying the frequency manually in the expected region.

2. Set the attenuator db level to give approximately 1 volt maximum amplitude at the X-Y Recorder. (Use 0.2 volt/inch vertical scale on the X-Y.) This will generally ensure that the signal is much greater than the noise.

3. Select the appropriate X-Y Recorder horizontal scale, so that the resonance curve is wide enough to give accuracy in the half-width measurement.

Plotting a Resonance Curve:

4. With X-Y servo switch off, turn on the triangular wave generator. Then turn X-Y servo on (activates pen) and curve will be plotted.

Notes:

a) Adjust plotting rate with function generator dial. Too rapid plotting may cut off the top of the peak.

b) The frequency range covered depends on the Frequency Synthesizer setting and the function generator output level, as outlined in Section B. Adjust these to plot the resonance curve.

c) Baseline: To obtain the baseline, set the attenuator to a very high db level (so that essentially zero signal goes to magnet) and replot as before;
or plot a sufficient region around the peak, and project back the baseline.

5. After plotting, turn off servo, then turn off function generator, returning instrument to manual operation: Turn on servo again. Using the CAD, locate the resonance frequency f_o, by manually adjusting to maximum amplitude. Record this frequency (or the period) and (immediately) take temperature readings. If temperature is changing very quickly, record it before and after plotting the resonance curve.

6. Repeat steps 4. and 5. as a function of temperature.

E: OPERATING PROBLEMS:

1. Noise:

Some noise (mostly 60 cycle) is unavoidable in the test. In general, signal is easily much greater than noise, but the following should be noted:

a) The heater creates very great noise and must be off during measurements;

b) The thermocouple meter also produces considerable noise and must be off during measurement. The same is true for manual potentiometer measurements.

Low frequency A.C. noise (e.g. 60 cycle) can readily be detected by using the X-Y Recorder zero check at an off-resonance frequency (the drop in signal is noise) or by looking at the waveform on a 'scope' (noise produces distortion).

c) Erratic noise may result from dirty X-Y Recorder switches.

d) Noise spikes may arise from too rapid cooling or heating of the piezoelectric transducer, probably due to uneven forces.

2. Temperature Measurement Below -200°C:

The Fluke Thermocouple meter is not calibrated for operation below -200°C. Therefore, a millivolt potentiometer must be used at lowest temperatures, such as those obtained for pumped liquid nitrogen.

FIGURE II-5

TYPICAL VIBRATING REED AMPLITUDE - FREQUENCY PLOT ILLUSTRATING HALF-WIDTH AND RESONANCE FREQUENCY

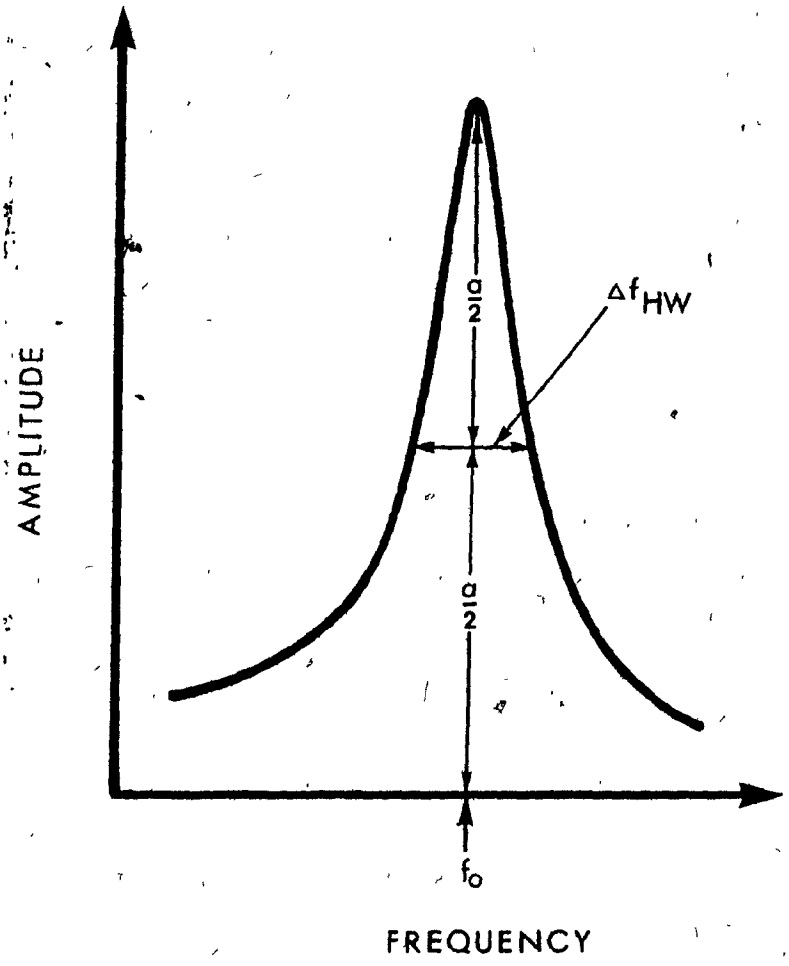
AMPLITUDE
a/2
Δf HW
a/2
f o
FREQUENCY

IV. RESULTS AND CALCULATIONS:

Figure II-5 shows a typical amplitude-frequency plot, from which the resonance frequency, f_o, and the half width, $\Delta f_{H.W.}$, are obtained.

Loss Tangent:

$$\tan \delta = \frac{(\Delta f)_{H.W.}}{\sqrt{3} f_o} \qquad \ldots \text{(II-2)}$$

If half width, $(\Delta f)_{H.W.}$, is measured in cm, then

$$(\Delta f)_{H.W.} = \text{H.W. (cm)} \times \frac{1 \text{ inch}}{2.54 \text{ cm}} \times S \left(\frac{\text{volts}}{\text{inch}}\right) \times \text{factor} \left(\frac{\text{Hz}}{\text{volt}}\right) \quad \ldots \text{(II-3)}$$

where S is the XY Recorder Scale setting and 'factor' is the Frequency Synthesizer frequency/voltage factor.

Example: For 0.5 volt/inch horizontal scale on XY Recorder and 10 Hz ≡ 0.3 v on Frequency Synthesizer,

$$\tan \delta = \frac{3.79 \times \text{H.W. (cm)}}{f_o \text{ (Hz)}} \qquad \ldots \text{(II-4)}$$

Dynamic Storage Modulus:

The Storage modulus or Young's modulus is calculated as follows: [II-3]

$$E' = \rho \left(\frac{\ell}{k_i}\right)^4 \left(\frac{2\Pi}{t}\right)^2 \cdot 12 \, (f_o)^2 \qquad \ldots \text{(II-5)}$$

where: $k_1 = 1.875$ (fundamental)

$k_2 = 4.694$ (1st overtone)

$k_3 = 7.855$ (2nd overtone)

and ρ, ℓ and t are sample density, length and thickness respectively.

Thus, for the fundamental, $E' = 38.33 \left[\frac{\ell^4 \rho}{t^2}\right] f_o^2$, ... (II-6)

with the constant 38.33 replaced by 0.9758 and 0.1244 for the first and second overtones respectively.

Dynamic Loss Modulus:

$$E'' = \tan \delta \, (E'). \qquad \ldots \text{(II-7)}$$

V SOURCES OF ERROR:

The vibrating reed design has been based on that of Fielding-Russell and Wetton[II-2], which is capable of detecting small mechanical dispersions. For methyl group motions in particular, it is necessary to detect modulus changes of the order of one part per thousand in a sample which is being cooled (or warmed) through the relaxation region. To achieve such high precision in modulus, a Frequency Counter capable of measuring resonance frequency (or period) with an accuracy approaching one part per million was incorporated into the design. The error in f_o was then determined mainly by the ability of the operator to manually set the vibration to resonance. For polymer samples at low temperatures (say, tan $\delta \sim 0.001$), use of a sensitive X-Y Recorder X-scale (say $\sim$1Hz/inch) probably allows f_o to be set to 1 part in 50,000.

Fielding-Russell and Wetton[II-2] found standard errors of ± 8% in E' and ± 0.001 in tan δ for regions of low loss; they attributed this variation to sample preparation conditions and accuracy of measurement of sample dimensions. The same degree of variation in E' and tan δ has been observed in the present experiments with PMMA samples at low temperatures.

Effect of Noise:

The presence of noise can easily account for the error in tan δ

level. Figure II-6 shows the effect of 60 Hz noise on f_o and tan δ for a PMMA-H_8 sample at 22.2°C and 1 atmosphere pressure. It can be seen that signal/noise ratios less than ~40 produce low values of tan δ by the mechanism shown, but no significant change in f_o (and therefore modulus). This experiment suggests that a constant signal/noise ratio throughout a test done as a function of temperature, would produce a constant error in tan δ without effect on the temperature position of a mechanical dispersion.

Effect of Manual Measurements:

An error of ~ 1% in individual tan δ values results from measuring Δf_{HW} off the chart. Errors in measurement of sample length and thickness can account for ~ 4% error in the modulus. Also, no correction was made for the gradual change in sample dimensions with temperature.

Effect of the Metal Tab:

The mass of the metal tab has been neglected in the modulus calculation. If desired, however, correction can be made with the use of the following equation[II-2]:

$$E' = \frac{4\pi^2 \ell^3 f_o^2}{35\, t^3 w} \left(140\, M_L + 33\, \rho w t \ell\right) \quad \ldots \text{(II-8)}$$

where M_L is the mass of the tab attached to the free end of the sample

and all other variables are as previously defined. Equation II-8 implies that modulus values given in this report are ~ 5% low from this source. This is not serious, since it is the temperature location of the relaxations (obtained from changes in modulus with temperature) which is of importance in the present study, and not the absolute value of modulus.

Effect of Pressure and Temperature:

The effect of gas pressure within the sample cell is important. In similar experiments at ~ 10 KHz, Bordoni et al.[II-4] found that a pressure of 1 atmosphere gave a 0.001 contribution to tan δ. The present experiments have confirmed this and have also shown that modulus is reduced by ~ 1% on changing from vacuum to atmospheric pressure. Vibrating reed tests were therefore conducted under a controlled low pressure of ~ 2.0 cm, which was considered to minimize these errors. At the same time, this pressure level allows sufficient heat transfer within the cell to achieve reasonable warming rates (say, 10^{o}C/hour) and low temperature gradients along the sample (generally $<1^{o}$ and often as low as 0.1^{o}C). Measurements are carried out during sample warm-up, with typical temperature changes of $\sim 0.2^{o}$C during a frequency sweep (tan δ measurement) and $<0.1^{o}$C during an f_o determination (modulus measurement). Precise temperatures ($\pm$ 0.1^{o}C) can therefore be assigned to the data points, enabling accurate location of low strength mechanical relaxations.

FIGURE II-6

EFFECT OF 60 Hz NOISE ON LOSS TANGENT AND RESONANCE FREQUENCY FOR PMMA-H_8 AT 22.2°C AND 1 ATMOSPHERE PRESSURE. THE INSERTS SHOW TWO VOLTAGE/FREQUENCY SWEEPS ILLUSTRATING LOW NOISE AND HIGH NOISE (NOISE = ΔV) SITUATIONS.

(Signal/Noise) Ratio	f_0 (Hz)	tan δ x10^2
75.	177.4	5.89
41.	177.4	5.82
22.	177.7	5.64
12.	177.2	5.43
6.2	178.3	4.86
3.1	177.6	4.48
1.4	177.4	3.86

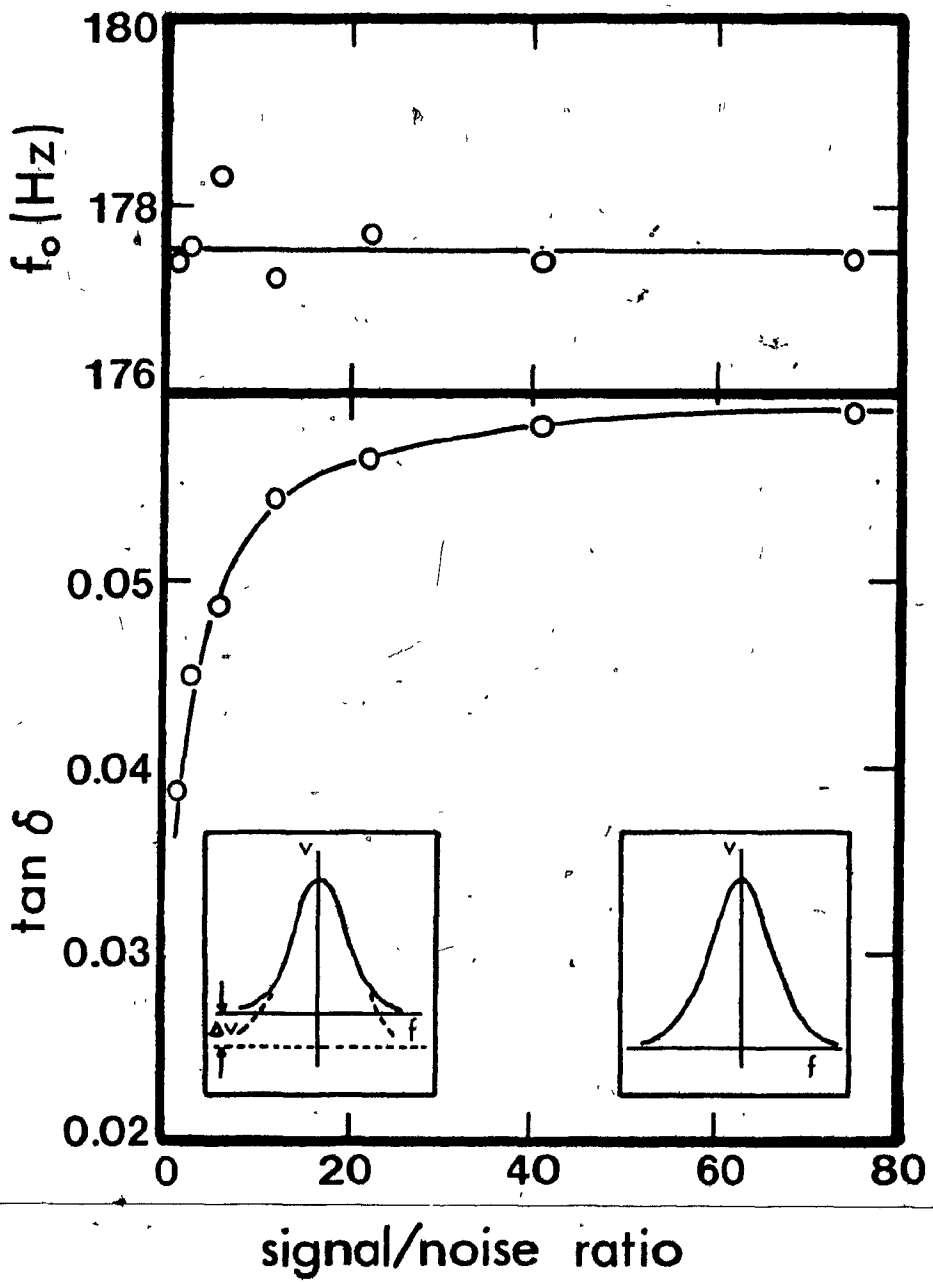
180
178
176
f_o (Hz)
0.05
0.04
0.03
0.02
tan δ
0
20
40
60
80
signal/noise ratio
v
Δv
f
v
f

VI REFERENCES:

II-1 S. Reich and A. Eisenberg, Rev. Sci. Instrum. 41, 1905 (1970).

II-2 G.S. Fielding-Russell and R.E. Wetton, Plastics and Polymers, 179 (June, 1970).

II-3 M. Barmatz, H.J. Leamy, and H.S. Chen, Rev. Sci. Instrum. 42, 885 (1971).

II-4 P.G. Bordoni, M. Nuovo, and L. Verdini, Il Nuovo Cimento 20, 667 (1961).

APPENDIX III

ULTRASONIC INSTRUMENT

DESCRIPTION AND MODE OF OPERATION

In this section, a detailed description of the ultrasonic apparatus employed in this study is presented, so as to allow the reader to assess the precision of the technique and to repeat the experiments if he so desires. As was the case for the vibrating reed instrument, very small relaxations have been detected. The design of this instrument is based on that employed by Dr. J. Krause of Bell Laboratories.

APPENDIX III

ULTRASONIC INSTRUMENT, DESCRIPTION AND MODE OF OPERATION

SINGLE CRYSTAL PULSE ECHO TECHNIQUE

INDEX

ULTRASONIC APPARATUS - SINGLE CRYSTAL PULSE ECHO TECHNIQUE

I PRINCIPLES OF OPERATION

The dynamic mechanical properties of materials at higher-than-audible frequencies (greater than ~ 20,000 Hz) can be determined from tests utilizing ultrasonic waves. These waves are generated by piezoelectric transducers (e.g. quartz crystal sections) which change dimensions in an electric field. In the commonly-used pulse echo experimental technique, a single crystal is used both to generate an initial ultrasonic pulse which is coupled into a sample and to detect echoes from the opposite face of the sample. The method has been successfully applied to polymeric solids from room to cryogenic temperatures.

The apparatus described here permits measurements of attenuation coefficient and speed of sound for longitudinal waves in low loss solid samples ($\tan \delta$ less than ~ 0.02) over a frequency range of 1 to 20 MHz. From these experimental values, the loss tangent ($\tan \delta$), real Young's modulus (E') and imaginary Young's modulus (E'') can be calculated.

Temperature Range: Liquid nitrogen temperature ($-196^{\circ}C$) to $+50^{\circ}C$, the latter being attained with the use of a low wattage heater.

Pressure Range: Normally 1 atmosphere throughout a test. Vacuum operation is also possible, with suitable experimental technique.

II DESCRIPTION OF INSTRUMENT

A: SCHEMATIC DIAGRAM OF APPARATUS:

A schematic diagram of the ultrasonic pulse echo apparatus has been given in Figure 13 of the Experimental section and is reproduced as Figure III-1 for convenience in the present discussion. The Pulse Generator main frame - R.F. plug-in combination (A+B) generates pulses of radio frequency at the desired frequency; these pulses are applied via impedance matching network D to piezoelectric transducer T, which vibrates at the frequency of the electrical signal. The transducer is attached by means of a thin layer of suitable bonding agent X to solid sample S which has closely parallel faces (as compared to the wavelength of the ultrasound). The ultrasonic pulse is coupled into the sample where it travels at a characteristic speed and undergoes a series of internal reflections from the sample faces until all the sound energy has been dissipated. The transducer also acts as a detector for the returning pulse echoes, producing electrical pulses which pass back through the matching network D and the stepped attenuator C to RF plug-in B where they are amplified and then rectified (leaving only the RF pulse envelopes). This video output is then displayed on Oscilloscope E where an exponentially decaying series of evenly spaced pulses is observed.

The stepped attentuator C is a variable resistance unit used to measure relative attenuation levels of the pulse echoes. The Oscilloscope yields accurate values for the time between these echoes. This information is analyzed to obtain the desired mechanical properties.

FIGURE III-1

SCHEMATIC DIAGRAM OF ULTRASONIC PULSE ECHO APPARATUS

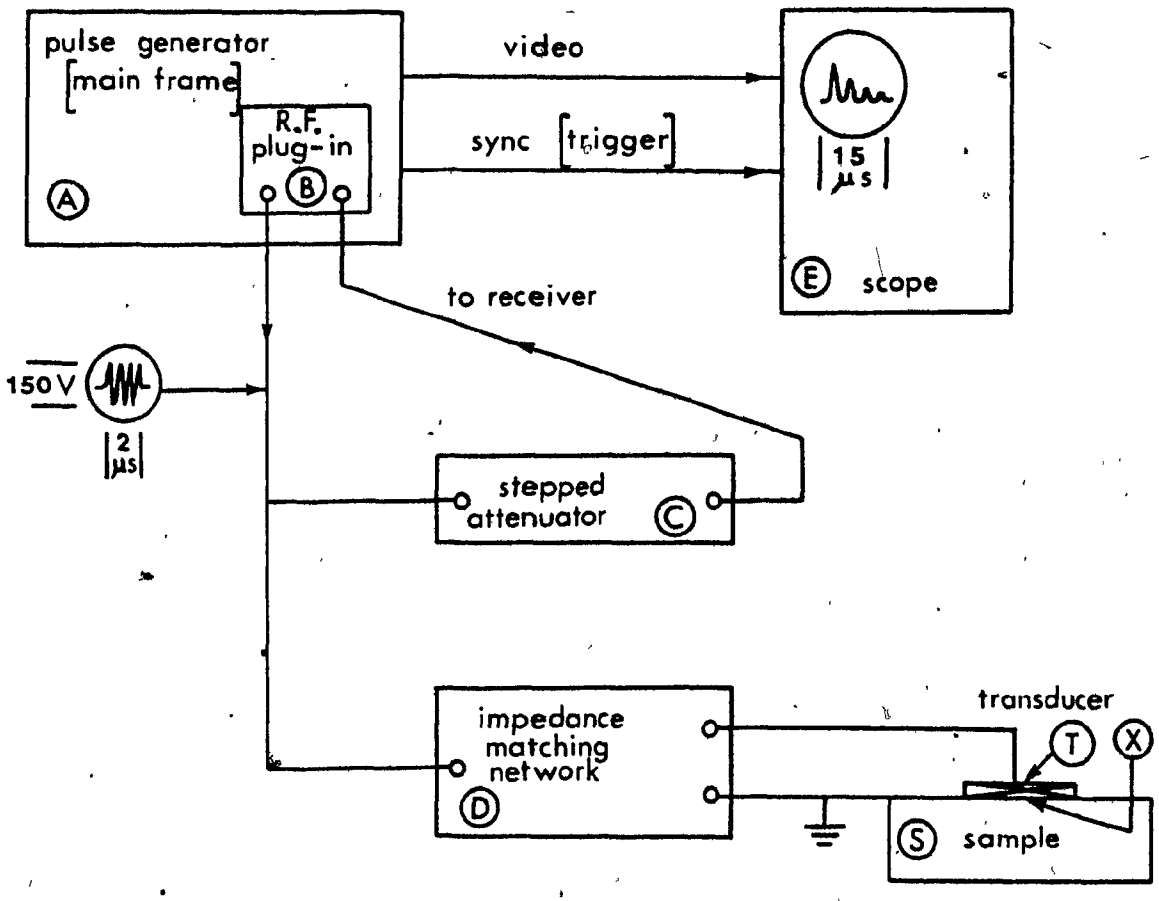

LEGEND

A *Pulse Generator, main frame: Matec model 6600*

B *Radiofrequency plug-in: Matec model 950, 1-20 MHz range*

C *Stepped Attenuator, 0-80 db in 0.1 db steps: Texscan LA's*

D *Impedance Matching Network, 0-28 μh: Matec model 65, rated 5-30 MHz*

E *Oscilloscope: Tektronix model 535A with type L amplifier*

T *Transducer: quartz, Valpey-Fisher Corp.; ceramic, Automation Industries*

S *Sample: cylindrical, with closely parallel faces (top face requires an electrode for use with quartz transducer)*

X *Bonding liquid layer between transducer and sample*

(numbers given in the figure are typical for 15 MHz operation)

B: RF PULSE GENERATOR AND OSCILLOSCOPE - Detailed Descriptions and Settings:

Radio Frequency Pulse Generator: (Parts A & B in Figure III-1):

The Matec model 6600 main frame, in conjunction with model 950 RF plug-in, produces high voltage RF pulses (~150 volts peak-to-peak) of variable width (0.5 to 5 μsec) and repetition rate (5 - 500 pulses/sec) over a nominal frequency range of 1 to 20 MHz. (The model 960 RF plug-in covering the frequency region 10 to 310 MHz is also available.)

Optimum Settings:

Main Frame (6600):

Mode of operation:	A - single pulse mode.
Pulse amplitude:	Maximum, ~150 v. peak-to-peak.
Pulse repetition rate:	Near maximum on 50 - 500 pulse/sec scale.
Pulse width:	~ 2 μsec - set for sharp echoes of maximum height; kept constant throughout a given test.
Receiver gain:	Maximum, ~ 70 db of amplification.

Plug-In (950):

RF tuning:	Range and tuning dials are set according to the calibration table supplied; fine adjustments are made after sample assembly so as to achieve maximum echo strength and symmetry.
Detector filter:	Position 1 for < 3 MHz Position 2 for ≥ 3 MHz.

Cable Connections:

RF out: The 'LOW-Z' output from the plug-in (BNC fitting) is connected directly to a BNC tee; the two arms of the tee are connected by cables (each 2 feet long) to the attenuator and matching network input respectively.

RF echoes in: The ultrasonic echo train to be amplified goes from the attenuator via 2 foot cable to the 'IN TO RECEIVER' connector on the plug-in.

Video output: Goes to the vertical scale of the oscilloscope from a rear main frame connector.

Sync output: Goes to the trigger connector of the B horizontal scale of the oscilloscope from a rear main frame connector.

All cables are coaxial with 50 Ω characteristic impedance, and BNC fittings.

Oscilloscope (Part E in Figure III-1): A Tektronix 535A oscilloscope equipped with a single trace L-type plug-in amplifier and viewing hood is operated in the 'A DELAYED BY B' mode. Here, the B time base is triggered by the pulse generator and the A time base is triggered after a time interval which can be varied manually with the delay time multiplier. This special feature of the model 535A oscilloscope permits very accurate measurement of the time between successive ultrasonic echoes.[III-1]

Optimum Settings:

Horizontal display: A delayed by B.

Time base A: Trigger input - from B delayed trigger connection

Triggering mode - external, negative

Triggering level, stability - approximately middle scale for both

Time/cm - 2 μsec/cm for thinner samples (as used with 15° and 25 MHz quartz transducers)

- 5 μsec/cm for thicker samples (as used with automation transducers).

Time base B: Trigger input - from pulse generator 'sync out' connection

Triggering mode - external, negative

Triggering level, stability - approximately middle scale for both

Delay time/cm - again 2 or 5 μsec/cm depending on sample thickness

Vertical Scale (type L plug-in):

2 volts/cm, A.C.; input from pulse generator 'video' connection

The oscilloscope viewing hood serves to reduce reflected light from the screen facilitating visual observation. An alignment mark placed on this hood may be used to diminish parallax error in the time measurements.

C: LOW TEMPERATURE CELL DESIGN:

1. Design for 15 and 25 MHz Quartz Transducers:

This low temperature cell is illustrated in Figure III-2. It is specifically designed for use with thin unplated ¼"-diameter X-cut quartz transducers. A principal feature of the cell is that the sample holder may be assembled independently of the body of the cell.

All parts are of copper for high thermal conductivity, unless otherwise noted on the diagrams, except for the pins which are all 1/8"-diameter stainless steel. The cell container is principally stainless steel, but silver soldered to copper at the supported end (see Figure III-2). This is to permit a soft solder joint to be made between the container and cell cover for operation of the cell under vacuum. However, the cell is generally operated at atmospheric pressure, so that this soft solder connection is not needed.

It is very important that the sample holder and cell body be in intimate contact in the assembled cell. This is to provide an effective ground connection for the unplated transducer. (The ground passes from cell body to sample holder to the sample's electrode surface (see part III A: 2).) The brass button thickness must also be carefully chosen so that the spring contact is

compressed when the sample holder and cell body surfaces are flush. This spring counteracts the differential shrinkage which occurs as temperature is decreased, thereby maintaining the transducer/sample contact.

Figure III-3 shows this low temperature cell in place for an experiment. The cell is surrounded with a close-fitting copper jacket which attaches over the cell cover by means of several set screws. This jacket serves both to hold the inner container in place and to achieve better temperature uniformity throughout the cell.

2. Design for 1 and 2.25 MHz Ceramic Transducers:

The frequency region from 1 to 10 MHz was studied using 1 MHz and 2.25 MHz Automation Industries mounted ceramic transducers at fundamental and overtone frequencies. The transducer and sample were simply clamped together in the sample holder described in part 1. A thermocouple was positioned and the appropriate coaxial cable connected. An aluminum foil container was fashioned about this cell and the assembly placed in a dewar vessel for cooling. These experiments were limited to temperatures greater than $\sim -100^{\circ}C$ in order to avoid cracking the mounted transducers.

FIGURE III-2

LØW TEMPERATURE CELL DESIGN FOR USE WITH ½"-DIAMETER SAMPLES AND ¼"-DIAMETER QUARTZ TRANSDUCERS (FREQUENCY RANGE 15 - 25 MHz).

ASSEMBLY DRAWING - ACTUAL SIZE.

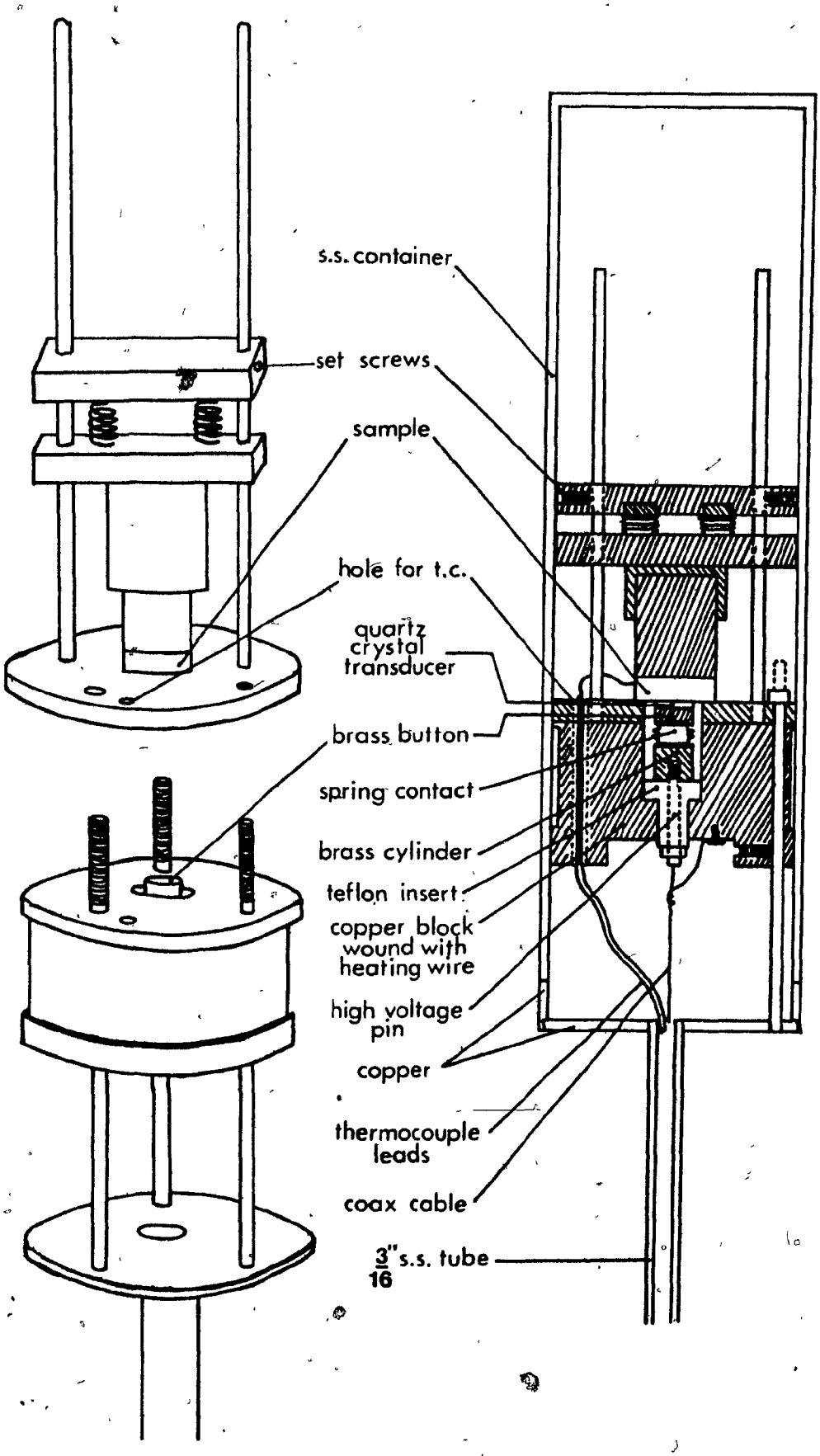
s.s. container
set screws
sample
hole for t.c.
quartz crystal transducer
brass button
spring contact
brass cylinder
teflon insert
copper block wound with heating wire
high voltage pin
copper
thermocouple leads
coax cable
3/16" s.s. tube

FIGURE III-3

LOW TEMPERATURE CELL (FREQUENCY RANGE 15 - 25 MHz)
IN PLACE IN SPECIAL DEWAR.

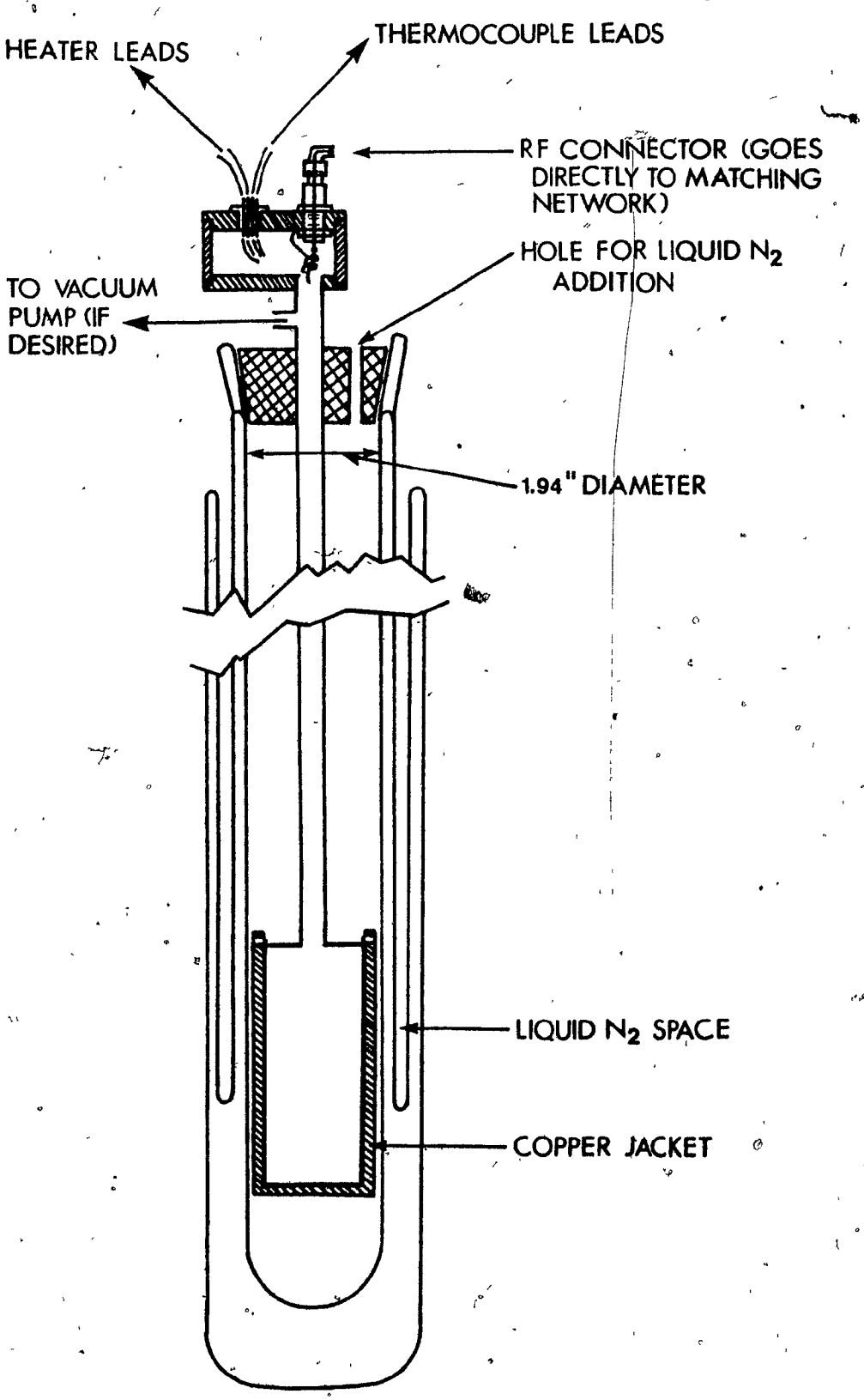
HEATER LEADS
THERMOCOUPLE LEADS
RF CONNECTOR (GOES DIRECTLY TO MATCHING NETWORK)
HOLE FOR LIQUID N_2 ADDITION
TO VACUUM PUMP (IF DESIRED)
1.94" DIAMETER
LIQUID N_2 SPACE
COPPER JACKET

III MODE OF OPERATION

A: SAMPLE PREPARATION:

Samples, which are cylindrical in shape, may be prepared by the compression molding technique. They must be free of air bubbles and imperfections which would absorb and scatter ultrasonic waves. Impurities also contribute to ultrasonic absorption at specific temperatures and frequencies.

1. Optimum Dimensions:

The sample diameter must be sufficiently greater than the transducer diameter to minimize the effects of beam spread. Beam spread increases as frequency and transducer diameter decrease.[III-2] Consequently larger diameter transducers are used at lower frequencies.

The thickness must be large enough so that consecutive echoes do not overlap and therefore interfere with each other. However, too large a thickness will result in fewer observable echoes, reducing accuracy in the velocity and tan δ calculations. There exists an optimum thickness depending on the pulse width used ($\sim$2 μsec) and on the attenuation coefficient (db/cm).

Opposite sample faces must be parallel to within a tenth of a wavelength to minimize wave cancellation (which causes too

high tan δ's). For the polymeric materials studied, the wavelength varies from ~0.01 cm at 25 MHz to ~0.25 cm at 1 MHz, so parallelisms better than 0.001 cm are necessary. The parallelism can be obtained by measuring the sample thickness at many points using a narrow bore micrometer and it may be improved by sanding or machining, if necessary.

Recommended sample and quartz transducer dimensions have been given.[III-3] In practice, however, these requirements cannot always be met, and acceptable results have been achieved using the dimensions listed below in Table III-1.

TABLE III-1. SAMPLE AND TRANSDUCER DIMENSIONS USED IN PULSE ECHO EXPERIMENTS (PULSE WIDTH ~2.0 μSEC).

Transducer Frequency (MHz)	Transducer Type	Transducer (Element) Diameter (")	Sample Diameter (Inch)	Sample Thickness (cm)	Sample Parallelism (cm)
15-25	X-Cut Quartz	0.25	0.5	0.42-0.54	±0.0005-0.001
2.25*	Ceramic-Mounted	0.312	0.75	0.6265	±0.0005
1	Ceramic-Mounted	0.75	1.375	1.243	±0.001

* also operated at overtone frequencies

2. Electrode:

Samples to be tested with unplated quartz transducers (15 - 25 MHz) must have a grounding electrode on the face which is against the transducer. A simple technique of glueing an aluminum foil electrode (0.001" thick) to the sample with epoxy glue was adopted. A smooth flawless electrode is essential and obtainable in the following way:

a) Place a smooth piece of aluminum foil on a hard flat surface, such as a glass slide.

b) Prepare an excess of epoxy cement, mixing 50% resin and 50% hardener, and spread thickly on one spot on the aluminum foil. (Use epoxy with three hour hardening time.)

c) Press the sample firmly face-down onto the glue. Then transfer carefully (slide and all) into a clamp (such as the sample holder of the low temperature cell) and tighten securely.

d) Allow the glue to harden overnight (in a desiccator if the sample is sensitive to moisture). Then remove it from the clamp and cut away excess foil and glue with scissors.

The result is a thin uniform glued layer about 0.005 cm thick (glue and electrode) which will not break at temperatures down to -200°C. Tests were done comparing such an electrode with vacuum evaporated and pressed-on aluminum electrodes, using poly (ethyl methacrylate) samples (Figure III-4). No significant differences were observed.

FIGURE III-4

COMPARISON OF ULTRASONIC DATA FOR POLY (ETHYL METHACRYLATE) SAMPLES WITH VARIOUS ELECTRODE TYPES AND BONDING AGENTS, AT 13.5 MHz.

	Electrode type	Sample-to-transducer bond	Test Pressure
○	evaporated aluminum	epoxy cement	0.4 mm Hg
△	glued aluminum	rubber cement	1 atm.
□	pressed aluminum	silicone oil	0.4 mm Hg

T (°C)	tan δ x10^2	T (°C)	tan δ x10^2	T (°C)	tan δ x10^2
39.	1.19	25.	1.09	32.5	1.00
36.	1.17	5.	0.76	24.	1.06
23.	1.11	-2.	0.74	4.	0.82
18.	0.91	-9.	0.69	-5.	0.70
13.	0.84	-13.5	0.70	-23.	0.59
3.5	0.77	-19.	0.64	-41.5	0.69
		-19.5	0.57		
		-26.	0.63		
		-37.	0.64		
		-40.	0.64		
		-44.	0.63$_5$		

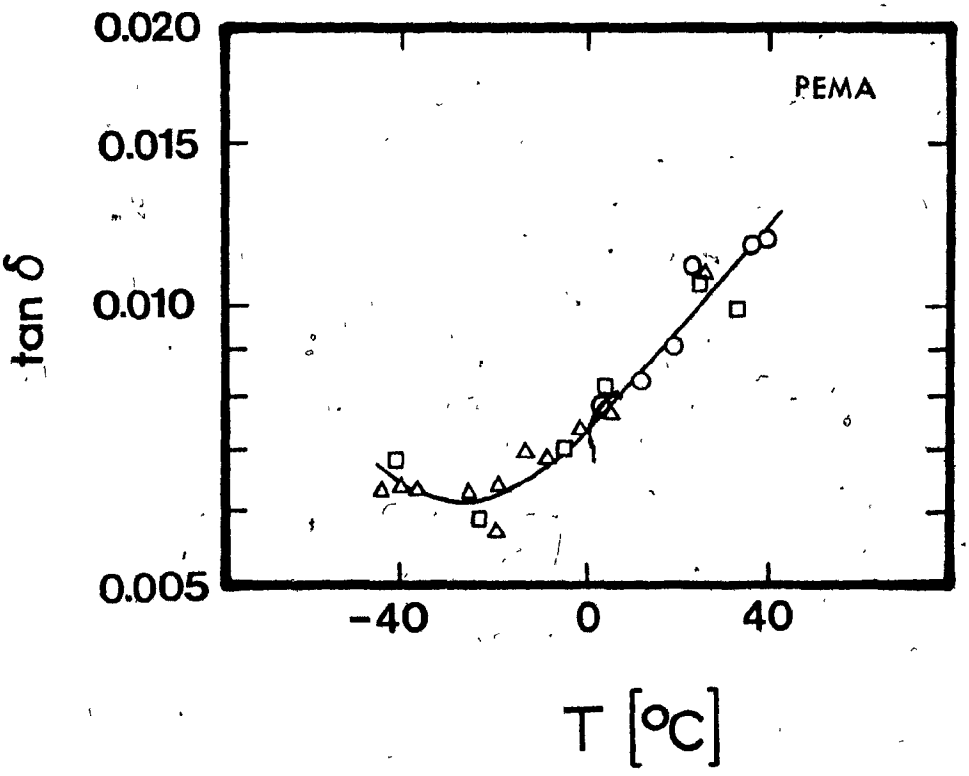
0.020
0.015
0.010
0.005
tan δ
PEMA
-40
0
40
T [°C]

An electrode is not needed on samples to be tested with the Automation mounted transducers, which contain their own ground.

3. Thermocouple Positioning:

A small hemispherical indentation ($\frac{1}{32}$ to $\frac{1}{16}$ inch diameter) carefully drilled into the side edge of the sample, may be used to accommodate the tip of a fine copper-constantan thermocouple. This technique would not be usable with very brittle samples which may crack.

4. Storage:

Samples with a tendency to absorb moisture should be stored in a dry environment - e.g. over drierite (anhydrous $CaSO_4$).

B: BONDING AGENT SELECTION:

The medium used to bond the transducer to the sample is critical and must be carefully selected according to the temperature region to be studied. Bateman[III-4] has stated that "it is desirable to obtain the thinnest possible bond that will adhere to both transducer and specimen over the largest temperature range". In a note on low viscosity liquids, Matheson[III-5] claims that the "best bonds are formed by liquids which supercool in the bulk to form stable glasses". Some properties of four

very useful bonding agents used in conjunction with the apparatus described here (for longitudinal waves) are summarized in Table III-2 below.

TABLE III-2. SOME PROPERTIES OF SELECTED ULTRASONIC BONDING AGENTS.

Bonding Agent		Temp. Range Achieved (°C)	Notes	Ref. #
General Type	Name			
High viscosity liquids	Nonaq grease	-131 to +57	Easy to handle and compatible with many materials; background losses of 0.5 db/reflection are common	III-4
	DC200 silicone oil	-128 to +45	Can form thinner bond than nonaq	III-4
Low viscosity liquids	3-phenyl propyl chloride	-188 to +25	Forms low temperature glass (Tg = 147°K); scatter in data is considerable around room temperature.	III-5
	3-phenyl-1-propanol	-157 to +28	Forms low temperature glass (Tg = 176°K).	III-5

C: CELL ASSEMBLY:

1. Operation with Quartz Crystal Transducers:

The sample in place in the cell has been shown in Figure III-2 Steps to be taken in assembling this cell are as follows:

a) Clean the electrode surface of the sample if necessary, using a cotton swab wetted with a suitable solvent (e.g. ethanol). Care must be taken that solvent does not contact the polymer.

b) Place the sample in the holder with the electrode side toward the circular opening in the holder plate. Center the sample and position it so that the thermocouple indentation is aligned with the thermocouple hole in the holder plate. Manually compress the springs as tightly as possible, to secure the sample, and tighten the two set screws. Place the holder in a suitable stand with the sample's electrode side up.

c) Apply the quartz transducer as follows:

i) Remove the transducer to be used from storage in acid-dichromate cleaning solution using plastic-coated forceps and rinse with distilled water. Gently dry the crystal with a cotton swab.

ii) With the tip of a pin, place a drop of bonding agent near the center of the sample's electrode surface which is visible through the hole in the holder plate.

Note: There must be sufficient bonding agent to bond

over the entire face of the transducer, but not enough to give spreading to both sides of the transducer (which results in ultrasonic pulses traveling into the brass button as well as the sample, producing erratic results). For nonaq grease bonds, a $\frac{1}{32}$" diameter drop has been found appropriate.

iii) Place the crystal gently onto the drop of bonding agent, again using the plastic coated forceps. Then press it down firmly with a cotton swab to spread the bonding liquid, making sure that the crystal is well centered.

d) Position the gold-plated spring contact (Servometer Company part # 2023) and the brass button as shown in Figure III-2, so that they are well centered. Then invert the sample holder (with the transducer now attached to the sample) and fit it carefully onto the copper block, matching the thermocouple holes in each. Tighten the nuts firmly around the three pins, and position the thermocouple, bending it so that the tip touches the sample wall at the indentation.

Note: At this point, it may be advisable to check if any bonding liquid has spread to the brass button side of the transducer, and, if it has, to remove the excess.

e) Invert the assembled cell and slide it into the copper/stainless steel cell container (which may contain some drierite to maintain dry conditions). Then install the outer copper container tightening the three screws at the top, as shown in Figure III-3.

Note: For vacuum operation, the inner container must be soldered shut using soft solder.

f) Finally, place the entire assembly into the dewar vessel and make the appropriate electrical connections (Figure III-3).

2. Operation with Automation Industries Mounted Ceramic Transducers:

Clamp the sample (which requires no electrode) firmly against the transducer, using an excess of bonding liquid. The sample holder described above may be employed as a clamp. Install a thermocouple and the appropriate coaxial cable and place the assembly into a wide dewar vessel. An aluminum foil container partly filled with drying agent, may be fashioned about the sample/transducer assembly.

D. MEASUREMENT PROCEDURE:

1. Setting up the Electronics:

a) Turn on the Pulse Generator (first main power, then high voltage) and the Oscilloscope.

Note: The scope sweep may not function immediately, producing a very bright spot on the screen. When this happens, turn down the beam intensity to avoid damaging the phosphor on the face of the CRT.

b) Adjust scale settings as described in the instrumental section.

Note: For a delay time scale of 2 μsec/cm, the signal vanishes if the delay time multiplier is close to zero. It is

necessary to start each set of readings with the multiplier dial at (say) 0.10. No such problem exists with the 5 μsec/cm delay time scale, which can be set initially to zero.

c) Once a scope trace has been obtained, set the frequency approximately to resonance using the R.F tuning and range knobs. The detector filter must be on "1" or "2" for frequencies less than or greater than 3 MHz respectively. Finally adjust the RF tuning and the impedance matching network setting so as to achieve the best ultrasonic echo train - as characterized by sharp, symmetric peaks of maximum amplitude which follow a uniform exponential decay.

Note: The matching network may not be needed with the 25 MHz quartz transducer.

The test frequency can be obtained from the RF dial setting using the calibration tables; this frequency is not normally changed during an ultrasonic test. The pulse width is also kept constant at ∿2 μsec, but it may occasionally have to be increased slightly to remove any instability of the trace.

There is also a problem of instrument recovery from the high voltage initiating pulse, which can cause interference with the first ultrasonic echo. If this echo is not exponential with respect to the others, it should be omitted from the calculations.

2. Taking a Set of db/time Readings:

a) Record the initial temperature.

b) Set the delay time multiplier to zero (0.10 for the 2 μsec/cm scale). Then use horizontal position knob to bring the first ultrasonic peak to be measured into coincidence with the center vertical line on the oscilloscope graticule. (This can be done visually, minimizing parallax by sighting past a mark on the scope viewing hood.)

c) Bring the peak to a predetermined height (say 4 cm for a vertical scale of 2 volts/cm) using the stepped attenuator, and record the attenuator reading in db.

d) Center the next ultrasonic peak on the scope using the delay time multiplier and bring it to the predetermined voltage level using the attenuator. Record the delay time and db readings.

e) Continue this procedure for as many peaks as is practical (say five peaks for polymeric samples with tan $\delta \lesssim 0.01$, tested at $\sim$15 MHz). The amount of noise present and the temperature change during the measurements also determine the number of peaks to be measured.

f) Record the final temperature.

FIGURE III-5

GASEOUS NITROGEN COOLING SYSTEM

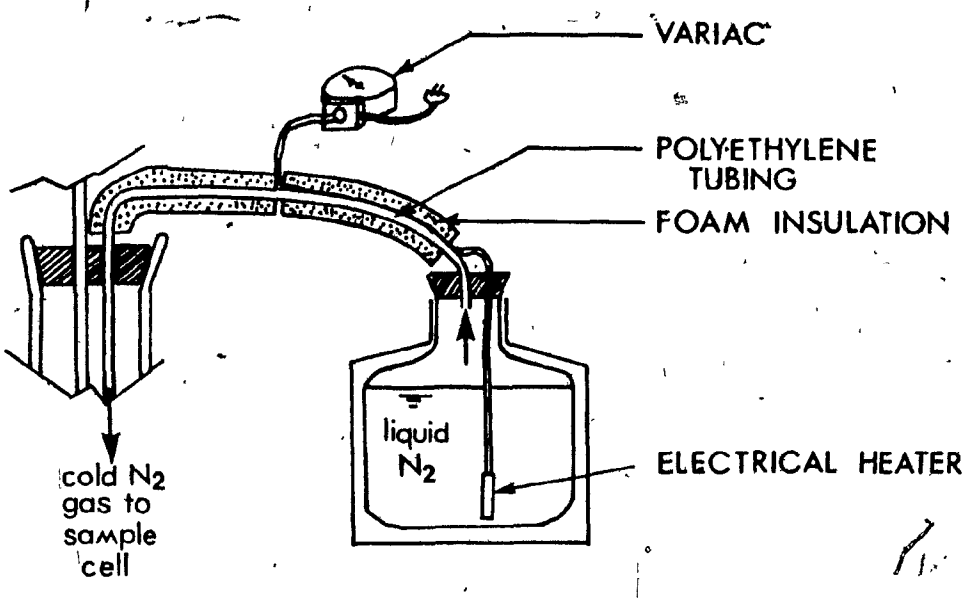
VARIAC
POLYETHYLENE TUBING
FOAM INSULATION
liquid N_2
ELECTRICAL HEATER
cold N_2 gas to sample cell

3. Cool-Down and Warm-Up Procedures:

Readings are taken as a function of temperature during cooling or warming. Cooling is achieved either by direct addition to the dewar of small amounts of liquid nitrogen or by directing a stream of cold gaseous nitrogen onto the sample cell. The latter technique permits a more uniform cooling rate but cannot achieve very low temperatures due to limitations of the transfer system used (shown in Figure III-5).

A warming run may also be done by first cooling directly (at, say, 100°C/hour) to the lowest temperature desired (taking care not to break the sample-to-transducer bond) and then reheating with the sample cell heater (40 Ω, constantan thermocouple wire). The variac setting for this latter heater should not exceed ~20 volts to prevent burning the heating wire. This useful technique can give a very uniform warming rate.

Note: In cooling and warming tests of this nature, sample temperature may lag behind the thermocouple temperature, to an extent which depends on the cooling or warming rate.

IV RESULTS AND CALCULATIONS

A: THEORY: III-6a, b

Ultrasonic intensity I decays exponentially with distance x in a solid due to dissipative mechanisms (such as molecular motion):

$$I = I_o e^{-2\alpha x}, \qquad \ldots \text{(III-1)}$$

where α is the attenuation coefficient with units of nepers/unit distance in the direction of propagation and I_o is the intensity at $x = o$. Figure III-6 illustrates this relation with respect to the pulse echo experiment.

Since the range of intensities is very large, a logarithmic scale - the decibel or db scale - is generally used, where

$$db = 10 \log \left(\frac{I}{I_o}\right) = -8.68\alpha x. \qquad \ldots \text{(III-2)}$$

FIGURE III-6

EXPONENTIAL DECAY OF SOUND INTENSITY IN A SOLID. THE SINGLE CRYSTAL PULSE ECHO EXPERIMENT CONSISTS OF COUPLING AN INITIAL PULSE INTO THE SAMPLE (AT X = 0) AND OBSERVING THE ECHOES CORRESPONDING TO 'ROUND TRIPS' THROUGH THE SAMPLE (AT X = 2t, 4t, ..., WHERE t IS THE SAMPLE THICKNESS). INSERT SHOWS RF NATURE OF DECAY.

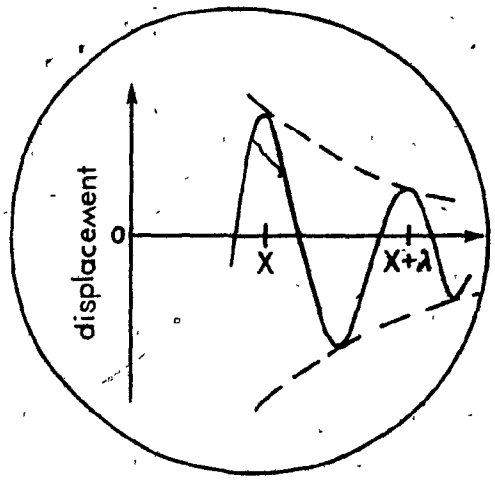
displacement
0
X
X+λ

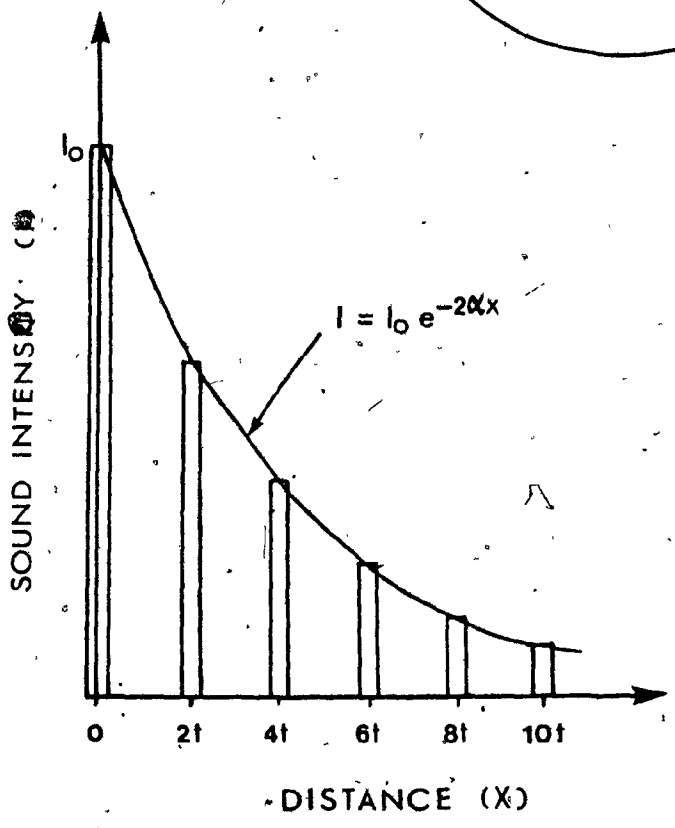
I_o
$I = I_o e^{-2\alpha x}$
SOUND INTENSITY
0
2t
4t
6t
8t
10t
DISTANCE (X)

Derivation of tan δ:

$$\frac{\Delta W}{W_{st.}} = \frac{\text{Energy dissipated in one cycle}}{\text{Energy stored}} \quad \ldots(\text{III-3})$$

$$= \frac{I(x) - I(x+\lambda)}{I(x)}, \text{ where } \lambda \text{ is the ultrasonic wavelength (Figure III-6)} \quad \ldots (\text{III-4})$$

$$\approx \frac{e^{-2\alpha x} - e^{-2\alpha(x+\lambda)}}{e^{-2\alpha x}} \quad \ldots (\text{III-5})$$

$$\approx 1 - e^{-2\alpha\lambda} \quad \ldots (\text{III-6})$$

$$\approx 2\alpha\lambda \text{ for } (\alpha\lambda) << 1 \quad \ldots (\text{III-7})$$

$$\text{loss tangent } \tan\delta = \frac{1}{2\pi}\frac{\Delta W}{W_{st.}} \quad \ldots (\text{III-8})$$

$$= \frac{\alpha\lambda}{\pi} \quad (\alpha\lambda << 1) \quad \ldots (\text{III-9})$$

Substituting for $\lambda = v/f$

where v and f are sound velocity and frequency respectively, yields:

$$\tan\delta = \frac{\alpha v}{\pi f} = \frac{1}{\pi f}\left[\frac{\Delta(db)}{8.68\Delta x}\right]\left[\frac{\Delta x}{\Delta t'}\right] = \frac{1}{8.68\pi f}\left[\frac{\Delta(db)}{\Delta t'}\right] \quad \ldots (\text{III-10})$$

$$\therefore \tan\delta \simeq \frac{0.0367}{f}\frac{\Delta(db)}{\Delta t'} \quad \ldots (\text{III-11})$$

which is a form suitable for the pulse echo experiment. (Note that, in this derivation, t' refers to time.)

Real and Imaginary Young's Moduli:

Real Young's Modulus: $E' = \rho v^2$ ... (III-12)

where ρ is the density of the medium.

Imaginary Young's Modulus: $E'' = (\tan \delta)\, E'$ ... (III-13)

E' (the in-phase stress/strain) is related to energy stored by the medium, while E'' (the out-of-phase stress/strain) is related to energy dissipated.

B: RESULTS:

Figures III-7a and III-7b show attenuation versus time and time versus distance respectively for a poly (ethyl methacrylate) sample at 24°C and 13.5 MHz. The slope of the upper curve $(\frac{\Delta db}{\Delta t'})$ yields a tan δ = 0.0106. The slope of the lower curve (proportional to $\frac{\Delta t'}{\Delta x}$) permits calculation of the speed of sound. The slopes and standard deviations are calculated by the least squares fitting technique.[III-7] A complete experiment consists of obtaining such data as a function of temperature, so that curves of tan δ and velocity versus temperature are established. Peaks in tan δ and inflections in the velocity (proportional to $\sqrt{E'}$) can then be correlated with molecular mechanisms of energy dissipation.

Single Peak Measurement:

Plots of attenuation level (db) for a single RF echo, as a function of temperature, can exhibit local minima which may be interpreted in terms of molecular motion. This technique would be especially

FIGURE III-7A & B

ULTRASONIC RESULTS

A: ULTRASONIC ATTENUATION VERSUS TIME FOR POLY (ETHYL METHACRYLATE) AT 24°C AND 13.5 MHz. THE SLOPE YIELDS A TAN δ = 0.0106.

B: TIME VERSUS DISTANCE FOR POLY (ETHYL METHACRYLATE) AT 24°C AND 13.5 MHz. (1 ROUND TRIP ≡ 0.544 cm).

Peak #	Time (μsec x 1/2)	db level
1	0.10	45.5
2	1.42	37.
3	2.72	25.
4	3.96	15.
5	5.14	7.

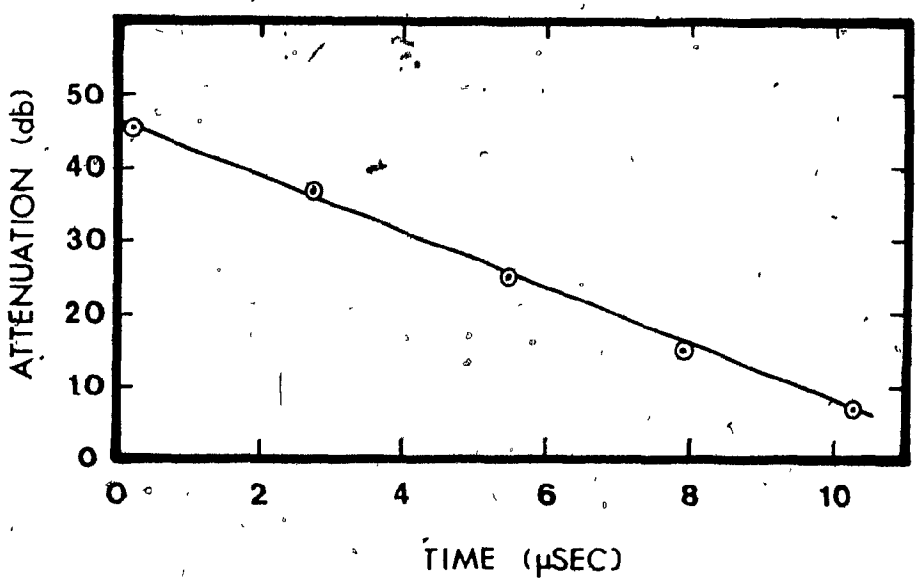
ATTENUATION (db)
50
40
30
20
10
0
0
2
4
6
8
10
TIME (μSEC)

A

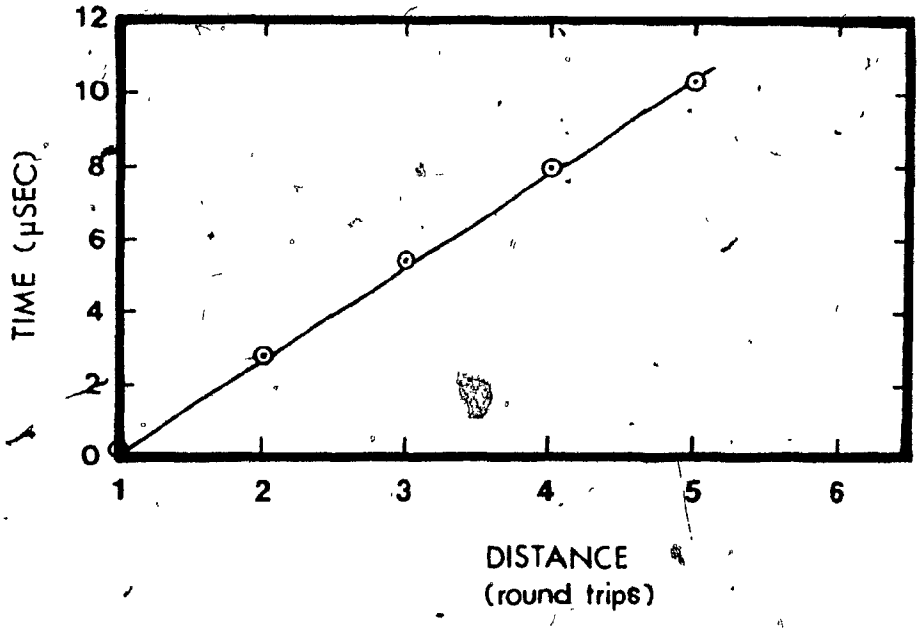
TIME (μSEC)
12
10
8
6
4
2
0
1
2
3
4
5
6
DISTANCE
(round trips)

B

useful when only one echo is observable, as in high loss materials or higher frequency tests. Here, the initiating pulse frequency, width and amplitude must be constant throughout the test and transducer behavior must not change much with temperature. Interpretation of any db vs temperature minima found must still be done with great care - perhaps only in cases where positions of molecular motion are already indicated by previous experiments at other frequencies.

C. CALCULATIONS:

A computer program has been developed to calculate tan δ, speed of sound, and standard deviations in each of these quantities from ultrasonic data on two or more echoes. A least squares fit[III-7] is first applied to the db versus time data, and tan δ together with its standard deviation is calculated. Then time versus distance data is fitted for the same echo train, yielding the velocity and its standard deviation.

The calculations are summarized as follows:

Least squares fit: For n values of y as a f (x), assuming that x values are precise and that all uncertainty is contained in the y-values, whose weights are all equal,

$$y = Ax + B \qquad \text{... (III-14)}$$

where

$$A = \frac{n \Sigma (x_i y_i) - \Sigma x_i \Sigma y_i}{n \Sigma x_i^2 - (\Sigma x_i)^2} \qquad \text{...(III-15)}$$

and $$B = \frac{\Sigma x_i^2 \, \Sigma y_i - \Sigma x_i \Sigma (x_i y_i)}{n\Sigma x_i^2 - (\Sigma x_i)^2} \quad \ldots \text{(III-16)}$$

The standard deviation of Δy values (where $\Delta y_i = y_i - (Ax_i + B)$) is:

$$Sy = \sqrt{\frac{\Sigma(\Delta y_i)^2}{n-2}} \quad \ldots \text{(III-17)}$$

and the standard deviation of the slope is:

$$S_A = Sy \sqrt{\frac{n}{n\Sigma x_i^2 - (\Sigma x_i)^2}} \quad \ldots \text{(III-18)}$$

The calculations of tan δ, standard deviation in tan δ and speed of sound are all straight forward.

However, velocity $v \alpha \frac{1}{A_2}$ (where A_2 denotes slope of time vs distance data) ... (III-19)

$$\therefore \Delta v \alpha \frac{1}{A_2^2} \Delta A_2 \quad \ldots \text{(III-20)}$$

$$\text{i.e. } \Delta v \alpha v^2 \Delta A_2 \quad \ldots \text{(III-21)}$$

so that the calculation of standard deviation for the velocity involves not only the standard deviation of the slope, but also the square of the velocity itself and a constant factor.

The ultrasonic computer program (Fortran-level Watfiv) is reproduced below. Here the variables T, TAND, SDTAND, VEL, and SDVEL represent the temperature, tan δ, standard deviation in tan δ, velocity, and standard deviation in the velocity respectively.

```
C PROGRAMME TO COMPUTE LEAST SQUARES FIT TO ULTRASONIC DATA -
C X IS TIME (USEC*1/2)† AND Y IS ATTENUATION IN DB FOR TAN DELTA CALCULATION
C THEN TIMES ARE REASSIGNED TO Y'S FOR VELOCITY CALCULATION
C DATA CARDS- FIRST IS # OF RUNS, NEXT IS # OF CARDS OF DATA FOR FIRST RUN + FREQ
C OF RUN (MHZ) + WIDTH OF SAMPLE (CM) + TIME SCALE.† EACH DATA CARD HAS TEMP(C)+
C # OF PEAKS + TIME FOLLOWED BY DB FOR THE PEAKS IN ORDER. THEN CARDS FOR THE
C SECOND RUN. ETC.

      DIMENSION X(10),Y(10),V(10),TMULT(10)
      READ,NRUN
      NRUNC=0
400   NCC=0
      READ,NC,FREQ,W,TIMESC
      DO 45 I=1,6
45    TMULT(I)=1./TIMESC
      NRUNC=NRUNC+1
      WRITE(6,5)NRUNC,FREQ
5     FORMAT(1H1,'RUN # ',I2,5X,'FREQUENCY = ',F5.2,' MHZ')
      WRITE(6,40)
40    FORMAT(1HO,'  TEMP   TAN D  STD DEV   VEL   STD DEV    #      T1
     1DB1       T2  DB2       T3  DB3       T4  DB4       T5  DB5
     2T6  DB6')
      WRITE(6,42)(TMULT(I),I=1,6)
42    FORMAT(1H+,46X,F3.1,    5(11X, F3.1))
      WRITE(6,41)
41    FORMAT(1H ,'    (C)          (TAN D) (CM/US)   (VEL)    PTS (USEC)
     1      (USEC)       (USEC)         (USEC)       (USEC)')
11    READ,T,N,(X(K),Y(K),K=1,N)
      NSUB=0
      NCC=NCC+1
13    SUMX=0.0
      SUMY=0.0
      SUMX2=0.0
      SUMXY=0.0
      DO 12 K=1,N
      SUMX=SUMX+X(K)
      SUMY=SUMY+Y(K)
      SUMX2=SUMX2+X(K)*X(K)
12    SUMXY=SUMXY+X(K)*Y(K)
      XN=FLOAT(N)
      A=(SUMXY-(SUMX*SUMY)/XN)/(SUMX2-SUMX*SUMX/XN)
      B=(SUMX*SUMXY-SUMY*SUMX2)/(SUMX*SUMX-XN*SUMX2)
      SUM=0.0
      DO1I=1,N
      V(I)=(Y(I)-(A*X(I)+B))**2
1     SUM=SUM+V(I)
      STDDEV=0.
```

```
      IF(N.EQ.2)GOTO35
      STDY=SQRT(SUM/FLOAT(N-2))
      STDDEV=STDY*(SQRT(XN/(XN*SUMX2-SUMX**2)))
35    NSUB=NSUB+1
      IF(NSUB.NE.1)GOTO55
      FACTOR=.0367/FREQ
      TAND=(-1.)*FACTOR*A*TMULT(1)
      SDTAND=FACTOR*STDDEV*TMULT(1)
      WRITE(6,50)T,TAND,SDTAND,N,(X(K),Y(K),K=1,N)
50    FORMAT(1HO,F7.1,2F8.5,16X,I5,1X,12F7.3)
      DO21J=1,N
      Y(J)=X(J)
21    X(J)=FLOAT(J-1)
      GOTO13
55    VEL=(W/A)*2.*TMULT(1)
      SDVEL=STDDEV*VEL**2/(2.*W*TMULT(1))
      WRITE(6,51)VEL,SDVEL
51    FORMAT(1H+,23X,2F8.5)
      IF(NCC.NE.NC)GOTO11
      IF(NRUNC.NE.NRUN)GOTO400
      STOP
      END
```

† for X as time in μsec x $\frac{1}{2}$, enter the timescale (denoted TIMESC) as 2. X may also be time in μsec x 1/5, corresponding to TIMESC = 5.

V REFERENCES

III-1 D.Y. Chung, Rev. Sci. Instrum. 42, 878 (71).

III-2 Automation Industries Report # TR 67-4, Ultrasonic Search Units, p. 18 (67).

III-3 Valpey-Fisher Corporation, An Introduction to Piezoelectric Transducers, p. 11 (72).

III-4 T.B. Bateman, J. Acoust. Soc. Amer. 41, 1011 (67).

III-5 A.J. Matheson, J. Phys. E. 4, 796 (71).

III-6a H.F. Olson, Elements of Acoustical Engineering (Van Nostrand, New York, 1947).

III-6b N.G. McCrum, B.E. Read, and G. Williams, Anelastic and Dielectric Effects in Polymeric Solids (John Wiley, New York, 1967).

III-7 D.C. Baird, Experimentation: An Introduction to Measurement Theory and Experiment Design, (Prentice Hall, New Jersey, 1962) pp. 138 and 186.

APPENDIX IV

VIBRATING REED GRAPHICAL AND NUMERICAL DATA FOR FREE-RADICAL PMMA-H_8 AND PMMA-D_8 AT VARIOUS TEST FREQUENCIES (for Figures not shown in the text.)

Vibrating reed graphical data in support of results cited in Tables 2 and 3 of the text for free-radically prepared PMMA-H_8 and PMMA-D_8 respectively are given in this section to avoid repetition in the text. Experimental curves of E' and $\tan\delta$ as a function of temperature are reported along with the corresponding numerical data. Initial and final values of resonance frequency are given for each experiment, so that the constant factor relating f_o^2 and E' (and therefore the f_o value for any experimental point) may be calculated, if desired.

INDEX : VIBRATING REED GRAPHICAL AND NUMERICAL DATA.

(see also Figures 14 and 15 of the text.)

FIGURE IV-1

PMMA-H_8 : VIBRATING REED RESULTS AT ~230 HZ. A° γ_2 relaxation is present at -200.5°C and 225.3 Hz. (f_o varied from 225.58 Hz at -205.7°C to 224.14 Hz at -173.2°C.)

T (°C)	E'x10^{-10} (dynes/cm^2)
-205.7	8.2741
-205.0	8.2727
-204.2	8.2705
-203.7	8.2683
-203.2	8.2646
-202.1	8.2661
-201.3	8.2587
-201.0	8.2609
-200.1	8.2492
-198.9	8.2448
-197.8	8.2441
-196.6	8.2389
-195.6	8.2309
-193.8	8.2324
-192.6	8.2236
-192.0	8.2287
-190.7	8.2177
-190.3	8.2214
-189.1	8.2141
-188.0	8.2104
-186.7	8.2038
-185.8	8.2053
-184.4	8.1907
-183.7	8.1900
-182.5	8.1944
-181.4	8.1936
-180.5	8.1965
-179.2	8.1907
-177.0	8.1819
-175.5	8.1688
-174.1	8.1666
-173.2	8.1688

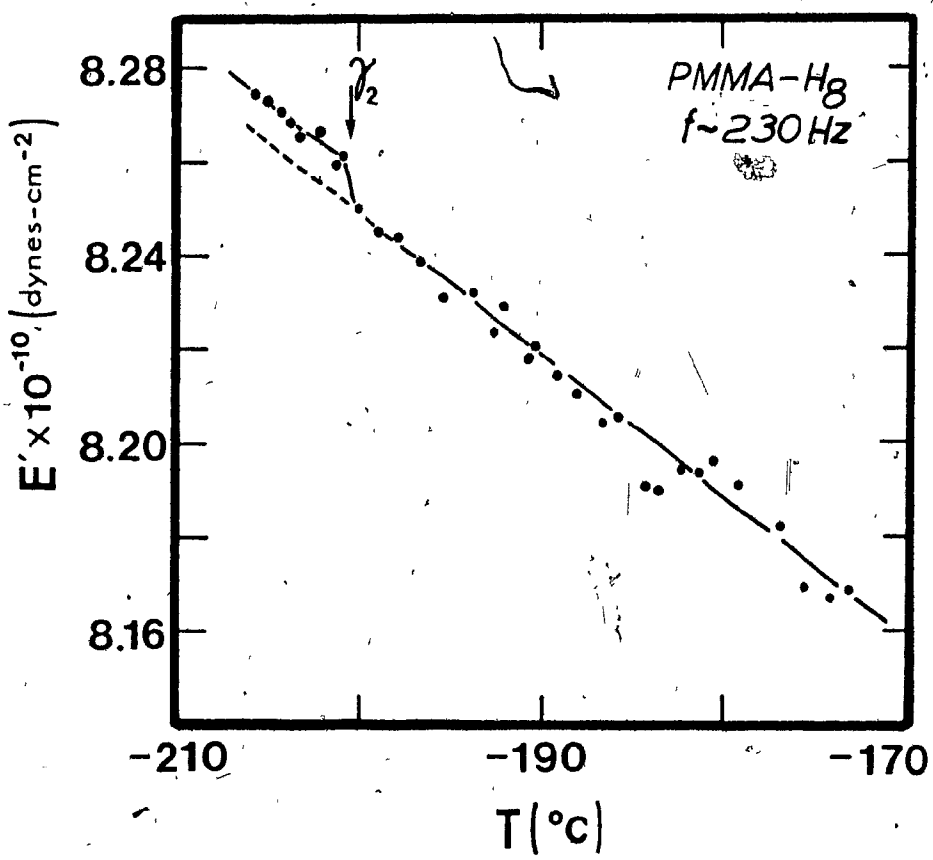
8.28
8.24
8.20
8.16
E' x 10^-10 (dynes-cm^-2)
γ2
PMMA-H8
f~230 Hz
-210
-190
-170
T(°C)

FIGURE IV-2

PMMA-H_8 : VIBRATING REED RESULTS AT ~275 HZ. The γ_1 relaxation is present at -162° and 274 Hz. (f_o varied from 275.43 Hz at -183.3°C to 271.55 Hz at -141.7°C.)

T (°C)	E'x10^{-10} (dynes/cm^2)
-183.3	7.6924
-182.3	7.6952
-176.8	7.6667
-173.0	7.6455
-170.2	7.6338
-168.5	7.6272
-166.8	7.6194
-164.6	7.6077
-162.8	7.6022
-160.9	7.5849
-158.8	7.5750
-156.5	7.5639
-154.6	7.5550
-150.2	7.5318
-146.1	7.5053
-141.7	7.4772

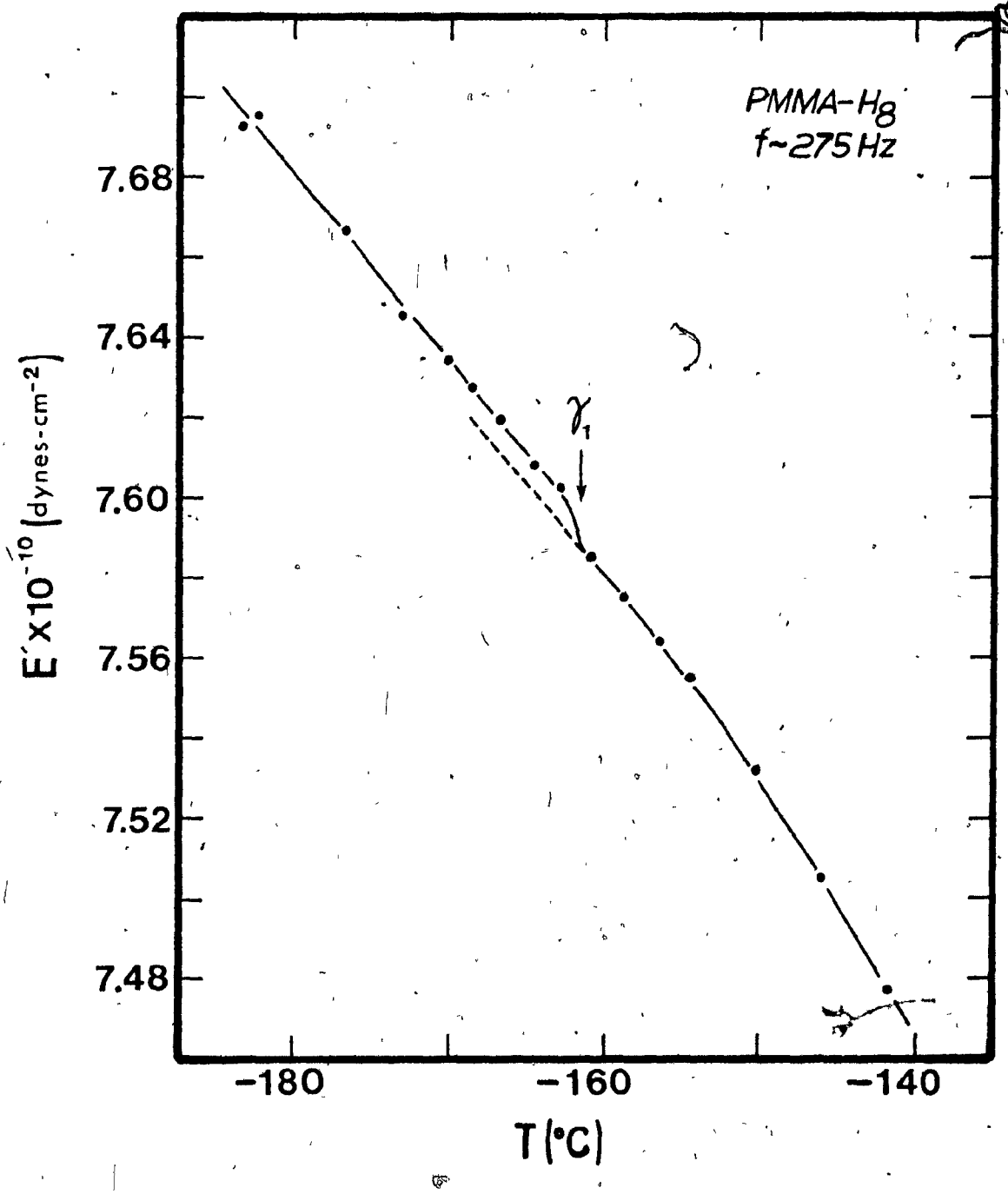
PMMA-H8
f~275 Hz
7.68
7.64
7.60
7.56
7.52
7.48
E' X10^-10 (dynes-cm^-2)
γ1
-180
-160
-140
T(°C)

FIGURE IV-3

PMMA-H_8 : VIBRATING REED RESULTS AT ~275 Hz. The γ_2 relaxation is present at -198°C and 277 Hz. (f_o varied from 277.6 Hz at -202.4°C to 274.55 Hz at -165.8°C.)

T (°C)	$\tan\delta$ x10^3
-202.4	2.60
-200.0	2.63
-199.8	2.71
-197.0	2.67
-195.3	2.65
-193.5	2.60
-192.3	2.57
-190.2	2.58
-189.2	2.57
-186.7	2.63
-182.7	2.68
-179.7	2.79
-176.7	2.88
-173.5	3.00
-172.0	3.08
-170.5	3.18
-169.0	3.25
-167.3	3.41
-165.8	3.52

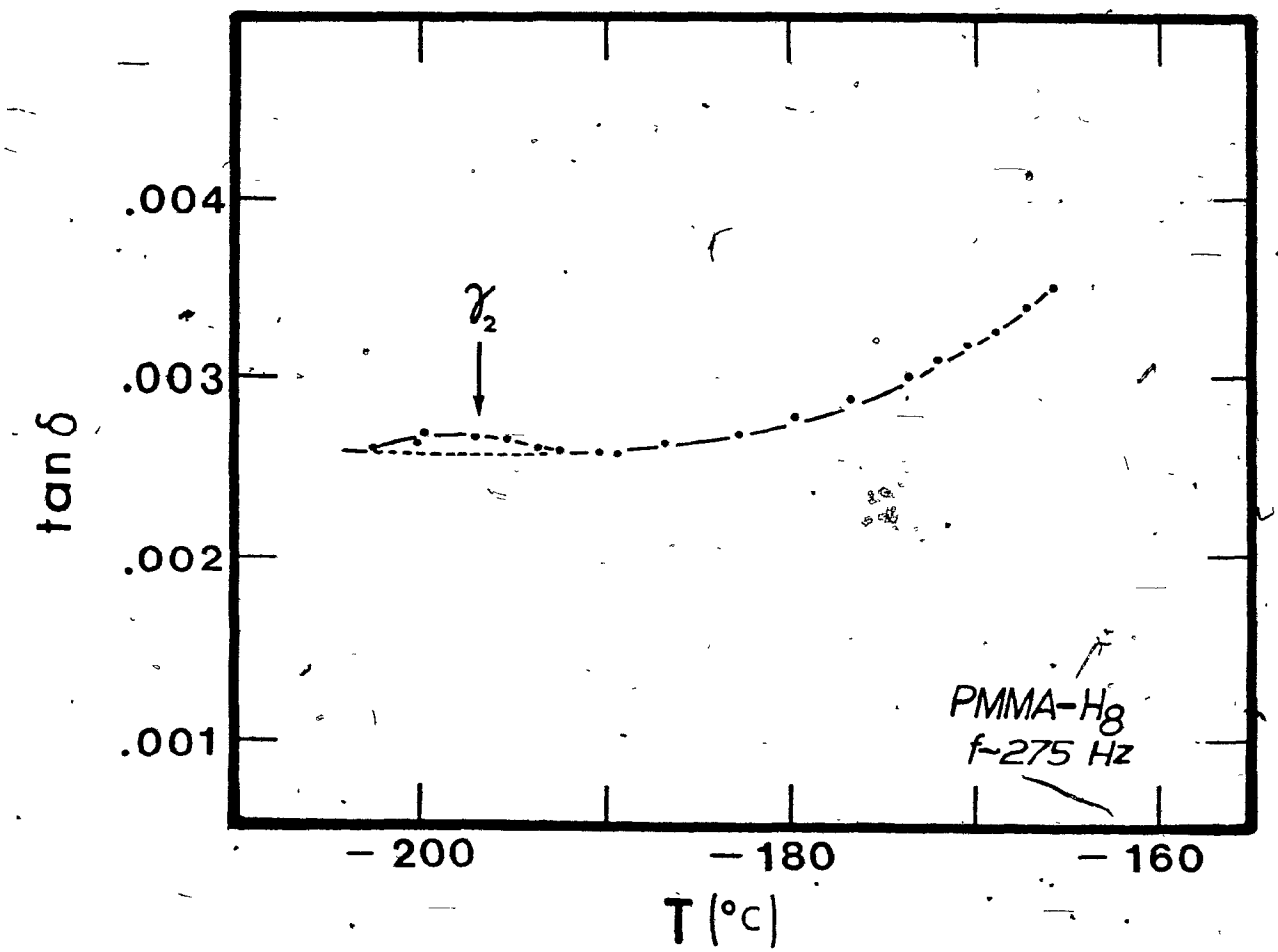
.004
.003
.002
.001
tan δ
γ2
PMMA-H8
f~275 Hz
−200
−180
−160
T (°C)

FIGURE IV-4

PMMA-H_8 : VIBRATING REED RESULTS AT ~295 HZ. The γ_2 relaxation is present at -196.5°C and 295.3 Hz. (f_o varied from 295.64 Hz at -200.2°C to 293.27 Hz at -171.4°C.)

T (°C)	E'x10^{-10}(dynes/cm^2)	T (°C)	E'x10^{-10}(dynes/cm^2)
-200.2	7.3392	-190.9	7.3001
-199.1	7.3338	-189.5	7.2931
-197.8	7.3308	-188.7	7.2897
-197.4	7.3293	-186.9	7.2832
-196.1	7.3204	-184.1	7.2733
-195.1	7.3164	-180.2	7.2580
-194.7	7.3154	-177.9	7.2506
-193.4	7.3080	-176.0	7.2408
-192.6	7.3040	-171.4	7.2220
-191.5	7.3030		

FIGURE IV-5

PMMA-H_8 : VIBRATING REED RESULTS AT ~495 HZ. The γ_1 relaxation is present at -167.5°C and 496 Hz. (f_o varied from 497.04 Hz at -177.0°C to 493.29 Hz at -138.7°C.)

T (°C)	E'x10^{-10} (dynes/cm^2)	T (°C)	E'x10^{-10} (dynes/cm^2)	T (°C)	E'x10^{-10} (dynes/cm^2)
-177.0	6.7124	-163.3	6.6838	-153.8	6.6577
-176.5	6.7090	-162.5	6.6821	-153.0	6.6556
-176.1	6.7111	-161.6	6.6805	-152.0	6.6519
-174.6	6.7071	-161.1	6.6791	-151.0	6.6486
-173.4	6.7054	-160.4	6.6760	-150.1	6.6460
-172.6	6.7044	-159.8	6.6746	-149.4	6.6437
-171.2	6.7027	-159.0	6.6711	-148.6	6.6420
-169.1	6.6997	-158.6	6.6694	-147.8	6.6398
-168.2	6.6981	-157.8	6.6690	-146.2	6.6359
-167.0	6.6931	-157.2	6.6669	-145.0	6.6324
-166.2	6.6917	-156.4	6.6642	-143.8	6.6275
-165.8	6.6898	-155.9	6.6633	-142.2	6.6222
-164.8	6.6881	-155.2	6.6610	-140.3	6.6156
-164.0	6.6858	-154.5	6.6592	-138.7	6.6113

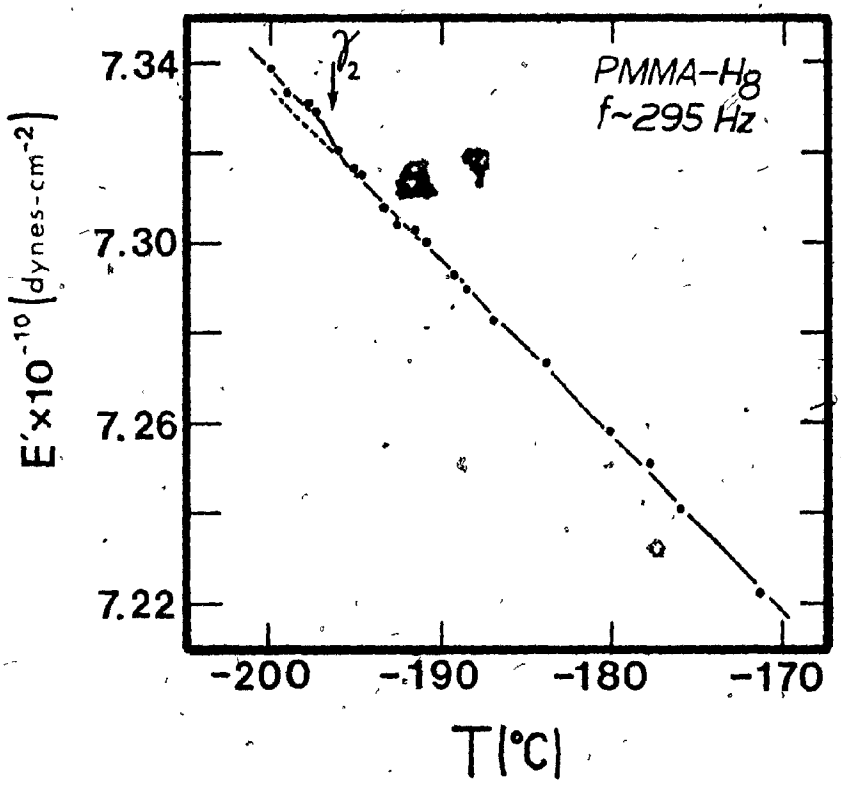
PMMA-H8
f~295 Hz
γ2
7.34
7.30
7.26
7.22
E'x10^-10 (dynes-cm^-2)
-200
-190
-180
-170
T(°C)

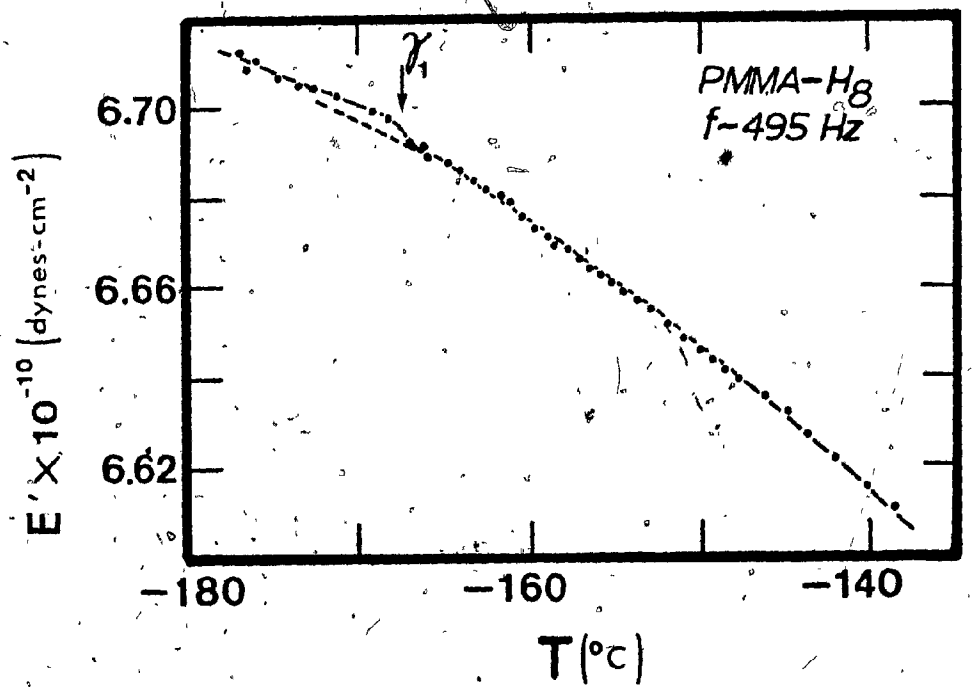
PMMA-H8
f~495 Hz
γ1
6.70
6.66
6.62
E'x10^-10 (dynes-cm^-2)
-180
-160
-140
T(°C)

FIGURE IV-6

PMMA-H_8 : VIBRATING REED RESULTS AT ~500 HZ. γ_1 and γ_2 relaxations are apparent at ~ -170°C (497 Hz) and ~ -190°C (499 Hz) respectively. (f_o varied from 500.53 Hz at -198.7°C to 488.23 Hz at -97.7°C.)

T (°C)	E'x10^{-10} (dynes/cm^2)	tan δ x10^3	T (°C)	E'x10^{-10} (dynes/cm^2)	tan δ x10^3
-198.7	6.8068		-148.0	6.6818	2.03
-195.4	6.7983	1.67	-146.4	6.6758	
-193.0	6.7928		-145.3	6.6719	2.09
-190.0	6.7884	1.72	-142.8	6.6626	
-187.0	6.7823		-141.7	6.6606	2.20
-184.4	6.7749	1.65	-139.4	6.6534	
-181.8	6.7708		-138.2	6.6488	2.26
-179.1	6.7654		-135.8	6.6389	
-176.6	6.7570	1.60	-135.2	6.6376	2.36
-171.8	6.7472		-132.8	6.6284	
-170.0	6.7442	1.73	-130.6	6.6206	
-166.1	6.7331		-129.6	6.6160	2.58
-164.2	6.7291	1.73	-126.8	6.6066	
-162.4	6.7241		-123.7	6.5945	
-160.6	6.7204	1.78	-122.3	6.5887	2.95
-158.4	6.7134		-118.4	6.5722	
-157.2	6.7101	1.85	-116.4	6.5641	3.24
-156.2	6.7064		-109.2	6.5319	
-154.8	6.7037		-107.2	6.5262	3.79
-153.7	6.6994	1.85	-102.0	6.4994	
-151.9	6.6944		-100.0	6.4905	4.26
-150.8	6.6904	1.96	-97.7	6.4766	
-149.1	6.6838				

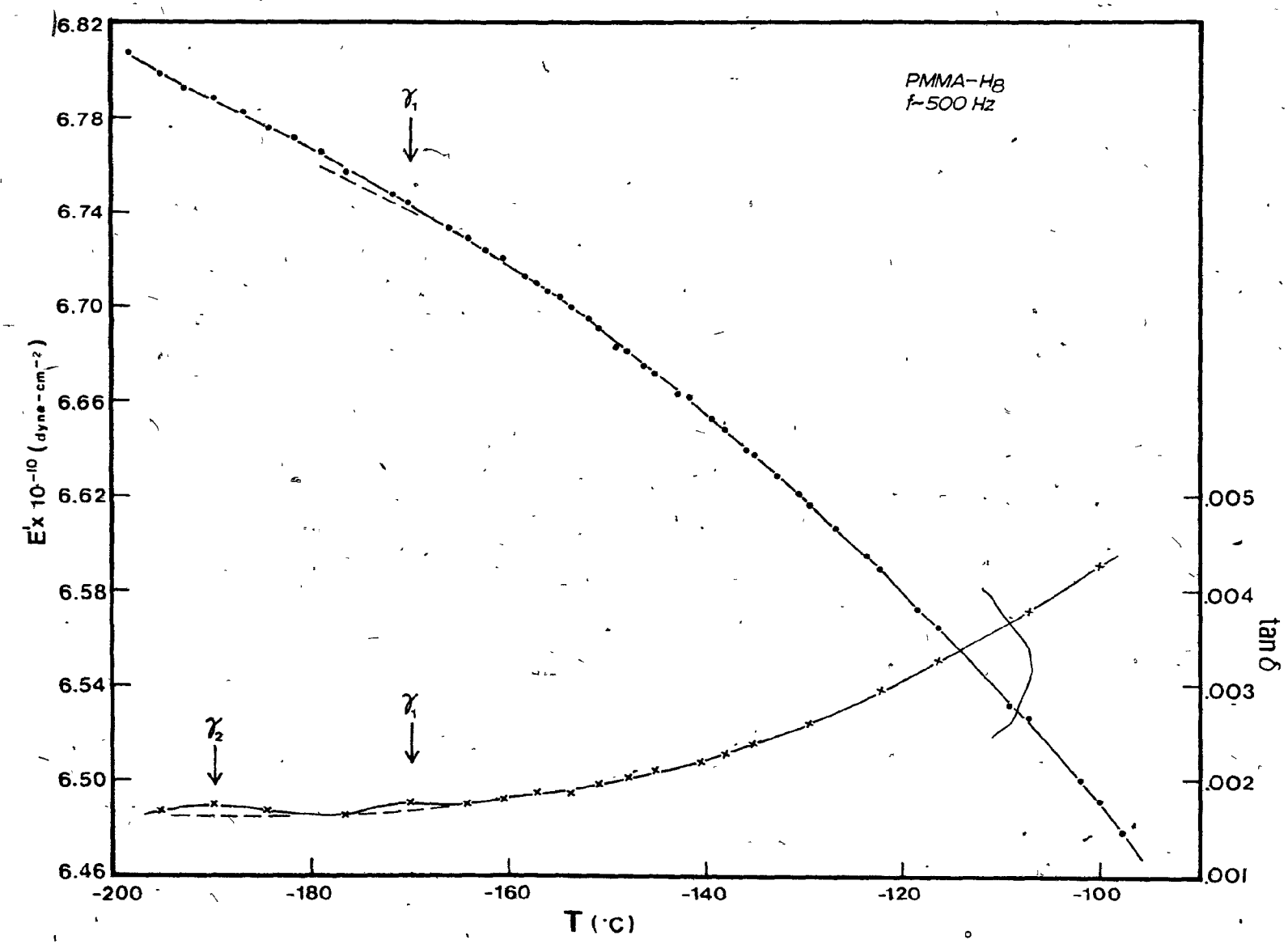
PMMA-H8
f~500 Hz
γ1
γ2
γ1
E' x 10^-10 (dyne-cm^-2)
tan δ
T (°C)
6.82
6.78
6.74
6.70
6.66
6.62
6.58
6.54
6.50
6.46
.005
.004
.003
.002
.001
-200
-180
-160
-140
-120
-100

FIGURE IV-7

PMMA-H_8 : VIBRATING REED RESULTS AT ~565 HZ. The γ_1 relaxation is present at ~-156°C (568 Hz). (f_o varied from 568.8 Hz at -167.1°C to 560.7 Hz at -105.5°C.)

T (°C)	E'x10^{-10}(dynes/cm^2)	T (°C)	E'x10^{-10}(dynes/cm^2)
-167.1	6.778	-136.8	6.707
-166.2	6.776	-135.0	6.704
-164.6	6.773	-134.3	6.697
-163.8	6.768	-132.5	6.695
-161.3	6.768	-131.9	6.692
-160.3	6.766	-129.8	6.685
-159.1	6.766	-129.2	6.685
-157.9	6.759	-127.2	6.676
-155.2	6.754	-126.6	6.678
-154.5	6.740	-124.7	6.669
-154.0	6.742	-124.1	6.664
-152.5	6.742	-121.2	6.655
-151.0	6.738	-120.6	6.655
-149.8	6.735	-118.4	6.643
-148.7	6.740	-117.5	6.641
-147.5	6.733	-115.5	6.631
-146.7	6.728	-114.7	6.626
-145.3	6.728	-111.4	6.617
-144.8	6.728	-110.8	6.612
-143.0	6.728	-107.2	6.593
-142.3	6.723	-106.8	6.591
-140.3	6.719	-106.0	6.589
-139.4	6.714	-105.5	6.586
-137.7	6.709		

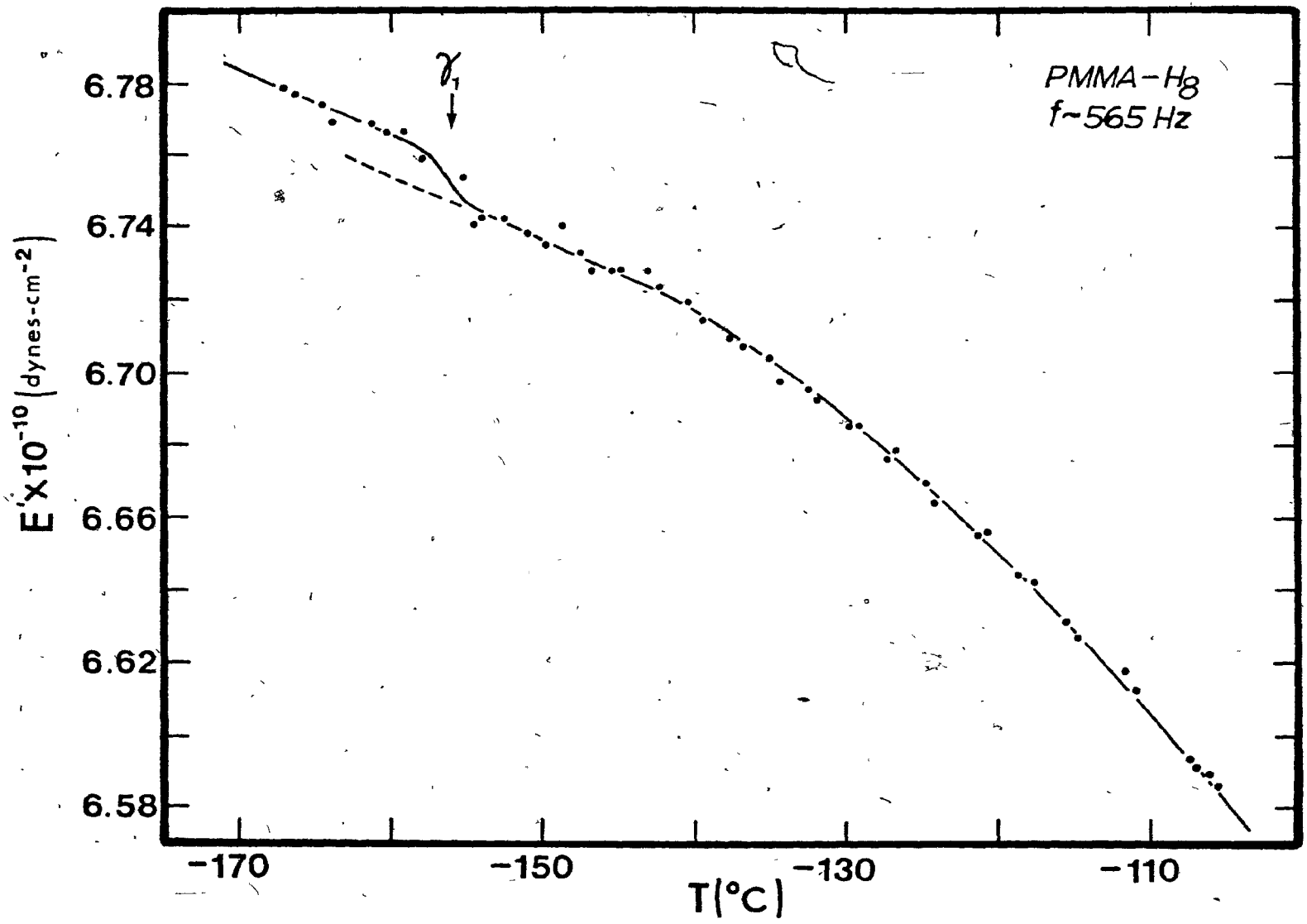
PMMA-H8
f~565 Hz
γ1
E' X10^-10 (dynes-cm^-2)
6.78
6.74
6.70
6.66
6.62
6.58
-170
-150
-130
-110
T(°C)

FIGURE IV-8

PMMA-H_8 : VIBRATING REED RESULTS AT ~570 HZ. The γ_1 and γ_2 relaxations are present at ~-162.5°C (569.5 Hz) and ~-188°C (571 Hz) respectively. (f_o ranged from 571.9 Hz at -197.0°C to 567.7 Hz at -147.2°C.)

T (°C)	E'x10^{-10}(dynes/cm^2)	T (°C)	E'x10^{-10}(dynes/cm^2)
-197.0	6.852	-173.0	6.821
-194.9	6.847	-171.3	6.816
-194.6	6.850	-171.0	6.819
-193.3	6.850	-170.3	6.814
-192.8	6.845	-169.8	6.811
-191.8	6.847	-169.5	6.814
-191.2	6.847	-168.5	6.814
-190.1	6.843	-168.2	6.814
-189.7	6.840	-167.5	6.811
-188.8	6.845	-166.8	6.807
-188.3	6.843	-166.4	6.809
-187.6	6.838	-165.9	6.807
-187.0	6.840	-164.8	6.804
-186.3	6.838	-164.2	6.804
-186.0	6.835	-163.4	6.802
-185.0	6.835	-162.2	6.792
-184.6	6.835	-161.8	6.790
-183.3	6.835	-161.1	6.790
-182.8	6.835	-160.6	6.788
-181.4	6.831	-158.9	6.780
-181.1	6.833	-153.5	6.776
-179.8	6.831	-153.1	6.773
-179.5	6.828	-151.3	6.766
-177.8	6.828	-151.0	6.766
-177.4	6.831	-149.9	6.759
-176.3	6.826	-149.0	6.761
-175.8	6.826	-148.5	6.759
-174.7	6.823	-147.5	6.752
-174.4	6.823	-147.2	6.752
-173.5	6.823		

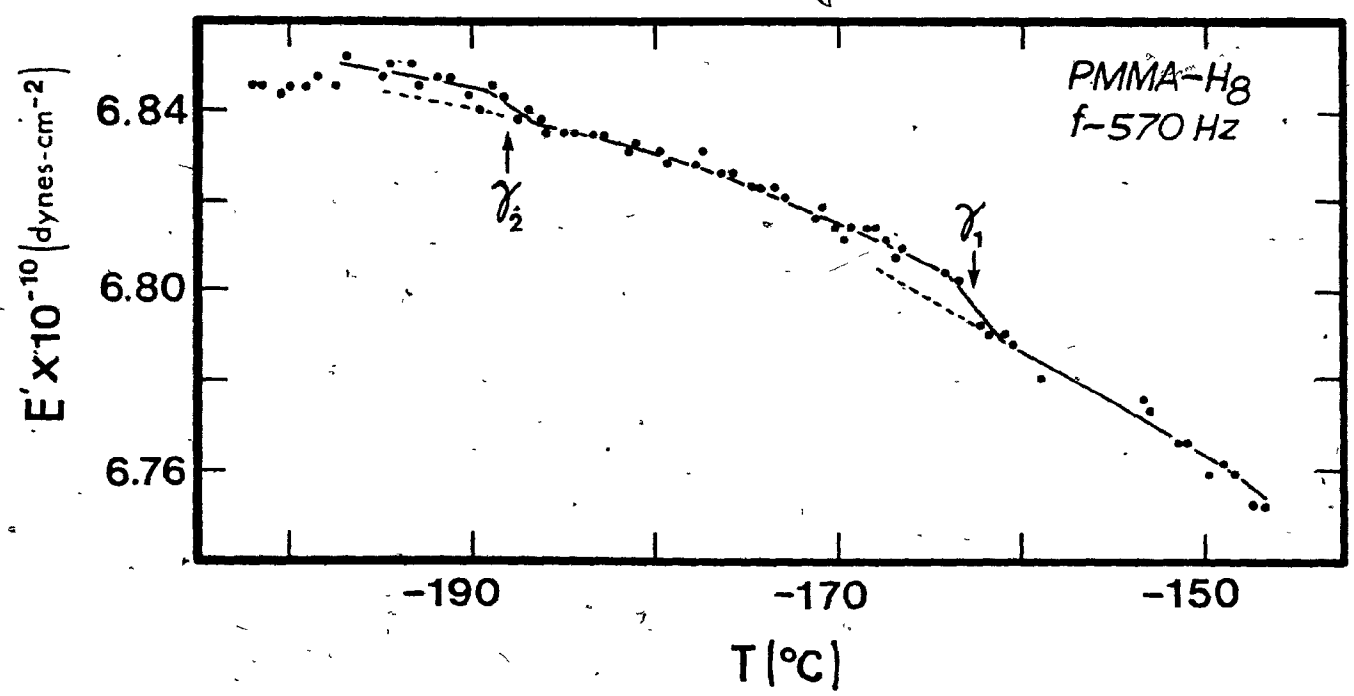
PMMA-H8
f-570 Hz
6.84
6.80
6.76
E' x10^-10 (dynes-cm^-2)
γ2
γ1
-190
-170
-150
T (°C)

FIGURE IV-9

PMMA-H_8 : VIBRATING REED RESULTS AT ~710 HZ. The γ_1 relaxation is present at ~-145°C (710 Hz). (f_o varied from 721.1 Hz at -197.3°C to 702.8 Hz at -121.5°C.)

T (°C)	E'x10^{-10} (dynes/cm^2)	T (°C)	E'x10^{-10} (dynes/cm^2)	T (°C)	E'x10^{-10} (dynes/cm^2)
-197.3	7.274	-165.8	7.159	-139.4	7.0155
-196.0	7.273	-164.9	7.152	-137.8	7.006
-195.2	7.270	-164.7	7.152	-136.3	6.999
-193.5	7.267	-164.1	7.150	-134.8	6.991
-193.0	7.264	-163.0	7.144	-133.4	6.984
-191.9	7.262	-162.8	7.143	-132.2	6.978
-191.5	7.258	-162.6	7.143	-131.0	6.971
-190.8	7.256	-161.7	7.140	-129.6	6.963
-189.8	7.252	-161.5	7.137	-128.4	6.956$_5$
-189.0	7.252	-160.5	7.133	-126.8	6.945$_5$
-188.3	7.250	-160.2	7.130	-125.5	6.938$_5$
-187.9	7.246	-159.3	7.127	-121.5	6.915
-187.2	7.243	-158.3	7.125		
-186.8	7.243	-158.1	7.121		
-186.2	7.240$_5$	-156.8	7.115		
-185.8	7.240$_5$	-156.7	7.116		
-185.4	7.237$_5$	-155.7	7.111		
-184.9	7.235$_5$	-155.4	7.107		
-184.4	7.232$_5$	-154.6	7.106		
-183.7	7.230$_5$	-154.3	7.101		
-182.6	7.226$_5$	-153.2	7.097		
-182.0	7.225$_5$	-153.2	7.097		
-181.2	7.223$_5$	-151.6	7.091		
-179.8	7.217$_5$	-151.7	7.091		
-176.8	7.205$_5$	-150.2	7.084$_5$		
-174.8	7.197	-150.0	7.082$_5$		
-174.0	7.192	-148.3	7.075$_5$		
-172.5	7.189	-146.5	7.061$_5$		
-171.0	7.181	-144.9	7.053$_5$		
-169.8	7.175	-143.5	7.039$_5$		
-168.5	7.169	-141.7	7.030$_5$		
-166.9	7.163	-140.3	7.021$_5$		

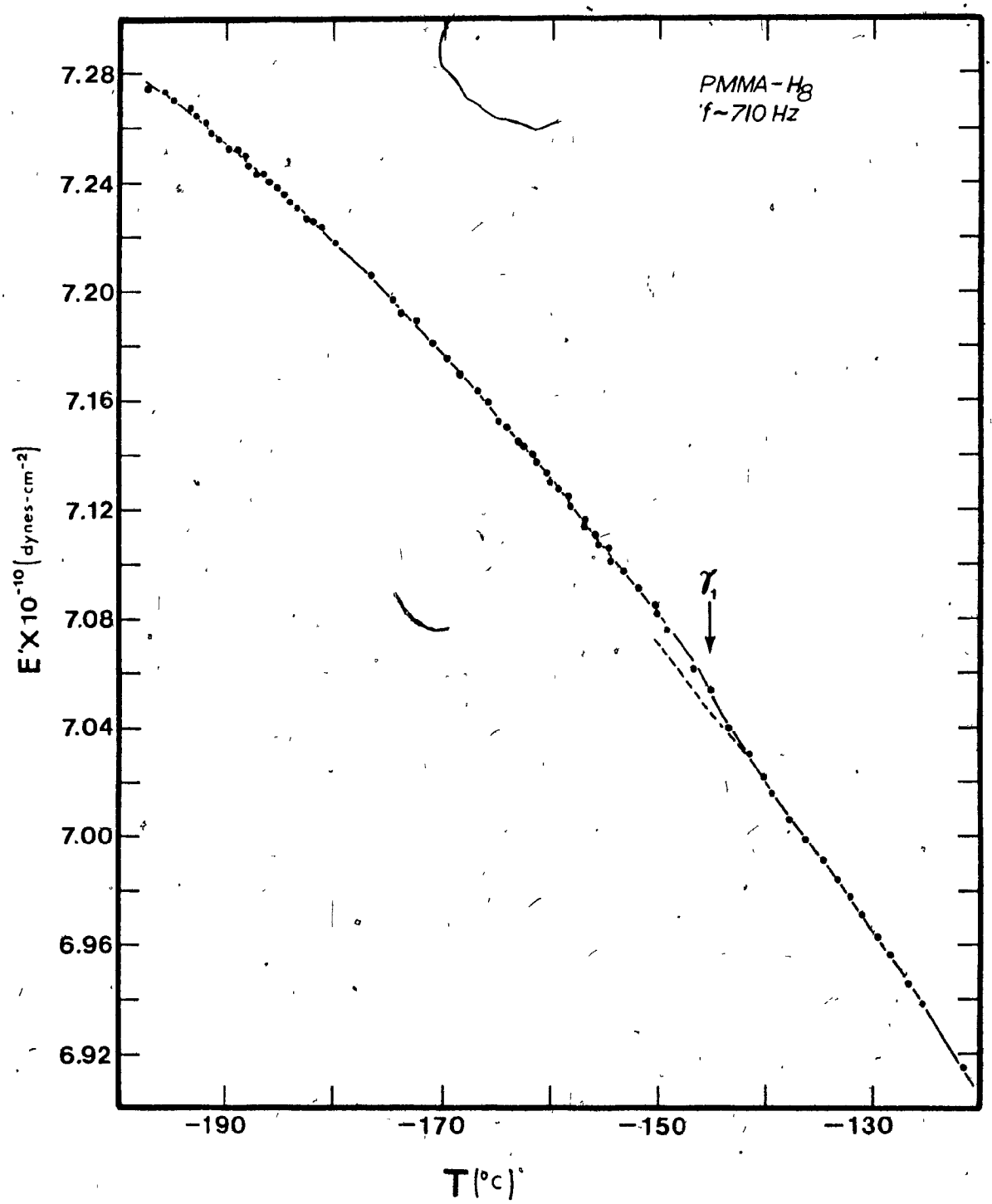
PMMA-H8
f~710 Hz
γ1
7.28
7.24
7.20
7.16
7.12
7.08
7.04
7.00
6.96
6.92
E' X 10^-10 (dynes-cm^-2)
-190
-170
-150
-130
T (°C)

FIGURE IV-10

PMMA-H_8 : VIBRATING REED RESULTS AT ~715 HZ. The γ_1 relaxation is present at ~-151°C (712.5 Hz). (f_o ranged from 714.55 Hz at -159.5°C to 709.8 Hz at -141.1°C.)

T (°C)	E'x10^{-10}(dynes/cm^2)	T (°C)	tanδ x10^3
-159.5	7.1481	-158.6	1.76
-158.2	7.1431	-156.3	1.80
-158.5	7.1451	-154.4	1.84_5
-157.5	7.1391	-152.8	1.90_5
-156.2	7.1331	-150.6	1.99
-156.5	7.1351	-148.3	2.06_5
-154.2	7.1262	-145.9	2.13
-154.6	7.1272	-144.6	2.19_5
-153.3	7.1192	-142.6	2.26
-152.5	7.1162	-141.0	2.29_5
-152.8	7.1152		
-151.6	7.1112		
-150.6	7.1032		
-150.9	7.1032		
-149.8	7.0972		
-149.2	7.0932		
-148.3	7.0892		
-148.0	7.0892		
-146.9	7.0853		
-145.9	7.0793		
-146.0	7.0793		
-144.4	7.0713		
-144.5	7.0703		
-143.5	7.0683		
-142.5	7.0634		
-142.8	7.0624		
-141.7	7.0574		
-141.0	7.0514		
-141.1	7.0534		

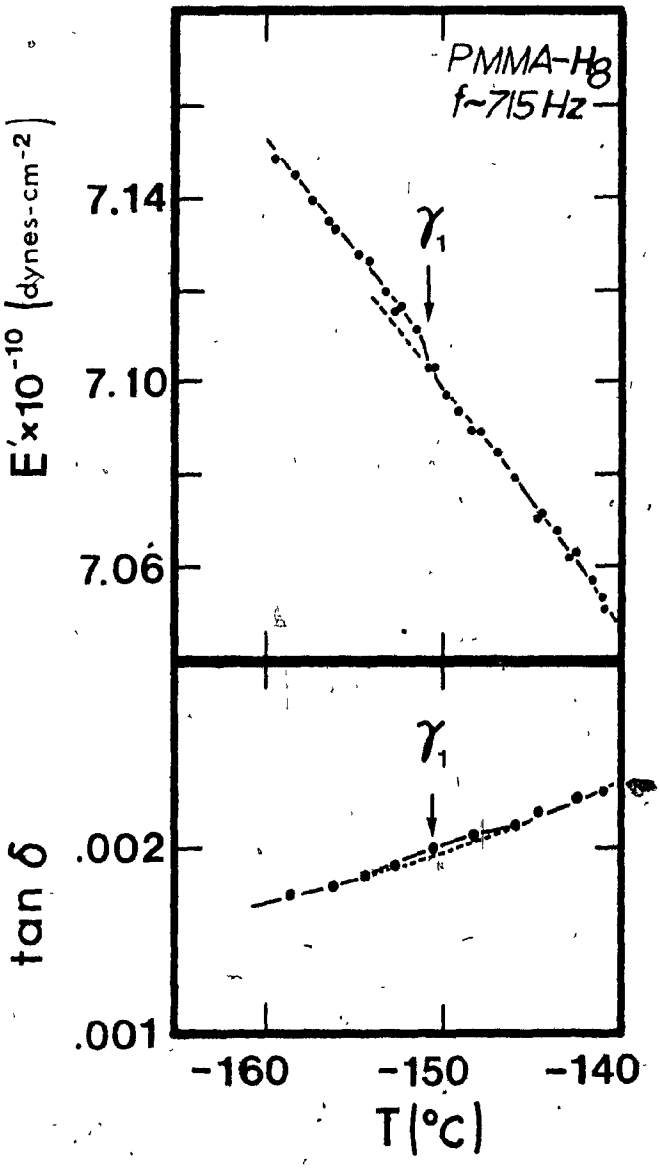
PMMA-H8
f~715 Hz
E'×10^-10 (dynes-cm^-2)
7.14
7.10
7.06
γ1
tan δ
.002
.001
γ1
-160
-150
-140
T(°C)

FIGURE IV-11

PMMA-H_8: VIBRATING REED RESULTS AT ~1325 HZ AND ~1630 HZ (INSERT). γ_2 relaxations are apparent at ~-179.5°C (1322 Hz) and ~-179°C (1633 Hz). (In the experiment at 1325 Hz, f_o varied from 1330.8 Hz at -207.6°C to 1318.1 Hz at -168.7°C.)

~1325 HZ		~1630 HZ	
T (°C)	E'x10^{-10}(dynes/cm^2)	T (°C)	tanδ x10^3
-207.6	7.3316	-182.2	1.74
-208.0	7.3303	-180.0	1.97
-205.4	7.3199	-177.3	2.07
-203.3	7.3131	-175.8	2.03
-200.1	7.3023	-173.8	2.13
-197.6	7.2960	-172.2	2.24
-197.3	7.2920	-170.7	2.31
-195.0	7.2880	-169.2	2.38
-194.5	7.2861		
-192.6	7.2795		
-190.8	7.2744		
-189.5	7.2698		
-187.8	7.2652		
-186.1	7.2595		
-185.	7.2554		
-183.3	7.2512		
-181.9	7.2470		
-180.3	7.2413		
-178.8	7.2334		
-177.5	7.2293		
-176.2	7.2264		
-174.8	7.2197		
-173.5	7.2142		
-172.2	7.2087		
-170.9	7.2035		
-168.7	7.1928		

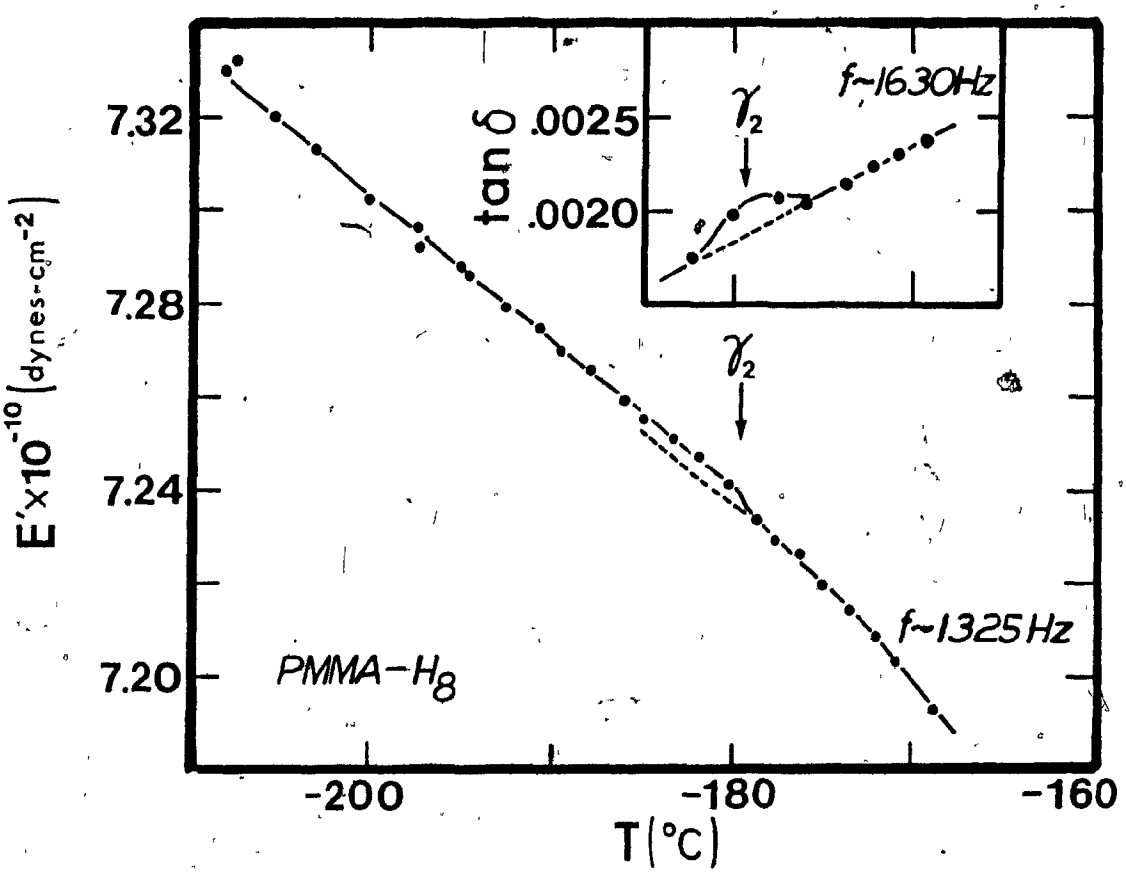
7.32
7.28
7.24
7.20
E'x10^-10 (dynes-cm^-2)
tan δ
.0025
.0020
f~1630Hz
γ2
γ2
f~1325Hz
PMMA-H8
-200
-180
-160
T(°C)

FIGURE IV-12

PMMA-H_8 : VIBRATING REED RESULTS AT ~1750 HZ. The γ_1 relaxation is present at ~-147°C and 1761 Hz. (f_o varied from 1781.45 Hz at -191.6°C to 1731.71 Hz at -91.6°C.)

T (°C)	E'x10^{-10} (dynes/cm^2)	T (°C)	E'x10^{-10} (dynes/cm^2)	T (°C)	E'x10^{-10} (dynes/cm^2)
-191.6	6.8168	-154.2	6.6891	-123.6	6.5767
-189.4	6.8105	-153.4	6.6864	-122.8	6.5728
-188.1	6.8049	-152.4	6.6819	-121.8	6.5711
-187.0	6.8011	-151.4	6.6792	-120.7	6.5666
-185.8	6.7968	-150.2	6.6748	-119.7	6.5621
-184.6	6.7930	-149.1	6.6701	-118.1	6.5569
-183.6	6.7896	-148.4	6.6679	-116.8	6.5517
-182.7	6.7862	-147.6	6.6653	-115.4	6.5468
-181.8	6.7843	-147.2	6.6613	-114.2	6.5419
-180.6	6.7810	-146.8	6.6578	-112.0	6.5315
-179.8	6.7775	-145.6	6.6535	-109.9	6.5233
-178.6	6.7738	-144.4	6.6483	-108.1	6.5154
-177.3	6.7696	-142.7	6.6419	-105.8	6.5062
-176.1	6.7662	-141.4	6.6380	-103.4	6.4946
-174.6	6.7608	-139.9	6.6338	-100.8	6.4838
-174.0	6.7576	-139.2	6.6311	-97.6	6.4693
-173.2	6.7545	-138.4	6.6289	-93.8	6.4527
-172.2	6.7516	-137.8	6.6264	-91.6	6.4414
-171.1	6.7473	-136.9	6.6247		
-170.4	6.7445	-136.4	6.6211		
-169.4	6.7416	-135.7	6.6187		
-168.9	6.7395	-134.8	6.6161		
-167.8	6.7368	-133.8	6.6111		
-167.0	6.7340	-131.9	6.6055		
-166.0	6.7306	-130.8	6.6019		
-164.9	6.7255	-128.9	6.5938		
-164.2	6.7242	-127.8	6.5922		
-162.8	6.7198	-126.6	6.5871		
-162.2	6.7174	-125.7	6.5840		
-161.2	6.7127	-124.9	6.5810		
-159.7	6.7079	-123.6	6.5767		
-158.6	6.7017	-122.8	6.5728		
-157.6	6.7031	-121.8	6.5711		
-156.7	6.6989	-120.7	6.5666		
-156.3	6.6977	-119.7	6.5621		
-154.9	6.6914	-118.1	6.5569		

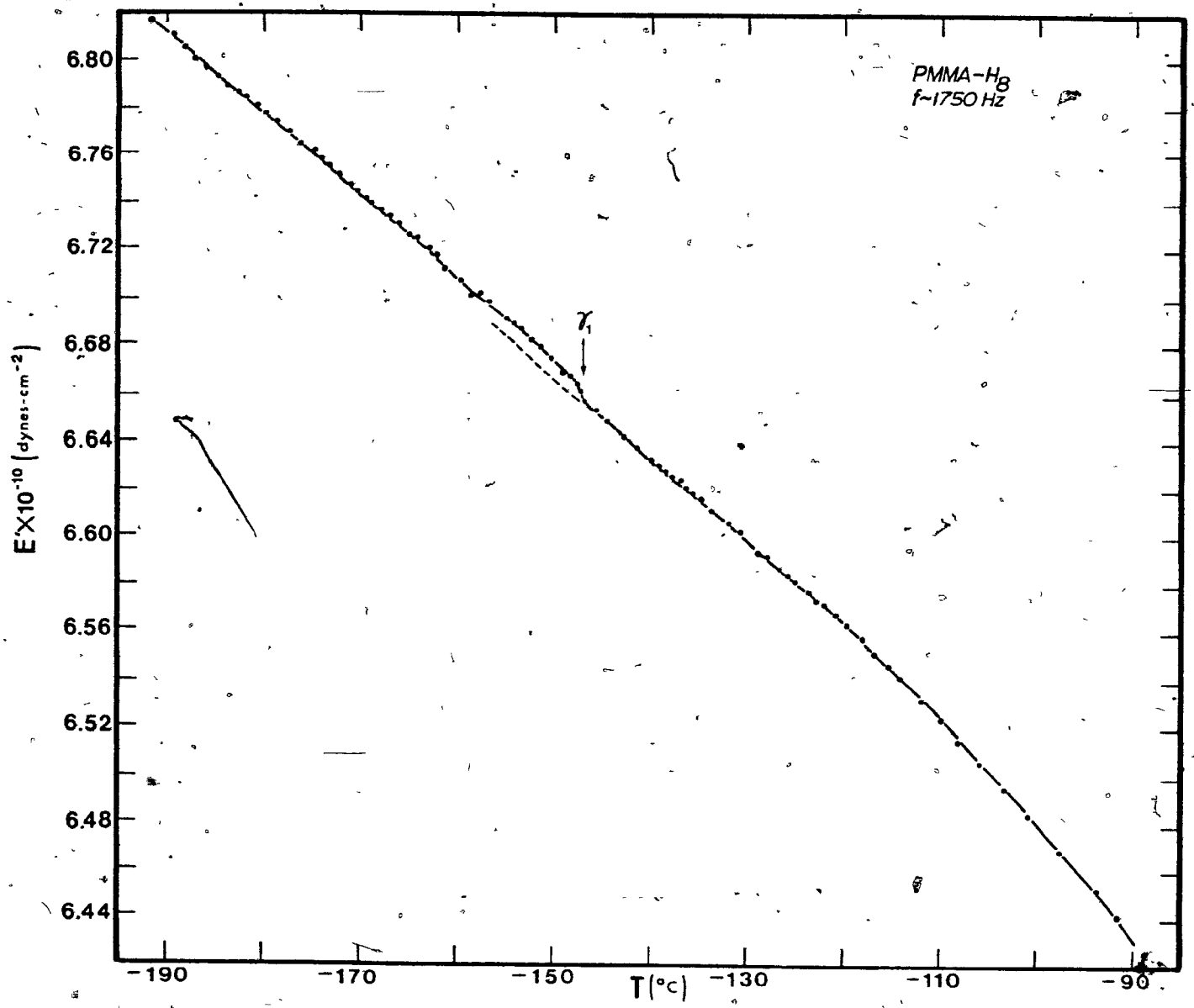
PMMA-H8
f~1750 Hz
γ1
E'X10-10 (dynes-cm-2)
6.80
6.76
6.72
6.68
6.64
6.60
6.56
6.52
6.48
6.44
-190
-170
-150
-130
-110
-90
T(°C)

FIGURE IV-13

PMMA-H_8 : VIBRATING REED RESULTS AT ~1770 HZ. The γ_2 relaxation is apparent at ~-175°C (1770 Hz). (f_0 varied from 1782.2 Hz at -199.8°C to 1765.4 Hz at -166.5°C.)

T (°C)	E'x10^{-10}(dyne/cm^2)
-199.8	6.7908
-198.0	6.7778
-196.1	6.7748
-193.8	6.7649
-191.7	6.7565
-189.7	6.7497
-187.9	6.7429
-185.6	6.7345
-184.4	6.7315
-182.7	6.7254
-181.6	6.7209
-180.6	6.7171
-179.3	6.7118
-178.6	6.7103
-177.9	6.7072
-177.2	6.7050
-176.6	6.7019
-175.9	6.6997
-175.4	6.6966
-174.2	6.6928
-173.3	6.6891
-172.5	6.6860
-171.8	6.6838
-170.3	6.6777
-169.7	6.6762
-168.8	6.6717
-168.1	6.6702
-167.1	6.6664
-166.5	6.6634

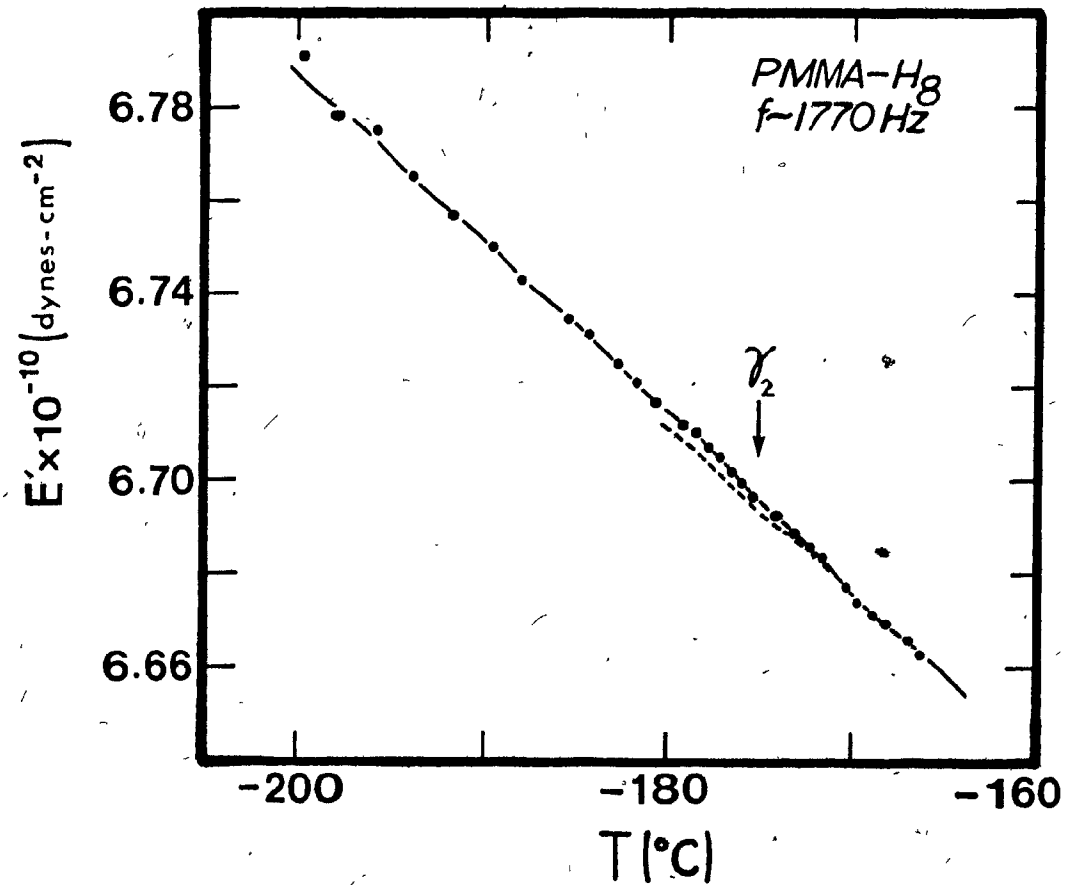
PMMA-H8
f-1770 Hz
6.78
6.74
6.70
6.66
E'x10^-10 (dynes-cm^-2)
γ2
-200
-180
-160
T (°C)

FIGURE IV-14

PMMA-H_8 : VIBRATING REED RESULTS AT ~3 KHZ. The γ_1 relaxation is apparent at ~ -118°C (3025 Hz). (f_o varied from 3051.7 Hz at -163.6°C to 3020.8 Hz at -111.4°C.)

T (°C)	E'x10^{-10} (dynes/cm^2)	T (°C)	E'x10^{-10} (dynes/cm^2)
-163.6	6.4418	-126.7	6.3563
-161.4	6.4384	-126.1	6.3557
-158.8	6.4323	-125.0	6.3527
-156.2	6.4280	-124.4	6.3498
-153.8	6.4245	-123.7	6.3482
-151.2	6.4157	-123.2	6.3479
-148.1	6.4083	-121.9	6.3448
-146.0	6.4032	-121.4	6.3425
-144.0	6.3981	-120.8	6.3413
-141.6	6.3919	-120.2	6.3398
-140.8	6.3911	-119.4	6.3371
-140.2	6.3900	-118.6	6.3344
-139.6	6.3878	-117.3	6.3304
-138.4	6.3849	-116.8	6.3279
-137.8	6.3830	-116.0	6.3268
-137.2	6.3814	-115.2	6.3227
-136.7	6.3811	-114.6	6.3208
-135.8	6.3783	-114.0	6.3187
-134.9	6.3768	-112.8	6.3159
-133.3	6.3745	-112.0	6.3140
-132.5	6.3716	-111.4	6.3119
-131.9	6.3696		
-131.2	6.3694		
-130.3	6.3667		
-129.2	6.3621		
-128.6	6.3609		
-127.9	6.3598		
-127.3	6.3577		

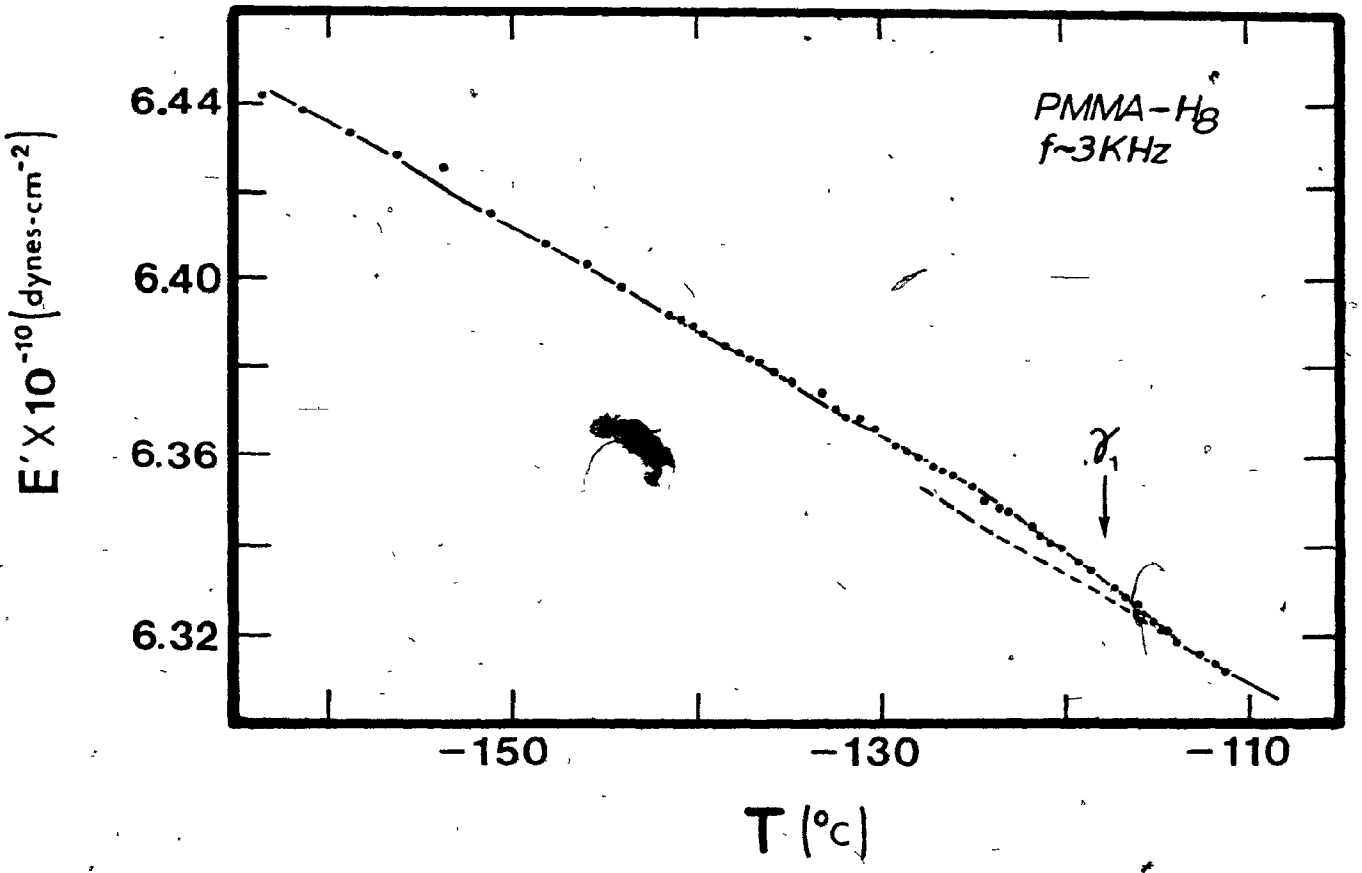
PMMA-H8
f~3KHz
6.44
6.40
6.36
6.32
E' X 10^-10 (dynes-cm^-2)
γ1
-150
-130
-110
T (°C)

FIGURE IV-15

PMMA-H_8 ; VIBRATING REED RESULTS AT-3 KHZ. The γ_1 relaxation is present at ~-117°C (3025 Hz). (f_o varied from 3040.9 Hz at -138.0°C to 3014.8 Hz at -103.2°C.)

T (°C)	E'x10^{-10} (dynes/cm^2)	T (°C)	E'x10^{-10} (dynes/cm^2)
-138.0	6.3962	-118.4	6.3360
-136.9	6.3931	-118.0	6.3354
-135.9	6.3910	-117.6	6.3338
-134.5	6.3861	-117.2	6.3317
-133.6	6.3838	-117.0	6.3309
-132.0	6.3799	-116.4	6.3292
-131.2	6.3772	-115.9	6.3275
-130.2	6.3741	-115.3	6.3252
-129.5	6.3722	-114.8	6.3242
-128.9	6.3700	-114.2	6.3231
-128.6	6.3697	-113.8	6.3203
-128.2	6.3677	-113.3	6.3191
-127.2	6.3647	-112.8	6.3174
-126.5	6.3631	-111.8	6.3143
-125.7	6.3602	-110.8	6.3106
-125.0	6.3583	-110.2	6.3082
-124.4	6.3565	-109.0	6.3048
-123.6	6.3539	-108.3	6.3029
-123.0	6.3517	-107.8	6.3005
-122.6	6.3508	-107.2	6.2993
-121.6	6.3479	-106.6	6.2975
-121.0	6.3458	-105.8	6.2956
-120.0	6.3426	-104.9	6.2923
-119.6	6.3404	-103.8	6.2892
-119.2	6.3392	-103.2	6.2871
-118.8	6.3378		

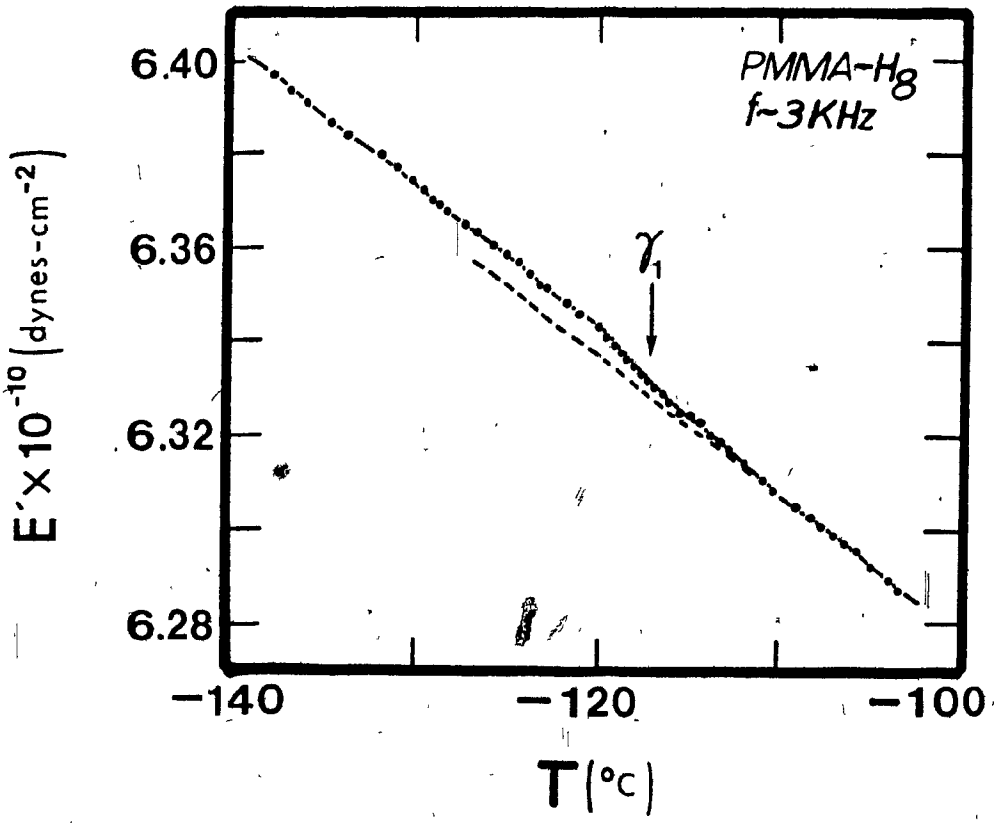
PMMA-H8
f~3KHz
γ1
6.40
6.36
6.32
6.28
E'X10-10 (dynes-cm-2)
-140
-120
-100
T(°C)

FIGURE IV-16.

PMMA-H_8 : VIBRATING REED RESULTS AT ~3 KHZ. The γ_1 relaxation is present at ~-121°C (3036 Hz). (f_o varied from 3061.6 Hz at -155.4°C to 3012.4 Hz at -90.7°C.)

T (°C)	E' x 10^{-10} (dynes/cm^2)
-155.4	6.4834
-152.6	6.4763
-149.8	6.4676
-147.3	6.4611
-143.8	6.4502
-140.7	6.4420
-137.6	6.4310
-136.4	6.4274
-134.6	6.4212
-133.6	6.4178
-132.2	6.4141
-131.0	6.4114
-129.0	6.4054
-127.8	6.4015
-126.1	6.3958
-124.7	6.3915
-121.6	6.3814
-119.4	6.3737
-115.6	6.3606
-114.0	6.3536
-110.1	6.3423
-106.0	6.3275
-104.2	6.3203
-99.4	6.3069
-98.2	6.3012
-97.4	6.2983
-95.7	6.2930
-93.4	6.2868
-90.7	6.2769

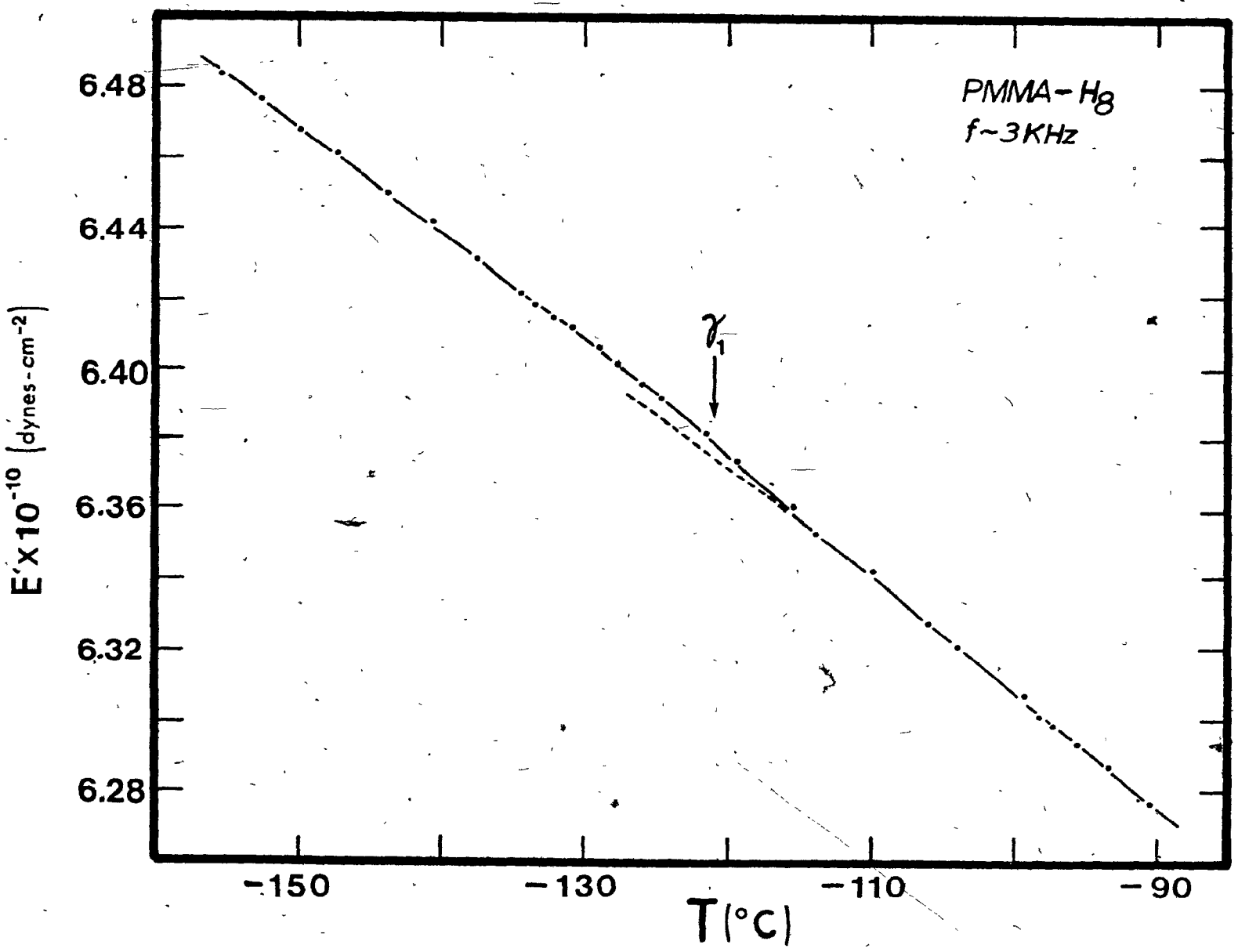
PMMA-H8
f~3KHz
γ1
E'X10^-10 (dynes-cm^-2)
6.48
6.44
6.40
6.36
6.32
6.28
-150
-130
-110
-90
T(°C)

FIGURE IV-17

PMMA-H_8 : VIBRATING REED RESULTS AT ~4.3 KHZ. The γ_1 and γ_2 relaxations are in evidence at ~ -125°C (4319 Hz) and ~ -172.5°C (4379 Hz) respectively. (f_o varied from 4393 Hz at -197.2°C to 4286.5 Hz at -110.°C)

T (°C)	E'x10^{-10} (dynes/cm^2)	T (°C)	E'x10^{-10} (dynes/cm^2)	T (°C)	E'x10^{-10} (dynes/cm^2)
-197.2	6.880	-166.9	6.816	-136.1	6.715
-196.2	6.881_5	-165.8	6.814_5	-134.7	6.708_5
-194.9	6.880	-165.7	6.814_5	-133.4	6.702_5
-194.0	6.877	-164.9	6.811	-132.2	6.696_5
-193.0	6.877	-164.7	6.808	-131.0	6.691_5
-192.4	6.877	-164.6	6.808	-129.8	6.684^5
-191.3	6.875	-164.2	6.809_5	-128.5	6.673
-190.2	6.873_5	-163.8	6.808	-126.9	6.668_5
-189.5	6.872	-162.8	6.808	-125.4	6.653
-188.8	6.869	-161.0	6.803_5	-124.2	6.641
-187.5	6.869	-160.3	6.802	-122.7	6.628_5
-186.4	6.867_5	-159.5	6.800_5	-121.4	6.619_5
-185.6	6.867_5	-158.3	6.792_5	-119.8	6.613
-184.6	6.862_5	-157.8	6.789_5	-118.3	6.601
-183.0	6.861	-157.0	6.788	-116.1	6.582_5
-181.4	6.859_5	-156.7	6.786_5	-115.1	6.578
-180.4	6.856_5	-155.5	6.786_5	-114.0	6.573_5
-179.6	6.851_5	-154.6	6.781_5	-112.8	6.576_5
-176.7	6.848_5	-153.2	6.777	-111.7	6.561
-174.8	6.842_5	-151.7	6.774	-110.9	6.561
-173.5	6.839	-149.9	6.767_5	-110.0	6.550_5
-172.5	6.836	-148.3	6.758_5		
-171.0	6.830	-146.6	6.755		
-170.9	6.831_5	-144.8	6.747_5		
-170.0	6.828_5	-143.5	6.743		
-169.7	6.825	-141.6	6.736_5		
-168.6	6.823_5	-140.5	6.733_5		
-168.4	6.820_5	-139.3	6.727_5		
-167.2	6.817_5	-137.8	6.724		

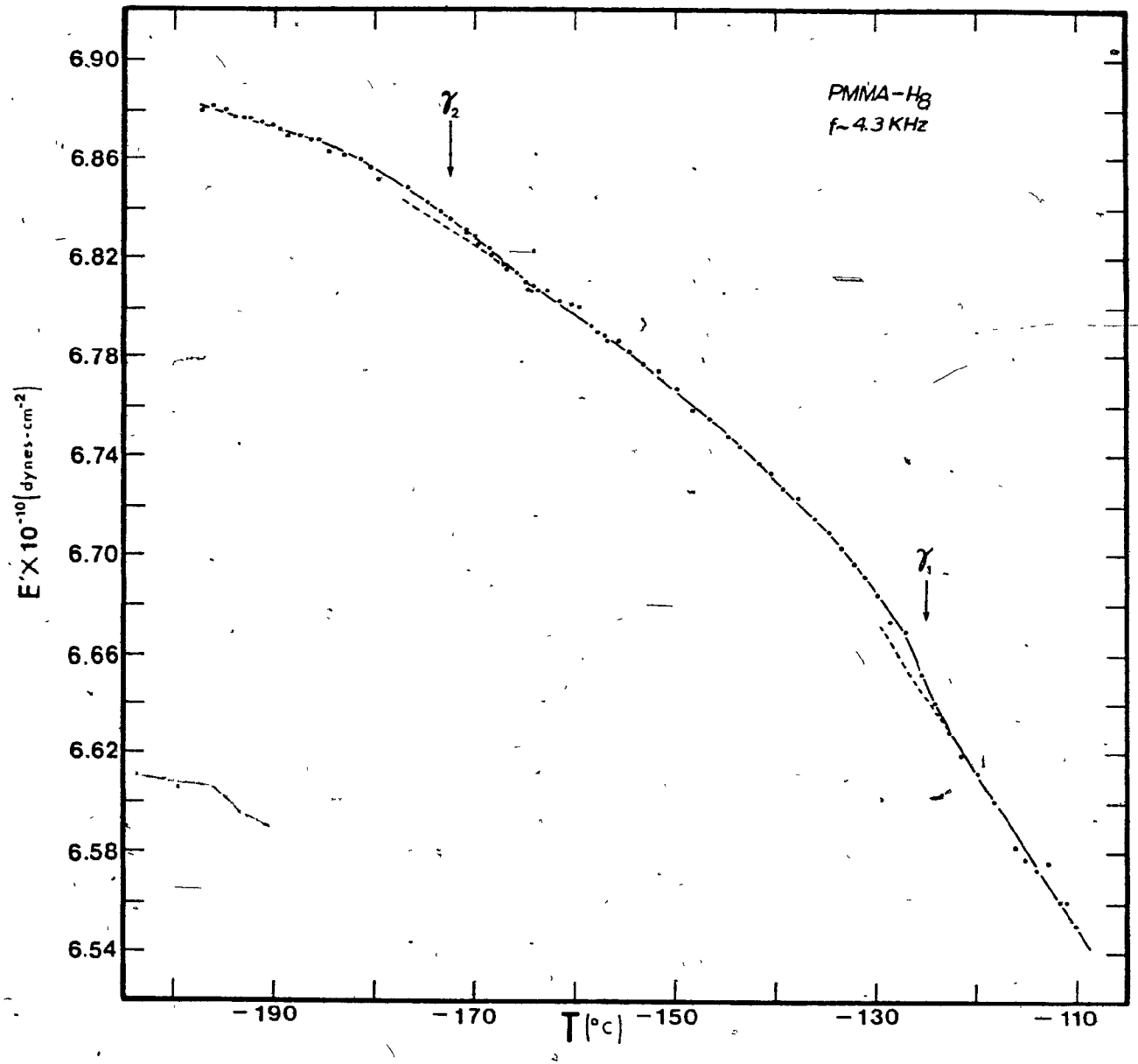
PMMA-H8
f~4.3 KHz
γ2
γ1
E'X10-10(dynes-cm-2)
6.90
6.86
6.82
6.78
6.74
6.70
6.66
6.62
6.58
6.54
-190
-170
-150
-130
-110
T(°C)

FIGURE IV-19

PMMA-H_8 : VIBRATING REED RESULTS AT ~9.25 KHZ. the γ_2 relaxation is apparent at ~-164°C (9243 Hz). (f_o varied from 9251 Hz at -180.4°C to 9227 Hz at -146.7°C.)

T (°C)	E'x10^{-10} (dynes/cm^2)	T (°C)	E'x10^{-10} (dynes/cm^2)	T (°C)	E'x10^{-10} (dynes/cm^2)
-180.4	5.819_5	-170.8	5.814_5	-161.3	5.804_5
-180.2	5.819_5	-170.4	5.816	-159.9	5.803
-179.2	5.819_5	-169.0	5.813	-159.5	5.804_5
-178.7	5.821	-168.8	5.814_5	-153.	5.801
-177.0	5.821	-167.2	5.813	-152.7	5.797
-176.5	5.818	-167.0	5.813	-152.2	5.797
-175.3	5.818	-165.7	5.812	-150.9	5.794
-175.0	5.817	-165.3	5.813	-150.6	5.794
-174.2	5.817	-163.3	5.806	-148.3	5.790_5
-173.8	5.816	-162.8	5.804_5	-148.0	5.789
-172.6	5.817	-162.7	5.804_5	-147.0	5.789
-172.1	5.817	-162.3	5.806	-146.7	5.789
		-161.7	5.804_5		

FIGURE IV-18

PMMA-H_8 : VIBRATING REED RESULTS AT ~9.1 KHZ. The γ_1 relaxation is in evidence at ~-116°C (9105 Hz). (f_o varied from 9129 Hz at -131.0°C to 9089 Hz at -105.2°C.).

T (°C)	E'x10^{-10} (dynes/cm^2)	T (°C)	E'x10^{-10} (dynes/cm^2)
-131.0	5.667	-114.2	5.632
-130.2	5.663	-113.4	5.626
-130.0	5.663	-109.0	5.620
-129.0	5.664_5	-107.9	5.620
-128.3	5.664	-107.4	5.619
-126.1	5.659_5	-106.9	5.619
-125.4	5.657	-105.9	5.620
-123.8	5.656	-105.2	5.617_5
-123.1	5.653		
-120.4	5.651		
-119.7	5.647		
-117.3	5.642		
-116.8	5.640		

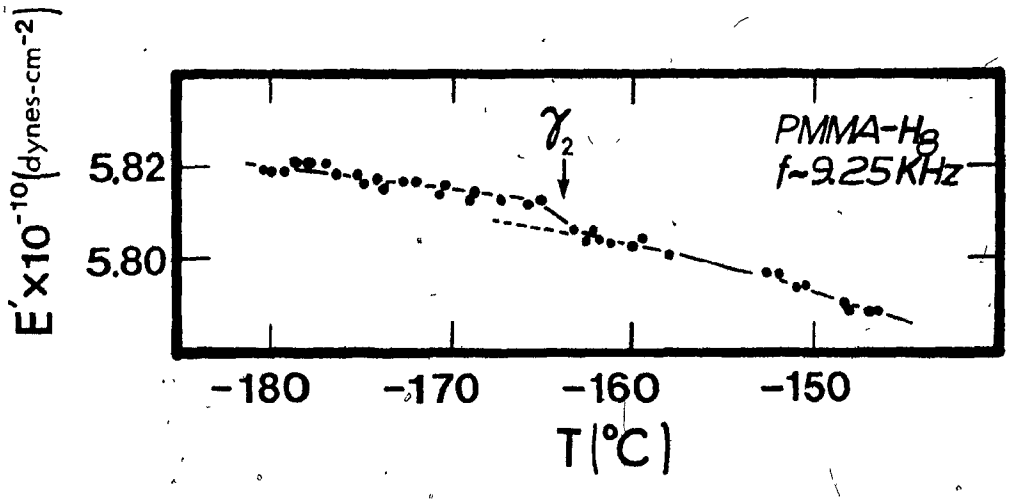
E'x10^{-10}(dynes-cm^{-2})
5.82
5.80
γ_2
PMMA-H_8
f~9.25KHz
-180
-170
-160
-150
T(°C)

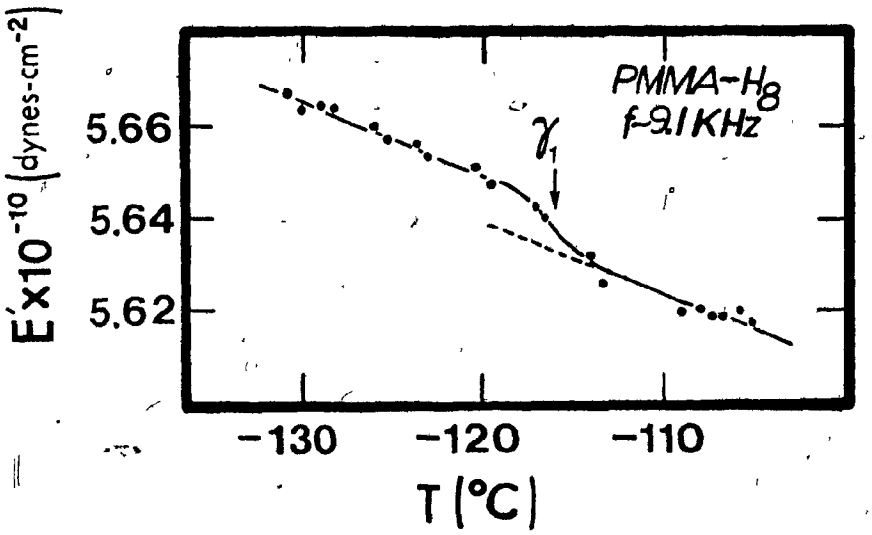
E'x10^{-10}(dynes-cm^{-2})
5.66
5.64
5.62
γ_1
PMMA-H_8
f~9.1KHz
-130
-120
-110
T(°C)

FIGURE IV-20

PMMA-D_8#: VIBRATING REED RESULTS AT ~370 HZ. The γ_1 relaxation is present at ~-119°C (368 Hz). (f_o varied from 376.0 Hz at -195.5°C to 365.2 Hz at -97.4°C).

T (°C)	E'x10^{-10} (dynes/cm^2)	T (°C)	tanδ x 10^3
-195.5	5.5504	-189.8	1.24
-191.2	5.5433	-187.6	1.25
-188.8	5.5356	-185.0	1.27
-186.2	5.5321	-183.0	1.29
-184.2	5.5285	-181.1	1.26
-182.2	5.5238	-178.0	1.26
-179.3	5.5173	-176.7	1.28
-177.5	5.5132	-174.5	1.30
-175.5	5.5079	-172.4	1.30
-173.5	5.5061	-169.4	1.35
-170.5	5.4984	-166.7	1.34
-167.8	5.4925	-164.2	1.38
-165.1	5.4843	-161.5	1.44
-162.7	5.4784	-158.6	1.49
-159.8	5.4702	-155.5	1.55
-157.1	5.4631	-153.1	1.61
-154.7	5.4579	-149.5	1.68
-151.0	5.4461	-146.3	1.80
-147.5	5.4362	-144.5	1.87
-145.0	5.4297	-143.2	1.91
-143.8	5.4268	-142.3	1.94
-142.6	5.4227	-142.3	1.91
-142.3	5.4227	-139.6	2.01
-140.3	5.4180	-135.5	2.11
-136.2	5.4052	-131.7	2.31
-132.5	5.3935	-128.7	2.49
-129.5	5.3836	-125.5	2.73
-126.2	5.3731	-123.8	2.88
-124.3	5.3655	-121.5	3.29
-122.0	5.3574	-119.9	3.64
-120.5	5.3493	-117.5	3.83
-118.3	5.3376	-115.25	3.60
-115.8	5.3272	-112.3	3.51
-112.9	5.3179	-109.7	3.69
-110.1	5.3063	-107.2	3.81
-107.6	5.2994	-100.0	4.23
-101.8	5.2769	-97.2	4.48
-97.4	5.2590		

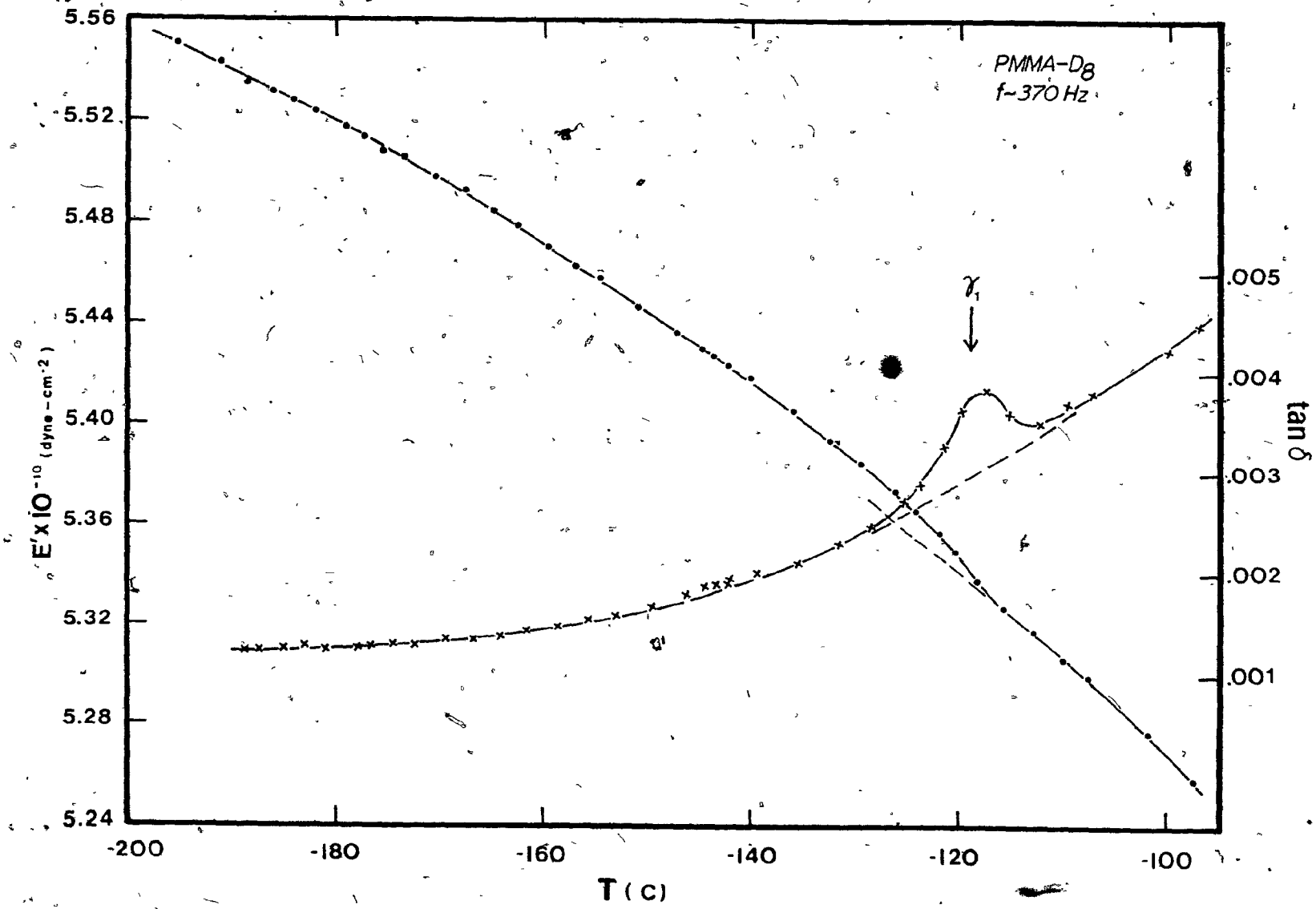
PMMA-D8
f~370 Hz
γ1
E' x 10^-10 (dyne-cm^-2)
tan δ
T (C)
5.56
5.52
5.48
5.44
5.40
5.36
5.32
5.28
5.24
.005
.004
.003
.002
.001
-200
-180
-160
-140
-120
-100

FIGURE IV-21

PMMA-D_8: VIBRATING REED RESULTS AT ~550 Hz. The γ_1 relaxation is present at ~ -120°C and 540.5 Hz. (f_o varied from 548.50 Hz at -171.7°C to 536.96 Hz at -103.6°C.)

T (°C)	E'x10^{-10} (dynes/cm^2)	T (°C)	E'x10^{-10} (dynes/cm^2)	T (°C)	tanδ x10^3	T (°C)	tanδ x10^3
-171.7	7.6627	-138.6	7.5317	-169.6	0.968	-135.8	1.76
-170.2	7.6591	-136.4	7.5228	-168.9	0.966	-133.8	1.82
-169.3	7.6549	-134.5	7.5142	-167.2	0.966	-131.7	1.92
-167.8	7.6471	-132.4	7.5040	-165.9	1.01	-129.5	2.01
-166.4	7.6432	-130.5	7.4952	-163.9	1.03	-127.2	2.14
-164.3	7.6353	-128.0	7.4835	-162.7	1.04	-125.5	2.27
-163.2	7.6317	-126.2	7.4742	-161.2	1.08	-123.3	2.42
-161.8	7.6253	-124.3	7.4631	-159.8	1.10	-121.2	2.62
-160.2	7.6200	-122.0	7.4524	-158.5	1.12	-119.5	2.74
-158.7	7.6158	-120.2	7.4408	-156.8	1.15	-117.5	2.80
-157.6	7.6094	-118.3	7.4298	-155.3	1.19	-115.7	2.85
-155.8	7.6022	-116.5	7.4180	-153.7	1.22	-113.5	2.93
-154.4	7.5977	-114.3	7.4070	-152.4	1.26	-111.2	3.04
-153.0	7.5916	-112.1	7.3933	-151.2	1.29	-108.5	3.18
-151.6	7.5863	-109.3	7.3776	-149.2	1.33	-106.4	3.34
-149.6	7.5794	-107.1	7.3664	-147.8	1.36	-104.4	3.48
-148.2	7.5741	-105.1	7.3541	-146.0	1.41	-102.8	3.56
-146.4	7.5658	-103.6	7.3437	-144.5	1.46		
-145.0	7.5600			-142.7	1.50		
-143.3	7.5530			-140.2	1.60		
-140.9	7.5425			-137.8	1.66		

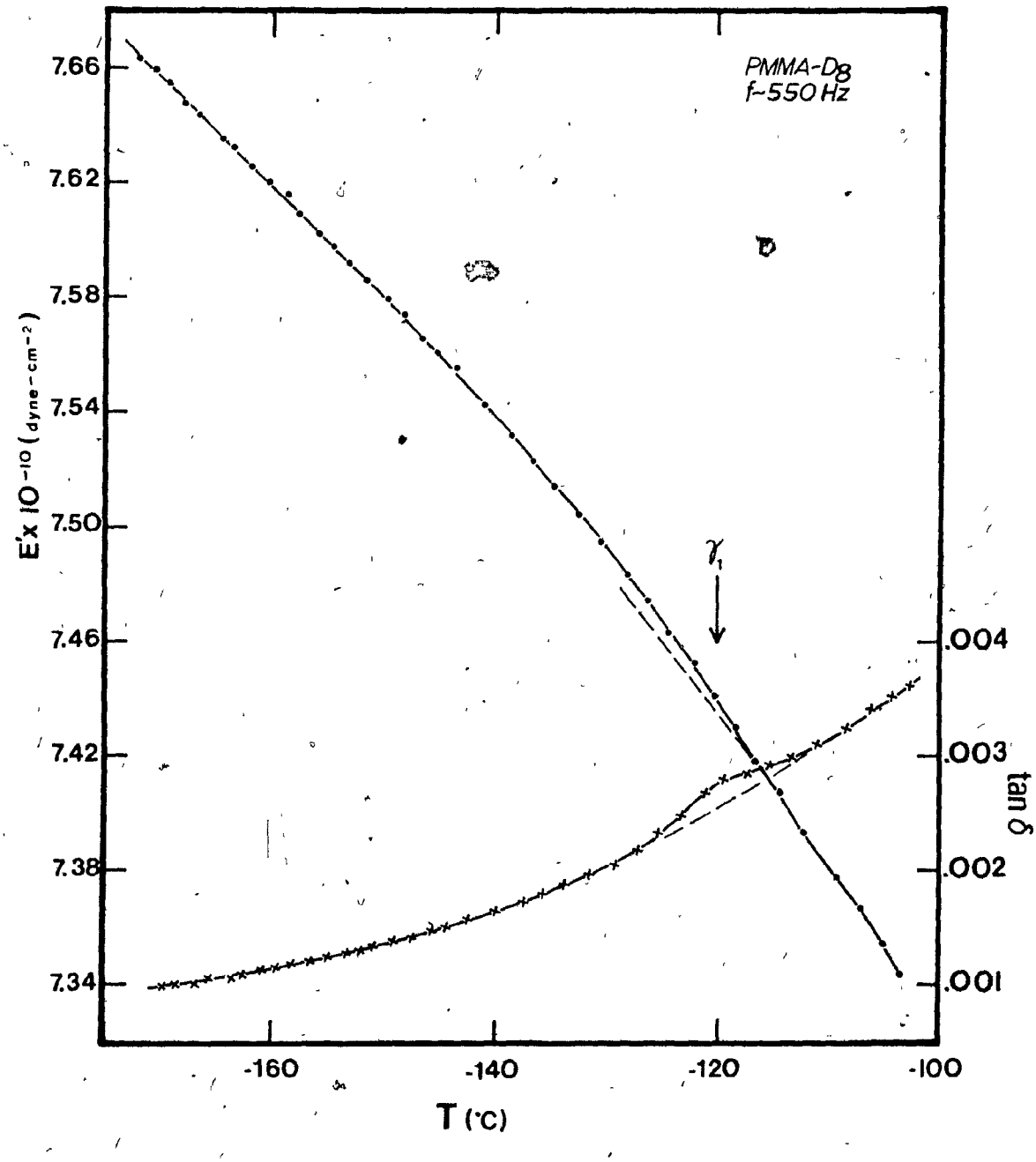
PMMA-D8
f-550 Hz
7.66
7.62
7.58
7.54
7.50
7.46
7.42
7.38
7.34
E'x 10⁻¹⁰ (dyne-cm⁻²)
γ1
.004
.003
.002
.001
tan δ
-160
-140
-120
-100
T (°C)

FIGURE IV-22

PMMA-D_8 : VIBRATING REED RESULTS AT ~1 KHZ. The γ_1 and γ_2 relaxations are evident at ~ -118°C (1007 Hz) and ~ -175°C (1017 Hz) respectively. (f_o varied from 1018.61 Hz at -185.2°C to 998.70 Hz at -93.3°C.)

T (°C)	E'x10^{-10} (dynes/cm^2)	tanδ x10^3	T (°C)	E'x10^{-10} (dynes/cm^2)	tanδ x10^3	T (°C)	E'x10^{-10} (dynes/cm^2)	tanδ x10^3
-185.2	5.3933		-147.3	5.3471		-112.3	5.2495	3.48
-184.4	5.3922	1.42	-146.1	5.3451		-110.9	5.2460	
-183.7	5.3913		-145.7	5.3450	1.98	-110.2	5.2431	3.63
-182.5	5.3903		-145.0	5.3435		-109.0	5.2387	
-181.4	5.3892		-143.8	5.3425		-107.9	5.2349	
-180.3	5.3884	1.41	-143.1	5.3404		-107.4	5.2338	3.83
-179.7	5.3873		-141.8	5.3376		-106.5	5.2300	
-178.7	5.3863		-141.3	5.3373	2.12	-105.6	5.2269	
-177.7	5.3853	1.47	-140.3	5.3346		-104.8	5.2247	4.01
-176.9	5.3845		-139.0	5.3324		-104.0	5.2222	
-175.8	5.3818		-138.2	5.3309		-103.0	5.2196	
-175.1	5.3813	1.44	-137.8		2.25	-102.0	5.2159	
-173.5	5.3787		-134.9		2.41	-101.5	5.2138	4.22
-172.9	5.3777		-132.1		2.49	-100.2	5.2095	
-172.2	5.3772	1.46	-128.8		2.64	-98.7	5.2041	
-169.2	5.3742		-128.2	5.3026		-97.9	5.2022	4.47
-168.3	5.3732	1.52	-127.2	5.2997		-97.1	5.1984	
-166.8	5.3717		-126.3	5.2968		-95.8	5.1937	
-164.7	5.3705		-125.6	5.2945	2.81	-94.8	5.1905	
-164.3	5.3695	1.56	-124.4	5.2910		-94.4	5.1890	4.77
-162.0	5.3684		-123.7	5.2891		-93.3	5.1845	
-161.4	5.3672	1.61	-122.8	5.2871	2.97			
-160.3	5.3649		-121.9	5.2838				
-159.2	5.3633		-121.2	5.2819				
-158.6	5.3642	1.66	-120.5	5.2794				
-158.2	5.3626		-119.8	5.2769	3.24			
-157.7	5.3617		-118.6	5.2727				
-156.9	5.3613		-117.8	5.2681				
-155.7	5.3593		-117.0	5.2660	3.35			
-155.3	5.3586	1.76	-116.3	5.2636				
-154.2	5.3571		-115.5	5.2598				
-152.7	5.3548		-114.6	5.2577				
-152.3	5.3546	1.82	-114.0	5.2548	3.43			
-150.8	5.3523		-113.1	5.2527				
-149.7	5.3507							
-149.3	5.3507	1.89						
-148.2	5.3488							

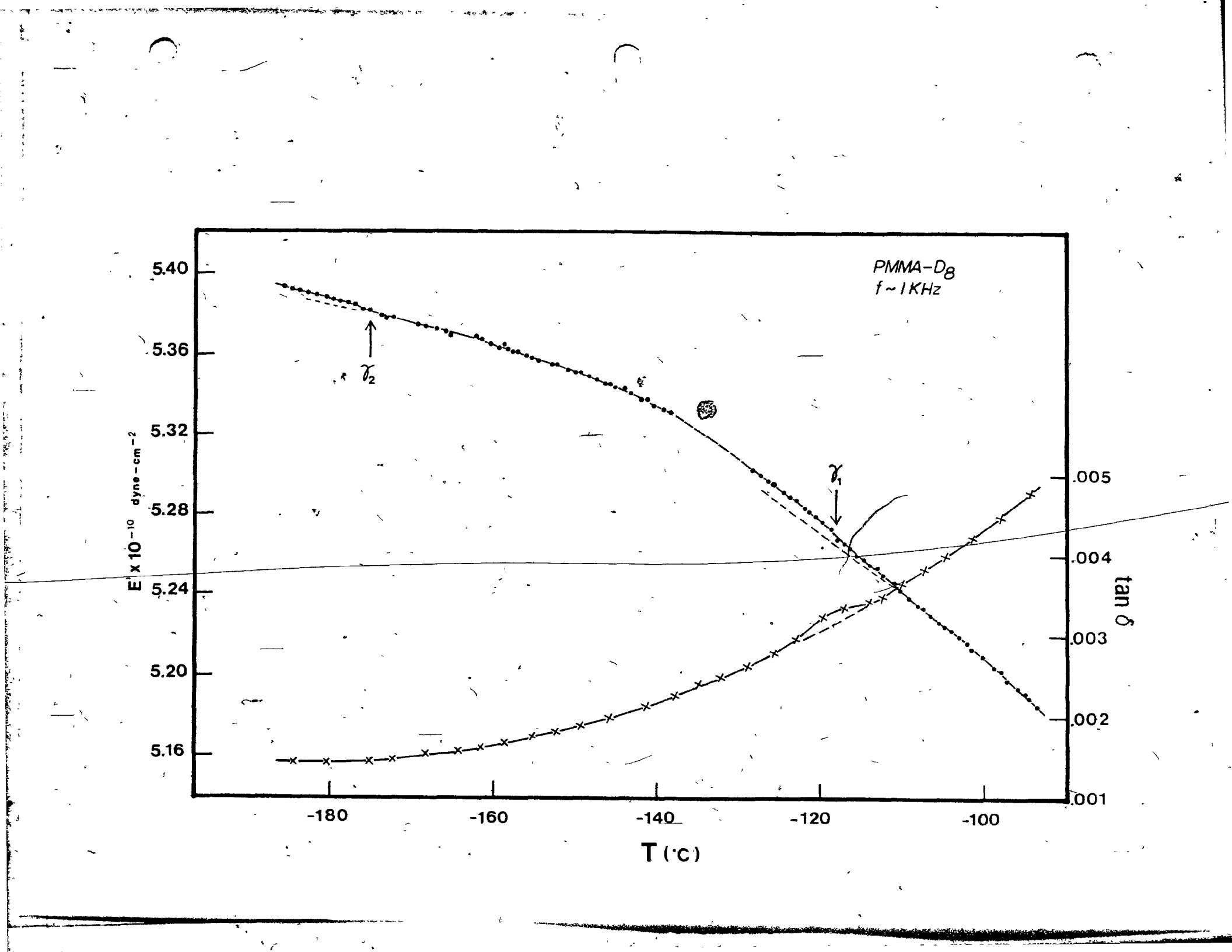
PMMA-D_8
$f \sim 1$ KHz
γ_2
γ_1
E' x 10^{-10} dyne-cm^{-2}
5.40
5.36
5.32
5.28
5.24
5.20
5.16
tan δ
.005
.004
.003
.002
.001
-180
-160
-140
-120
-100
T (°C)

FIGURE IV-23

PMMA-D_8 : VIBRATING REED RESULTS AT ~1400 HZ. The γ_1 and γ_2 relaxations are apparent at ~-119°C (1392 Hz) and ~-176°C (1416 Hz) respectively. (f_o varied from 1421.02 Hz at -191.6°C to 1383.24 Hz at -102.4°C.)

T (°C)	E'x10^{-10} (dynes/cm^2)
-191.6	6.1003
-189.0	6.0927
-186.0	6.0843
-183.2	6.0780
-181.0	6.0723
-178.6	6.0662
-176.2	6.0580
-174.7	6.0518
-172.6	6.0465
-170.0	6.0380
-168.2	6.0335
-165.7	6.0262
-163.6	6.0192
-161.2	6.0115
-158.8	6.0033
-155.8	5.9941
-153.4	5.9863
-150.4	5.9758
-147.3	5.9645
-145.0	5.9572
-141.0	5.9432
-138.5	5.9344
-136.0	5.9256
-133.2	5.9135
-130.5	5.9043
-127.5	5.8918
-124.7	5.8803
-121.2	5.8658
-118.5	5.8520
-116.1	5.8399
-113.7	5.8302
-111.8	5.8218
-109.3	5.8112
-107.0	5.8006
-104.2	5.7884
-102.4	5.7802

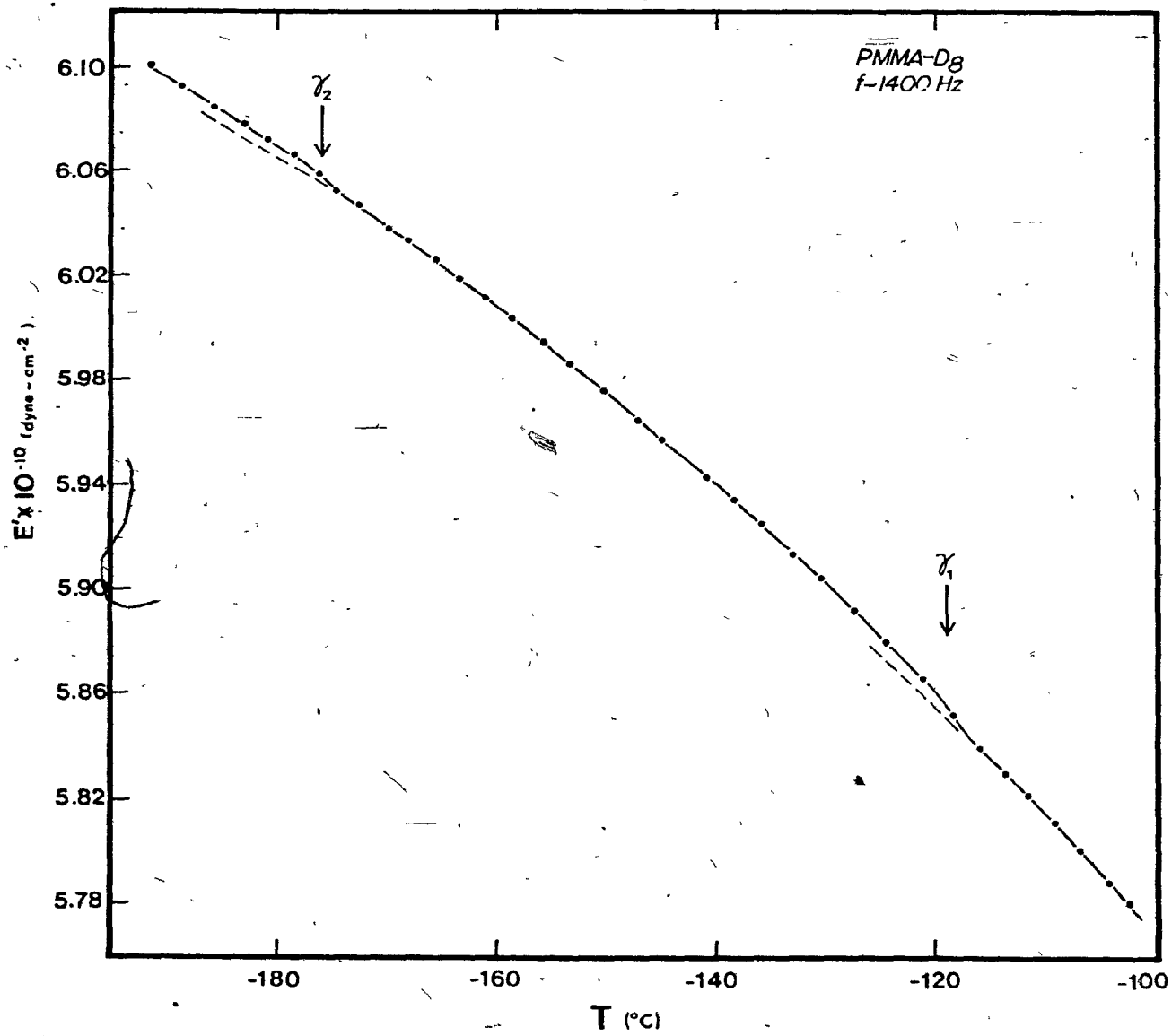
PMMA-D8
f-1400 Hz
γ2
γ1
6.10
6.06
6.02
5.98
5.94
5.90
5.86
5.82
5.78
E' x 10-10 (dyne - cm-2)
-180
-160
-140
-120
-100
T (°C)

FIGURE IV-24

PMMA-D_8 : VIBRATING REED RESULTS AT ~1730 Hz. The γ_1 relaxation is apparent at ~ -118.5°C and 1731 Hz. (f_o varied from 1741.16 Hz at -140.1°C to 1723.32 Hz at -102.0°C.)

T (°C)	E'x10^{-10} (dynes/cm^2)	T (°C)	tanδ x 10^3
-140.1	6.2421	-139.7	2.54
-137.9	6.2358	-137.2	2.65
-136.9	6.2331	-135.4	2.70
-136.0	6.2295	-133.5	2.72
-134.0	6.2239	-131.5	2.77
-131.9	6.2174	-129.5	2.82
-129.9	6.2115	-127.5	2.84
-128.0	6.2061	-125.6	2.88
-126.0	6.1999	-123.4	3.09
-124.0	6.1932	-121.4	3.26
-121.8	6.1871	-119.4	3.35
-119.8	6.1793	-116.9	3.40
-117.4	6.1696	-115.4	3.44
-115.9	6.1631	-113.1	3.44
-113.5	6.1558	-110.7	3.59
-111.3	6.1487	-109.2	3.70
-109.7	6.1422	-107.3	3.79
-107.8	6.1362	-105.5	3.83
-105.9	6.1295	-103.6	3.95
-103.9	6.1226	-101.5	4.06
-102.0	6.1149		

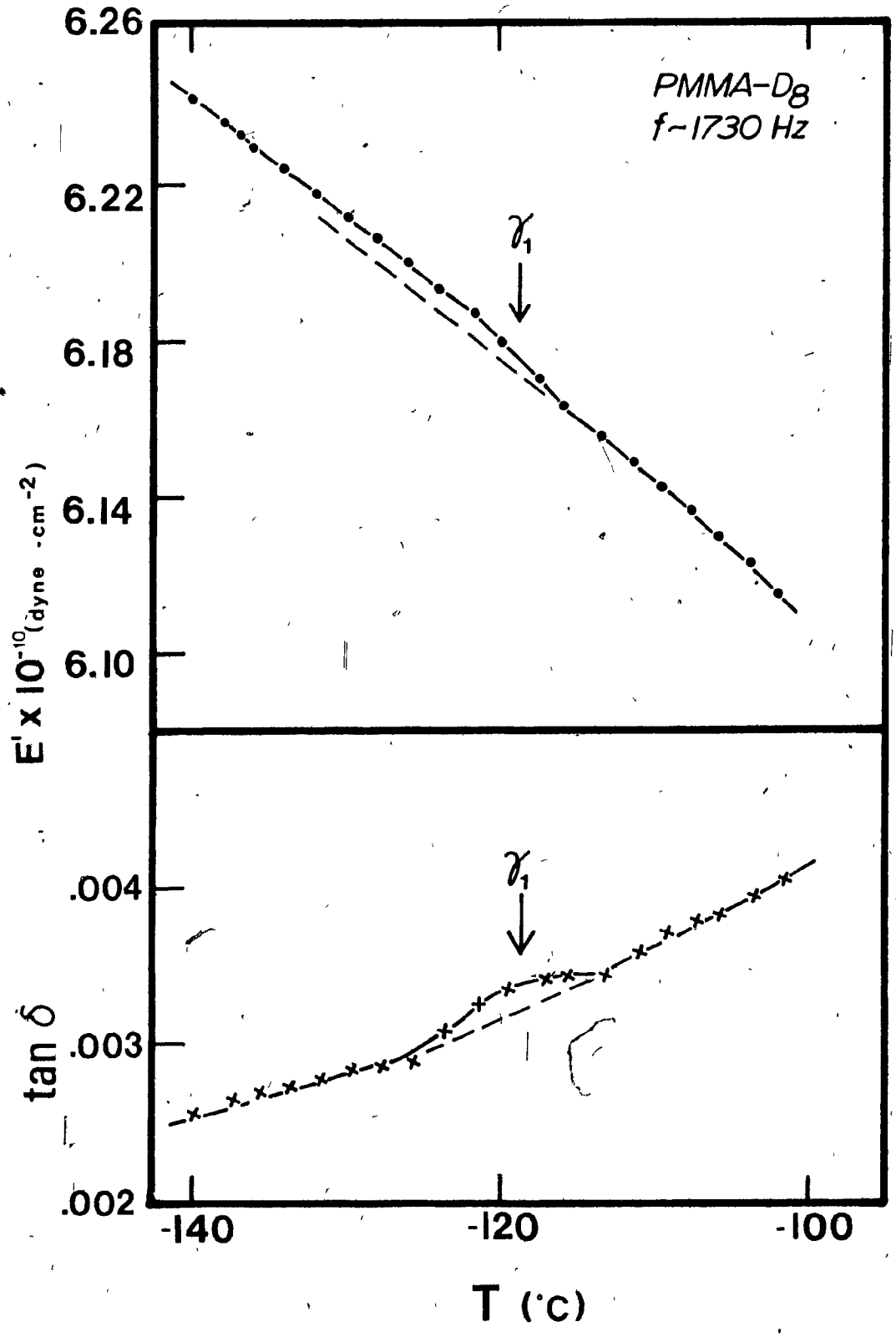
PMMA-D8
f~1730 Hz
γ1
γ1
E' x 10^-10 (dyne -cm^-2)
6.26
6.22
6.18
6.14
6.10
tan δ
.004
.003
.002
-140
-120
-100
T (°C)

FIGURE IV-25

PMMA-D_8 : VIBRATING REED RESULTS AT ~4000 HZ. The γ_1 and γ_2 relaxations are in evidence at ~ -106°C (3934 Hz) and ~ -175°C (4015 Hz) respectively. (f_o varied from 4034.8 Hz at -197.7°C to 3923.8 Hz at -99.3°C.)

T (°C)	E' x 10^{-10} (dynes/cm^2)	T (°C)	tanδ x 10^3
-197.7	6.2693	-187.3	1.61
-195.8	6.2624	-181.9	1.54
-192.8	6.2547	-179.6	1.62
-190.6	6.2491	-177.0	1.66
-188.0	6.2444	-175.3	1.61
-185.0	6.2351	-173.2	1.51
-182.4	6.2283	-171.1	1.49
-180.3	6.2231	-168.9	1.44
-177.6	6.2163	-166.9	1.51
-175.8	6.2091	-164.6	1.53
-173.8	6.2011	-162.2	1.59
-172.2	6.1946	-159.9	1.61
-169.3	6.1872	-157.3	1.77
-167.2$_5$	6.1816	-154.7	1.86
-165.1	6.1755	-151.7	1.83
-162.9	6.1690	-148.9	1.94
-160.5	6.1622	-146.8	2.19
-158.1	6.1548	-142.0	2.36
-155.2	6.1456	-139.7	2.71
-152.1	6.1354	-137.0	2.76
-149.4	6.1271	-134.8	3.06
-146.6	6.1170	-132.0	3.06
-143.1	6.1054	-129.1	3.08
-140.3	6.0980	-126.2	3.52
-137.7$_5$	6.0909	-123.2	3.86
-135.2	6.0808	-120.2	4.21
-132.5	6.0717	-116.5	4.69
-129.7	6.0613	-112.2	5.32
-126.8	6.0527	-107.4	6.93
-123.7	6.0417	-104.9	7.74
-120.7	6.0271	-100.2	7.52
-117.2	6.0146	-98.8	7.50
-112.8	5.9965	-96.0	9.36
-108.0	5.9766	-93.6	10.34
-105.5	5.9596		
-100.6	5.9348		
-99.3	5.9291		

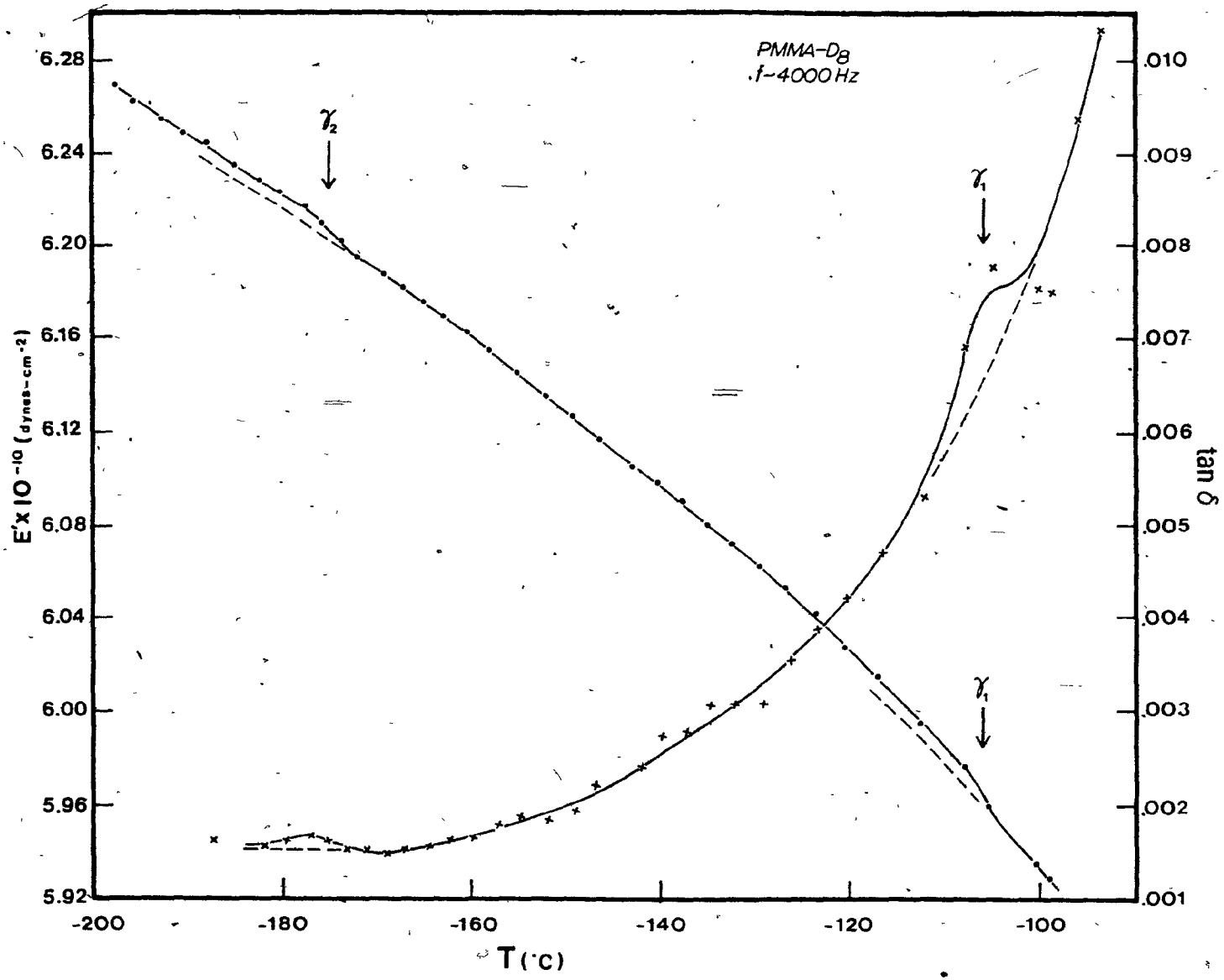
PMMA-D8
f~4000 Hz
γ2
γ1
γ1
E' x 10^-10 (dynes-cm^-2)
tan δ
6.28
6.24
6.20
6.16
6.12
6.08
6.04
6.00
5.96
5.92
.010
.009
.008
.007
.006
.005
.004
.003
.002
.001
-200
-180
-160
-140
-120
-100
T(°C)

APPENDIX V

ULTRASONIC GRAPHICAL AND NUMERICAL DATA FOR FREE-RADICAL PMMA-H_8 COVERING THE 1.3 TO 20.0 MHZ FREQUENCY RANGE (for Figures not shown in the text.)

Ultrasonic graphical data in support of results cited in Table 6 of the text for free-radically prepared PMMA-H_8 are given in this section to avoid repetition in the text. Tanδ and, in some cases, speed of sound and decibel level for a single echo have been plotted as a function of temperature, with detailed numerical data (consisting, in most cases, of the computer print-out obtained from the ultrasonic computer program given in Appendix III) also reported.

INDEX : ULTRASONIC GRAPHICAL AND NUMERICAL DATA FOR FREE-RADICAL PMMA-H_8

(see also Figure 17 of the text.)

FIGURE V-1

ULTRASONIC RESULTS FOR PMMA-H_8 AT 1.3 MHZ. The γ_1 and water dispersions are in evidence at $\sim -38^{\circ}C$ and $\sim +6^{\circ}C$ respectively.

TEMP (C)	TAN D	STD DEV (TAN D)	VEL (CM/US)	STD DEV (VEL)	# PTS	(•2)T1 (USEC)	DB1	(•2)T2 (USEC)	DB2	(•2)T3 (USEC)	DB3	(•2)T4 (USEC)	DB4	(•2)T5 (USEC)	DB5	(•2)T6	DB6
24.8	0.01833	0.00014	0.26344	0.00097	6	0.000	40.6	1.896	34.8	3.818	28.3	5.690	22.3	7.596	16.3	9.417	10.0
23.1	0.01813	0.00017	0.26428	0.00099	6	0.000	40.7	1.895	34.9	3.796	28.3	5.661	22.5	7.575	16.7	9.385	10.5
21.2	0.01759	0.00013	0.26478	0.00098	6	0.000	40.8	1.895	35.0	3.803	28.8	5.665	23.0	7.560	17.5	9.373	11.5
18.8	0.01720	0.00015	0.26533	0.00116	6	0.000	41.0	1.902	35.6	3.800	29.2	5.657	23.9	7.555	18.3	9.352	12.5
16.8	0.01702	0.00011	0.26604	0.00093	6	0.000	41.5	1.884	36.0	3.773	29.9	5.640	24.5	7.522	18.9	9.326	13.4
14.7	0.01578	0.00012	0.26679	0.00079	6	0.000	41.7	1.879	36.4	3.757	30.5	5.529	25.2	7.489	19.4	9.305	14.2
12.4	0.01626	0.00009	0.26710	0.00070	6	0.000	41.9	1.875	36.7	3.741	31.0	5.619	25.8	7.476	20.4	9.294	15.2
10.0	0.01577	0.00008	0.26778	0.00068	6	0.000	42.2	1.859	37.2	3.726	31.7	5.600	26.6	7.453	21.4	9.266	16.4
7.5	0.01534	0.00011	0.26869	0.00058	6	0.000	42.4	1.857	37.6	3.717	32.2	5.582	27.4	7.422	22.2	9.241	17.4
5.4	0.01489	0.00010	0.25940	0.00072	6	0.000	42.5	1.850	37.9	3.705	32.7	5.568	28.0	7.411	23.0	9.210	18.3
3.2	0.01454	0.00014	0.27001	0.00056	6	0.000	42.6	1.838	38.3	3.687	33.2	5.538	28.7	7.389	23.8	9.189	19.0
1.4	0.01404	0.00012	0.27063	0.00062	6	0.000	42.8	1.841	38.6	3.684	33.7	5.537	29.3	7.374	24.6	9.170	20.1
-0.8	0.01389	0.00010	0.27130	0.00062	6	0.000	43.2	1.839	39.0	3.674	34.3	5.529	29.9	7.352	25.2	9.150	20.8
-2.8	0.01354	0.00007	0.27180	0.00048	6	0.000	43.4	1.836	39.2	3.663	34.6	5.507	30.3	7.338	25.8	9.135	21.6
-5.0	0.01322	0.00007	0.27243	0.00052	6	0.000	43.6	1.827	39.5	3.656	35.0	5.491	30.9	7.323	26.5	9.111	22.3
-7.1	0.01254	0.00023	0.27267	0.00079	6	0.000	43.3	1.841	39.7	3.679	35.4	5.499	31.7	7.326	27.5	9.109	23.0
-8.8	0.01246	0.00015	0.27304	0.00068	6	0.000	43.8	1.831	39.9	3.674	35.8	5.485	32.1	7.314	27.9	9.095	23.6
-10.4	0.01227	0.00012	0.27351	0.00047	6	0.000	44.0	1.830	40.2	3.669	36.0	5.478	32.4	7.300	28.3	9.081	24.2
-12.3	0.01211	0.00014	0.27387	0.00066	6	0.000	44.2	1.823	40.3	3.662	36.3	5.467	32.8	7.290	28.7	9.067	24.6
-14.4	0.01200	0.00009	0.27462	0.00058	6	0.000	44.4	1.811	40.6	3.637	36.7	5.447	33.0	7.267	29.1	9.038	25.1
-16.0	0.01179	0.00007	0.27496	0.00056	6	0.000	44.6	1.814	40.8	3.639	36.8	5.442	33.3	7.258	29.4	9.031	25.7
-18.2	0.01142	0.00012	0.27485	0.00048	6	0.000	44.4	1.827	40.8	3.650	37.1	5.447	33.7	7.253	29.9	9.048	26.0
-20.4	0.01117	0.00010	0.27570	0.00062	6	0.000	44.6	1.820	40.9	3.643	37.4	5.430	34.0	7.241	30.4	9.014	26.6
-22.5	0.01092	0.00012	0.27616	0.00048	6	0.000	44.7	1.816	41.1	3.627	37.7	5.415	34.4	7.225	30.9	9.000	27.1
-25.0	0.01059	0.00017	0.27699	0.00063	6	0.000	44.9	1.813	41.2	3.627	37.9	5.425	34.6	7.207	31.4	8.973	27.6
-27.4	0.01036	0.00014	0.27739	0.00056	6	0.000	44.9	1.811	41.4	3.615	38.2	5.392	35.1	7.197	31.9	8.950	28.2
-29.8	0.01045	0.00104	0.27755	0.00044	6	0.000	45.1	1.811	41.5	3.611	41.5	5.390	35.5	7.184	32.3	8.950	28.6
-32.2	0.00990	0.00019	0.27828	0.00048	6	0.000	45.3	1.788	41.7	3.600	38.5	5.372	35.8	7.160	32.7	8.929	29.3
-34.5	0.00990	0.00017	0.27929	0.00029	6	0.000	45.5	1.775	41.9	3.567	38.8	5.343	36.0	7.131	32.9	8.893	29.6
-36.3	0.00967	0.00025	0.27945	0.00043	6	0.000	45.7	1.767	41.9	3.576	38.9	5.342	36.2	7.119	33.2	8.890	30.1
-38.8	0.00965	0.00020	0.28074	0.00063	6	0.000	45.8	1.761	42.2	3.556	39.1	5.329	36.4	7.102	33.4	8.839	30.4
-41.3	0.00939	0.00022	0.28076	0.00027	6	0.000	45.9	1.764	42.3	3.542	39.3	5.317	36.7	7.091	33.8	8.845	30.9
-43.5	0.00913	0.00021	0.28122	0.00046	6	0.000	45.8	1.752	42.4	3.543	39.4	5.310	36.9	7.080	34.2	8.826	31.2
-45.6	0.00872	0.00022	0.28100	0.00049	6	0.000	45.6	1.759	42.3	3.557	39.5	5.319	37.3	7.086	34.5	8.837	31.6
-47.6	0.00894	0.00022	0.28169	0.00049	6	0.000	45.8	1.746	42.5	3.537	39.6	5.298	37.4	7.058	34.5	8.816	31.7
-49.7	0.00866	0.00021	0.28208	0.00049	6	0.000	45.7	1.740	42.5	3.533	39.6	5.294	37.4	7.050	34.7	8.802	31.9
-51.6	0.00849	0.00022	0.28289	0.00060	6	0.000	45.6	1.738	42.4	3.530	39.6	5.278	37.4	7.040	34.8	8.772	32.1
-53.6	0.00819	0.00020	0.28295	0.00048	6	0.000	45.3	1.757	42.3	3.533	39.6	5.283	37.6	7.046	34.9	8.777	32.3
-56.4	0.00810	0.00019	0.28326	0.00071	6	0.000	45.5	1.748	42.4	3.547	39.9	5.280	37.6	7.032	35.3	8.770	32.6
-58.4	0.00798	0.00022	0.28401	0.00033	6	0.000	45.4	1.751	42.3	3.514	39.8	5.262	37.7	7.014	35.3	8.747	32.7
-59.9	0.00793	0.00025	0.28430	0.00055	6	0.000	45.4	1.743	42.2	3.514	39.8	5.266	37.7	7.007	35.4	8.733	32.7
-61.0	0.00817	0.00029	0.28585	0.00072	6	0.000	45.5	1.723	42.2	3.499	39.5	5.229	37.5	6.974	35.0	8.679	32.6
-65.2	0.00793	0.00026	0.28536	0.00041	6	0.000	45.3	1.732	42.2	3.499	39.6	5.233	37.7	6.975	35.3	8.704	32.7
-67.4	0.00798	0.00034	0.28594	0.00059	6	0.000	45.5	1.727	42.0	3.500	39.6	5.226	37.7	6.966	35.3	8.683	32.7

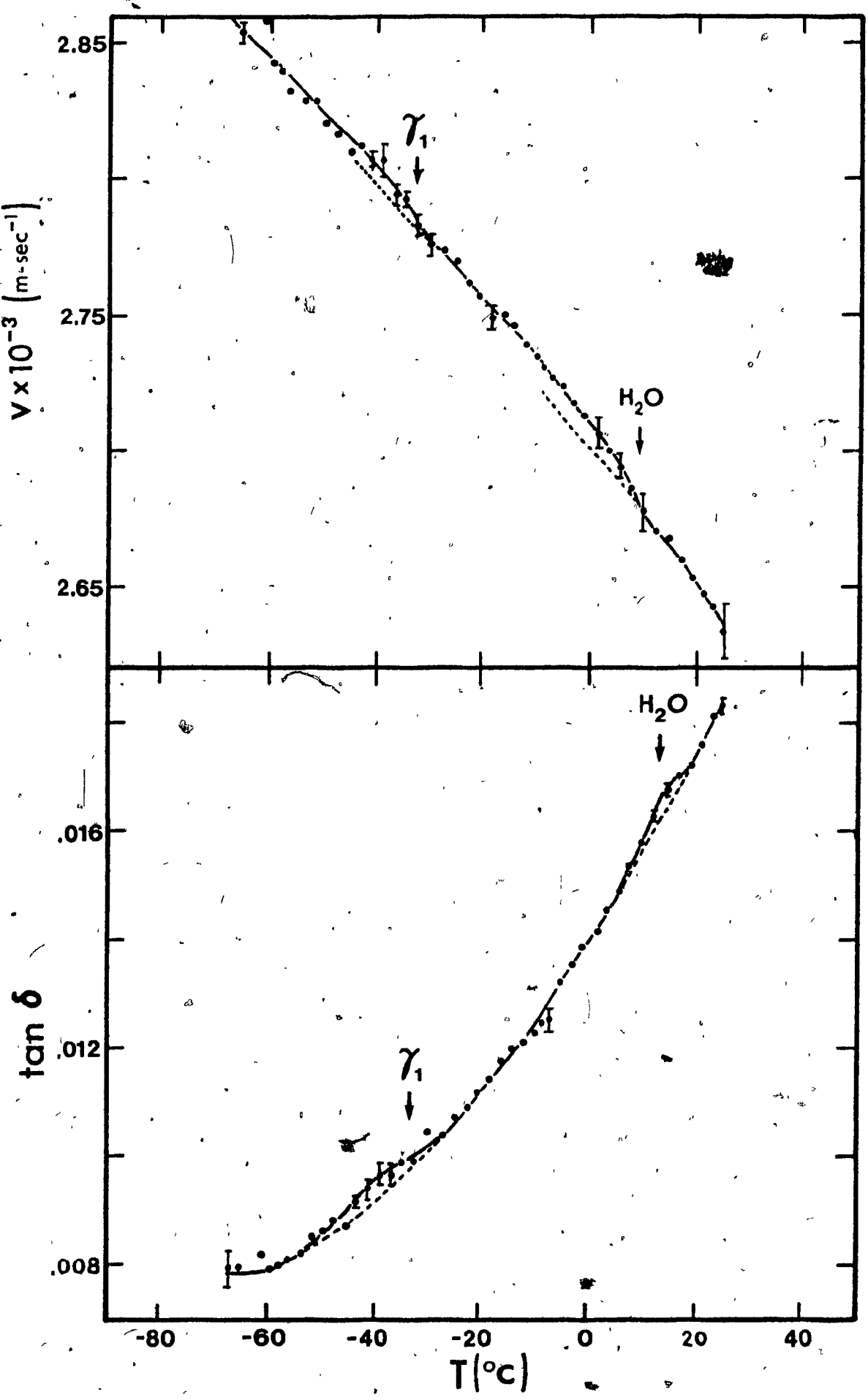
2.85
2.75
2.65
V x 10⁻³ (m-sec⁻¹)
γ1
H2O
.016
.012
.008
tan δ
H2O
γ1
-80
-60
-40
-20
0
20
40
T(°C)

FIGURE V-2

ULTRASONIC RESULTS FOR PMMA-H_8 AT 3.4 MHZ. The γ_1 relaxation is present at ~ -20°C.

TEMP (C)	TAN D	STD DEV (TAN D)	VEL (CM/US)	STD DEV (VEL)	# PTS	(.5)T1 (USEC)	DB1	(.5)T2 (USEC)	DB2	(.5)T3 (USEC)	DB3	(.5)T4 (USEC)	DB4	(.5)T5 (USEC)	DB5
-81.4	0.01144	0.00020	0.28896	0.00080	5	0.100	49.6	2.433	45.0	4.759	39.9	7.064	34.6	9.343	30.3
-78.0	0.01142	0.00020	0.28850	0.00080	5	0.100	49.8	2.434	45.3	4.767	40.1	7.074	34.9	9.357	30.5
-72.7	0.01165	0.00025	0.28782	0.00068	5	0.100	50.2	2.445	45.6	4.775	40.5	7.086	34.9	9.384	30.5
-67.7	0.01187	0.00022	0.28630	0.00053	5	0.100	50.5	2.456	45.8	4.786	40.5	7.122	34.9	9.433	30.3
-60.7	0.01229	0.00030	0.28598	0.00083	5	0.100	50.8	2.452	46.1	4.800	40.8	7.142	34.7	9.434	29.9
-57.0	0.01250	0.00039	0.28556	0.00054	5	0.100	50.9	2.450	46.4	4.803	40.9	7.137	34.6	9.453	29.7
-51.7	0.01297	0.00040	0.28468	0.00074	5	0.100	51.3	2.472	46.5	4.834	40.9	7.157	34.3	9.490	29.2
-46.7	0.01328	0.00040	0.28392	0.00063	5	0.100	51.5	2.477	46.7	4.841	40.8	7.173	34.2	9.516	28.8
-43.0	0.01349	0.00048	0.28359	0.00070	5	0.100	51.6	2.481	46.9	4.850	41.0	7.184	34.2	9.526	28.5
-37.2	0.01397	0.00050	0.28268	0.00092	5	0.100	52.0	2.502	46.9	4.874	41.0	7.219	33.7	9.557	28.0
-32.0	0.01465	0.00057	0.28214	0.00083	5	0.100	52.1	2.486	47.0	4.878	40.7	7.228	33.1	9.567	26.9
-27.0	0.01525	0.00061	0.28184	0.00116	5	0.100	52.2	2.508	46.8	4.905	40.4	7.241	32.6	9.584	25.8
-21.5	0.01576	0.00057	0.28079	0.00088	5	0.100	52.3	2.504	46.6	4.908	39.9	7.258	31.9	9.618	24.9
-16.2	0.01590	0.00041	0.27922	0.00114	5	0.100	52.2	2.540	45.9	4.951	39.1	7.300	31.2	9.682	24.3
-11.0	0.01613	0.00033	0.27811	0.00081	5	0.100	52.2	2.515	45.6	4.951	38.7	7.316	30.8	9.709	23.7
-6.0	0.01656	0.00029	0.27780	0.00083	5	0.100	52.0	2.527	45.1	4.950	38.0	7.345	29.9	9.714	22.7
-2.7	0.01708	0.00031	0.27594	0.00052	5	0.100	51.8	2.540	44.8	4.973	37.3	7.374	29.0	9.787	21.4
4.6	0.01775	0.00029	0.27433	0.00055	5	0.100	51.6	2.564	44.2	5.000	36.3	7.414	27.7	9.850	19.8

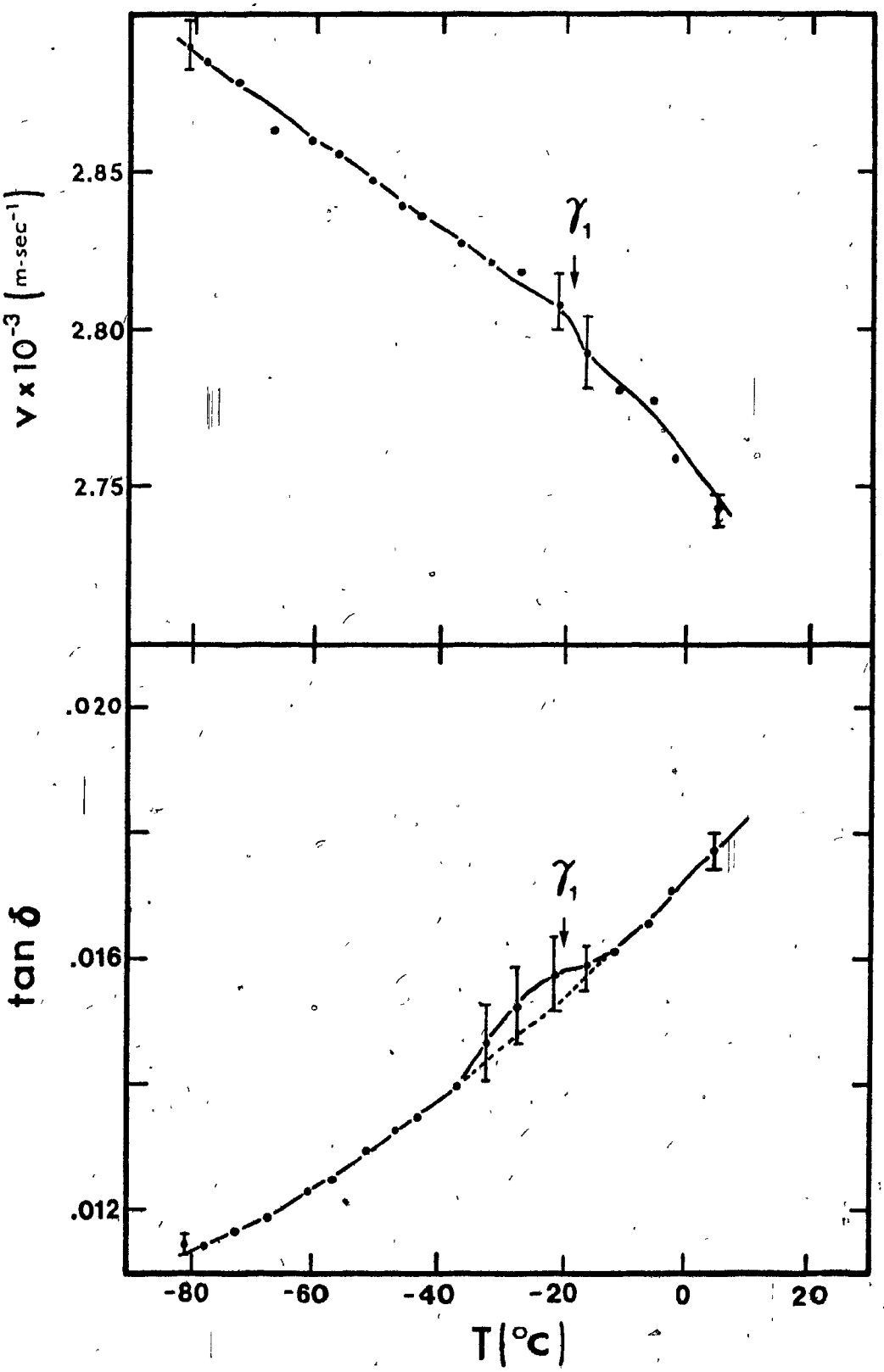
2.85
2.80
2.75
V x 10^-3 (m-sec^-1)
γ1
.020
.016
.012
tan δ
γ1
-80
-60
-40
-20
0
20
T(°C)

FIGURE V-3

ULTRASONIC RESULTS FOR PMMA-H_8 AT 13.0 (±0.1) MHZ: A γ_2 relaxation is possibly present at ~-56°C, with a peak thought due to bonding agent (3-chloropropyl benzene) appearing at~-85°C. (Tan δ has been calculated from the first two peaks only, for consistency.)

TEMP (C)	TAN D	STD DEV (TAN D)	VEL (CM/US)	STD DEV (VEL)	# PTS	0.5 T1 (USEC)	DB1	0.5 T2 (USEC)	DB2	0.5 T3 (USEC)	DB3	0.5 T4 (USEC)	DB4	0.5 T5 (USEC)	DB5	TAN D [CALC. FROM TWO PTS. ONLY]
23.5	0.01868	0.00000	0.25665	0.00000	2	0.100	40.1	1.830	17.2							
19.5	0.01412	0.00000	0.25814	0.00000	2	0.100	40.6	1.820	23.4							
14.0	0.01345	0.00000	0.26272	0.00000	2	0.100	42.0	1.790	25.9							
6.5	0.01254	0.00000	0.26118	0.00000	2	0.100	43.4	1.800	28.3							
2.5	0.01408	0.00074	0.26041	0.00309	3	0.100	44.4	1.770	29.3	3.510	10.4					0.01276
-2.5	0.01289	0.00088	0.26350	0.00226	3	0.100	45.5	1.810	31.7	3.470	14.7					0.01139
-6.0	0.01202	0.00055	0.26429	0.00182	3	0.100	45.6	1.760	32.6	3.460	17.0					0.01105
-11.5	0.01134	0.00059	0.26828	0.00234	3	0.100	46.9	1.780	34.6	3.410	20.3					0.00981
-15.0	0.01077	0.00051	0.26797	0.00117	3	0.100	47.7	1.770	35.2	3.415	22.4					0.00972
-20.5	0.01044	0.00027	0.26950	0.00048	4	0.100	48.5	1.750	37.4	3.405	25.0	5.040	12.0			0.00950
-25.0	0.00952	0.00028	0.26909	0.00000	4	0.100	49.1	1.750	39.0	3.400	27.9	5.050	15.7			0.00864
-31.0	0.00855	0.00016	0.26812	0.00155	4	0.100	50.4	1.730	41.1	3.380	30.8	5.070	20.0			0.00805
36.5	0.00812	0.00009	0.27231	0.00030	5	0.100	51.7	1.735	43.0	3.370	33.4	5.000	23.8	6.620	14.4	0.00751
-40.5	0.00759	0.00005	0.27306	0.00034	5	0.100	52.3	1.720	44.0	3.360	35.0	4.980	26.2	6.600	17.5	0.00723
-44.5	0.00712	0.00004	0.27357	0.00017	5	0.100	53.4	1.720	45.5	3.350	37.0	4.970	28.8	6.590	20.8	0.00688
-48.5	0.00678	0.00004	0.27441	0.00039	5	0.100	54.0	1.720	46.5	3.350	38.5	4.960	30.6	6.570	23.1	0.00653
-52.5	0.00638	0.00003	0.27424	0.00051	5	0.100	54.7	1.710	47.4	3.350	39.8	4.960	32.6	6.570	25.5	0.00640
-57.0	0.00598	0.00003	0.27612	0.00020	5	0.100	55.4	1.710	48.5	3.320	41.6	4.930	34.8	6.530	28.2	0.00605
-63.5	0.00540	0.00003	0.27664	0.00017	5	0.100	56.2	1.710	50.2	3.310	43.8	4.920	37.8	6.520	31.7	0.00526
-68.5	0.00507	0.00005	0.27724	0.00033	5	0.100	56.8	1.695	51.4	3.305	45.3	4.910	39.5	6.500	34.0	0.00478
-74.5	0.00482	0.00006	0.27846	0.00017	5	0.100	57.5	1.690	52.3	3.290	46.4	4.885	41.1	6.475	35.4	0.00462
-80.0	0.00453	0.00007	0.27889	0.00020	5	0.100	58.3	1.690	53.3	3.280	47.7	4.880	42.8	6.465	38.0	0.00444
-86.0	0.00430	0.00004	0.27925	0.00029	5	0.100	58.8	1.680	53.9	3.280	48.9	4.870	44.1	6.455	39.5	0.00438
-99.5	0.00391	0.00005	0.28013	0.00018	5	0.100	59.4	1.680	54.9	3.270	50.3	4.850	46.0	6.440	41.9	0.00402
-94.5	0.00351	0.00005	0.28083	0.00021	5	0.100	59.9	1.675	56.0	3.260	51.8	4.845	47.9	6.420	44.3	0.00350
-98.5	0.00329	0.00006	0.28101	0.00018	5	0.100	60.5	1.675	56.9	3.255	52.9	4.835	49.3	6.420	45.9	0.00323
-104.0	0.00290	0.00004	0.28155	0.00010	5	0.100	61.0	1.680	57.7	3.255	54.2	4.830	51.3	6.410	48.0	0.00295
-110.5	0.00248	0.00006	0.28119	0.00047	5	0.100	62.4	1.660	59.4	3.245	56.5	4.830	53.8	6.410	51.3	0.00271
-118.0	0.00222	0.00008	0.28190	0.00036	5	0.100	63.4	1.665	60.8	3.240	58.0	4.815	55.6	6.400	53.6	0.00234
-124.0	0.00202	0.00005	0.28280	0.00033	5	0.100	63.5	1.660	61.0	3.235	58.6	4.800	56.5	6.380	54.5	0.00226
-127.5	0.00197	0.00004	0.28289	0.00027	5	0.100	63.8	1.660	61.5	3.240	59.0	4.805	57.0	6.375	55.1	0.00208
-133.0	0.00184	0.00008	0.28389	0.00046	5	0.100	64.0	1.645	61.7	3.220	59.4	4.785	57.5	6.350	55.9	0.00210
-137.0	0.00178	0.00008	0.28471	0.00027	5	0.100	64.5	1.655	62.2	3.215	60.0	4.770	58.3	6.340	56.6	0.00209
-141.5	0.00169	0.00005	0.28452	0.00033	5	0.100	64.5	1.650	62.4	3.210	60.4	4.775	58.7	6.340	57.0	0.00191
-146.5	0.00165	0.00009	0.28599	0.00026	5	0.100	64.9	1.645	62.8	3.200	60.7	4.750	59.0	6.310	57.7	0.00192
-151.5	0.00160	0.00009	0.28627	0.00028	5	0.100	65.0	1.640	62.9	3.200	60.9	4.750	59.3	6.300	58.0	0.00192
-157.0	0.00156	0.00009	0.28645	0.00000	5	0.100	65.4	1.650	63.3	3.200	61.5	4.750	59.8	6.300	58.6	0.00191
-163.0	0.00143	0.00006	0.28765	0.00026	5	0.100	64.8	1.635	63.0	3.180	61.4	4.730	59.8	6.270	58.6	0.00166
-167.5	0.00136	0.00007	0.28831	0.00046	5	0.100	64.5	1.630	62.7	3.165	61.1	4.710	59.7	6.260	58.6	0.00166
-172.5	0.00145	0.00000	0.28599	0.00027	3	0.100	66.1	1.655	64.5	3.205	62.9					0.00145

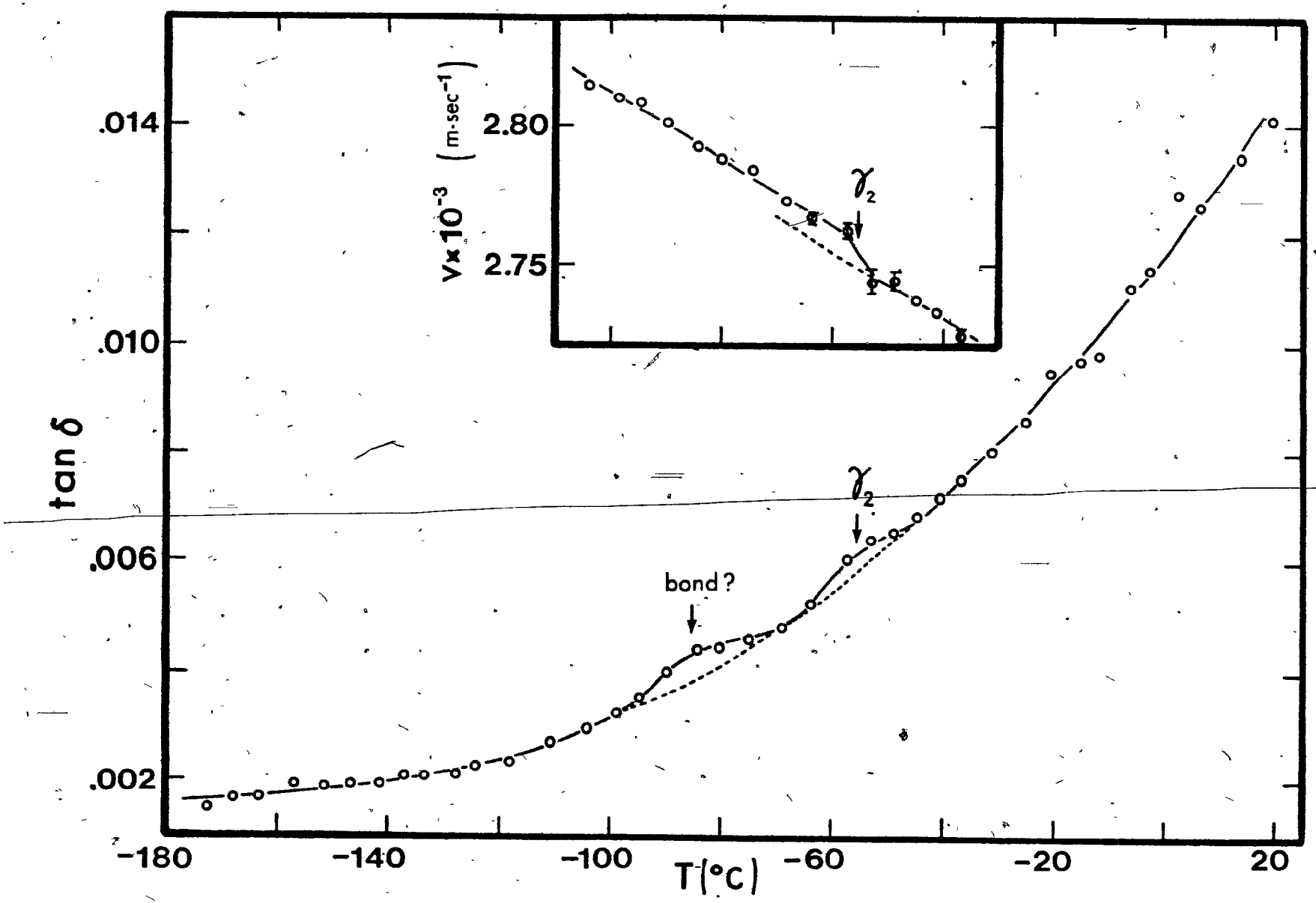
.014
.010
.006
.002
tan δ
-180
-140
-100
-60
-20
20
T(°C)
bond ?
γ2
γ2
V×10^-3 (m·sec^-1)
2.80
2.75

FIGURE V-4

ULTRASONIC RESULTS FOR PMMA-H_8 AT 13.6 MHZ. A γ_1 peak is present at $\sim -1^{\circ}C$ and the water dispersion is apparent at $\sim +34^{\circ}C$ as a local minimum in the db level of the second echo. (Tan δ has been calculated from two peaks throughout.)

TEMP (C)	TAN D	(.5)T1 (USEC)	DB1	(.5)T2 (USEC)	DB2
-54.8	0.00715	0.100	51.6	1.760	42.8
-50.5	0.00739	0.100	51.5	1.762	42.4
-46.0	0.00774	0.100	50.8	1.773	41.2
-41.7	0.00804	0.100	50.2	1.778	40.2
-36.8	0.00854	0.100	48.8	1.775	38.2
-32.7	0.00907	0.100	47.7	1.781	36.4
-29.0	0.00949	0.100	46.8	1.792	34.9
-25.1	0.01018	0.100	45.8	1.797	33.0
-21.0	0.01076	0.100	44.5	1.793	31.0
-17.3	0.01143	0.100	43.0	1.800	28.6
-14.3	0.01201	0.100	41.8	1.808	26.6
-10.7	0.01278	0.100	40.3	1.800	24.2
-8.0	0.01331	0.100	39.1	1.813	22.2
-5.2	0.01404	0.100	38.1	1.810	20.3
-3.0	0.01443	0.100	37.5	1.820	19.1
-1.0	0.01471	0.100	36.9	1.825	18.1
1.7	0.01508	0.100	36.2	1.818	17.0
5.0	0.01577	0.100	35.0	1.837	14.7
6.2	0.01604	0.100	34.6	1.833	14.0
7.7	0.01642	0.100	33.9	1.826	12.9
10.0	0.01701	0.100	33.4	1.821	11.7
13.0	0.01713	0.100	32.8	1.841	10.7
15.0	0.01791	0.100	32.4	1.825	9.5
18.0	0.01796	0.100	31.9	1.865	8.4
20.7	0.01887	0.100	31.1	1.845	6.7
24.1	0.01969	0.100	30.0	1.813	5.0
27.0	0.02052	0.100	28.6	1.810	2.6
29.3	0.02149	0.100	26.9	1.770	0.3

TEMP (C)	DB_1
32.9	24.8
35.5	23.8
37.3	22.7
39.8	22.2
43.5	20.0
49.4	15.4
51.5	13.8
53.0	12.2

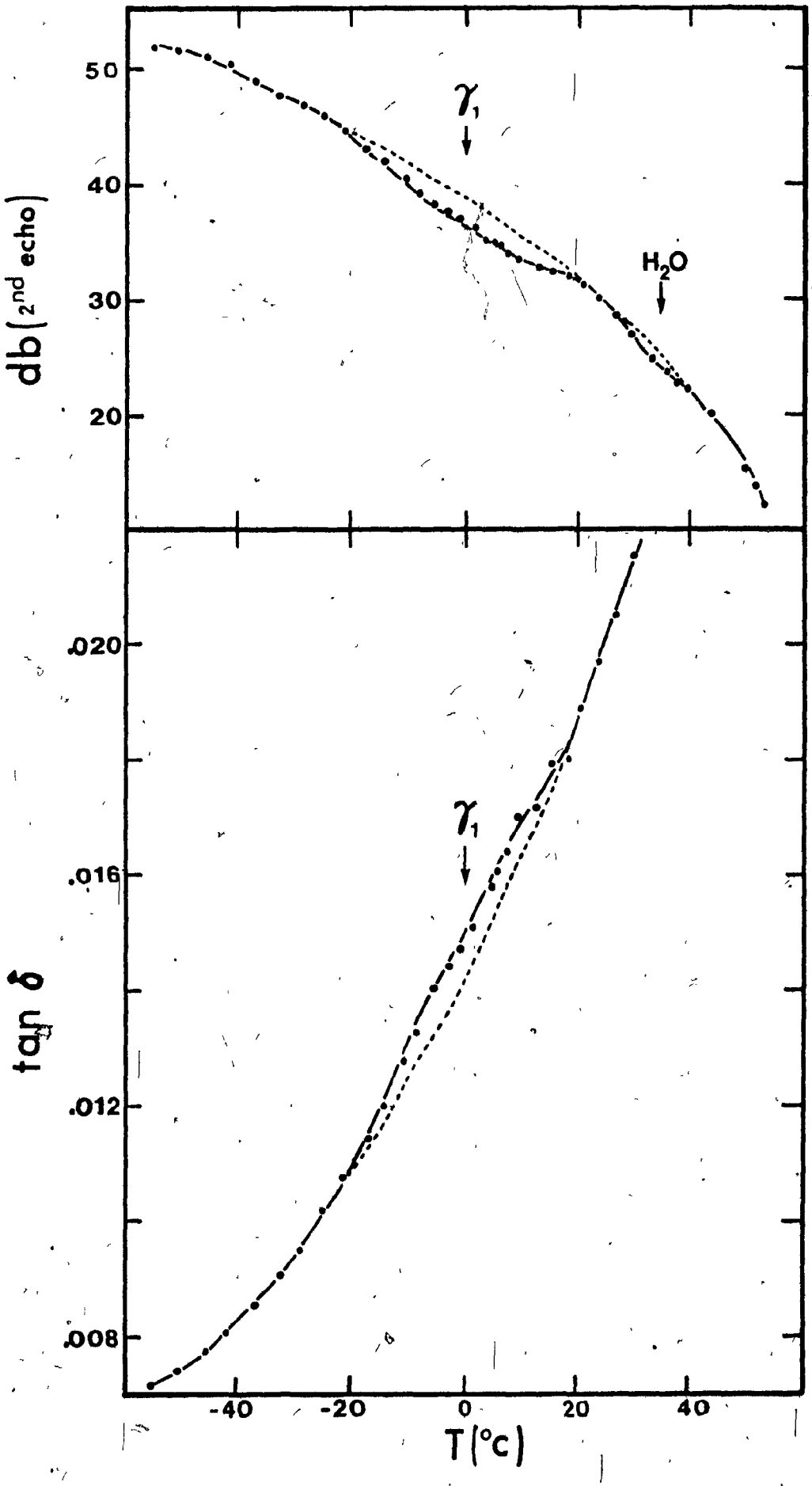
50
40
30
20
db(2nd echo)
γ1
H2O
.020
.016
.012
.008
tan δ
γ1
-40
-20
0
20
40
T(°C)

FIGURE V-5

ULTRASONIC RESULTS FOR PMMA-H_8 AT 18.5 MHZ. A $\tan\delta$ peak (labeled γ_3) may be present at $\sim -92.5^{o}C$ and a hint of the water relaxation is evident at $\sim +42^{o}C$ from the db versus temperature data.

TEMP (C)	TAN D	STD DEV (TAN D)	VEL (CM/US)	STD DEV (VEL)	# PTS	(.5)T1 (USEC)	DB1	(.5)T2 (USEC)	DB2	(.5)T3 (USEC)	DB3	(.5)T4 (USEC)	DB4	(.5)T5 (USEC)	DB5
-118.0	0.00260	0.00004	0.29614	0.00059	5	0.100	48.3	1.610	44.6	3.116	40.8	4.611	36.7	6.096	32.6
-115.0	0.00267	0.00003	0.29636	0.00036	5	0.100	48.5	1.600	44.7	3.108	40.7	4.598	36.6	6.092	32.4
-112.0	0.00275	0.00005	0.29592	0.00056	5	0.100	48.1	1.612	44.3	3.117	40.2	4.614	35.9	6.101	31.5
-108.9	0.00288	0.00004	0.29561	0.00040	5	0.100	47.8	1.613	43.7	3.111	39.4	4.617	34.9	6.108	30.4
-105.5	0.00303	0.00005	0.29519	0.00052	5	0.100	47.3	1.618	42.9	3.124	38.5	4.623	33.7	6.118	28.9
-101.7	0.00324	0.00005	0.29449	0.00066	5	0.100	46.7	1.621	42.1	3.138	37.3	4.634	32.1	6.132	27.1
-98.1	0.00344	0.00002	0.29386	0.00043	5	0.100	46.1	1.625	41.0	3.135	35.8	4.640	30.4	6.147	25.2
-94.2	0.00370	0.00004	0.29326	0.00060	5	0.100	45.5	1.623	40.1	3.146	34.5	4.655	28.6	6.154	23.0
-90.4	0.00396	0.00004	0.29321	0.00045	5	0.100	45.0	1.627	39.3	3.141	33.2	4.654	27.0	6.158	20.9
-86.9	0.00415	0.00005	0.29218	0.00051	5	0.100	44.6	1.631	38.7	3.157	32.3	4.667	25.7	6.160	19.3
-83.9	0.00434	0.00005	0.29168	0.00066	5	0.100	44.3	1.630	38.1	3.167	31.4	4.678	24.5	6.191	17.8
-80.8	0.00455	0.00006	0.29163	0.00034	5	0.100	44.0	1.631	37.5	3.157	30.5	4.670	23.2	6.193	16.2
-77.6	0.00505	0.00008	0.29124	0.00051	5	0.100	44.0	1.640	36.9	3.164	29.2	4.685	21.1	6.200	13.1
-74.8	0.00531	0.00010	0.29035	0.00049	5	0.100	43.9	1.640	36.6	3.172	28.4	4.700	19.8	6.216	11.4
-71.6	0.00561	0.00011	0.28931	0.00050	5	0.100	43.7	1.647	35.9	3.187	27.4	4.712	18.1	6.241	9.2
-68.4	0.00591	0.00010	0.28771	0.00010	5	0.100	43.2	1.647	34.9	3.187	25.8	4.731	15.9	6.274	6.7

T(C)	Db1
30.1	6.0
32.2	5.7
34.3	5.6
36.8	5.1
38.2	4.8
39.0	4.6
40.1	4.4
41.3	4.1
42.5	3.9
44.0	3.7
45.0	3.5
46.2	3.4
47.3	3.3
48.7	3.1
49.7	2.9
51.6	2.5
53.1	2.1

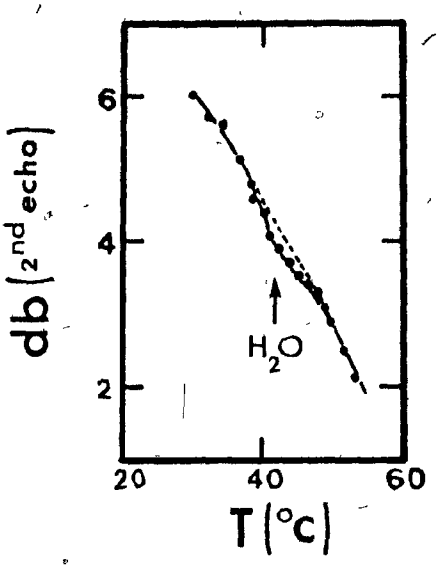
db (2nd echo)
6
4
2
H2O
20
40
60
T (°C)

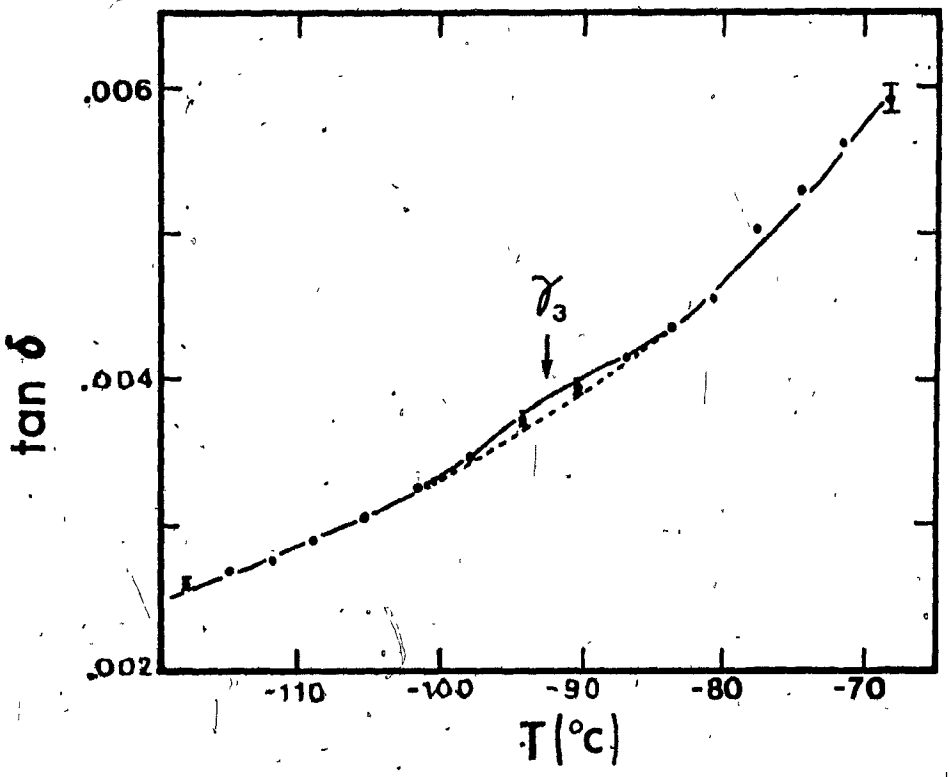
tan δ
.006
.004
.002
γ3
-110
-100
-90
-80
-70
T (°C)

FIGURE V-6

ULTRASONIC RESULTS FOR PMMA-H_8 AT 20.0 MHZ. The γ_1 relaxation is apparent at $\sim -1^{\circ}C$ as a local db minimum.

TEMP (C)	DB1
-33.0	39.5
-29.1	38.3
-25.1	36.5
-21.1	35.2
-15.7	32.8
-11.4	30.6
-8.5	29.3
-5.9	28.3
-3.4	27.2
-1.0	26.2
2.2	24.8
5.1	23.7
7.0	22.9
9.5	22.5
11.1	21.8
12.9	21.0
14.9	20.3
17.2	19.2
19.5	18.4
21.4	17.6
22.8	17.0
25.3	15.8
28.5	14.1

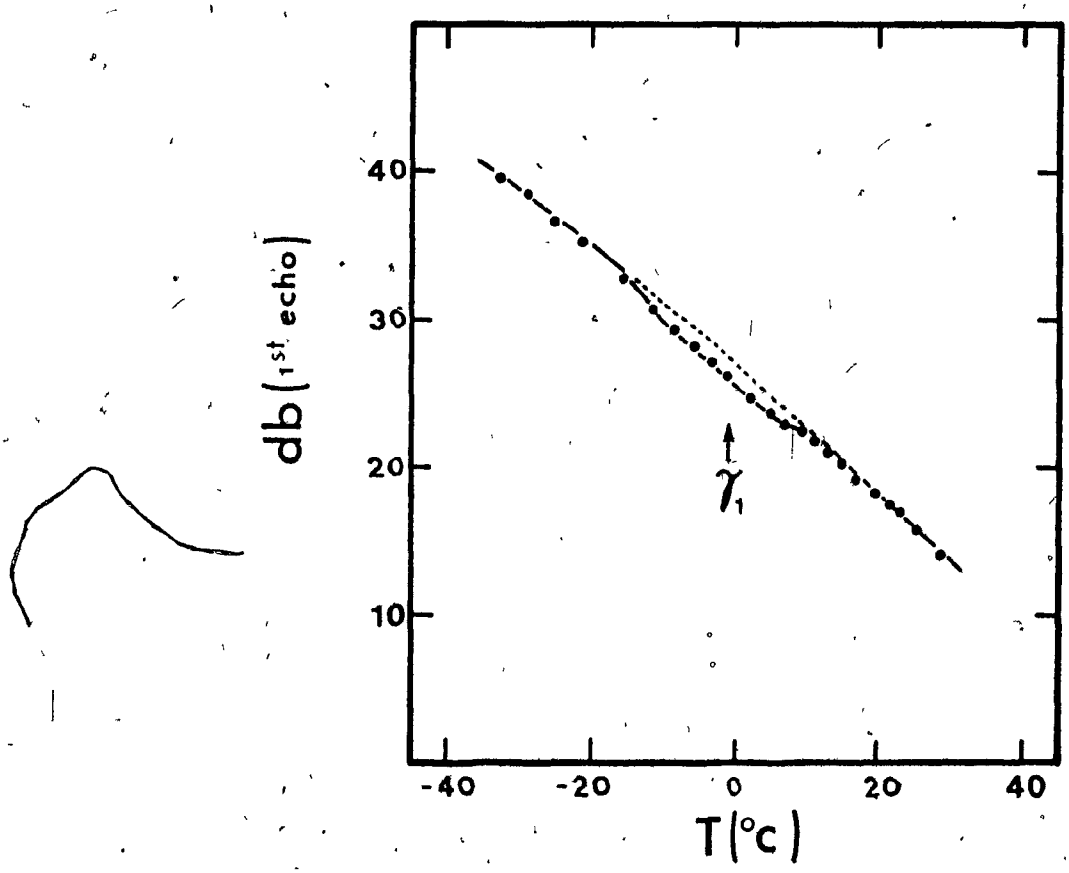
db (1st echo)
40
30
20
10
γ_1
-40
-20
0
20
40
T(°c)

APPENDIX VI

TABLES OF SUPPORTING DATA FOR FIGURES IN THE TEXT

Figure 4, Chapter I, page 15. Data for Methyl Chloroform (from Das[21].)

$\log \nu_c$ (Hz)	1000/T $(^oK)^{-1}$
6.2	5.0
5.8	5.2
5.6	5.5
5.4	5.8
5.2	6.1
5.2	6.5
4.9	7.0
4.7	7.4
4.4	8.1
4.3	8.8
4.0	9.7
3.8	10.7
3.5	12.0

Figure 9, Chapter I, page 33

Literature Data for the Backbone Methyl Relaxation in Conventional PMMA
(The points for the α, β, 'H_2O', and δ relaxations have been taken from McCrum, Read and Williams[11] and McCall[6], and need not be repeated here.)

NMR POINTS								DYNAMIC MECHANICAL POINTS				
log ν_c (Hz)	1000/T $(^oK)^{-1}$	Remarks	Ref.	log ν_c (Hz)	1000/T $(^oK)^{-1}$	Remarks	Ref.	log ν (Hz)	1000/T $(^oK)^{-1}$	tan δ peak ht.	Relax. strength	Ref.
7.51	3.6		6	5.35	4.05	[line width]	34	7.0	~4.0	~0.003		47
7.33	3.84	T_1 min	65	5.2	4.2	"	"	7.0	~4.55	-0.03	[hint of infl.]	"
7.6	3.8	"	63	5.0	4.45	"	"	6.48	~6.2	-0.003		61
7.5	4.0	[",<0.1% monomer]	64	4.85	4.65	"	"	6.48	~4.8	-0.001		"
				4.65	4.85	"	"	6.7	6.06		[v/T slope changes]	49
~4.7	~6.3	$T_{1\rho}$ min	66	4.5	5.1	"	"	6.7	6.66			"
~4.6	6.0±0.5	[line width 0.2% H_2O present]	62	4.4	5.35	"	"	6.0	6.80			"
				4.25	5.7	"	"	6.0	7.40			"
				4.1	6.0	"	"	6.2	4.1			62
4.4	5.8		6	4.05	6.35	"	"	5.8	4.7			"
4.8	5.9		"	3.8	6.75	"	"	4.1	6.65			"
4.4	6.2		"	3.6	7.2	"	"	3.35	7.6			"
4.4	6.7		"	3.25	7.75	"	"	3.844	9.09	-0.0002	-1/1000	56
4.2	6.7		"	2.8	8.4	"	"	3.83	6.25		-2/1000	"
5.8±0.3	4.0	line width	31					0.0	10.0			59
4.75±0.1	5.0	"	"									
4.3	6.0	"	"									
3.95	7.0	"	"									
3.75	8.0	"	"									

(VI-2)

Figure 14, Chapter III, page 57

Vibrating Reed data for free-radical PMMA-H_8 at ~565 Hz. (f_o varied from 567.0 Hz at -197.8°C to 562.7 Hz at -139.4°C.)

T(°C)	E'x10^{-10} (dynes/cm^2)	T(°C)	tanδ x10^3
-197.8	6.391	-196.0	1.94
-193.0	6.389	-191.0	1.81
-190.7	6.384	-188.2	1.83
-189.7	6.380	-186.0	1.86
-187.5	6.382	-183.0	1.85
-186.8	6.382	-180.3	1.79
-184.8	6.380	-177.6	1.85
-183.7	6.371	-174.8	1.89
-182.0	6.369	-172.1	1.92
-181.5	6.371	-168.8	2.01
-179.7	6.366	-164.2	2.14
-178.5	6.366	-161.5	2.24
-177.0	6.369	-159.0	2.36
-176.4	6.364	-154.9	2.42
-175.7	6.364	-150.3	2.40
-174.2	6.362	-147.4	2.56
-173.0	6.362	-143.8	2.74
-171.3	6.360	-138.2	2.97
-171.0	6.362	-135.5	3.05
-167.8	6.360	-133.6	3.17
-165.7	6.353	-132.0	3.20
-165.2	6.355	-130.1	3.48
-163.2	6.351		
-162.2	6.353		
-160.7	6.348		
-160.0	6.344		
-157.8	6.337		
-157.2	6.339		
-156.0	6.331		
-153.8	6.326		
-152.5	6.324		
-151.4	6.319		
-149.3	6.319		
-148.7	6.315		
-146.3	6.308		
-145.7	6.306		
-142.0	6.301		
-139.4	6.295		

Figure 15, Chapter III, page 59

Vibrating Reed Data for PMMA-D8 at ~540 Hz. (f_o varied from 548.96 Hz at -198.6°C to 536.52 Hz at -109.6°C.)

T (°C)	E'x10-10 (dynes/cm^2)	T (°C)	tanδ x 10^3
-198.6	7.6756	-199.5	0.787
-196.4	7.6694	-197.2	0.835
-194.1	7.6633	-195.1	0.832
-191.2	7.6549	-192.6	0.802
-189.0	7.6485	-189.8	0.839
-186.0	7.6418	-187.2	0.852
-183.1	7.6342	-184.3	0.891
-180.0	7.6214	-180.8	0.934
-178.0	7.6156	-178.7	0.939
-176.5	7.6097	-177.0	0.937
-174.9	7.6041	-175.5	0.942
-173.0	7.5983	-173.7	0.938
-171.7	7.5936	-172.3	0.961
-170.2	7.5900	-171.0	0.993
-168.4	7.5838	-169.0	1.04
-166.4	7.5788	-167.2	1.03
-164.0	7.5713	-165.2	1.08
-161.2	7.5613	-162.2	1.08
-159.3	7.5541	-159.9	1.14
-158.0	7.5483	-158.4	1.20
-157.3	7.5458	-157.5	1.22
-156.6	7.5430	-156.8	1.22
-154.8	7.5383	-155.9	1.24
-153.0	7.5347	-153.8	1.30
-150.5	7.5231	-151.7	1.32
-149.0	7.5181	-149.6	1.34
-146.5	7.5076	-147.6	1.41
-144.2	7.5012	-144.9	1.50
-141.3	7.4899	-142.2	1.58
-138.0	7.4753	-139.3	1.64
-135.9	7.4670	-136.5	1.78
-132.3	7.4499	-134.0	1.81
-127.5	7.4304	-130.4	1.93
-125.2	7.4188	-125.8	2.16
-122.9	7.4084	-123.8	2.32
-120.8	7.3963	-121.6	2.47
-118.1	7.3776	-119.4	2.67
-115.5	7.3650	-117.0	2.83
-112.2	7.3459	-113.9	2.85
-109.6	7.3316	-110.5	3.02
		-108.0	3.16
		-103.5	3.39
		-100.0	3.65
		- 95.5	3.95

Figure 16, Chapter III, page 63

Acoustic Data for Free-radical PMMA-H_8

Δ - Optical Vibrating Reed (~270 Hz)		□ - Acoustic Spectrometer (1240-1424 Hz)		○ - Piezoelectric Vibrating Reed (946-1112 Hz)	
T(°C)	tan δ x10^2	T (°C)	E'x10^{-10} (dynes/cm^2)	T (°C)	E'x10^{-10} (dynes/cm^2)
-120	0.48	26.	4.14	26.	3.76
-113	0.51	12.	4.37	13.	4.04
-107	0.59	-9.5	4.62	5.	4.16
-104	0.62	-37.	4.90	-4.	4.31
-98	0.67	-47.	5.12	-13.5	4.45
-92	0.79	-59.	5.20	-23.	4.55
-85	0.92	-66.5	5.27	-33.5	4.64
-79	1.01	-73.	5.27	-48.	4.84
-72	1.12	-78.5	5.35	-54.	4.91
-64.5	1.21	-88.5	5.36	-61.5	4.98
-57.	1.31	-98.5	5.39	-75.5	5.09
-51.	1.50	-116.	5.42	-93.	5.20
-40.	2.06	-134.	5.45		
		-144.5	5.45		

(VI-5)

Figure 17, Chapter III, page 65

Ultrasonic Data for Free-radical PMMA-H_8 at 8.4 MHz.

TEMP (C)	TAN D	STD DEV (TAN D)	VEL (CM/US)	STD DEV (VEL)	# PTS	(.5)T1 (USEC)	DB1	(.5)T2 (USEC)	DB2	(.5)T3 (USEC)	DB3	(.5)T4 (USEC)	DB4
25.5	0.01485	0.00017	0.27112	0.00176	4	0.100	50.2	2.611	32.4	5.080	16.4	7.490	-0.3
20.3	0.01459	0.00017	0.27194	0.00147	4	0.100	50.7	2.600	33.5	5.054	17.9	7.470	1.2
16.0	0.01402	0.00013	0.27210	0.00068	4	0.100	51.9	2.581	35.4	5.018	20.3	7.471	4.4
12.0	0.01366	0.00007	0.27317	0.00077	4	0.100	52.8	2.574	37.0	4.996	22.1	7.444	6.8
8.4	0.01335	0.00006	0.27482	0.00070	4	0.100	53.6	2.555	38.4	4.962	24.0	7.400	8.9
4.3	0.01303	0.00008	0.27634	0.00091	4	0.100	54.4	2.551	39.8	4.944	25.8	7.360	11.0
-0.3	0.01266	0.00006	0.27844	0.00100	4	0.100	55.0	2.535	41.0	4.905	27.4	7.307	13.2
-4.2	0.01246	0.00008	0.27954	0.00106	4	0.100	55.6	2.528	41.9	4.890	28.6	7.278	14.6
-8.3	0.01211	0.00009	0.28124	0.00136	4	0.100	56.0	2.524	42.8	4.865	29.9	7.237	16.4
-12.4	0.01169	0.00011	0.28294	0.00121	4	0.100	56.7	2.500	44.1	4.848	31.7	7.187	18.7
-16.3	0.01120	0.00013	0.28421	0.00145	4	0.100	57.1	2.495	45.2	4.834	33.3	7.155	20.9
-20.5	0.01069	0.00017	0.28507	0.00171	4	0.100	57.6	2.490	46.5	4.830	35.0	7.131	23.2
-24.7	0.01024	0.00015	0.28627	0.00177	4	0.100	58.1	2.478	47.5	4.813	36.5	7.100	25.3
-28.9	0.00990	0.00018	0.28726	0.00173	4	0.100	58.4	2.465	48.3	4.797	37.7	7.074	26.8
-33.0	0.00948	0.00018	0.28803	0.00138	4	0.100	58.8	2.451	49.2	4.775	39.1	7.056	28.6
-36.3	0.00919	0.00018	0.28833	0.00130	4	0.100	59.0	2.447	49.8	4.768	39.9	7.049	29.8

Figure 18, Chapter III, page 68

Ultrasonic Data for Free-radical PMMA-D_8 at 13.4 MHz.
(Upper data set - 0 ; lower data set - •)

TEMP (C)	TAN D	STD DEV (TAN D)	VEL (CM/US)	STD DEV (VEL)	# PTS	0.5 T1 (USEC)	DB1	0.5 T2 (USEC)	DB2
-24.2	0.00822	0.00000	0.24412	0.00000	2	0.100	61.6	1.803	51.4
-22.2	0.00821	0.00000	0.24142	0.00000	2	0.100	61.1	1.819	50.8
-19.6	0.00854	0.00000	0.24255	0.00000	2	0.100	60.3	1.811	49.5
-17.1	0.00886	0.00000	0.24397	0.00000	2	0.100	59.4	1.801	48.4
-15.4	0.00934	0.00000	0.24397	0.00000	2	0.100	59.2	1.801	47.6
-13.9	0.00942	0.00000	0.24397	0.00000	2	0.100	58.7	1.801	47.0
-12.0	0.00959	0.00000	0.24226	0.00000	2	0.100	58.1	1.813	46.1
-10.5	0.01004	0.00000	0.24142	0.00000	2	0.100	57.6	1.819	45.0
-9.5	0.01038	0.00000	0.24198	0.00000	2	0.100	57.6	1.815	44.6
-8.0	0.01064	0.00000	0.24255	0.00000	2	0.100	57.2	1.811	43.9
-6.4	0.01134	0.00000	0.24542	0.00000	2	0.100	57.2	1.791	43.2
-5.5	0.01140	0.00000	0.24340	0.00000	2	0.100	57.0	1.805	42.8
-4.2	0.01179	0.00000	0.24312	0.00000	2	0.100	56.9	1.807	42.2
-3.2	0.01206	0.00000	0.24369	0.00000	2	0.100	56.7	1.803	41.7
-2.2	0.01216	0.00000	0.24397	0.00000	2	0.100	56.5	1.801	41.4
-0.8	0.01235	0.00000	0.24469	0.00000	2	0.100	56.2	1.796	40.9
0.7	0.01260	0.00000	0.24644	0.00000	2	0.100	55.8	1.784	40.3
2.0	0.01265	0.00000	0.24732	0.00000	2	0.100	55.4	1.778	39.9
3.3	0.01285	0.00000	0.24644	0.00000	2	0.100	55.0	1.784	39.2
5.0	0.01297	0.00000	0.24571	0.00000	2	0.100	54.4	1.789	38.4
6.3	0.01315	0.00000	0.24441	0.00000	2	0.100	54.1	1.798	37.8
7.8	0.01355	0.00000	0.24732	0.00000	2	0.100	53.5	1.778	36.9
9.4	0.01372	0.00000	0.24455	0.00000	2	0.100	52.8	1.797	35.8
10.5	0.01390	0.00000	0.24354	0.00000	2	0.100	52.3	1.804	35.0
11.3	0.01405	0.00000	0.24198	0.00000	2	0.100	52.0	1.815	34.4
13.2	0.01454	0.00000	0.24484	0.00000	2	0.100	50.9	1.795	32.9
15.1	0.01502	0.00000	0.24880	0.00000	2	0.100	49.7	1.768	31.4

TEMP (C)	TAN D	STD DEV (TAN D)	VEL (CM/US)	STD DEV (VEL)	# PTS	0.5 T1 (USEC)	DB1	0.5 T2 (USEC)	DB2
-103.3	0.00304	0.00000	0.25554	0.00000	2	0.100	59.5	1.724	55.9
-98.5	0.00299	0.00000	0.25609	0.00000	2	0.100	59.0	1.703	55.5
-94.7	0.00316	0.00000	0.25971	0.00000	2	0.100	59.1	1.701	55.4
-90.8	0.00323	0.00000	0.25744	0.00000	2	0.100	59.0	1.712	55.2
-85.9	0.00321	0.00000	0.25601	0.00000	2	0.100	59.0	1.721	55.2
-81.0	0.00339	0.00000	0.25681	0.00000	2	0.100	59.1	1.716	55.1
-77.0	0.00362	0.00000	0.25491	0.00000	2	0.100	59.2	1.728	54.9
-72.4	0.00381	0.00000	0.25076	0.00000	2	0.100	59.2	1.755	54.6
-68.6	0.00400	0.00000	0.25228	0.00000	2	0.100	59.6	1.745	54.8
-64.0	0.00517	0.00000	0.25289	0.00000	2	0.100	61.5	1.741	55.3
-60.2	0.00541	0.00000	0.24821	0.00000	2	0.100	63.2	1.772	56.6
-56.9	0.00550	0.00000	0.24940	0.00000	2	0.100	63.9	1.764	57.1
-53.7	0.00575	0.00000	0.24880	0.00000	2	0.100	64.4	1.768	57.4
-50.2	0.00579	0.00000	0.24717	0.00000	2	0.100	64.4	1.779	57.3
-46.9	0.00587	0.00000	0.25060	0.00000	2	0.100	64.2	1.756	57.1
-43.7	0.00605	0.00000	0.24770	0.00000	2	0.100	64.1	1.775	56.7
-41.3	0.00649	0.00000	0.24895	0.00000	2	0.100	64.2	1.767	56.3
-36.2	0.00708	0.00000	0.24397	0.00000	2	0.100	64.0	1.801	55.2
-32.8	0.00748	0.00000	0.24629	0.00000	2	0.100	63.6	1.785	54.4
-30.3	0.00762	0.00000	0.24058	0.00000	2	0.100	63.2	1.825	53.6
-28.2	0.00796	0.00000	0.24369	0.00000	2	0.100	62.8	1.803	52.9
-25.2	0.00813	0.00000	0.24156	0.00000	2	0.100	62.0	1.818	51.8
-23.1	0.00836	0.00000	0.24142	0.00000	2	0.100	61.6	1.819	51.1
-21.4	0.00875	0.00000	0.23892	0.00000	2	0.100	61.2	1.837	50.1
-19.4	0.00892	0.00000	0.24128	0.00000	2	0.100	60.5	1.820	49.3

Figure 19, Chapter III, page 69

Ultrasonic Data for Isotactic PMMA-H_8 at 13.7 MHz

FREQUENCY = 13.7 MHZ

TEMP (C)	TAN D	STD DEV (TAN D)	VEL (CM/US)	STD DEV (VEL)	# PTS	(.5)T1 (USEC)	DB1	(.5)T2 (USEC)	DB2	(.5)T3 (USEC)	DB3	(.5)T4 (USEC)	DB4	(.5)T5 (USEC)	DB5
27.5	0.01266	0.00068	0.26344	0.00386	3	0.100	40.0	1.797	25.4	3.410	8.7				
24.5	0.01234	0.00075	0.26273	0.00297	3	0.100	40.5	1.792	26.5	3.419	9.9				
21.5	0.00998	0.00042	0.25405	0.00131	4	0.100	41.8	1.787	27.9	3.505	14.6	5.248	3.6		
18.5	0.01076	0.00014	0.25937	0.00009	3	0.100	42.5	1.780	28.7	3.462	15.5				
15.5	0.01035	0.00018	0.25797	0.00285	4	0.100	43.1	1.795	30.0	3.423	16.7	5.191	4.0		
11.3	0.00958	0.00005	0.26235	0.00211	4	0.100	43.9	1.788	31.7	3.470	19.9	5.079	8.2		
9.5	0.00974	0.00006	0.26346	0.00178	4	0.100	44.7	1.767	32.7	3.448	20.6	5.056	8.6		
6.5	0.00937	0.00007	0.25955	0.00236	4	0.100	46.1	1.759	34.8	3.407	22.9	5.150	10.9		
3.7	0.00878	0.00011	0.26392	0.00141	4	0.100	46.8	1.761	35.6	3.434	24.5	5.049	14.4		
1.0	0.00875	0.00004	0.26136	0.00057	4	0.100	47.2	1.754	36.2	3.427	25.3	5.163	14.5		
-2.7	0.00865	0.00007	0.26448	0.00134	3	0.100	47.7	1.763	37.1	3.357	26.4				
-5.3	0.00844	0.00006	0.26514	0.00100	4	0.100	48.2	1.759	37.9	3.410	27.6	5.031	17.1		
-9.0	0.00796	0.00001	0.26257	0.00018	4	0.100	49.0	1.756	39.2	3.421	29.3	5.060	19.4		
-13.0	0.00787	0.00008	0.26749	0.00079	4	0.100	50.0	1.747	40.7	3.374	31.0	4.991	21.3		
-15.8	0.00760	0.00011	0.26706	0.00027	4	0.100	50.7	1.739	41.8	3.365	32.6	5.000	22.9		
-17.8	0.00723	0.00003	0.26576	0.00014	4	0.100	51.2	1.743	42.4	3.380	33.6	5.023	24.6		
-19.2	0.00705	0.00002	0.26685	0.00058	4	0.100	51.6	1.734	43.0	3.379	34.4	4.998	25.8		
-22.0	0.00686	0.00002	0.26765	0.00062	4	0.100	52.0	1.736	43.7	3.371	35.3	4.985	27.0		
-25.2	0.00663	0.00006	0.26804	0.00052	4	0.100	52.6	1.737	44.6	3.363	36.7	4.980	28.4		
-28.0	0.00628	0.00009	0.26778	0.00019	4	0.100	53.2	1.726	45.9	3.359	38.3	4.983	30.3		
-30.3	0.00617	0.00010	0.26870	0.00021	4	0.100	53.7	1.727	46.6	3.349	39.1	4.968	31.3		
-33.0	0.00605	0.00010	0.26944	0.00053	4	0.100	54.3	1.717	47.4	3.346	40.0	4.951	32.4		
-36.0	0.00607	0.00016	0.27191	0.00057	4	0.100	54.9	1.713	48.2	3.318	40.9	4.910	33.1		
-39.0	0.00578	0.00007	0.27086	0.00026	4	0.100	55.3	1.704	48.7	3.320	41.6	4.927	34.5		
-42.0	0.00556	0.00005	0.27169	0.00007	4	0.100	55.6	1.703	49.2	3.309	42.5	4.914	35.7		
-47.0	0.00523	0.00004	0.27282	0.00040	5	0.100	56.4	1.706	50.4	3.311	44.2	4.903	37.8	6.492	31.8
-51.3	0.00487	0.00004	0.27373	0.00037	5	0.100	56.7	1.697	51.2	3.299	45.3	4.885	39.5	6.470	33.6
-56.0	0.00476	0.00006	0.27496	0.00041	5	0.100	57.4	1.685	52.1	3.282	46.6	4.864	40.8	6.438	35.0
-61.0	0.00452	0.00007	0.27618	0.00023	5	0.100	57.7	1.679	52.9	3.265	47.5	4.834	42.0	6.416	36.8
-65.5	0.00428	0.00008	0.27630	0.00018	5	0.100	58.1	1.675	53.6	3.260	48.5	4.831	43.3	6.412	38.0
-70.3	0.00415	0.00010	0.27716	0.00038	5	0.100	58.5	1.682	54.3	3.261	49.3	4.825	44.3	6.394	39.1
-75.5	0.00404	0.00008	0.27819	0.00045	5	0.100	58.9	1.671	54.6	3.251	49.9	4.808	45.1	6.386	40.0
-80.8	0.00386	0.00007	0.27840	0.00036	5	0.100	59.5	1.674	55.4	3.246	50.9	4.803	46.3	6.366	41.2
-85.0	0.00382	0.00009	0.27977	0.00035	5	0.100	60.0	1.656	56.1	3.227	51.7	4.778	47.0	6.331	42.3
-90.0	0.00372	0.00008	0.28067	0.00034	5	0.100	60.2	1.660	56.4	3.215	52.0	4.770	47.6	6.312	43.0
-95.7	0.00361	0.00006	0.28096	0.00041	5	0.100	60.7	1.660	57.0	3.216	52.7	4.766	48.4	6.306	44.1
-99.3	0.00353	0.00007	0.28266	0.00053	5	0.100	60.9	1.656	57.3	3.204	53.1	4.737	49.0	6.272	44.7
-104.5	0.00314	0.00007	0.28356	0.00032	5	0.100	61.1	1.650	57.7	3.181	54.3	4.720	50.6	6.253	46.6
-106.0	0.00315	0.00006	0.28330	0.00023	5	0.100	61.9	1.640	58.7	3.184	55.1	4.722	51.3	6.254	47.5
-110.0	0.00309	0.00004	0.28452	0.00044	5	0.100	62.1	1.644	58.8	3.178	55.2	4.708	51.7	6.230	48.0
-116.5	0.00270	0.00005	0.28530	0.00036	5	0.100	62.2	1.637	59.2	3.165	56.4	4.658	53.0	6.212	49.9
-120.5	0.00252	0.00000	0.28275	0.00000	2	0.100	62.7	1.642	59.8						

Figure 20, Chapter III, page 70

Ultrasonic Data for 'Syndiotactic' PMMA-H_8 at 13.5 MHz

TEMP (C)	TAN D	STD DEV (TAN D)	VEL (CM/US)	STD DEV (VEL)	# PTS	0.5 T1 (USEC)	DB1	0.5 T2 (USEC)	DB2	0.5 T3 (USEC)	DB3	0.5 T4 (USEC)	DB4	0.5 T5 (USEC)	DB5	0.5 T6	DB6
-104.1	0.00202	0.00005	0.27105	0.00021	6	0.100	69.0	1.659	65.8	3.207	63.3	4.750	60.7	6.304	58.7	7.849	56.7
-101.4	0.00197	0.00006	0.27101	0.00042	6	0.100	68.0	1.671	65.7	3.215	63.0	4.770	60.7	6.313	58.7	7.852	56.9
-98.9	0.00197	0.00004	0.27088	0.00041	6	0.100	68.0	1.662	65.7	3.213	63.0	4.764	60.7	6.321	58.6	7.848	56.9
-95.4	0.00190	0.00004	0.27074	0.00028	6	0.100	67.9	1.660	65.6	3.213	63.2	4.754	61.9	6.318	59.0	7.856	57.1
-91.4	0.00185	0.00004	0.27030	0.00049	6	0.100	67.8	1.662	65.6	3.221	63.2	4.789	61.2	6.319	59.1	7.869	57.3
-87.8	0.00182	0.00003	0.26999	0.00031	6	0.100	67.7	1.663	65.4	3.231	63.2	4.774	61.3	6.331	59.2	7.883	57.2
-85.8	0.00184	0.00001	0.27049	0.00039	6	0.100	67.7	1.649	65.6	3.216	63.4	4.771	61.1	6.319	59.3	7.856	57.2
-83.9	0.00184	0.00001	0.26985	0.00030	6	0.100	67.7	1.665	65.5	3.224	63.4	4.782	61.4	6.345	59.2	7.882	57.1
-81.2	0.00189	0.00002	0.26931	0.00032	6	0.100	67.7	1.660	65.5	3.230	63.4	4.785	61.3	6.348	59.0	7.892	56.8
-78.3	0.00192	0.00002	0.26945	0.00031	6	0.100	67.5	1.667	65.4	3.227	63.2	4.779	61.1	6.350	58.8	7.891	56.5
-76.3	0.00201	0.00004	0.26910	0.00030	6	0.100	67.5	1.656	65.4	3.221	63.2	4.790	61.1	6.350	58.4	7.895	56.0
-72.8	0.00216	0.00005	0.26871	0.00039	6	0.100	67.5	1.657	65.3	3.241	63.0	4.800	60.4	6.358	57.9	7.910	55.1
-66.6	0.00249	0.00004	0.26731	0.00014	6	0.100	67.5	1.673	65.1	3.249	62.3	4.819	59.2	6.389	56.2	7.955	53.3
-61.8	0.00275	0.00005	0.26703	0.00005	6	0.100	67.5	1.674	64.8	3.249	61.7	4.820	58.5	6.392	55.1	7.965	51.7
-58.2	0.00298	0.00005	0.26630	0.00016	6	0.100	67.4	1.681	64.5	3.262	61.0	4.840	57.4	6.410	53.6	7.987	50.3
-53.8	0.00310	0.00003	0.26474	0.00026	6	0.100	67.1	1.681	63.7	3.271	60.0	4.868	56.2	6.449	52.4	8.025	49.0
-50.6	0.00316	0.00005	0.26410	0.00045	6	0.100	66.8	1.703	63.1	3.309	59.1	4.891	55.3	6.475	51.8	8.052	48.5
-46.0	0.00313	0.00006	0.26343	0.00031	6	0.100	66.4	1.706	62.5	3.306	58.4	4.899	54.9	6.481	51.4	8.077	48.1
-42.6	0.00303	0.00006	0.26261	0.00034	6	0.100	66.0	1.712	61.9	3.312	58.2	4.919	54.7	6.502	51.5	8.100	48.0
-38.4	0.00300	0.00003	0.26268	0.00050	6	0.100	65.6	1.709	61.7	3.312	58.2	4.918	54.7	6.516	51.3	8.067	47.8
-35.0	0.00311	0.00001	0.26230	0.00038	6	0.100	65.3	1.699	61.7	3.312	58.0	4.907	54.1	6.504	50.8	8.085	47.6
-31.7	0.00331	0.00004	0.26214	0.00026	6	0.100	65.1	1.709	61.5	3.317	57.7	4.921	53.7	6.510	49.8	8.114	45.8
-28.0	0.00362	0.00005	0.26179	0.00040	6	0.100	65.0	1.721	61.0	3.329	56.9	4.929	52.6	6.535	48.2	8.122	43.8
-24.6	0.00397	0.00004	0.26170	0.00059	6	0.100	64.8	1.732	60.4	3.340	55.7	4.948	51.0	6.535	46.3	8.131	41.4
-20.9	0.00431	0.00002	0.26048	0.00051	6	0.100	64.4	1.733	59.4	3.359	54.4	4.954	49.2	6.554	44.1	8.159	38.9
-17.5	0.00461	0.00001	0.25994	0.00052	6	0.100	63.7	1.740	58.1	3.363	52.7	4.971	47.2	6.581	41.6	8.184	36.3
-13.8	0.00487	0.00002	0.25872	0.00031	6	0.100	62.7	1.721	56.9	3.360	51.0	4.980	45.1	6.600	39.3	8.212	33.7
-10.0	0.00500	0.00003	0.25817	0.00031	6	0.100	61.9	1.748	55.7	3.365	49.5	5.007	43.8	6.619	37.6	8.241	31.5
-6.6	0.00500	0.00002	0.25759	0.00070	6	0.100	61.2	1.760	55.2	3.400	49.2	5.031	43.3	6.637	37.2	8.261	31.2
-3.7	0.00507	0.00005	0.25770	0.00056	6	0.100	60.9	1.749	55.2	3.390	49.2	5.020	43.0	6.635	36.9	8.251	30.6
-0.5	0.00517	0.00005	0.25682	0.00051	6	0.100	60.9	1.753	55.1	3.389	48.9	5.031	42.5	6.650	36.3	8.277	29.9
2.3	0.00543	0.00005	0.25743	0.00051	6	0.100	60.7	1.743	54.7	3.378	48.2	5.010	41.6	6.652	34.9	8.250	28.3
6.5	0.00581	0.00006	0.25775	0.00069	6	0.100	60.7	1.754	54.2	3.400	47.3	5.021	40.1	6.641	33.1	8.250	26.0
9.8	0.00613	0.00004	0.25624	0.00039	6	0.100	60.3	1.755	53.2	3.399	45.9	5.021	38.5	6.675	30.9	8.297	23.4
14.1	0.00667	0.00010	0.25557	0.00106	6	0.100	59.6	1.753	52.0	3.419	44.1	5.061	36.2	6.678	28.0	8.271	19.4
18.5	0.00720	0.00008	0.25672	0.00095	6	0.100	58.2	1.767	50.1	3.432	41.4	5.010	32.4	6.653	23.6	8.305	15.2
25.2	0.00748	0.00009	0.25299	0.00057	6	0.100	56.3	1.778	47.6	3.448	38.8	5.114	29.6	6.758	20.2	8.400	10.6

Figure 21, Chapter III, page 72

Torsional Pendulum Data for Free-Radical PMMA-D_8 at ~0.75 Hz.

TEMP (C)	TAN D APP	TAN D CORR	STD DEVN TAN D C.	FREQ (HZ)	G1 (10**9)	G11 (10**9)
-192.0	0.001112	0.001118	0.000012	0.75390	26.7304	0.029883
-187.8	0.001224	0.001231	0.000010	0.75350	26.7019	0.032859
-182.7	0.001304	0.001311	0.000008	0.75290	26.6591	0.034951
-178.0	0.001440	0.001448	0.000008	0.75245	26.6271	0.038568
-174.9	0.001524	0.001532	0.000010	0.75160	26.5667	0.040713
-172.0	0.001720	0.001730	0.000011	0.75055	26.4920	0.045818
-168.0	0.001822	0.001832	0.000016	0.75025	26.4707	0.048500
-164.8	0.001974	0.001986	0.000018	0.74990	26.4459	0.052509
-161.5	0.002162	0.002165	0.000026	0.74970	26.4317	0.057224
-158.4	0.002224	0.002237	0.000021	0.74930	26.4034	0.059070
-156.1	0.002344	0.002358	0.000029	0.74800	26.3114	0.062036
-153.8	0.002658	0.002673	0.000061	0.74820	26.3255	0.070381
-152.5	0.002646	0.002661	0.000030	0.74795	26.2795	0.069934
-150.4	0.002676	0.002692	0.000049	0.74735	26.2654	0.070706
-148.0	0.003085	0.003103	0.000072	0.74685	26.2300	0.081395
-145.6	0.003118	0.003136	0.000037	0.74580	26.1559	0.082030
-142.6	0.003230	0.003249	0.000042	0.74520	26.1136	0.084835
-139.9	0.003488	0.003508	0.000044	0.74550	26.1348	0.091686
-136.8	0.003906	0.003929	0.000044	0.74390	26.0220	0.102239

Figure 21, Chapter III, page 72 (continued)
Torsional Pendulum Data for Free-radical PMMA-D_8 at ~2.35 Hz.

TEMP (C)	TAN D APP	TAN D CORR	STD DEVN TAN D C.	FREQ (HZ)	GI (10**9)	GII (10**9)
-194.0	0.001270	0.001277	0.000017	2.36300	26.5930	0.033961
-189.5	0.001284	0.001291	0.000012	2.36000	26.5251	0.034247
-185.0	0.001357	0.001365	0.000011	2.35800	26.4799	0.036154
-181.5	0.001404	0.001412	0.000008	2.35900	26.5025	0.037414
-178.0	0.001502	0.001511	0.000012	2.35800	26.4799	0.040006
-175.5	0.001517	0.001526	0.000010	2.35600	26.4348	0.040330
-173.0	0.001590	0.001599	0.000018	2.35600	26.4348	0.042269
-171.0	0.001670	0.001679	0.000014	2.35300	26.3671	0.044277
-168.5	0.001741	0.001751	0.000013	2.35400	26.3896	0.046213
-165.7	0.001817	0.001827	0.000019	2.35200	26.3445	0.048134
-162.5	0.001942	0.001954	0.000020	2.35000	26.2995	0.051383
-159.0	0.002018	0.002030	0.000017	2.34950	26.2882	0.053371
-157.0	0.002146	0.002158	0.000027	2.34800	26.2545	0.056663
-154.0	0.002299	0.002312	0.000026	2.34750	26.2433	0.060676
-151.7	0.002447	0.002461	0.000029	2.34300	26.1422	0.064341
-149.2	0.002627	0.002643	0.000038	2.34200	26.1197	0.069028
-145.0	0.002867	0.002884	0.000020	2.34100	26.0973	0.075262
-141.5	0.003027	0.003045	0.000033	2.33900	26.0525	0.079324
-137.0	0.003339	0.003359	0.000028	2.33700	26.0077	0.087364
-132.2	0.003750	0.003772	0.000025	2.33450	25.9518	0.097884

Figure 22, Chapter IV, page 74.

Experimental log ν versus 1/T data for the γ_1 relaxation of Free-radical PMMA-H_8 and PMMA-D_8.

PMMA-H_8		PMMA-D_8	
log ν	1000/T $(^oK)^{-1}$	log ν	1000/T $(^oK)^{-1}$
7.301	3.68	7.127	3.69
7.134	3.68	3.595	5.99
6.924	3.80	3.238	6.47
6.532	3.98	3.144	6.49
6.114	4.26	3.003	6.45
3.959	6.37	2.733	6.54
3.635	6.76	2.731	6.54
3.483	6.58	2.566	6.49
3.481	6.41	0.371	8.33
3.481	6.45	-0.125	8.62
3.246	7.94		
2.853	8.20		
2.851	7.81		
2.756	9.05		
2.754	8.55		
2.752	8.85		
2.696	9.71		
2.696	9.48		
2.438	9.01		

Figure 23, Chapter IV, page 76

Complete Transition Map Data for PMMA-H_8 and PMMA-D_8

(The literature data of Figure 9 (given on page VI-2) and the experimental data for the γ_1 relaxation of free-radical PMMA-H_8 and PMMA-D_8 (given on page VI-12) need not be repeated here).

Polymer	PMMA-H_8 (free-radical)		PMMA-D_8 (free-radical)		PMMA-H_8 (isotactic)		PMMA-H_8 (syndiotactic)	
Relaxation	log ν	1000/T $(^oK)^{-1}$	log ν	1000/T $(^oK)^{-1}$	log ν	1000/T $(^oK)^{-1}$	log ν	1000/T $(^oK)^{-1}$
water	7.267	3.17						
	7.134	3.26						
	6.114	3.58						
	3.135	4.33						
	3.031	4.48						
	2.430	5.18						
γ_2	7.111	4.61	7.127	4.65			7.131	4.61
	3.966	9.17	3.604	10.20				
	3.641	9.95	3.151	10.31				
	3.248	10.20	3.007	10.20				
	3.213	10.64	2.738	10.87				
	3.121	10.70						
	2.757	11.76						
	2.753	11.24						
	2.698	12.05						
	2.470	13.07						
	2.443	13.33						
	2.353	13.79						
γ_1							7.131	3.89
γ_3 -experimental	7.267	5.54			7.137	5.68		
Literature Reference					7.333	4.55		
Literature Reference					-4.7	-8.0		

METHYL-GROUP TUNNELING IN VISCOELASTIC RELAXATION: EXPERIMENTAL VERIFICATION

physical review letters

VOLUME 35, NUMBER 14 OCTOBER 6, 1975,
leaves 951-953

BY J. WILLIAMS, E. SHOHAMY, S. REICH, AND A. EISENBERG

DEPARTMENT OF CHEMISTRY, MCGILL UNIVERSITY,
MONTREAL, CANADA H3C 3G1

(CORRESPONDENCE CONCERNING THIS MATERIAL
SHOULD BE ADDRESSED TO A. EISENBERG.)